Mass Spectrometric Studies on Some Materials of Relevance to Nuclear Technology

By

Suranjan Bera

(Enrolment No: CHEM02201104002)

Indira Gandhi Centre for Atomic Research,

Kalpakkam

A thesis submitted to the
Board of Studies in Chemical Sciences
In partial fulfillment of requirements
for the Degree of
DOCTOR OF PHILOSOPHY
of
HOMI BHABHA NATIONAL INSTITUTE

August, 2018

Homi Bhabha National Institute

Recommendations of the Viva Voce Committee

As members of the Viva Voce Committee, we certify that we have read the dissertation prepared by **Suranjan Bera** entitled "**Mass Spectrometric Studies on Some Materials of Relevance to Nuclear Technology**" and recommend that it may be accepted as fulfilling the thesis requirement for the award of Degree of Doctor of Philosophy.

Chairman - Dr. N. Sivaraman **Date:** 15/3/19

Guide / Convener - Dr. T. S. Lakshmi Narasimhan **Date:** 15/03/19

Examiner - Dr. Ravi Bhushan **Date:** 15-03-2019

Member 1 - Dr. M. Joseph **Date:** 15/3/2019

Member 2 - Dr. D Ponraju **Date:** 15/3/2019

Final approval and acceptance of this thesis is contingent upon the candidate's submission of the final copies of the thesis to HBNI.

I hereby certify that I have read this thesis prepared under my direction and recommend that it may be accepted as fulfilling the thesis requirement.

Date: 15/03/19

Place: Kalpakkam

Guide

STATEMENT BY AUTHOR

This dissertation has been submitted in partial fulfillment of requirements for an advanced degree at Homi Bhabha National Institute (HBNI) and is deposited in the Library to be made available to borrowers under rules of the HBNI.

Brief quotations from this dissertation are allowable without special permission, provided that accurate acknowledgement of source is made. Requests for permission for extended quotation from or reproduction of this manuscript in whole or in part may be granted by the Competent Authority of HBNI when in his or her judgment the proposed use of the material is in the interests of scholarship. In all other instances, however, permission must be obtained from the author.

Suranjan Bera

SURANJAN BERA

DECLARATION

I, hereby declare that the investigation presented in the thesis has been carried out by me. The work is original and has not been submitted earlier as a whole or in part for a degree / diploma at this or any other Institution / University.

Suranjan Bera

SURANJAN BERA

List of Publications arising from the thesis

Journals

1. "Burn-up measurements on dissolver solution of mixed oxide fuel using HPLC-Mass spectrometric method", **S. Bera**, R. Balasubramanian, Arpita Datta, R. Sajimol, S. Nalini, T. S. Lakshmi Narasimhan, M. P. Antony, N. Sivaraman, K. Nagarajan, P. R. Vasudeva Rao, *International. Journal of Analytical Mass Spectrometry and Chromatography*, **2013**, 1, 55-60.
2. "Knudsen effusion mass spectrometric studies over (USn_3+U_3Sn_7) two-phase region of U-Sn system", P. Manikandan, V.V. Trinadh, **Suranjan Bera**, T.S.Lakshmi Narasimhan, K. Ananthasivan, M. Joseph, U. Kamachi Mudali, *Journal of Nuclear Materials,* **2017**, 491, 31-36.
3. "Knudsen effusion mass spectrometric studies on U-Al system: Thermodynamic properties over (UAl_2+UAl_3) biphasic region", **Suranjan Bera**, V.V. Trinadh, P. Manikandan, T. S. Lakshmi Narasimhan, K. Ananthasivan, M. Joseph, *Journal of Nuclear Materials,* **2018**, 509, 613-619.
4. "Thermodynamic properties over ($GdAl_3$+$GdAl_2$) of Gd-Al system: A High temperature mass spectrometric study", **Suranjan Bera**, P. Manikandan, V. V. Trinadh, T. S. Lakshmi Narasimhan, K. Ananthasivan, *Journal of Nuclear Materials*, **2018**, 511, 480-486.
5. "Molybdenum and lanthanum as alternate burn-up monitors - Development of chromatographic and mass spectrometric methods for determination of atom percent fission", **Suranjan Bera**, K. Sujatha, N. Sivaraman, T. S. Lakshmi Narasimhan, *Radiochimica Acta*, **2018**, https://doi.org/10.1515/ract-2018-3017.

Conferences

1. "Isotopic analysis of magnesium by thermal ionization mass spectrometry-A new sample loading approach for ion emission enhancement", **S. Bera**, R. Sajimol, S. Nalini, R. Balasubramanian, T. S. Lakshmi Narasimhan, *DAE-BRNS Theme Meeting on Recent Trends in Analytical Chemistry (TRAC-2012), August 30-31,* **2012**, held at VIT, Chennai.

2. “Thermal Ionization Mass Spectrometric studies on sodalite- a candidate material for nuclear waste containment”, **S. Bera**, R. Sajimol, S. Nalini, R. Balasubramanian, T. S. Lakshmi Narasimhan, *Theme meeting on recent trends in material chemistry, July 25-27,* **2013**, held at VIT, Chennai.
3. “IDMS studies on sodalite- a candidate material for nuclear waste containment”, **S. Bera**, R. Sajimol, S. Nalini, R. Balasubramanian, T. S. Lakshmi Narasimhan, *28th ISMAS symposium cum workshop on mass spectrometry, March 9-13*, **2014**, held at Parwanoo, Himachal Pradesh.
4. “Development of chromatographic and mass spectrometric methods for separation and quantification of molybdenum as burn-up monitor in dissolver solution of nuclear reactor fuels”, **Suranjan Bera**, S. Nalini, T. S. Lakshmi Narasimhan, N. Sivaraman, M. Joseph. *In 13th National Symposium on Nuclear and Radiochemistry on February 6-10*, **2017**, held at KIIT University, Bhubaneswar.
5. “Knudsen Effusion Mass Spectrometric studies over (U_3Sn_7+USn_3) phase region of U-Sn System”, P. Manikandan, V.V. Trinadh, **Suranjan Bera**, T. S. Lakshmi Narasimhan, K. Ananthasivan, M. Joseph, U. Kamachi Mudali, *31st ISMAS Symposium, March 23-25*, **2017**, held at BARC, Mumbai.
6. “Knudsen effusion mass spectrometric studies on U-Al system”, **Suranjan Bera**, V.V. Trinadh, P. Manikandan, N. Sivaraman, T. S. Lakshmi Narasimhan, K. Ananthasivan, M. Joseph, *21st Workshop & Symposium on Thermal Analysis (THERMANS - 2018), January 16-20*, **2018**, held at Goa University, Goa.
7. “High Temperature Mass Spectrometric studies on ($GdAl_2$+$GdAl_3$) two phase mixture”, **Suranjan Bera**, V.V. Trinadh, P. Manikandan, C. V. S. Brahmmananda Rao, T. S. Lakshmi Narasimhan, N. Sivaraman, K. Ananthasivan, *7th Interdisciplinary Symposium on Materials Chemistry (ISMC - 2018), December 4-8,* **2018**, held at BARC, Mumbai.

Others

a. Journals

1. “Effect of laser parameters on the measurement of U/Nd ratio using Pulsed Laser Deposition followed by Isotopic Dilution Mass Spectrometry”, R. Sajimol, P. Manoravi, **S. Bera**, M. Joseph, *International Journal of Mass Spectometry*, **2015**, 387, 51-55.

2. “Preferential Removal of Sm by Evaporation from Nd-Sm Mixture and its Application in Direct Burn-up Determination of Spent Nuclear Fuel”, R. Sajimol, **S. Bera**, S. Nalini, N. Sivaraman, M. Joseph, T. Kumar, *Journal of Radioanalytical and Nuclear Chemistry*, **2016**, 309, 563-573.
3. “High Temperature Mass Spectrometric studies on U-Ga system: Thermodynamic properties over (U_3Ga_5+UGa_2) and (UGa_2+UGa_3) phase regions”, P. Manikandan, V. V. Trinadh, **Suranjan Bera**, T.S. Lakshmi Narasimhan, M. Joseph**,** *Journal of Nuclear Materials,* **2016**, 475, 87-93.
4. “Direct burn-up determination of fast reactor mixed oxide (MOX) fuel by preferential evaporation of interfering elements”, R. Sajimol, **S. Bera**, N. Sivaraman, M. Joseph, *Journal of Radioanalytical and Nuclear Chemistry*, **2017**, 311, 1593-1603.
5. “Mass spectrometric studies on U-Pu-Zr alloy”, P. Manikandan, V.V. Trinadh, **Suranjan Bera**, T. S. Lakshmi Narasimhan, K. Ananthasivan, M. Joseph, *Journal of Nuclear Materials,* **2018**, 507, 339-346.

b. Conferences/Symposiums

1. “PLD-IDMS studies towards direct measurement of Burn-up of nuclear fuel”, R. Sajimol, P. Manoravi, S. Nalini, R. Balasubramanian, **Suranjan Bera**, T.S. Lakshmi Narasimhan, M. Joseph, *12th ISMAS- Triennial International Conference on Mass Spectrometry, March 3-8*, **2013**, held at Goa.
2. “PLD-IDMS studies towards direct measurement of burn-up of nuclear fuel”, R.Sajimol, P. Manoravi, S. Nalini, R. Balasubramanian, **S. Bera**, M. Joseph, *28th ISMAS symposium cum workshop on mass spectrometry, March 9-13*, **2014**, held at Parwanoo, Himachal Pradesh.
3. “Vaporisation studies over Sn-Te-O system”, V.V.Trinadh, P. Manikandan, **Suranjan Bera**, Ashish Jain, T. S. Lakshmi Narasimhan, K. Ananthasivan, M. Joseph, U. Kamachi Mudali, *31st ISMAS symposium on mass spectrometry*, *March 23-25*, **2017**, held at BARC, Mumbai.

Suranjan Bera
SURANJAN BERA

Dedicated to

My Family

&

Almighty

ACKNOWLEDGEMENTS

Foremostly, I would like to express my deep sense of gratitude to my research supervisor *Dr. T. S. Lakshmi Narasimhan* for his valuable guidance, immense support and the care that I was bestowed, despite his busy schedule. His exhaustive experience in KEMS and TIMS, enhanced my capability to explore various aspects while conducting experiments. I express my sincere indebtedness to *Dr. N. Sivaraman* for his continuous motivation and persistent encouragement throughout this work. His in-depth knowledge and experience in HPLC helped me immensely during the experiments. I express my obligations to *Dr. C. V. S. Brahmmananda Rao* for his valuable suggestions during preparation of manuscript. I would like to acknowledge my colleagues *Dr. P. Manikandan* and *Mr. V.V. Trinadh,* whose helps were invaluable for completing the experiments. My acknowledgements deservedly find the name *Shri. R Balasubramanian* and *Dr. R. Viswanathan*, whose deep knowledge in mass spectrometry enriched me during my initial days. I would like to express gratitude to *Dr. M. Joseph* for his fruitful suggestions and wholehearted cooperation. My overwhelming gratitude to *Mrs. S. Nalini, Mrs. R. Sajimol* and *Ms. B. Suhasini* for their profound support and continuous inspiration. I would like to thank *Dr. D. Ponraju* for his valuable suggestions during doctoral committee meeting. I owe my sincere thank to *Dr. K. Sankaran* for his critical comments and suggestion during correction of the manuscript. A special thanks to all my colleagues of MC&MFCG, IGCAR, in particular to *Dr. N. Sivakumar*, *Mr. Ujjwal Kumar Maity, Mrs. S. Jayalakshmi, Dr. Soumen Das* and *Dr. G. Gopakumar* for their help in some way or the other during the course of my work. I would like to thanks *Mrs. K. Revathy, Mrs. M. Mythili, Mr. Rahul Trikha* and *Mr. Sourabh Agarwal* for their support in the form

of technical and non technical discussions. I would like to thank my batch mates *Satendra, Binoy, Siva Kumar, Ashok Kumar* for sharing their valuable thoughts during lunch hours. I would like to mention some of my close friends *Ganesh, Naresh, Lucky, Pradeep* who always stood with me when ever required and their help was phenomenal.

I express my sincere gratitude from my heart to my wife *Priyanka* and daughter *Nandini* for their unconditional support, care and affection. My words are not enough to express my gratitude to my *parents*, whose blessings made my path less cumbersome. Least but not last, I would like to honour my *teachers*, whose moral lesion and trainings are inherent part of my life.

Finally, I would like to acknowledge the Director, IGCAR and administrative authorities of IGCAR, Kalpakkam for giving me permission and all the facilities to do the work.

Suranjan Bera
SURANJAN BERA

CONTENTS

1AA High Performance Liquid Chromatography (HPLC)

1AB Alpha spectrometry

CHAPTER 1B Knudsen Effusion Mass Spectrometry (KEMS)

CHAPTER 2 **Burn-Up Measurements on Dissolver Solution of Mixed Oxide Fuel Using HPLC-Mass Spectrometric Method**

CHAPTER 3 **Use of Molybdenum and Lanthanum as alternate burn-up monitors**

CHAPTER 3A **Molybdenum as alternate burn-up monitor**

CHAPTER 3B **Lanthanum as alternate burn-up monitor**

CHAPTER 4 **Other TIMS studies on materials of relevance to nuclear fuel cycle**

CHAPTER 4A **Improved magnesium loading method to employ MAGnesium Tracer Technique for the Accountability of Plutonium (MAGTRAP)**

CHAPTER 4B **IDMS Studies on Sodalite - a Candidate Material for Nuclear waste Immobilisation**

CHAPTER 4C **Gadolinium enrichment studies by using HPLC and TIMS**

CHAPTER 5 **Knudsen effusion mass spectrometric studies on some of the systems relevant to fuel, structural materials and reprocessing**

CHAPTER 5A **Knudsen effusion mass spectrometric studies on U-Al system: Thermodynamic properties over (UAl_2+UAl_3) biphasic region**

CHAPTER 5B **Knudsen Effusion Mass Spectrometric studies over (USn_3+U_3Sn_7) two-phase region of U-Sn System**

CHAPTER 5C **Thermodynamic properties over ($GdAl_3$+$GdAl_2$) of Gd-Al system: A High temperature mass spectrometric study**

SYNOPSIS

1. Introduction

Energy plays a vital role in the country's development and per capita consumption of energy is one of the yard stick. The flow of energy begins with a source (e.g. coal, uranium, petroleum, sun) and passes through several intermediate processes for conversion to different forms (electricity, diesel oil, methane) and finally utilised by consuming devices (e.g. furnace, motor etc). The world is strongly dependent on finite resources of fossil fuels. As demand of energy increases and supply becomes scarce, the problem becomes more acute, with severe economic and social consequences. Nuclear power is a robust facilitator of energy security in countries with inadequate domestic fossil and renewable energy resources, and also a way to deliver energy free from carbon footprint and with negligible impact on the Global warming. In India nuclear power is the fifth-largest source of electricity after those obtained from coal, gas, hydroelectricity and wind power. India has twenty two commercial power reactors which are operating and seven more are under construction [1]. India has planned for a rapid increase in nuclear power capacity from the present installed capacity of 6780 MWe to 20,000 MWe by 2020, and 63,000 MWe by 2032 [2]. India has limited reserves of uranium whereas thorium is abundantly available. However, the production of ^{239}Pu and ^{233}U fissile nuclides in breeder reactors overcomes this limitation. Keeping this in view, India has a three stage nuclear power program linking the fuel cycles of Pressurised Heavy Water Reactors (PHWRs), Fast Breeder Reactors (FBRs) and thorium based FBRs and Advanced Heavy Water Reactors (AHWR) [3,4]. Accordingly, India has embraced a closed fuel cycle to effectively utilise limited uranium reserves and abundant thorium resources [5]. The nuclear fuel cycle, is the progression of nuclear fuel through a series of differing stages. It consists of steps in the front end, which include mining, conversion, enrichment (if required), deconversion, fabrication of the fuel, irradiation in the reactor and steps in the back end, which are necessary to safely contain, manage, and either reprocess or dispose the spent nuclear fuel. The fuel discharged from nuclear reactors is referred to as 'spent fuel' which contains fission fragments and transuranic actinides produced by the absorption of neutrons in addition to the un-used fuel [6]. If spent fuel is not reprocessed, the fuel cycle is referred to as an open fuel cycle (or a once-through fuel cycle); if the spent fuel is reprocessed, it is referred to as a closed fuel cycle. The present thesis deals with use of mass spectrometric methods to characterise the nuclear materials at different stages of fuel cycle.

2. Scope of the present study

Mass spectrometer plays an important role in addressing different aspects of characterisation of nuclear materials at various stages. The works carried out in this thesis include determination of both analytical and thermo-chemical properties of materials relevance to nuclear technology. The mass spectrometric techniques used are (i) Thermal Ionisation Mass Spectrometry (TIMS), (ii) Knudsen Effusion Mass Spectrometer (KEMS). TIMS is a mass spectrometric technique in which, determination of isotopic ratios are carried out by vaporising and ionising an element of interest loaded on a surface of a metallic filament strip using resistive heating. TIMS is well known for its accurate and precise measurement of isotopic ratio and is considered as a gold standard for nuclear material accounting (NUMAC). Accurate and precise determination of isotopic ratios especially for elements like Li, B, Nd, Gd, U and Pu are of vital importance in various stage of nuclear fuel cycle. Burn-up (in atom %) is defined as the number of fissions per hundred heavy nuclides initially present in the fuel or the integrated energy released by fission of heavy nuclides initially present in the fuel (MWd/t). Burn-up is a measure of utilisation of important fissile materials in the nuclear reactor. One of the well established methods for the determination of burn-up is by fission product monitor method, in which, a suitable fission product monitor/isotope is quantified and its concentration is correlated with residual heavy element contents (uranium and plutonium) for atom % burn-up. For burn-up determination, although neodymium is commonly used as fission product monitor for thermal reactor fuels, it is important to find an alternate fission product monitor which serve not only for thermal reactor but also for fast reactor fuels with different fuel composition.

Determination of thermo-chemical properties like vapour pressure, enthalpy and Gibbs energy of a chemical reaction is of important to understand the vapour behavior, thermodynamic stabilities of the nuclear materials. KEMS is a powerful tool for the determination of the thermodynamic properties of various substances. During controlled nuclear reaction, a host of fission products are formed inside the reactor. The thermo-chemical data on compounds or alloys formed due to interaction of fission products with other fission products, fuel and clad are of important to understand the behavior of these materials at high temperature [7, 8, 9, 10, 11]. Mass spectrometry coupled with Knudsen effusion, commonly known as Knudsen Effusion Mass Spectrometry (KEMS), is a powerful tool for the determination of vapour pressure on a wide dynamic range (~10 Pa to 10^{-5} Pa), and other thermodynamic properties like enthalpy and Gibbs energy of reaction and formation. This technique is useful especially for samples which are less volatile even at very high temperatures. Knudsen effusion mass spectrometry also known as high temperature mass spectrometry is a powerful tool for the determination of vapour pressures and other thermodynamics properties. In this method the sample is taken inside a small cup with a lid containing a small orifice of negligible thickness at the top. This cell is called as Knudsen cell. The vapour which is in thermodynamic equilibrium with the condensed phase effuses through the small hole to form a molecular beam. The vapour is ionised by a suitable ionisation source and the ions produced are mass anlaysed and detected by a suitable detector. These studies are essential to understand the interaction, behaviour of nuclear materials at high temperatures under normal and transient conditions.

3. Structure of the thesis

The thesis titled "**Mass Spectrometric Studies on Some Materials of Relevance to Nuclear Technology**" is divided into seven chapters. A brief description of the individual chapters is given below.

Chapter 1: Introduction

The scope and the importance of nuclear energy in the Indian context are discussed in detail. The different stages of nuclear fuel cycle in a reactor operation and role of mass spectrometry at various stages are out-lined in this chapter. As present study deals with Thermal Ionisation Mass Spectrometric (TIMS) and Knudsen Effusion Mass Spectrometric (KEMS) methods, the basic principles of these techniques are given in chapter 1A and 1B respectively. This subchapter (1A) further covers a detailed study on the applications of TIMS in nuclear industry and concludes with description on scope of the work. High Performance Liquid Chromatography (HPLC) technique is used for effective and rapid separation of elements of interest from the mixtures and hence the principle of this technique is also explained in this section. In subchapter 1B, the experimental methods, instrumentation and application of KEMS to generate the data such as vapour pressure, Gibbs energy and enthalpy of formation are discussed in detail.

Chapter 2: Burn-Up Measurements on Dissolver Solution of Mixed Oxide Fuel Using HPLC-Mass Spectrometric Method

This chapter describes the importance of burn-up determination in a nuclear reactor and different methods available for its determination. In the present work, the atom percent fission is determined using fission product monitor method. The fuel, U-Pu mixed oxide (MOX) of composition $(U_{0.79}\ Pu_{0.21})O_2$ with uranium having an enrichment of 53.5% ^{233}U was irradiated in Fast Breeder Test Reactor (FBTR) for a peak burn-up of ~110 GWd/t, was used for the study. The dissolver solution of irradiated MOX fuel was passed through the HPLC column for rapid separation of lanthanides and actinides of interest from the mixture of fission products. Lanthanide fission products (La to Eu) were separated from each other using dynamic ion-exchange chromatographic technique whereas actinides (uranium and plutonium) were separated from each other using reversed phase chromatographic technique. The pure fractions of neodymium, uranium and plutonium obtained after HPLC separation, were subjected to TIMS analysis. The concentration of individual elements was determined by using HPLC and TIMS techniques. From these data, atom percent fission (burn-up) was determined. In the TIMS method, isotopic ratios of lanthanides and actinides were first obtained and these ratios were further used to derive concentration using well established IDMS method. The atom % burn-up deduced from the concentrations of U, Pu and Nd was 10.8 (elemental Nd as monitor), 10.9

(^{148}Nd as monitor) and 10.9 ($^{(145+146)}$ Nd as monitors). The burn-up data obtained using different fission product monitors from HPLC method, were also compared with well established neodymium monitor.

Chapter 3: Use of Molybdenum and Lanthanum as alternate burn-up monitors

This chapter focuses on establishing alternate fission product monitors for neodymium which is used conventionally for thermal reactor. Accordingly methods have been developed for establishing molybdenum and lanthanum as burn-up monitors. This chapter is divided into two subchapters based on the selection of different fission product monitor for burn-up determination. The chapter 3A, explains briefly about the possibility of using molybdenum as alternate burn-up monitor. It covers in detail the literature survey on various separation methods employed to obtain pure fraction of molybdenum from zirconium and ruthenium mixtures and on various sample loading methods employed in TIMS. The dissolver solution collected from Pressurised Heavy Water Reactor (PHWR) spent fuel was used for these experiments. Reverse phase chromatography method was developed to separate molybdenum from dissolver solution using 0.1 M mandelic acid as mobile phase. The HPLC technique was selected for this work because of it efficiency and rapid separation of molybdenum from other fission product elements to reduce the radiation dose. For TIMS analysis, a sample loading method was developed, where mixture of solution containing molybdenum and ascorbic acid in 4 M HCl was loaded onto an out-gassed rhenium filament followed by deposition of a layer of silicic acid above this mixture. This sample loading method helps in providing stable and intense Mo^+ ion beam formation. The concentrations of molybdenum, neodymium, uranium and plutonium were derived using IDMS method. From this, burn-up was computed using total elemental Mo as well as ^{100}Mo isotope as fission product monitor. The burn-up values were compared with the data obtained using ASTM standard, Nd-148 method. The fractional fission contribution from ^{235}U and ^{239}Pu was computed using isotopic ratio of ^{97}Mo / ^{95}Mo. The atom % burn-up determined from concentrations of U, Pu and Mo was found to be 0.79 (^{100}Mo as fission monitor), 0.80 (elemental Mo as monitor). In chapter 3B, work related to considering lanthanum as alternate fission product monitor for burn-up determination is described. This includes literature survey on lanthanum analysis using TIMS. The dissolver solution obtained from PHWR spent fuel was used for these experiments. The HPLC procedures followed for separation of lanthanum from PHWR dissolver solution is explained briefly in this chapter. Dynamic ion exchange chromatography technique was employed for the separation of lanthanum as well as neodymium from dissolver solution. A novel sample loading method has been developed for lanthanum analysis using TIMS, in which a mixture of graphite + H_3BO_3 + silica gel was employed to obtain enhanced and steady ion beam formation of LaO^+ instead of La^+ ion. For accurate and precise determination of La, Nd, U and Pu concentrations in the dissolver solution, IDMS method was employed. The burn-up data obtained using La as fission product monitor was compared with Nd-148 monitor. The atom % burn-up determined from concentrations of U, Pu, Nd and La was found to be 0.82 (^{148}Nd as fission monitor), 0.80 (elemental Nd as monitor) and 0.81 (^{139}La as fission monitor). The present study is the first investigation on lanthanum as fission product monitor for computing burn-up using TIMS.

Chapter 4: TIMS studies on materials of relevance to nuclear fuel cycle.

This chapter explains about some of the TIMS studies relevance to nuclear industry. It contains three subchapters.

Chapter 4A: Improved magnesium loading method to employ MAGnesium TRacer technique for the Accountability of Plutonium (MAGTRAP)

Nuclear materials accounting in reprocessing input tank is essential to have efficient and economic operation, to prevent proliferation of nuclear weapons and to provide assurance that all the materials are present in the correct quantities. The "tracer technique" is based on the addition of a known amount of a specific element (tracer) to the hot solution and then measuring the concentration of tracer in an aliquot of the solution drawn from the tank after homogenisation. The ratio between the concentrations of the tracer added and estimated after mixing, gives volume of solution in the reprocessing tank. The measurement of the tracer concentration in the drawn sample is performed by IDMS with the aid of a well calibrated spike. This subchapter covers, complete literature survey on various tracer techniques employed all over the world to determine volume of the reprocessing tanks for accountability of plutonium. In addition, various measurement techniques available in the literature for volume measurement in reprocessing tank are also described. In the present study, magnesium is selected as a tracer to determine the volume of the reprocessing tank. For this, a new sample loading method using tantalum activator was developed for stable and accurate measurement of magnesium concentration in the storage tank. The sample loading method thus developed for magnesium isotopic ratio analysis was verified for its accuracy and precision using Standard Reference Material for magnesium (National Bureau Standards-980).

Chapter 4B: IDMS Studies on Sodalite - a Candidate Material for Nuclear waste Immobilisation

Nuclear waste management is one of the important aspects of nuclear fuel cycle from environmental and safety consideration point of view. Different forms of waste storage matrices are known to be applicable for different kinds of nuclear waste. Glass bonded sodalite (GBS) [$Na_8(AlSiO_4)_6Cl_2$], a glass-ceramic is a promising candidate for the immobilisation of the chloride waste resulting from pyro-metallurgical reprocessing of nuclear fuels. Characterisation of individual components in waste containing matrix is essential for the development of waste storage material, which is expected to undergo different physicochemical conditions during immobilisation process. In the present study the concentrations of individual components (Li and Nd) in GBS were determined by employing IDMS owing to its capability to ensure precise and accurate data for multi-element analysis in a matrix. For these experiments, lighter element lithium and heavier element neodymium were used to determine their concentration in a single sample without any chemical separation. The IDMS data on actual sodalite sample are presented in this subchapter.

Chapter 4C: Gadolinium enrichment studies by using HPLC followed by TIMS analysis

Gadolinium, one of the strong neutron absorbing element and has an important role in nuclear industry. In the reprocessing tanks, especially in plutonium rich fuels, enriched gadolinium which acts as neutron poison is added to prevent criticality. Currently natural gadolinium is used as a burnable poison in nuclear fuel but the use of gadolinium enriched with 155 and 157 isotopes would create more effective burnable poison. Hence the use of enriched gadolinium ($^{155,\ 157}Gd$) will reduce the gadolinium inventory and this provides a good economic incentive. This subchapter describe briefly about various techniques generally employed for enrichment of isotopes. In the present study, the HPLC technique was used to enrich gadolinium isotopes. Enrichment up to 1% for ^{157}Gd with respect to natural isotope was observed. The challenges and efforts involved in the enrichment experiments are discussed.

Chapter 5: Knudsen effusion mass spectrometric studies on some of the systems relevant to fuel, structural materials and reprocessing

This chapter deals with KEMS studies on some of the compounds which are of relevance to nuclear programme. This chapter is divided into three subchapters.

Chapter 5A: Knudsen effusion mass spectrometric studies on U-Al system: Thermodynamic properties over (UAl_2+UAl_3) biphasic region

Thermodynamic properties of U-Al alloys are of interest in nuclear technology since these alloys are used as fuel in some research reactors [12]. Thermodynamic properties of U-Al phases are essential to understand their behaviour at high temperature under normal and in transient conditions. High temperature mass spectrometric study was carried out on (UAl_2+UAl_3) biphasic region using the KEMS facility. The vaporisation studies were performed on the compositions 28 and 30 at.% U and in the temperature range 1115-1253 K. The vaporisation reaction occurs incongruently and Al(g) was found to be the neutral gaseous species in the equilibrium vapour. Partial pressure-temperature relation was derived and is given as $\log(p_{Al}/Pa) = (-18215 \pm 157)/T + (12.12 \pm 0.13)$. From the partial pressures, the enthalpy of reaction $UAl_3(s) = UAl_2(s) + Al(g)$ at 298.15 K was deduced by applying the second and third law methods. Subsequently, enthalpy and Gibbs energy of formation of UAl_3 were deduced as $\Delta_f H^{\circ}_{298.15} = -112.1 \pm 12.8$ kJ mol^{-1} and

$\Delta_f G^\circ_T$ (±3.4) = −158.8 + 0.0591 T (kJ mol^{-1}). The vaporisation studies on this system are being reported for the first time.

Chapter 5B: Knudsen Effusion Mass Spectrometric studies over (USn_3+U_3Sn_7) two-phase region of U-Sn System

Intermetallic compounds of uranium and plutonium with tin (fission yield is 0.3% in fast reactors) and noble metal fission products have been reported to exist in irradiated mixed oxide fuel [13]. Post irradiation examination of the defective mixed oxide fuel pins has revealed the presence of (U, Pu)Sn$(Rh, Pd)_2$ [13]. Further, the actinide-tin alloys are of interest from the point of view of molten tin process [14], an alternate method to pyro reprocess of the spent oxide fuel. In this process, the spent oxide fuel is dissolved in the molten tin bath in a graphite crucible maintained at 1900 K. The solution consisting of actinides and the fission products is treated with nitrogen and the nitrides of actinides get precipitated out while the fission products remain in the solution. In the next step, the molten bath is cooled to 700 - 900 K to precipitate any residual actinide left over in the solution. Hence, it is useful to derive thermodynamic data on U-Sn system to assess the thermodynamic stabilities of different U-Sn intermetallic compounds. In this subchapter, vaporisation studies over (USn_3+U_3Sn_7) “two-phase” field were carried out by employing KEMS in the temperature range of 1050-1226 K. Sn(g) was the species observed in the mass spectrum of the equilibrium vapour phase over the samples (71.5 at.% Sn and 73.0 at.% Sn). The partial pressure of Sn(g) was measured as a function of temperature over (USn_3+U_3Sn_7) “two-phase” field and the p-T relation was derived as $\log(p_{Sn}/Pa) = (-14580 \pm 91)/T + (8.82 \pm 0.08)$ (1050-1226 K). The vaporisation reaction $3USn_3(s) = U_3Sn_7(s) + 2Sn(g)$ was evaluated by second law method. The Gibbs energy of formation of USn_3(s) was derived as $\Delta_f G^\circ_{T,USn_3(s)}$ (±1.8) = $-173.4 + 0.055$ T (K) (kJ mol^{-1}) (1050-1226 K). The mass spectrometric studies on this system have been carried out for the first time.

Chapter 5C: Thermodynamic properties over ($GdAl_3$+$GdAl_2$) of Gd-Al system: A High temperature mass spectrometric study

Pyrochemical reprocessing is envisaged as an alternative to the well established aqueous reprocessing to treat metallic fuels. This process employs molten chloride/ fluoride salts of various metals such as Cd, Bi, Zn, Sn, Ga and Al, which act as solvent for effecting the mutual separation of actinides and lanthanides. It had been reported in the literature that among the metals studied, Al shows superior selectivity for actinides over lanthanides [15]. Among the lanthanides, gadolinium is one of the fission products present in nuclear spent fuel. Hence thermodynamic properties of Gd-Al system are of interest to pyrochemical reprocessing. In the present study, the high temperature mass spectrometric study was carried out on ($GdAl_2$+$GdAl_3$) two phase region using the KEMS technique. In the case of ($GdAl_2$+UAl_3) two phase region, the vaporisation studies were performed on the compositions 70 and 72 at.% Al in the temperature range 1131-1258 K. The vaporisation reaction occurs incongruently and Al(g) was found to be the neutral gaseous species in the equilibrium vapour. Partial pressure-temperature relation was derived and is given as $\log(p_{Al}/Pa) = (-18743 \pm 213)/T + (12.61 \pm 0.18)$. From the partial pressures, the enthalpy of reaction $GdAl_3$(s) = $GdAl_2$(s) + Al(g) at 298.15 K was deduced by applying the second and third law methods. Subsequently, enthalpy and Gibbs energy of formation of $GdAl_2$ were deduced as $\Delta_f H^\circ_{298.15} = -148.7 \pm 17.1$ (kJ mol^{-1}) and

$\Delta_f G^\circ_T$ = (−179.2 ± 4.4) + (0.047 ± 0.004) T (kJ mol^{-1}). The vaporisation studies on this system are being reported for the first time.

Chapter 6: Conclusions

This chapter gives a summary of studies described in this thesis, which explains application of mass spectrometer at different stages of nuclear fuel cycle. Rapid HPLC and standard TIMS techniques were employed to determine burn-up of MOX dissolver solution. A quick and effective separation technique using 1.8 µm particle HPLC column was demonstrated for the separation of fission products, Mo, La, Nd and actinides (U and Pu) from PHWR dissolver solution. New sample loading methods were developed for molybdenum and lanthanum analysis and they provide stable and enhanced ion intensity during TIMS analysis. The burn-up was determined for PHWR dissolver solution using different isotopes of fission product monitors (molybdenum and lanthanum) and the data were in good agreement with established ASTM standard Nd-148 method. A new sample loading method using tantalum activator was also developed for accurate and precise measurement of magnesium in reprocessing tank using TIMS instrument. The isotopic ratio and concentration of lighter (lithium) and heaver (neodymium) elements were determined simultaneously, without any chemical separation using TIMS. Experimental conditions required for effective enrichment of gadolinium isotopes were examined using quick HPLC separation followed by TIMS analysis. High temperature mass spectrometry was employed to generate vapour pressure data on U-Al, Gd-Al, U-Sn system. From partial pressure data, enthalpy and Gibbs energy of formation of UAl_3, $GdAl_2$ and USn_3 were deduced respectively for U-Al, Gd-Al, U-Sn systems.

Chapter 7: Future work

This chapter describes the perspectives of future scope from the studies described in this thesis. Further experiments on HPLC separation and TIMS analysis will provide enhanced enrichment of gadolinium isotopes and insight into the understanding of the process involved. Absence of literature data on enthalpy increment of Gd-Al and U-Sn system demands further studies on these systems. These data can be determined by employing calorimetric method.

References

[1] https://www.iaea.org/PRIS/CountryStatistics.CountryDetails.aspx?current=IN.

[2] "India eyeing 64,000 MW nuclear power capacity by 2032: NPCIL". The Economic Times, 11th October (2010).

[3] http://www.dae.nic.in/?q=node/212.

[4] Venkataraman, Ganesan, Bhabha and His Magnificent Obsessions, Universities Press (India) Ltd., ISBN 81- 7371-007-4 (1994).

[5] H. J. Bhabha, Proc. Internatl. Conf. on the Peaceful uses of Atomic Energy, 1, Geneva (1955) 103.

[6] 'Standard Test Method for atom percent fission in Uranium Plutonium Fuel (Neodymium-148 method)', Annual of ASTM Standards, E321 (1996) 96.

[7] D. Darwin Albert Raj, Ph.D. Thesis (University of Madras) (2008).

[8] A. Matraszek, M. Miller, L. Singheiser, K. Hilpert, J. Euro. Ceram. Soc. 24 (2004) 2649.

[9] P. Chiotti, J. A. Kateley, J. Nucl. Mater. 32 (1969) 135.

[10] C. B. Alcock, V. P. Itkin, M. K. Horrigan, Can., Metall. Quart. 23 (1984) 309.

[11] T. S. Lakshmi Narasimhan, R. Viswanathan, Knudsen effusion mass spectrometric study of some congruently and incongruently vaporising systems, Workshop on Knudsen Effusion Mass Spectrometry (KEMS) 23th - 25th April (2012), Juelich. Proceedings published in ECS Transactions. 46, 1 (2013) 229.

[12] S. Usha, R. R. Ramanarayanan, P. Mohanakrishnan, R. P. Kapoor, Nucl. Engg. Design 236 (2006) 872.

[13] H. Kleykamp, S. G. Kang, J. Nucl. Mater. 230 (1996) 280.

[14] O. H. Krikorian, Review of the Thermodynamic and Kinetic Data for the Molten-Tin Process, Lawrence Livermore Laboratory, Report No. UCID-18262, 6th August (1979).

[15] O. Conocar, N. Douyere, J. Lacquement, J. Nucl. Mater. 344 (2005) 136.

LIST OF FIGURES

LIST OF TABLES

CHAPTER 1

==

Introduction

Energy growth is directly linked to well-being and prosperity across the globe. Meeting the growing demand for energy in a safe and environmentally responsible manner is a key challenge. The world demands energy and in increasing quantities to build a better quality of life, for social progress and to support economic development. For developing nations, the requirement of reliable and affordable energy is more fundamental to support industry, transportation, increased trade and modern agriculture. Today most of the energy the world consumes comes from hydrocarbons, with crude oil being the source of fuel for transport machineries and coal being the basic fuel material for thermal energy plants. As demand for energy increases due to rapid growth in population, supply would become scarce, problems will become more acute, with potential severe economic, social consequences and ever raising concerns about climate changes due to green house effect. Nuclear power, like solar, hydro and wind energy can generate electricity with no carbon dioxide or other greenhouse gas emissions. The critical difference is that Nuclear Energy is the only option to produce vastly expanded supplies of clean electricity on a global scale.

Energy is produced in a nuclear reactor by fission. Nuclear reactor is a system in which controlled nuclear chain reaction (fission) is maintained for the production of energy. Fission is a nuclear reaction where a heavy atom (mass $\geq$ 225 Da) is bombarded with a neutron and the heavy atom splits into mainly two atoms (fission products). Fission, apart from generating fission products, generates more than one neutron and also releases large amount of thermal energy (~200 MeV of energy per fission). Such fission reactions are possible in heavy atoms such as ^{235}U, ^{239}Pu and ^{233}U, which are called fissile isotopes. Nuclear reactors can be classified into many types depending on neutron energies, fuel material, types of moderator, design, fuel state etc. But based on the energy of the neutrons used for fission, reactors are classified as thermal reactors, where the neutron energy is ~ 0.025 eV; and fast reactors in which neutrons possess the energy in the range of 500-600 keV. A nuclear reactor comprises mainly of i) reactor core, consisting of fuel (which undergo fission to produce energy), clad material (which encapsulate fuel material), coolant (which act as medium to remove heat from source and transfer to sink) and moderator (which slows down the kinetic energy of neutrons) and control rods (which helps in controlling and maintaining of nuclear chain reaction), ii) steam generator (which convert thermal energy to mechanical energy) and turbine (which convert mechanical energy to electrical energy).

India pursues a three stage nuclear program as visioned by Dr. H. J. Bhabha, the pioneer of Indian atomic energy program [1]. Accordingly, India has adopted a closed fuel cycle to effectively utilise limited uranium reserves and abundant thorium resources. In the three stage nuclear program, the first stage reactors uses natural uranium dioxide as the fuel (in Pressurised Heavy Water Reactor) or uranium dioxide enriched in U-235 to the extent of ~2-3% (in Pressurised Water Reactor and Boiling Water Reactors). In addition to the generation of electricity, U-238 is transmuted into Pu-239, which is a man made and highly useful fissile element. The second stage reactor employs ^{239}Pu based systems (uranium-plutonium mixed oxide or carbide or nitride or alloy with zirconium) as the fuel in the Fast Breeder Reactors (FBRs). ^{232}Thorium dioxide kept as a blanket (at inner periphery of reactor core), which upon capturing the escaping neutrons, transforms into ^{233}U, another man made fissile nucleus. The third stage reactor (Advanced Heavy Water Reactor) uses (^{233}U-Th) or (Pu-Th) mixed oxide as the fuel. Kalpakkam, India, is the only place in world, where all the three stages of nuclear reactors are present at one location viz., commercial thermal reactor (Madras Atomic Power plant), representing the first stage, Fast Breeder Test Reactor (FBTR), representing the second stage and the KAlpakkam MINI reactor (KAMINI) which comes under third stage of Indian nuclear programme. The Nuclear Fuel Cycle supporting the nuclear power programme for clean and safe production of electricity consists of 'front end' i.e. mining, fuel fabrication, irradiation in reactor and 'back end', i.e. fuel reprocessing and waste management. The fuel discharged from nuclear reactors after irradiation, known as spent fuel, contains fission products and transuranic actinides produced by the absorption of neutrons in addition to the un-used fuel. Since the spent fuel is reprocessed and utilised materials are recovered for reuse, the complete cycle is referred as closed nuclear fuel cycle.

A vast variety of Nuclear Analytical Techniques (NATs) (destructive and non-destructive) are used for characterisation and quantitative determination of various materials used in the nuclear industry. Among these, mass spectrometer plays an important role in addressing different aspects of characterisation of nuclear materials at various stages.

1.1 Mass Spectrometry

Mass spectrometry is a highly powerful and informative analytical technique for assaying a material on the basis of mass to charge ratio of the analyte ions [2-5]. It is useful to identify the unknown compounds by determining their molecular weights and their qualitative and quantitative determination in trace and ultra trace levels. It is also used as a tool to derive basic thermodynamic information on materials of interest. It is used in characterisation of both organic compounds and inorganic elements in different matrices. Compared with other analytical techniques like radio-active emission counting, spectroscopy etc., mass spectrometry is a more precise and sensitive technique [6].

1.2 Applications of mass spectrometry in nuclear industry

The technique provides highly valuable information in various fields like nuclear technology, geochronology, chemistry, biology, planetary science, pharmaceutical industry, petrochemical industry, material science, environmental science, forensic science, archeology, cosmochemistry etc. The role of mass spectrometry in nuclear technology was demonstrated in mid 20th century by A. O. C. Nier and colleagues by showing that ^{235}U was the fissionable component of natural uranium [7]. This breakthrough was a decisive step in the success of the Manhattan Project, which involved the development of isotope separation and the construction of a nuclear reactor. These developments led to the necessity of measuring the isotopic composition of uranium and other related elements on a routine basis. Some of the contributions of mass spectrometry towards nuclear science are as follows,

i. Determination of isotopic abundance
ii. Determination of burn-up and nuclear material accounting
iii. Detection of ultra-trace quantities of elements
iv. Predicting chronology of events in tracing the nucleosynthetic processes.
v. Determination of neutron capture cross section for a nuclear reaction
vi. Determination of thermodynamic properties of nuclear materials
vii. Discovery of the Oklo natural reactor
viii. Identification of radioactive nuclides and their stable daughter products
ix. Determination of half-lives and the age of a nuclide

x. Monitoring nuclear materials inventory (uranium, plutonium and fission products)
xi. Determination of fission yield
xii. Determination of isotopic enrichment level of an element in enrichment plants.
xiii. Understanding the transfer/migration mechanisms of radio chemicals in environment
xiv. Finding radioactive contamination due to accidental fallout from nuclear reprocessing plants and nuclear power plants
xv. Controlling on illegal trafficking and proliferation of nuclear materials.

1.3 Components of a mass spectrometer

Most of the mass spectrometer consists of five principal components: 1) a sample inlet system, 2) ion source, 3) mass analyser, 4) detector and 5) data acquisition and vacuum systems [8]. Samples are introduced through the inlet either manually or through a suitable separations or injection system (solid/liquid/gas with or without passing through gas chromatography, ion chromatography or High Performance Liquid Chromatography). Sample is ionised within the source chamber by suitable means, the gaseous ions thus formed in source are passed through analyser to facilitate separation/filtration based on mass to charge ratio (m/z), and finally detected using efficient detectors under high vacuum. Present day mass spectrometers use computer interfaces and specialised software to acquire and interpret data. A brief description of important components is given below.

1.3.1 Ion Source

The main objective of ion source is to produce gaseous charged species with high efficiency. The gaseous charged ions can be generated either by removing (positive charged ion) or sometimes adding a single electron (negative charged ion) to atom or molecule to produce a singly charged ion. Ions can also be produced by addition of proton to a molecule. Generally, ion production is accomplished in a variety of ways.

The commonly used ion sources are i) Thermal ionisation or Surface ionisation source, ii) Electron ionisation or Electron bombardment source, iii) Spark source, iv) Glow discharge source, v) Inductively coupled plasma source, vi) Secondary ion source etc.

1.3.2 Analyser

In the analyser region, ions produced in the source chamber are accelerated and mass separated into different ion beams according to their mass to charge ratios (m/z) using different physical principles. Commonly used analysers are i) Magnetic sector, ii) Quadruple, iii) Time of flight, iv) Ion cyclotron resonance.

1.3.3 Detector

The separated ions are detected by a variety of sensors. The commonly used detectors are i) Faraday cup, ii) Secondary Electron Multiplier (SEM), iii) Daly, iv) Ion-sensitive photographic plates, v) Channeltron etc. For detection of trace amount of samples and low abundance isotopes, the ion current produced will be in the range of 10^{-14} to 10^{-16} A, detectors with electron multiplication are used.

1.4 Types of mass spectrometers

Based on specific application, required mass spectrometer is employed. Some of the mass spectrometers developed for specific application are Thermal Ionisation Mass Spectrometer (TIMS), Multiple ion Collectors ICP-MS (MC-ICP-MS), Fourier-Transform Ion Cyclotron Resonance MS (FTICR-MS), Knudsen effusion mass spectrometer (KEMS), Secondary Ion MS (SIMS), Glow Discharge MS (GDMS), Laser Ablation Inductively Coupled Plasma MS (LA-ICP-MS), Resonance Ionisation MS (RIMS), Accelerator MS (AMS) etc.

In the present work, two mass spectrometers, thermal ionisation mass spectrometer and Knudsen effusion mass spectrometer have been extensively used for the study of nuclear materials.

CHAPTER 1A

Thermal Ionisation Mass Spectrometry (TIMS)

This chapter describes the methodology employed for measurement of isotopic ratios of an element using TIMS. The principles relating to IDMS and burn-up measurements techniques are explained in detail. The HPLC and alpha spectrometric techniques, which are used in the present work, are also described briefly.

1A.1 Introduction

In Thermal ionisation mass spectrometry (TIMS), determination of isotopic ratios are carried out by vaporising and ionising an element of interest loaded on a surface of a metallic ribbon using resistive heating, separation of charged ions by magnetic sector analyser and detection by Faraday cup/ Daly scintillation detector/ SEM. TIMS is a single element analysis technique. TIMS technique in combination with IDMS method provides data with (better than 0.1%) high precision and accuracy. It has played a key role in the isotopic analysis of elements that are particularly important in nuclear technology and geo-cosmology. The major components of TIMS are described below.

1A.2 Sample inlet

Sample introduction system comprises of coating/depositing a small quantity of pure fraction of sample on a suitable filament surface (tantalum, rhenium or tungsten ribbon) in a filament holder. Present TIMS instruments are accomplished by mounting twenty or more filament assemblies on the periphery of a circular magazine (barrel). An advantage of this multiple sample magazine is that while one sample is being analysed, the next sample in the selected sequence can be preheated to condition it.

1A.2.1 Sample preparation methods

A good sample preparation technique ensures reliability of a mass spectrometric analysis. Best possible sensitivity and precision are achieved by careful control of chemistry at this stage. The development of novel sample loading/deposition procedures provides stable and better ion signal even with small quantity of samples.

1A.2.2 Choice of filament material

Work function and melting point are the two necessary criteria to select a filament material for loading the sample. The other features of a good filament material are weldability and low vapour pressure. Of the pure metals, platinum was the first widely used filament material due to highest work function (5.32 eV) and its availability in ribbon form. But its relatively low melting point (1772 ^{0}C) led to the use of other materials such as W, Ta and Re. Rhenium is widely used in many applications, because of the attractive compromise that it provides between work function and melting point.

1A.2.3 Filament configuration

Before loading the sample, filaments are welded onto the metal posts attached to the base through a ceramic insulator, in different configurations for achieving better sensitivity and focusing conditions. Single filament configuration is generally used for species with low volatility. In this configuration, vaporisation and ionisation take place at the same surface. However, for the species that are highly volatile but difficult to ionise, (in which case sample evaporates before the ionisation temperature is reached) multifilament configuration come in handy. The limitation of a single filament can be avoided by separating the evaporation and ionisation processes using double/ triple filaments assemblies. In this arrangement, the sample evaporates from one or two filaments (sample/ vaporisation filament) at a relatively low temperature (thus prolonging the sample utility) and ionisation takes place using another filament at a higher temperature giving rise to good ionisation efficiency. In a triple filament source, two sample filaments are welded sideways symmetrically with respect to the ionisation filament positioned at centre. A schematic of triple filament assembly is shown in Figure 1A.1.

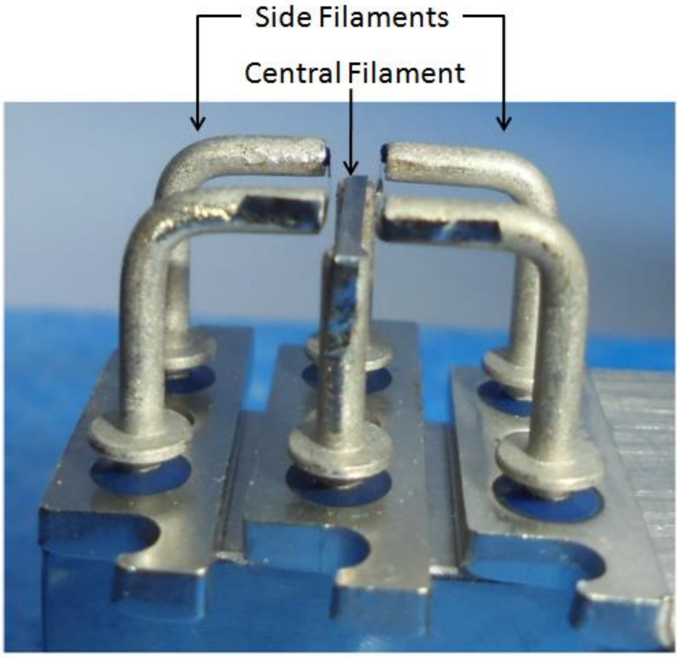

Fig. 1A.1 Photograph of triple filament assembly.

1A.2.4 Sample preparation

Samples for TIMS analysis should be available in the purest possible chemical form in order to ensure good ion emission. The thermal energy provided by the hot filament should not be lost by way of evaporating or forming ions of contaminant species. Different procedures for complete dissolution, followed by pre concentration techniques like solvent extraction and or chromatographic techniques are adopted for individual elements [2].

1A.2.5 Loading techniques

Choice of proper loading technique is one of the prerequisites for obtaining a stable ion beam and the nature of chemical form of the species for analysis varies for different elements. Normally, a dilute solution in nitrate form is used for metallic samples. Some of the loading techniques commonly used for different elements are (i) electro deposition (ii) resin bead and (iii) silica gel technique. Elements having first ionisation energy (IE) more than 7 eV are loaded along with some additives/ activator for enhancing the ion emission. For element like boron (having IE of 8.3 eV), the sample is converted into easily volatile alkali metal borates for directly loading onto the filament.

1A.3 Ion production

Ion production on a hot filament is described by the Saha-Langmuir equation. This equation gives the degree of ionisation (the ratio of positive ions n^+ to neutral atoms, n_0 leaving the surface) as

$$\frac{n^+}{n_0} = \left(\frac{g^+}{g_0}\right) \cdot \left[\frac{(1-r^+)}{(1-r_0)}\right] \cdot exp^{\left(\frac{(W-IE)}{kT}\right)} \tag{1A.1}$$

where g^+ and g_0 are the statistical weights for an ion and neutral atom, r^+ & r_0 are the reflection coefficients of the positive and neutral particles at the surface, W is the work function of the filament (eV), IE is the ionisation energy of the element (eV), T is the temperature of the filament surface (K) and k is the Boltzmann constant (eV/K).

As can be seen the ionisation efficiency (n^+/N, where $N = n_0 + n^+$, with negligible n^-) depends on parameters like work function of filament material, ionisation energy of the analyte element and temperature of the filament. In the case of elements with low ionisation energy (IE < W), W-IE term in equation (1A.1) is positive, which implies that the ionisation efficiency increases with reduced temperature. In this case, single filament is sufficient for sample evaporation as well as ionisation. The filament is heated to a temperature just enough for the sufficient vaporisation of the sample to get the ions in gas phase.

In the case of elements with high IE (>W), the term W-IE becomes negative and hence the ionisation efficiency increases with the increase in temperature. In this case the sample is required to be heated at much higher temperature for high sensitivity that can lead to evaporation of the sample before sufficient ionisation takes place if single filament is used. Hence, the use of multiple filament assembly whereby double or triple filaments are employed to decouple the evaporation and ionisation processes. In such multifilament configuration, temperature of the filament coated with the sample can be adjusted for steady and sufficient evaporation of neutral species onto a nearby filament whose temperature can be independently adjusted for good ionisation efficiency.

As the ionisation efficiency is dependent on the work function of the filament, there are various techniques used for enhancing the work function for specific element with very high IE (> 7eV). To mention a few, graphite coating of the filament for enhancing ionisation of actinides, deposition of silica gel, phosphoric acidic/boric acid on the filament before sample loading for Pb, Fe, Cr, Cu, Cd etc. and resin bead technique to analyse nanograms of U and Pu samples.

Negative ion production on a hot metal surface is given by a modified form of Saha-Langmuir equation as follows:

$$\frac{n^-}{n_0} = \left(\frac{g^-}{g_0}\right) \cdot \left[\frac{(1-r^-)}{(1-r_0)}\right] \cdot exp^{\left(\frac{(EA-W)}{kT}\right)} \qquad (1A.2)$$

where EA denotes electron affinity of analyte element and other terms represents same meaning as in equation (1A.1). Efficiency of negative ion formation is high for elements with high electron affinity evaporating from a filament with low work function and are analysed by negative thermal ionisation mass spectrometry (NTIMS). Positive and negative thermal ionisation modes are applied based on the values of ionisation energy and electron affinity of the elements to be analysed.

1A.4 Ion collimation

Ions emitted from the filament surface must be quantitatively extracted, accelerated with homogeneous energy and focused into a fine beam with a very small divergence before mass separation and this is accomplished by ion collimator unit. The acceleration and focusing is done by stack of electrode plates with different geometry of slits and extraction voltages. A highly stable positive dc voltage of about 8000 to 10000 Volts is applied on the filaments, and successively lower voltage on the other plates with the last plate containing the final source slit at ground potential. Ions formed by thermal ionisation have very small energy spread (~0.2 eV), and accelerated to about 8 to 10 K Volt provides ion beam which is extremely homogeneous in energy.

1A.5 Magnetic sector analyser

Thermal ionisation mass spectrometers employ magnetic and quadrupole mass analysers either separately or in series. The combination of thermal ionisation with quadrupole analyser provides rapid peak switching, rapid mass scanning and fast switching between positive and negative ionisation. However, magnetic sector type mass analyser is more popular among TIMS especially for precise measurements of isotopic ratios.

For the best separation of masses, one must provide an ion beam as homogeneous in energy as possible. The applied magnetic field acts both as an optical lens and as a prism for the ions. It exhibits unique feature of passing ions (within given mass range) simultaneously thereby making provision for their simultaneous collection at different collectors of multicollector system which increases the precision of the given analysis. The system parameters like resolution, dispersion and magnification are decided by the geometry of the magnetic sector. A schematic of the TIMS instrument is presented in Figure 1A.2.

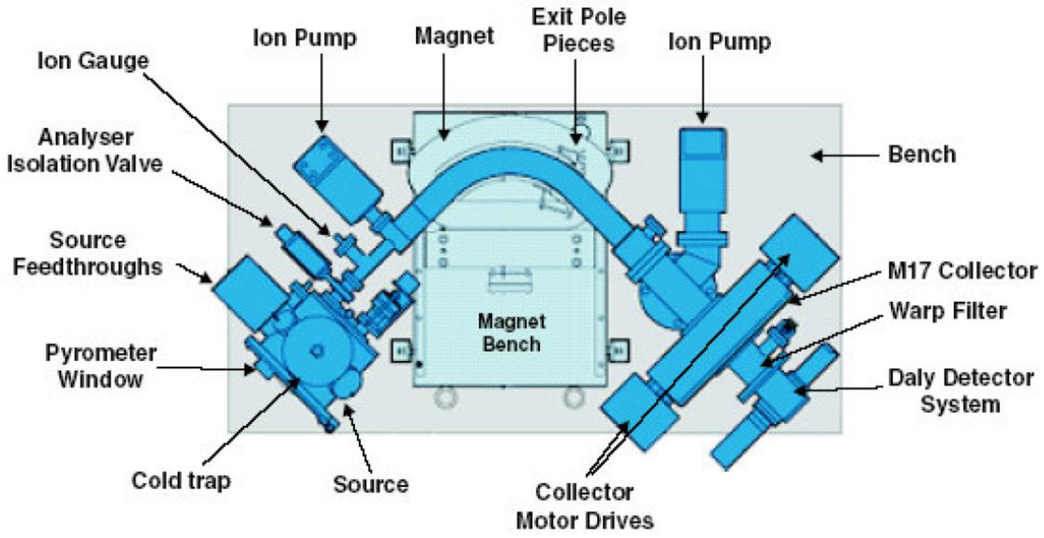

Fig. 1A.2 Schematic of TIMS instrument reproduced from IsotopX engineers manual.

1A.5.1 Mass analyser geometry

The present generation TIMS instruments are incorporated with modern sector instruments incorporating 60^o or 90^o analyser. The sector geometry creates focal points of the ion beam that are away from the magnet, which allows the use of ion detectors, such as electron multipliers, that would be away from the strong magnetic field of the analyser.

A significant advance in basic geometry in the form of extended or stigmatic geometry was made by including the effects of the fringing fields at the entrance and exit of the magnet. The use of the fringe fields by allowing the ion beam to enter and exit the magnet at an angle of 26.5^o with respect to the normal entry and exit to the magnet pole pieces, adds advantages like, two-dimensional focusing (axial and z-direction focusing), twice the mass separation for the same size of magnet, improved resolution without loss during transmission and hence sensitivity, and accommodation of multiple detectors due to relatively flattening of focal plane.

1A.6 Ion collection and detection

Different kinds of detectors are in use based on requirements. The desirable properties of a detector are: better multiplication efficiency, precise and accurate measure of the number of ions received, low time constant, long life without degradation, low cost, ease of maintenance, possibility of rejuvenation, minimum mass and energy discrimination. Some of the commonly used ion detectors for TIMS are: Faraday cup collector and Secondary Electron Multipliers (SEM).

The Faraday cup which is also referred as Faraday cage is well known for its simple design and accurate ion detection. Due to its simple construction, compact size, independency of ion detection irrespective of energy, mass and chemical nature of the ions, long life and highly reliable output, Faraday cups are the most preferred in TIMS instrument with multiple collector assembly. The poor sensitivity and long time constants, generally considered to be the demerits of this detector.

Secondary electron multiplier (SEM) detects the secondary electrons emitted upon striking of sample ion on detector surface (conversion dynode). The advantage of secondary electron multiplier is extremely high sensitivity and fast response. Secondary electron emission is a function of the velocity, mass, incident angle of striking ion, work function of dynode, and physical condition of the dynode surface. This will result in over estimation of the lighter mass relative to the heavier mass and this effect is known as mass discrimination effect. Another concern of the SEM comes from the fact that they lose efficiency over time. The problem of mass discrimination associated with electron multipliers can be solved in the following ways. i) a standard sample of known composition can be analysed and from the deviation from the expected value a correction factor per Dalton can be arrived at, ii) if a measurement can be done simultaneously with the SEM and a Faraday detector (latter does not suffer from mass discrimination), the correction factor can be calculated, iii) pulse counting devises if employed as an detector, mass discrimination errors can be avoided.

1A.7 Instrument control/Data handling

The modern TIMS instruments are focused on development with full automation without operator intervention to provide reliable data with effective utilisation of time.

1A.8 Concentration measurement using Isotope Dilution-Thermal Ionisation Mass Spectrometry (ID-TIMS)

1A.8.1 ID-TIMS Principle

Thermal ionisation mass spectrometer provides isotopic ratios of an analyte element. For quantification of analyte species in a given solution, Isotopic Dilution Mass Spectrometry (IDMS) method is employed using TIMS, which is commonly known as ID-TIMS [9, 10]. The important advantage of ID-TIMS is that the concentration determination depends only upon the change in isotopic ratio, and does not require quantitative recovery of the analyte during chemical separation and purification. ID-TIMS is termed as a definitive analytical methodology whose source of errors is known and is used as a reference method to calibrate other analytical methodologies. It is a highly accurate and precise method for concentration measurements. The method involves, addition of specific amount of a pre calibrated spike (whose isotopic composition and concentration are known) to a known quantity of sample (whose isotopic composition is known but concentration to be determined), homogeneous mixing of sample and spike, determination of isotopic composition of resultant mixture (spiked solution), which is directly related to the concentration of sample. The spike (also called as internal standard) contains analyte element in a different isotopic composition, preferably enriched with respect to isotopes which are present in lower abundance in sample. The pictorial presentation of IDMS method is shown below (Fig.1A.3).

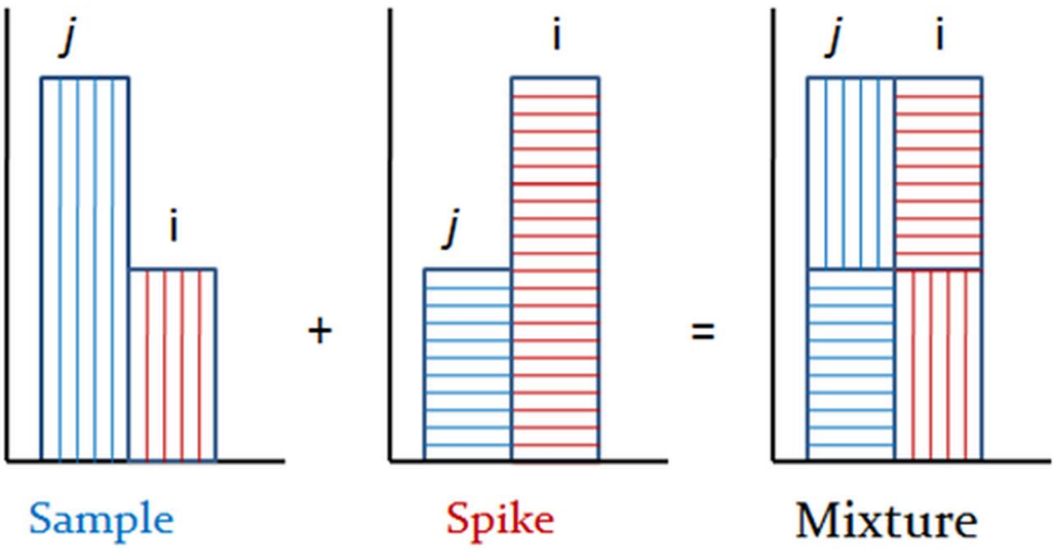

Fig. 1A.3 Pictorial presentation of sample-spike mixing in IDMS.

The IDMS equation which links isotopic ratios with quantity of element can be derived from the following equations

$$\textbf{Sample:}\qquad \boldsymbol{R}_{(j/i)S} = \left(\frac{N_j}{N_i}\right)_S \tag{1A.3}$$

$$\textbf{Spike:}\qquad \boldsymbol{R}_{(j/i)Sp} = \left(\frac{N_j}{N_i}\right)_{Sp} \tag{1A.4}$$

$$\textbf{Mixture:}\qquad \boldsymbol{R}_{(j/i)mix} = \left(\frac{N_j}{N_i}\right)_{mix} \tag{1A.5}$$

and concentration of the sample (C_s) is given as,

$$\boldsymbol{C_S} = \frac{C_{Sp} * W_{Sp}}{W_S} \times \left(\frac{R_{(j/i)Sp} - R_{(j/i)mix}}{R_{(j/i)mix} - R_{(j/i)S}} \times \frac{1}{R_{(j/i)Sp}} \right) \times \frac{<AF_{j,Sp}>}{<AF_{i,S}>} \times \frac{(AW)_S}{(AW)_{Sp}} \tag{1A.6}$$

where C_{Sp}: concentration of spike; W_{Sp}: weight of spike; W_S: weight of sample; $<AF_{i,S}>$, $<AF_{j,Sp}>$: atom fractions of isotopes *i* and *j* in sample and spike respectively; $(AW)_S$, $(AW)_{Sp}$: average atomic weights of sample and spike respectively and $R_{(j/i)S}$, $R_{(j/i)Sp}$ and $R_{(j/i)mix}$: ratio of isotopes *j* and *i* in sample , spike, and mixture solution.

All the isotopic ratio terms in equation (1A.6) can be obtained from TIMS analysis. From these isotopic ratio values, atom fraction and average atomic weights for an element are deduced.

IDMS methodology required certain criteria like:

A) Selection of suitable spike isotope

The criteria for selecting suitable spike are:

i) The spike isotope should be absent or least abundant in the given sample.
ii) Should not have any isobaric interference from the adjacent or other elements
iii) For radioactive isotopes, it should be long lived
iv) Easily available and should not be very expensive

v) It should preferably be in the same chemical form as the element in the sample for easy homogenisation or mixing.

B) Homogeneous mixing of sample and spike, if solid sample, must be chemically decomposed.

C) Optimised amount of spike should be added to sample so that the isotopic ratio of element in final mixture is near to one. This is required to minimise error in IDMS calculations.

1A.8.2 Sources of errors in IDMS

The sources of errors associated with an IDMS methodology are as follows:

1. Chemical errors: can be caused by incomplete decomposition of the sample on the filament, incomplete mixing with tracer in the solution
2. Isotopic fractionation during analysis.
3. Purity, stoichiometry and quantity of the standard (spike).
4. Isobaric interference.
5. Contamination from reagents, apparatus or wrong laboratory practice.
6. Blank correction
7. Selection of inappropriate spike isotope

The advantages of IDMS include precise and accurate analysis, non-quantitative isolation of the substance to be analysed, ideal internal standardisation, high sensitivity and low detection limits. However, the limitations of this method are, destructive nature, necessity of chemical preparation of sample, time consumption and use of expensive spikes.

In the present study, concentration of U, Pu, Nd, Mo, La and Li were derived by using ID-TIMS method. Isotopic dilution was carried out using ^{233}U, ^{239}Pu, ^{142}Nd (^{150}Nd for sodalite work (chapter 4B)), ^{94}Mo, ^{138}La, ^{6}Li spikes for samples containing U, Pu, Nd, Mo, La and Li, respectively. The spike solutions used for present work were calibrated in our laboratory by reverse IDMS (R-IDMS) method. In this method concentration of above spike solutions were determined using standard solutions. These standard solutions were characterised for their concentration using more than one technique like ICP-MS and ICP-OES etc.

1A.9 Burn-up determination of irradiated nuclear fuels

During nuclear chain reaction, neutrons interact with heavy elements (mass number ≥ 225 Da) to produce series of fragmented fission products along with release of energy. Burn-up determination on irradiated nuclear fuel is essential in establishing the amount of energy produced by the fuel and to measure net change in fissionable isotope content of the fuel [11]. Burn-up studies on dissolver solutions of nuclear reactor fuels helps in fuel management, quantification of transuranium elements, waste treatment etc. These experimental data are very useful to check and develop computer codes for the build-up and depletion of different heavy element isotopes. The burn-up is commonly expressed in units of atom percent fission or megawatt day/tonne (MWd/t) or gigawatt day/tonne (GWd/t). The atom percent burn-up is defined as number of fissions per hundred initial heavy element atoms (heavy elements includes fertile and fissile nuclides). Burn-up can be determined either by destructive or non destructive methods.

The nondestructive method for burn-up measurements is carried out by radiochemical technique using gamma spectrometry. It is based on the measurement of gamma activity of fission products, those having sufficient energy and ability to leave the irradiated fuel without appreciable attenuation.

Destructive methods available for burn-up determination are (i) heavy atoms difference method, (ii) Heavy elements isotopic ratio method and (iii) Fission product monitor method. The detail of destructive methods for burn-up determination is explained below.

1A.9.1 Heavy atoms difference method

In this method, burn-up is determined by measuring the total difference of heavy element atom contents in both un-irradiated and irradiated fuel specimens. This is also called as “atom percent depletion” method and is defined as net change in the number of atoms of fissionable heavy-element nuclide per hundred initial atoms of that nuclide. The advantages of this method include determination of burn-up using any standard chemical analysis method and does not require any fission yield or capture to cross section data for burn-up calculation. Limitations of this method are, it is applicable for relatively higher burn-up fuels i.e., 5 to 10 atom percent burn-up and requires information on initial inventory composition.

1A.9.2 Heavy elements isotopic ratio method

In this method, burn-up of spent fuel is determined by measuring the isotopic ratio of heavy elements (e.g., U and Pu) before and after irradiation of fuel specimen. This method is applicable generally for fuel with an appreciable burn-up. It needs additional information like composition of un-irradiated fuel and capture to fission cross section data for some isotopes.

1A.9.3 Fission products monitor method

In this method, the content of residual heavy elements (U and Pu) and that of a selected fission product element in irradiated fuel are determined and then using fission yield data of fission fragments, burn-up is calculated. The fission fragment element is called as fission product monitor. The estimation is carried out using radiochemical (if it is radioactive) or instrumental technique such as spectrophotometry, X-ray, mass spectrometry [12-16] and HPLC methods [17-19]. The atom percent fission in terms of fission product monitor can be expressed as

$$\text{Burn-up (atom \% fission)} = \frac{(A/Y)}{[H+(A/Y)]} \times 100 \qquad (1A.7)$$

where A is the numbers of atoms of fission product monitor, Y is the effective fractional fission yield for ‘A’ and H is the total number of residual heavy element atoms in the spent fuel. An ideal fission product monitor should satisfy the following criteria,

1. Should have low capture cross-section and low formation and burn-out cross section.
2. Preferably stable (if radioactive should have long half life).
3. Should not migrate in the fuel matrix at the operating temperature.
4. Should not have gaseous or volatile precursors
5. Chemical separation of fission product should be feasible. Fission product monitors should be amenable for accurate determination using chemical/radiochemical or mass spectrometric methods.
6. If to be used for isotope dilution, have a shielded isotope of the same element that permits monitoring for natural contamination and another stable or long lived isotope to be used as internal standards (spikes).
7. Have similar fission yields for all neutron energies and different fissioning isotopes.

The advantages of determining burn-up using fission product method are (i) only irradiated fuel to be analysed, (ii) it is applicable to low as well as high burn-up fuels, (iii) information of fractional fission contribution of fissile nuclides can be derived, (iv) capture to fission cross section data is not required.

1A.10 TIMS instrument used for present study

Thermal ionisation mass spectrometer of make ISOPROBE-T, M/s ISOTOPX, UK has been used in the present study and its photograph is shown in Fig. 1A.4. The Source chamber is attached with a detachable sample holder turret, which contains twenty sample holding positions. It enables continuous analysis of twenty samples without breaking vacuum in source region. Source chamber is equipped with two contact assemblies; one located just in front of the collimator, which is meant for sample heating during analysis, and the other which is away from the collimator is meant for preheating the sample before actual analysis (this reduces the sample analysis time). The contact assembly supplies, i) stable current to both the side and centre filaments independently for resistive heating and ii) stable high voltage (up to 8 KV) for providing constant acceleration potential to all the ions ejected out of filament surface. The source chamber can achieve a vacuum of ~ 3×10^{-8} mbar with the help of a turbo molecular pump backed by a rotary pump. To quickly achieve and maintain high vacuum during sample analysis, a cold trap unit is attached at top of the source chamber. The ions are accelerated, focused and directed towards analyser with the help of a collimator unit. The collimator unit contains a set of metallic slits connected with varying voltages to focus ions in X and Y direction. The source and analyser regions are separated by an isolation valve, which helps in maintaining ultra high vacuum (~ 4×10^{-9} mbar) in the analyser side, during sample change operation in the source region. The analyser region is connected with two ion pumps, one at the beginning of flight tube and the other near detector cabin to achieve ultra high vacuum. A 90^{o} sector magnet with an extended geometry of 26.5^{o} oblique incidence which provides a better mass dispersion and sensitivity is used as mass analyser. The collimated ions after dispersion by magnetic field, based on their mass to charge ratio, falls on the detectors for counting. The detector cabin houses nine movable Faraday cups and a Secondary Electron Multiplier (SEM) at the axial position. To have low noise to signal ratio, amplifiers for all the detectors were kept in a closed cabin at constant temperature

(~16 ^{o}C) and pressure. This is achieved by cooling the amplifiers by peltier cooling method and evacuating the cabin using a diaphragm pump.

After attaining required vacuum in source chamber, the samples were heated slowly by ramping up the filament current to the desired values. Initially central (ionisation) filament and side (vaporisation) filament currents were increased independently to 4.8 A and 1.0 A until rhenium ion signal were observed. At this setting, sufficient rhenium signal (~ 100 mV) required for focusing of ion beam using various focus plates was obtained. Subsequently central and side filament currents were increased slowly to get signals of metal ions of interest. The ion beam of a particular metal species was focused to obtain a flat “trapezoidal” isotopic peak. Depending on the number of isotopes of an element, collectors were arranged to have “coincidence” of isotopes, which indicate the exact positioning of the collectors for dispersed ion beams. These focusing and heating procedures were followed for all the analysis.

Ion intensities of different isotopes of an element can be acquired on single or multiple Faraday cups using dynamic or static mode with respect to the magnetic field. In the present work, isotopes of all the elements were measured in static multicollector mode. Isotopic ratios were measured by comparing ion intensities of all the isotopes of an element using inbuilt software which required programming for individual elements. During data acquisition, peak centering, base line corrections were carried out for all the isotopes independently at regular time intervals. Isotopic ratios obtained for an element corresponding to a single run is a mean of 36 (n) individual isotopic ratios with uncertainty of 95% confidence level. The mean of such five to ten runs (k) were considered to ascertain the final isotopic ratio of an element. The internal error (S_{int}) associated with each run is derived using the formula: $\sqrt{\sum_{i=1}^{n}\frac{(x-\bar{x})^2}{n(n-1)}}$. The external error

(S_{ext}) is calculated from the standard deviations of isotopic ratios associated with all the runs and is given as: $\sqrt{\sum_{i=1}^{k}\frac{(x-\bar{x})^2}{(k-1)}}$ and the total error (S_{total}) is computed by considering both internal and external errors: $\sqrt{S_{ext}^2 + \frac{1}{k}\sum S_{int}^2}$.

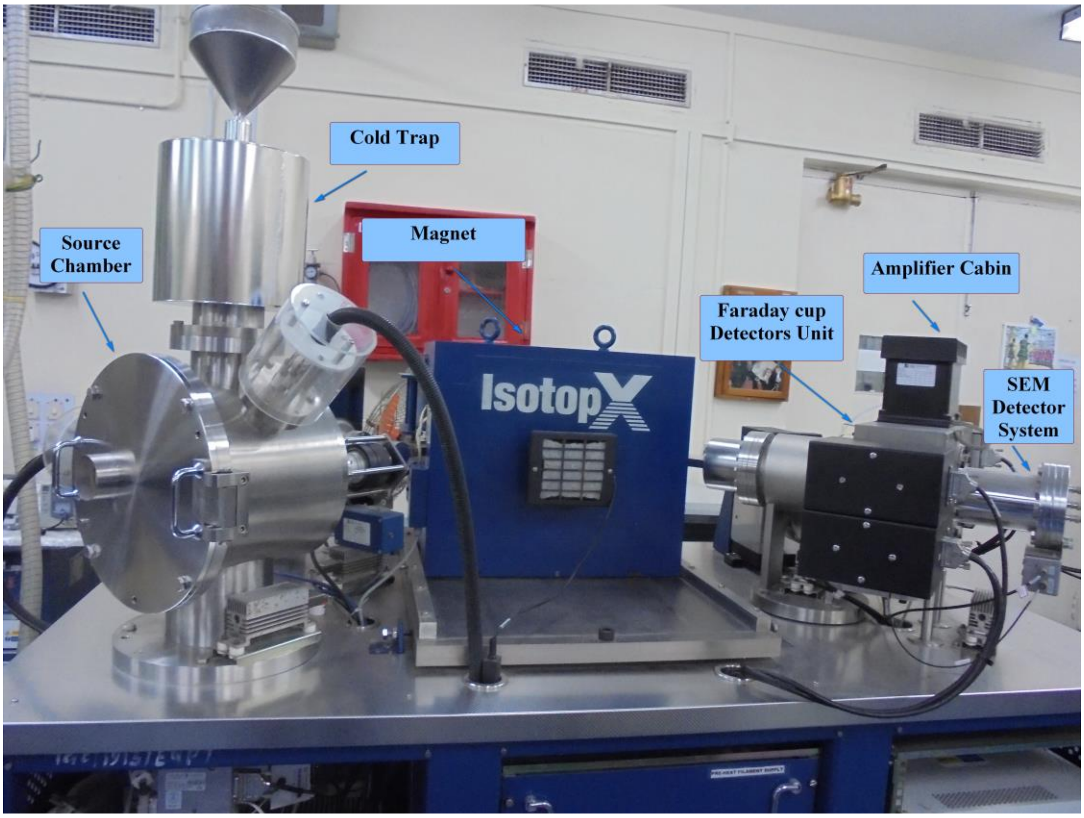

Fig. 1A.4 Photograph of TIMS instrument used in present study.

1A.11 Instrument calibration

1A.11.1 Mass calibration

The abscissa of mass spectrum which represents m/z is calibrated by analysing ranges of known elements at lower (^{7}Li, ^{23}Na, ^{40}Ca, ^{88}Sr), intermediate (^{133}Cs, ^{138}Ba, ^{142}Nd, ^{187}Re) and higher masses (^{238}U and ^{239}Pu). During mass calibration experiments, above isotopes are observed at particular mass positions on X-axis (exact mass number (up to four decimal places)) and is correlated with their true mass number by fitting to a polynomial equation. At the time of mass calibration magnetic current and acceleration voltage are kept constant.

1A.11.2 Amplifier gain calibration

The instrument equipped with nine Faraday cups, connected with nine separate amplifier units, required periodic calibration because their gain factor keeps changing with time. To normalise the gain factor for all the detectors, amplifier gain calibration is carried out periodically once in fifteen days. The calibration involves switching to a low reference current (200 mV), simulating the baseline, and a high reference current (9 V), simulating the signal, successively into each amplifier. The gain of each collector is baseline corrected and then calculated as a ratio relative to the axial Faraday.

1AA High Performance Liquid Chromatography (HPLC)

1AA.1 Introduction

Chromatography is a separation technique [20-21] which is used for the isolation of a pure sample component from a mixture. Quantitative as well as qualitative information about analytes can be obtained from chromatography. Qualitative information of analyte is obtained from retention time data, obtained experimentally. Quantitative information of analyte can be obtained from its corresponding peak area or peak height of a chromatogram using a calibration plot, which is generally prepared using standard solutions of an analyte. A typical chromatogram is shown in Fig. 1AA.1. In this figure, the identification of species A and B is made from its retention time i.e. t_{rA} and t_{rB} respectively. The amount of A and B present in a given solution is found out from the area under curves for species A and B respectively.

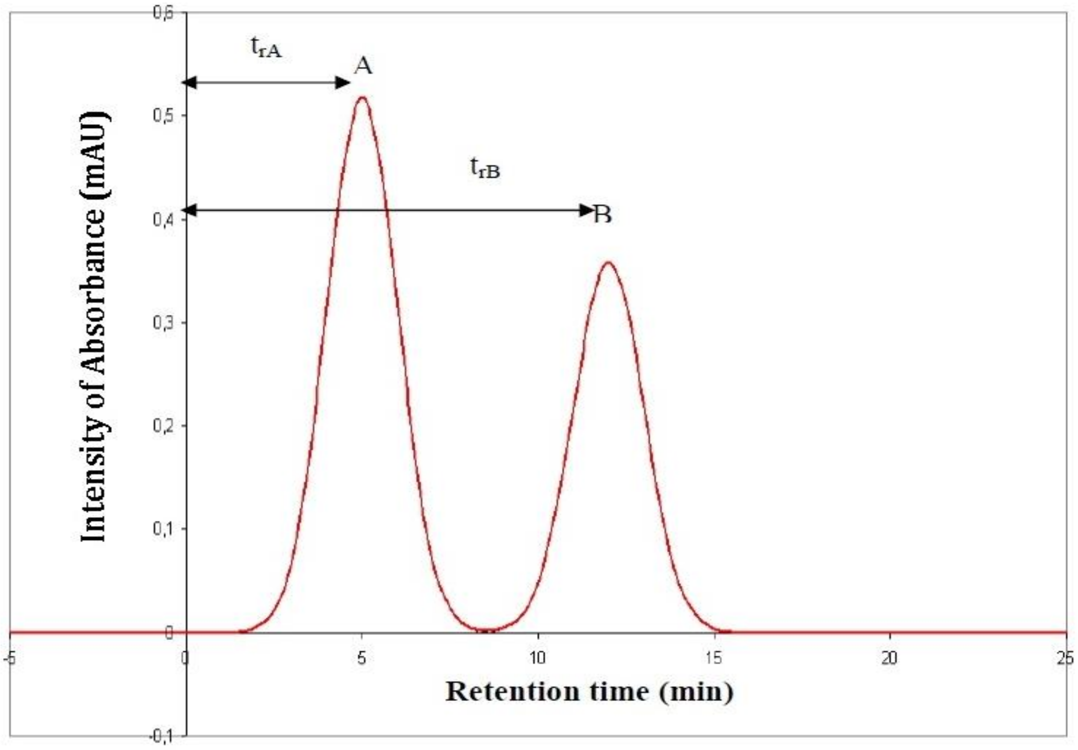

Fig. 1AA.1 Typical chromatogram of species A and B.

1AA.2 High Performance Liquid Chromatography (HPLC) technique

High performance liquid chromatography is a liquid chromatographic technique [21] that can separate the constituents from a mixture of compounds (in the liquid form) with very high speed and efficiency. Number of theoretical plate provides number of separation stages and is directly proportional to the length of the column (L) in which analytes equilibrate between two phases and is inversely proportional to the thickness of the plate (H). The number of theoretical plates (N) can be expressed as: $N = {}^{L}\!/_{H}$. For HPLC column, the number of separation stages is about 50,000 plates per meter.

1AA.3 HPLC separation modes

Depending upon the separation mechanism and the column type, HPLC can be divided into several related techniques. Some of the HPLC methods are:

i) Normal Phase Liquid Chromatography (NPLC): In this form of HPLC, the column packing materials used are polar in nature, e.g., silica and alumina; non-polar eluents such as hexane or hexane mixed with a slightly polar solvent are used as mobile phase.

ii) Reversed Phase Liquid Chromatography (RPLC): In this case, nature of stationary phase material and mobile phase are just opposite to the normal phase liquid chromatography, e.g., column packing material is non-polar (modified silica, i.e., siloxane) and mobile phase is polar in nature.

iii) Chromatography with particle column (size < 2 μm): Faster sample analysis and higher separation efficiency of HPLC column can be achieved by using spherically shaped small size particles as packing materials. Generally, column length of 3-5 cm is employed for separation of analytes with 1.8 μm particles.

iv) Separation using monolith based stationary phase: Monolith column consists of a single piece of porous, rigid material containing mesopores and micropores which provide faster analyte mass transfer [22, 23]. Compared to particle packed column, monolithic silica column has high permeability and separation efficiency with better resolution.

1AA.4 HPLC instrumentation

The HPLC system employed in the present work consisted of the following components (i) mobile phase reservoir, (ii) solvent delivery pumps (Jasco), (iii) sample injector (Rheodyne), (iv) reversed phase C_{18} column, (v) gradient mixer, (vi) post-column delivery system (Jasco), (vii) UV-VIS Spectro-photometric detector (190-900 nm wavelength) (Jasco) and (viii) data acquisition system.

The HPLC system was set-up in fume hood for studies involving radioactive materials. High pressure pumps used for the delivery of mobile phase and post-column reagent were placed outside the fume hood; Rheodyne sample injector, chromatographic column and detector were kept inside the fume hood. The eluate from the chromatographic experiment was collected inside the fume hood. The data acquisition from the UV-Vis detector was connected to a computer through a Borwin software interface, which was kept outside the fume hood. Post-column derivatisation technique was employed for the detection of lanthanides and actinides. In this method, the effluent from the column was mixed with a coloring reagent, arsenazo (III) after the column using a “Tee” connector and the complex was passed onto the UV-Vis detector. The schematic of HPLC system setup for radioactive sample analysis is shown in Fig. 1AA.2.

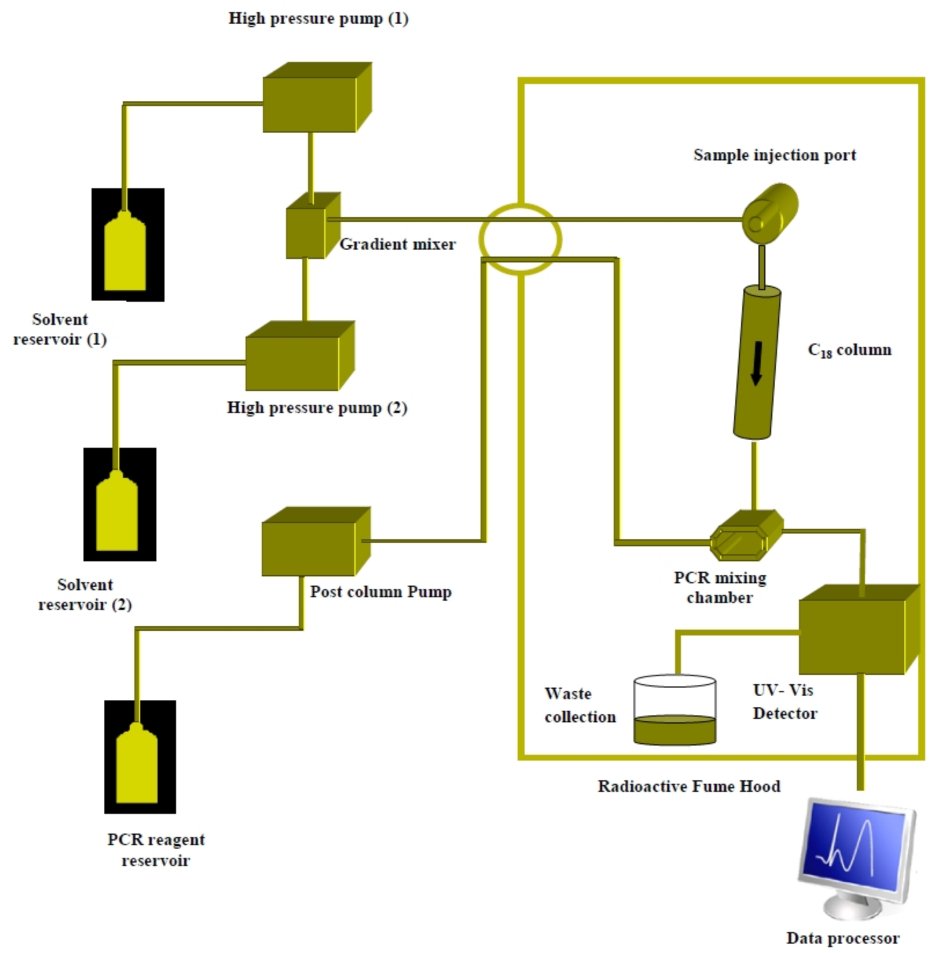

Fig. 1AA.2 Schematic of HPLC system for radioactive sample analysis.

1AB Alpha spectrometry

1AB.1 Introduction and Principle

Reactor produced uranium and plutonium mainly contain isotopes with mass numbers 233, 234, 235, 236, 238 and 238, 239, 240, 241, 242 respectively. Due to isobaric interference at mass number 238, chemical separation of uranium and plutonium is required before mass spectrometric analysis. However, during mass spectrometric analysis of plutonium, because of very high abundance of ^{238}U (> 50%) compared to ^{238}Pu (~0.2%) even small contamination from uranium results in isobaric interference at mass number 238, leading to erronius result. Hence, for accurate quantification of ^{238}Pu, alpha spectrometry was carried out and these results along with isotopic ratios from TIMS, were used for quantification of plutonium. Alpha decay is a spontaneous release of an alpha particle (^{4}He atomic nuclei) from heavy nuclei.

$$^{238}Pu_{94} \xrightarrow[\propto -decay]{t_{1/2}= 87.74\,Y} {}^{234}U_{92} \qquad (\alpha\text{- energy: 5.499 MeV}) \qquad (1AB.1)$$

$$^{239}Pu_{94} \xrightarrow[\propto -decay]{t_{1/2}= 2.411 \times 10^4\,Y} {}^{235}U_{92} \qquad (\alpha\text{- energy: 5.155 MeV}) \qquad (1AB.2)$$

$$^{240}Pu_{94} \xrightarrow[\propto -decay]{t_{1/2}= 6563\,Y} {}^{236}U_{92} \qquad (\alpha\text{- energy: 5.124 MeV}) \qquad (1AB.3)$$

In alpha spectrometry, alpha particles transfer their energy to the semiconductor detector through inelastic collisions, thus giving rise to electron-hole pairs. The number of these charge carriers is proportional to the energy of the alpha particles. The charge carriers created in the detector are collected through semiconductor contacts in preamplifier. The preamplifier integrates and converts the collected charge pulse to voltage pulse which is proportional to the alpha energy, which in turn is proportional to the number of alpha emitting heavy particles. Due to similar energy [24] of alpha particles emitted by plutonium 239 and 240, alpha spectrometer gives activity ratio for

$^{(239+240)/238}$Pu. Utilising half life ($t_{1/2}$) values for 238, 239 and 240 isotopes of plutonium [24], activity value for $^{(239+240)/238}$Pu from alpha spectrometry and 240/239 isotopic ratio value from TIMS, one can deduce the isotopic ratio of 238/239 for plutonium using the following equation.

$$^{238/239}Pu = \frac{\left(1 \times \frac{1}{t_{1/2(239)}}\right) + \left(^{240/239}Pu \times \frac{1}{t_{1/2(240)}}\right)}{\left(^{(239+240)/238}Pu \times \frac{1}{t_{1/2(238)}}\right)} \tag{1AB.4}$$

Above equation was derived using standard equation for radio activity i.e.

$A_i = N_i \times \frac{0.693}{t_{1/2(i)}}$, where A_i: activity of isotope i; N_i : number of atoms of isotope i and $t_{1/2(i)}$: half life of isotope i.

CHAPTER 1B

Knudsen Effusion Mass Spectrometry (KEMS)

In this chapter principle and methodology relating to KEMS which is relevant to this thesis will be discussed

1B.1 Introduction

All substances vaporise, but the extent of vaporisation and type of vaporisation might vary considerably from one system to the other. The vaporisation can take place either congruently or incongruently. The study of these evaporation processes is required for understanding the nature and composition of vapour phase, nature of phase equilibria that exist between the vapour and the condensed phase, and to establish the nature of chemical reactions that occur especially at high temperatures. The determination of rate of vaporisation and vapour pressures also enables one to obtain kinetics of vaporisation and condensation processes, thermodynamic data of gaseous and condensed phases, insight to bonding in molecules etc.

There are a number of methods available, both mass spectrometric and non mass spectrometric, for measuring the vapour pressures. These include (i) Static method, (ii) Boiling point method, (iii) Transpiration method, (iv) Isopiestic method, (v) Manometric method, (vi) Dew point method, (vii) Knudsen effusion based methods etc. Among these, Knudsen effusion based methods have advanges like better temperature control over sample and heating to high temperature for low vapour pressure species without significant loss of sample.

Vapour pressure measurement based on Knudsen effusion can be carried out by: (i) Knudsen effusion mass-loss method - from the molecular weight of vapour and rate of mass loss by using Hertz- Knudsen equation; (ii) Torsion method - by measuring the momentum of the effusing molecules; (iii) Collection technique - a known fraction of the effusate collected on a suitable target placed above the orifice and (iv) Knudsen effusion coupled with a mass spectrometer - from the measured ion intensities.

1B.2 Principle of effusion

In the effusion method, the sample in the form of condensed phase is placed inside a small container called Knudsen cell and heated by some suitable means. The cell can be considered as a closed container but with a small orifice of negligible thickness at the top. The atoms and molecules formed in the vapour over condensed phase collide with each other and with the walls of the container before escaping through the orifice. This process is referred to as effusion. The vapour inside the cell is assumed to be isotropic i.e. distribution of molecules is random in all directions and have a constant collisional rate at all surfaces. The vapour species effuse out in all directions following the cosine distribution law [25-27]. Since the molecules effuse out into vacuum in an effusion set up, they form a molecular beam in which, practically there are no collisions between the molecules. By keeping the diameter of the orifice much smaller than that of the mean free path of the molecules, the intermolecular collisions in the effusion orifice could be avoided. When the ratio of area of the effusion orifice to the surface area of sample which vaporises, becomes small (<<1), the equilibrium between vapour and condensed phase inside the Knudsen cell would not be perturbed by the process of effusion. Under these conditions, the vapour effusing out can be considered a representative of the vapour inside the cell, and hence, by a suitable method the vapour pressure and other thermodynamic information of the equilibrium existing inside the Knudsen cell can be obtained.

1B.3 Hertz - Knudsen equation

The Hertz-Knudsen is the fundamental equation which governs the process of effusion. It relates the rate of mass loss during effusion to the vapour pressure and is derived from the kinetic theory of gases. The Hertz-Knudsen equation for species having mass w, effusing in time t, through an orifice having an area a_0 can be presented as

$$w = p \cdot t \cdot a_0 \cdot \sqrt{\frac{M}{2\pi RT}} \tag{1B.1}$$

where M is the molar mass, R is the gas constant and T is the temperature. This equation is valid for an orifice with negligible thickness. It relates the vapour pressure to the rate of mass loss of the sample. If a small opening with an infinitesimal thickness is provided on the top of a container (Knudsen cell) and a high vacuum is maintained outside this opening, then all those molecules which might strike the surface of area equal to that of the opening (or orifice) can be assumed to be effusing out. Under such a situation, the measurement of the weight of the effusate can be used to calculate the equilibrium vapour pressure inside the container by using the equation (1B.1).

1B.4 Knudsen effusion mass spectrometer

The coupling of Knudsen effusion with mass spectrometer enables measurement of partial pressure of different vapour species present in the vapour phase. In this method, the effusate is mass analysed by allowing the molecular beam from the Knudsen cell into the ion source of the mass spectrometer. While the Knudsen cell serves as a source of production of molecular beam representative of the vapour phase in equilibrium with the condensed phase at various temperatures, the mass spectrometer assists in identifying the species present in the vapour. The KEMS system consists of following components.

1B.4.1 Cell chamber

It consists of Knudsen cell surrounded by filaments, which act as a heating source and enclosed by thermal shielding materials that helps in maintaining uniform temperature of the cell. The molecular beam effusing from a Knudsen cell serves as a source of equilibrium vapour for mass spectrometric analysis.

1B.4.1.1 Knudsen cell

The cells are generally made of metals like Mo, W, Ta, or ceramic oxides like alumina or graphite. Where the sample is inert and not expected to react with the container materials, these cells can be directly used. In the case of more reactive samples, inert materials like platinum can be used as liners for containing the sample. Hilpert [28-29] has reported a design of Knudsen cell which prevents chemical interactions of reactive samples with air or moisture during sample changing operations. Knudsen cells having a knife edged or channelled orifice of ~0.5 or ~0.7 mm diameter is used to contain the samples. The Knudsen cell is placed in an outer cup made of Mo, W, Ta or graphite.

1B.4.1.2 Furnace assembly

The sample is heated by electron bombardment mode, or resistive mode, or inductive mode. In the case of electron bombardment heating, tungsten filament wound around and at a distance from Knudsen cell emits radiation and electrons on passing current. To have uniformity in temperature, the cells are completely surrounded both at the sides and at the top and bottom by radiation shields made of materials such as tantalum which has a low emissivity. A good vacuum is maintained inside the mass spectrometer by a suitable high vacuum pumping system. This ensures that the molecular beam formed is not scattered by the background molecules, and also prevent oxidation, at high temperatures, of the components inside the mass spectrometer. The vacuum chamber surrounding the furnace assembly is cooled by chilled water to protect it from the heat radiated from the hot regions. Temperatures are measured by a thermocouple or an optical pyrometer depending on the temperature range of measurement.

1B.4.2 Source chamber

There are different ionisation methods available like electron impact ionisation, photoionisation, chemical ionisation, etc. Of these, the electron impact ionisation is the most commonly used method for ionising gaseous molecules. The molecular beam crosses the electron beam emitted from a heated filament and gets ionised. The filament is generally made of tungsten, rhenium, thoriated tungsten or oxide coated iridium. The positive ions produced are accelerated before reaching the mass analyser.

The beam of vapour from the Knudsen cell reaches the ionisation chamber through a series of coaxial holes present in radiation shields, shutter and ionisation chamber. Depending on the type of ionisation and application, a particular variety of mass analyser is used. If single focusing magnetic analysers with 60^o or 90^o sector are used, they can provide the required sensitivity and resolution. In cases where a rapid mass scan is required, one can use time-of-flight analysers, but the resolution and sensitivity are relatively lower than that of a magnetic sector instrument. Alternately one can use a quadrupole analyser, for better sensitivity. Because of its compact size, the quadrupole analyser and time of flight analysers can be taken much close to the ion source and hence, ions which have a relatively shorter life time can also be identified.

1B.4.2.1 Quadrupole analyser

In quadrupole analysers, mass separation is achieved solely with electric fields. It is a path-stability mass spectrometer where the quality determining the stability of ion path in quadrupole is the electric field. Thus, quadrupole mass analyser (QMS) is often referred as mass filter rather than as mass separator. QMS employs a combination of direct - current (dc) and a radio frequency (rf) field as a mass filter. An ideal quadrupole analyser consists of four long hyperbolic cylinders in a square array with specific inner space dimensions. Ions can be transmitted by the quadrupole mass filter only if they are stable in both x and y directions simultaneously i.e. their ‘a’ and ‘q’ values must lie in the region of overlap. Where ‘a’ is related to ‘dc’ and ‘q’ to ‘rf’ are dimensionless parameters, used to define the stability of the ion beam in a quadrupole electric field. For any given set of ‘dc’ and ‘rf’ voltages only ions of a specific m/z value avoid collisions with rods and successfully traverse the quadrupole along the z axis to reach the detector; all other ions collide with the quadrupole surfaces or get lost through the empty space between the rods. The mass scanning is achieved by varying both rf and dc voltages, while keeping their ratio constant.

1B.4.3 Detector

After the mass analysis, ions reach the detector. Secondary electron multiplier, Faraday cup, Daly scintillation and ion counting are some of the commonly used detectors. One or more of the detectors are generally attached to the mass spectrometer so that a suitable detector can be chosen depending on the sensitivity range in which the ion current is measured. For low ion current signals, secondary electron multiplier is used. The output from this detector is mass dependent. Faraday cup in which the mass dependency is practically non-existent can be used when the ion current to be measured is high. Daly detector is a scintillation type detector and whose conversion efficiency is reported to be hundred percent [3].

1B.5 Factors influencing the equilibrium conditions in Knudsen effusion

Knudsen method of measuring vapour pressures is only an attempt to approximate the ideal conditions well enough, so that the vapour pressures measured represent the true equilibrium pressure. This is because the cell is not a completely closed system and vapour is lost continuously from the Knudsen cell. So, the factors which influence the effusion process, would affect the accuracy of the pressures measured. Some of these factors are mentioned below and can be taken care either by some correction factors or by suitable experimental conditions.

I. The rate of effusion from an effusion cell is the difference between the rate of evaporation and rate of condensation of molecules inside the Knudsen cell. The vapour pressure measured from effusion (P_k) would be more close to the true equilibrium vapour pressure (P_e) which one would obtain, if the cell is completely closed, is given by [30]

$$P_e = P_k \ [1 + (a_o / a_s \alpha_v)\ ] \tag{1B.2}$$

where a_o is the area of the orifice; a_s area of the sample and α_v, the evaporation coefficient, which is the ratio of rate of evaporation from a free surface to the equilibrium rate of vaporisation in a closed cell. Thus, under conditions, where $a_o / a_s \leq 100$ and evaporation coefficient close to one, P_k would be more close to P_e. For example, when $a_o/a_s \sim 0.01$, $P_k/P_e \approx 0.99$ to 1.00 (for $\alpha_v \sim 1$). Hence, by keeping such low a_o/a_s a ratio, which is practically feasible, one can obtain almost true equilibrium pressures. If there exist a kinetic barrier for evaporation at the surface of sample such that the rate of evaporation is less than the ideal rate of effusion, α_v may become very small. Such a barrier would exist, if the molecular form of vapour is different from that of solid or if several vapour species are present [31]. Even when α_v is much less than one, by keeping an appropriate a_o / a_s ratio, one can have $P_k \sim P_e$.

II. The orifice thickness is assumed to be infinitely thin in deriving the equation for effusion. But practical inevitability is that the orifice has definite thickness. This leads to some transmission loss during the effusion through the orifice, as some molecules get reflected back to the cell by colliding with the wall of the orifice. Clausing [32] had, from a set of equations, calculated the correction factors, depending on the shape of the orifice. This factor is commonly referred to as Clausing factor, C or transmission coefficient. The combination of C and a_o (the orifice area), a_oC is called the "effective orifice area" which is available for molecules to effuse out. Thus by incorporating this factor into equation 1B.1 and writing in a more practical form, the Hertz-Knudsen equation becomes,

$$w = 10 \cdot p \cdot t \cdot a_0 \cdot C \cdot \sqrt{\frac{M}{2\pi RT}} \tag{1B.3}$$

where w = mass loss in grams; p = partial pressure in Pascal; a_o = orifice area in cm^2; C = Clausing factor (dimensionless); M = molar mass in g/mol; R = gas constant in erg/mol/K and T = temperature in Kelvin; t = time period in seconds.

III. Problems like temperature inhomogeneity within the cell, creeping of liquid samples to the outer walls of Knudsen cell, and diffusion of sample to the orifice lid can significantly alter the equilibrium pressures measured by Knudsen cell technique. If a movable beam defining slit is placed between the K-cell and the ionisation regions, one can differentiate whether the molecular beam consists of vapour, only due to effusion from Knudsen cell or from other location such as shields as well. The ion intensity profiles obtained by having slits of different shapes would result in peaks with normal shape if the vapour is only due to effusion. Any distortion in the peak shape like broadening would indicate that the molecular beam contains vapour from undesired sources also [33].

1B.6 Range of pressure measurements

The upper limit of vapour pressure measurement by Knudsen effusion mass spectrometric technique is mainly decided by the Knudsen flow conditions. Molecular flow occurs as long as the mean free path of the molecules effusing out is greater than the orifice diameter of the Knudsen cell. The lower limit is often set by the sensitivity of the mass spectrometer towards a particular species and interference from background gases. Generally, one can measure vapour pressures between 10^{-5} to 10 Pascal. By having a sensitive detector and a good pumping system which reduces the interference from background gases, the lower limit can further be extended. Double focusing instruments owing to their better resolution capabilities can separate the inorganic ions from the organic ions formed from the background gases thus enhancing the sensitivity. On the other hand, quadruple analyser, which combines the advantages of sensitivity and resolution, can also be used.

1B.7 Mass spectrometric measurements

Vaporisation studies using Knudsen effusion mass spectrometry, generally involve the following steps:

1) Identification of neutral species corresponding to the ions produced in the mass spectrum
2) Determination of partial pressures of neutral species
3) Evaluation of thermochemical data for the different gas phase and condensed phase- gas phase equilibria existing within the Knudsen cell
4) Determination of thermodynamic quantities for the various condensed phases and the gas phases.

5) Deriving phase diagram information.

Each of these will be discussed in detail in the following sections.

1B.7.1 Identification of neutral species

It is important that the ions detected in mass spectrum are correlated to proper neutral precursor from which they originate. The combination of one or more of the experimentally obtained information mentioned below help in identifying the neutral species:

1) Identification of ionic species
2) Ionisation efficiency curves
3) Temperature dependence of ion intensities

1B.7.1.1 Identification of ionic species

During ionisation, especially by electron impact mode, ions are formed due to both simple (both single and multiple) and dissociative ionisation. In simple ionisation, one or more electrons are removed from a gaseous molecule whereas in dissociative ionisation, in addition to electron removal, some of the bonds are also broken by the impinging electrons. Hence, the identification of neutral species starts with indexing of the ions observed in the mass spectrum. This is implemented, by scanning for all possible types of ions, viz. parent, fragment, polymeric and multiply charged ions and record the ion intensities as a function of mass to charge ratio. In the recorded spectrum, different types of ions may possess the same mass to charge ratio and hence appear at the same mass number. It is important to differentiate them, so that exact formula can be assigned to the vapour species. This is done by comparing the experimentally obtained pattern with the predicted relative isotopic abundances for a given ionic species.

Sometimes, the ions, which are formed in the ion source, dissociate in the transit between ion source and mass analyser and appear as peaks at unexpected mass numbers. These are called metastable peaks [3] and care must be taken not to attribute these to some neutral species.

To differentiate between ions formed from the species effusing from the Knudsen cell and those from background gases in the ionisation region, a shutter is interposed between the K-cell and the ionisation chamber. The design of the ion source configuration is usually such that the molecular, electron and ion beams are mutually perpendicular. The absence of residual ions in the vapour can be verified by switching off the ionising electron beam.

1B.7.1.2 Ionisation efficiency curves

These are obtained by recording intensities of ions as a function of electron energy. As long as the electron energy is less than the ionisation energy of ions under consideration, no ion signal is observed. After the threshold, with an increase in electron energy, the ion intensities increase in a linear fashion and reach a maximum value before decreasing a little. The energy obtained by extrapolating the linear portion of the curve to the electron energy scale is called the appearance energy. Apart from this linear extrapolation method, other methods like retarding potential method, vanishing current method, etc., [34] are also used to derive the appearance energy.

A parent ion has an experimentally obtained value comparable to the known first ionisation energy. If the measured appearance energy is higher than the reported value, then it can be concluded that the ion is a fragment with a different neutral precursor. In general, a parent ion would have higher intensities and lower appearance energy than that of the fragment resulting from the same neutral precursor, though there are known exceptions [35-36]. The general shapes in the ionisation efficiency curves like, any upward break or downward break also give information about fragmentation processes. For example, a downward break in the ionisation efficiency curve indicates that, at that energy, the neutral species undergoes dissociative ionisation resulting in the lowering of ion intensity. Similarly, if there is an upward break in the ionisation efficiency curve, it is an indication of more than one source contributing to the ion intensity.

Further information like temperature dependence of ion intensities also helps in identification of the neutral precursors.

1B.7.1.3 Temperature dependence of ion intensities

Another approach which is often adopted to assign a group of ions to a particular neutral species involves the measurement of ion intensities I^+ as a function of temperature. All ions, originating from the same neutral species would have the same temperature dependence of ion intensities i.e. similar heat of vaporisation (which may not correspond to the thermodynamic heat of vaporisation [37]). Sometimes, two ions having the same mass to charge ratio but appearing from different neutral precursor complicates the situation. This may result in a different heat of vaporisation and one may wrongly assign this to a totally different neutral species.

By making use of the information obtained by the procedures mentioned above, the nature of the neutral species can be identified unambiguously in most cases. As much as possible, the ion intensity measurements of a polyatomic ionic species are carried out at low electron energy (in electron impact ionisation) so as to minimise its fragmentation. Higher electron energy will result in higher ion intensity for itself (polyatomic ionic species) as well as contribute to the ion intensity of another ionic species by fragmentation.

There are also other experimental methods, which when used either separately or in conjunction with the technique described above provide further information regarding the nature of neutral species, extent of fragmentation etc. Once the neutral species corresponding to different ions are ascertained, their partial pressures can be obtained from the measured ion intensities as described in the following section.

1B.8 Relation between ion intensity and partial pressure

The expression which relates the ion intensity (I^+) measured at temperature T, using a mass spectrometer and the partial pressure (p) can be expressed as follows,

$$p = k' \cdot I^+ \cdot T \qquad (1B.4)$$

where $k' = k / (\sigma \,.\, \gamma \,.\, n)$ is the pressure calibration constant, n is the isotopic abundance of the ionic species measured, γ is the yield of secondary electron multiplier and k is the instrument constant. Hence by knowing the pressure calibration constant, the partial pressures can be calculated. k′ can be determined experimentally by any of the following methods.

1B.9 Determination of Pressure calibration constant (k′)

1B.9.1 Determination of instrument constant (k)

Instrument constant (k) for a particular KEMS set up can be determined by caring out either of the following methods

1. Measurement of ion intensities of a reference material whose vapour pressure is known.
2. Quantitative vaporisation of the sample while monitoring the ion intensities.
3. Use of M^+/M^{2+} ratio, provided ΔG° for the dissociation reaction is known. (M is monomer and M_2 is dimer)

Only the method used in present work is described here. The other two methods are described elsewhere [36, 41- 43].

1B.9.1.1 Using a reference substance whose vapour pressure is known

For selected elements, the vapour pressures as a function of temperature are certified (p_{ref}) by National Institute of Standards and Technology (NIST) and are known as vapour pressure standards [44]. By measuring the ion intensity for such substances, the pressure calibration constant k′ can be obtained.

$$p_{ref} = k'_{ref} \cdot I^{+} \cdot T \quad (k'_{ref} = k / (\sigma\gamma n)_{ref}) \tag{1B.5}$$

$$k'_{ref} = p_{ref} / (I^{+} T) \tag{1B.6}$$

The partial pressure of a gaseous species over the sample is given by

$$P_{sample} = k'_{sample} \cdot I^{+}_{sample} \cdot T \quad (k'_{sample} = k / (\sigma\gamma n)_{sample}) \tag{1B.7}$$

Substituting for k from the (k'_{ref}) obtained from equation (1B.5)

$$k'_{sample} = k'_{ref} \ (\sigma\gamma n)_{ref} \ / (\sigma\gamma n)_{sample} \tag{1B.8}$$

The ion intensities over the reference substance are measured at different temperatures and the calibration constant obtained at each temperature is averaged and this value is taken as k'_{ref}. This method requires the knowledge of ionisation cross sections for the reference as well as for the sample.

In those cases, where the vapour species over the given sample may also exist over some other substance with known vapour pressure data, use of factors such as ionisation cross section and detector responses can be avoided. The pressure calibration constant obtained over the known substance can be directly used.

1B.9.2 Determination of ionisation cross section (σ)

The ionisation cross section values have been measured experimentally for a limited number of molecules. These data are measured either absolutely or by a relative method. In the absolute method, from the known accurate values of parameters appearing in equation (1B.4), σ, is evaluated [38]. The determination of σ by relative method involves one or more of the following techniques.

1) Measuring the intensities of ions as a function of time and temperature over sample and a standard such as Ag(s): from the integrated ion intensities, mass loss of both sample and standard and with known ionisation cross section of standard, the ionisation cross section for the sample molecule can be deduced by using Hertz-Knudsen equation.

2) Ionisation cross section calculated by theoretical methods is largely used. Otvos and Stevenson [39] have calculated the ionisation cross section of atoms at the maximum of ionisation efficiency curves from quantum mechanical considerations. This method assumes that, the ionisation cross section of electrons in a particular shell of an atom is proportional to the mean square radius of the shell in which the electron is located. The ionisation cross sections obtained by this method differ from experimental data wherever available, by a factor of up to three. They have calculated the ionisation cross section for about 59 elements. A similar calculation was made by Mann [40], but by taking into consideration the energy of the electrons also and this yielded values which were much close to the experimental values (agree within 20 to 50 %) than those of Otvos and Stevenson. The agreement is better when comparison is made at the same electron energy. By this method ionisation cross section was calculated for almost all the elements in the periodic table.

1B.9.3 Determination of multiplier response (γ)

The ion current measured by a secondary electron multiplier (SEM) depends on (i) charge (ii) mass and (iii) kinetic energy of the ion falling on the first dynode of the multiplier. A correction factor, that takes into account these factors will yield appropriate secondary electron conversion efficiency. From the kinetic energy expression, this factor is assumed to be proportional to $1/\sqrt{M}$. In mass spectrometers where detectors like Faraday cup are also present, the detector response can be obtained by taking the ratio of ion currents measured using secondary electron multiplier and Faraday cup. If SEM is incorporated with pulse counting devise, mass discrimination factor can be avoided and multiplier factor for this can be considered as unity.

1B.10 Thermodynamic evaluation of partial pressures

From the partial pressures obtained for the vaporising species, enthalpies of the vaporisation reaction can be derived by using second- and third- law methods of thermodynamics [31]. Activities of the components and the Gibbs free energies of formation of the condensed phases can also be derived from the partial pressure data.

1B.10.1 Reaction enthalpies

1B.10.1.1 Second law method

The Gibbs free energy change of a reaction is given by the following expression.

$$\Delta_r G_T^o = -RTln(K_{eq}) = \Delta_r H_T^o - T\Delta_r S_T^o \tag{1B.9}$$

where $K_{eq} = \Pi (p_i / p^{\o})^n$, p_i is the measured partial pressure, $p^{\varphi} = 101325$ Pa, and 'n', is the stoichiometric coefficient. On rearranging the equation, we get

$$\ln (K_{eq}) = -\Delta_r H^o{}_T /(RT) + \Delta_r S^o{}_T/R \tag{1B.10}$$

Differentiating this expression with respect to 1/T results in vant Hoff's equation

$$d \ln (K_{eq})/ d(1/T) = - \Delta_r H^o{}_T /R \tag{1B.11}$$

Thus enthalpy of a reaction can be obtained from the slope of the plot of equilibrium constant of the reaction under consideration as a function of inverse temperature. In this method, variation of enthalpy with temperature is assumed to be negligible for change in the temperature range of about 100-150 K. Hence, the plot is taken as a straight line within the experimental uncertainty. The intercept of such a plot gives the entropy of the reaction. The enthalpy and entropy data obtained are assigned to the middle temperature of the investigation. These are converted to appropriate quantities at room temperature by the use of enthalpy and entropy increments.

$$\Delta_r H^0_{298.15} = \Delta_r H^0_T - \left[\sum\left(H^0_T - H^0_{298.15}\right)_{products} - \sum\left(H^0_T - H^0_{298.15}\right)_{reactants}\right] \qquad (1B.12)$$

$$\Delta_r S^0_{298.15} = \Delta_r S^0_T - \left[\sum\left(S^0_T - S^0_{298.15}\right)_{products} - \sum\left(S^0_T - S^0_{298.15}\right)_{reactants}\right] \qquad (1B.13)$$

1B.10.1.2 Third law method

In this method, the enthalpy of the reaction is directly obtained at the reference temperature for each data point. Substituting for $S^o_T = -(G^o_T - H^o_T) / T$ in equation (1B.10),

$$-RT \ln K_{eq} = \Delta_r H^o_T + \Delta_r (G^o_T - H^o_T) \qquad (1B.14)$$

adding $\Delta_r H^o_{298.15}$ on both sides and rearranging,

$$\Delta_r H^o_{298.15} = -T\,(R \ln K_{eq} + \Delta_r(G^o_T - H^o_{298.15}) / T) \qquad (1B.15)$$

The function $(G^o_T - H^o_{298.15}) / T$ is called the Gibbs energy function. In the expanded form it is given by

$$(G^o_T - H^o_{298.15})/T = \{(H^o_T - H^o_{298.15})/T\} - (S^o_T - S^o_{298.15}) - S^o_{298.15} \qquad (1B.16)$$

The Gibbs energy functions for the gaseous species are usually obtained from spectroscopic and structural data and those for the condensed phases from the measured heat capacities.

1B.10.1.3 Comparison of second and third law methods

In the second law method, only one enthalpy value is obtained for the whole range of measurement whereas in the third law method, for each temperature of measurement, enthalpy of reaction at the reference temperature can be calculated. This is the advantage of the third law method. Hence, even in those cases where measurements are possible only at a few temperatures, like in the case of minor species, enthalpies can still be obtained. Third law method enables one to check the consistency of the data obtained. If reliable Gibbs energy functions are available, then third law method provides more accurate value. If the Gibbs energy functions are not available and to be estimated, then third law values can be considered, provided there is no trend in the enthalpy value with temperature. The advantage of the second law method is that one need not plot the actual pressures. In mass spectrometric measurements, the enthalpy can be obtained from the log(I^+T) vs. 1/T plot. So, errors in ionisation cross section and other parameters used for deriving pressures do not affect the reliability. Third-law method requires absolute values of K_p and hence are affected by pressure calibration, ionisation cross section and detector responses. It is always better, wherever possible, to perform both second and third law analysis. Good agreements between these two values indicate that the enthalpies derived are reliable. In case of disagreement, and if the Gibbs energy functions are known accurately, then more weightage is to be given for third law value.

Uncertainties in the measured temperatures affect the second law values more than the third law values. The differential error in temperature, introduces more uncertainty than the absolute error in measured temperatures over the range of measurement. Drowart and Goldfinger [33] have given equations to calculate uncertainties in the enthalpies obtained by second and third law values due to measured temperature and pressure.

1B.10.2 Auxiliary thermodynamic quantities

The auxiliary thermodynamic data such as enthalpy and entropy increments and Gibbs energy functions used in second and third law evaluations for the condensed phase are obtained by calorimetric methods [45]. Usually bomb or drop type calorimeter is used. From the heat capacity data obtained as a function of temperature, the enthalpy and entropy functions are obtained by integration. Subsequently, the Gibbs energy function is also determined. For the gas phase, these data are obtained from spectroscopic and structural information. Wherever the data could not be obtained by the methods described above, empirical estimations can be made [45]. For example, one can estimate based on the values for analogous molecules or calculate from the values of constituent elements.

1B.10.3 Determination of activity

Knudsen effusion mass spectrometry provides a very useful way of studying the activities of components in alloys, and thus finds application in solution thermodynamic studies in metallurgical research. At low pressures where, fugacity can be approximated to partial pressure, the activity of a particular component in an alloy can be calculated knowing the partial pressures over the alloy and the pure component [45- 46]

$$a_i = [p_i / p^o_i]^{1/n} = [I_i^+ / I_i^{o+}]^{1/n} \tag{1B.17}$$

where p_i^o and I_i^{o+} are the partial pressures and ion intensities of species i over pure component and p_i and I_i^+, are that over the alloy system at a given temperature. n, is the atomicity of the vaporising species. Thus, by measuring the ion intensities of species ‘i’, over pure component and alloy phase, the activity of ‘i’ in the alloy phase can be obtained. This method of determining the activity assumes that the instrument calibration constant does not change between the two measurements.

1B.11 Phase diagram studies

One of the important applications of Knudsen effusion mass spectrometry, is in obtaining phase diagram information for two and three component systems by the application of Gibbs phase rule, $F = C - P + 2$, where F, is the degree of freedom, C, is the number of components and P is the number of phases which are in equilibrium for a given system. Since the ion intensity (and thus partial pressure) can be measured as a function of temperature and composition, its variation with time can be used to identify the different phase equilibria involved.

1B.12 KEMS used in present study

The vaporisation studies have been conducted using home built high temperature mass spectrometric system (KEMS). It consists of two chambers, one that houses the Knudsen cell assembly with a provision for heating the samples and the other in which mass analyser is mounted. The schematic of Knudsen effusion mass spectrometer used for present study is shown in Fig. 1B.1 and the photograph of KEMS is shown in Fig. 1B.2.

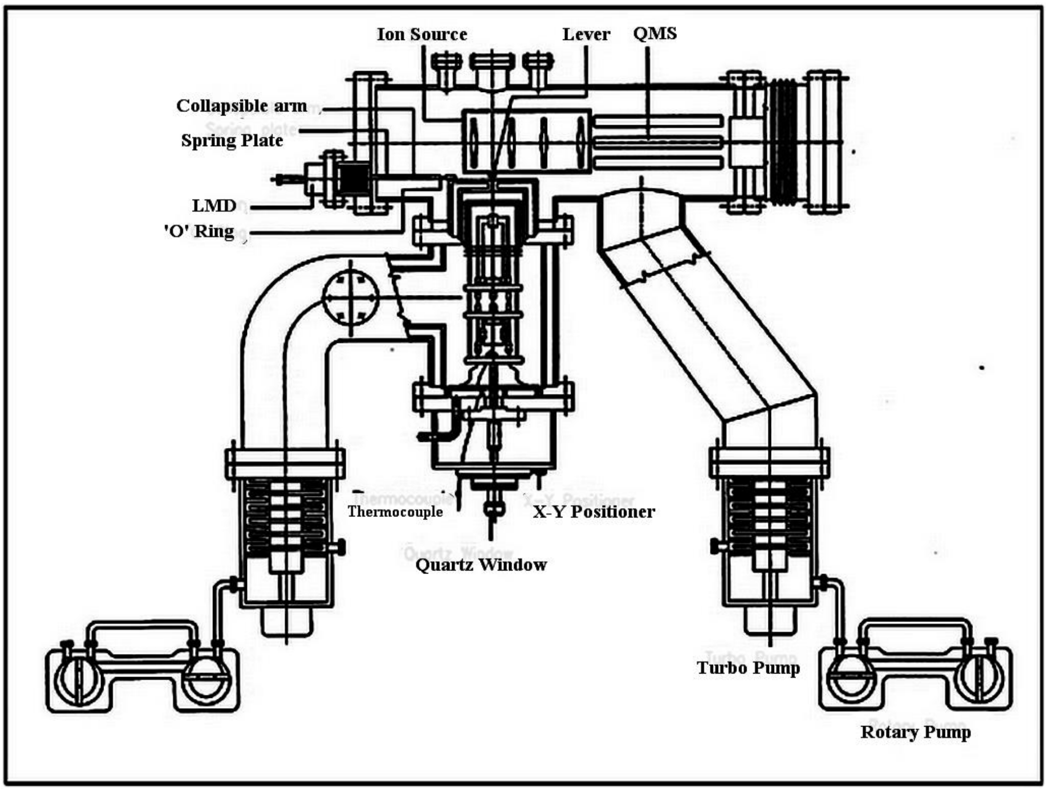

Fig. 1B.1 Schematic diagram of Knudsen effusion mass spectrometer used in the present study.

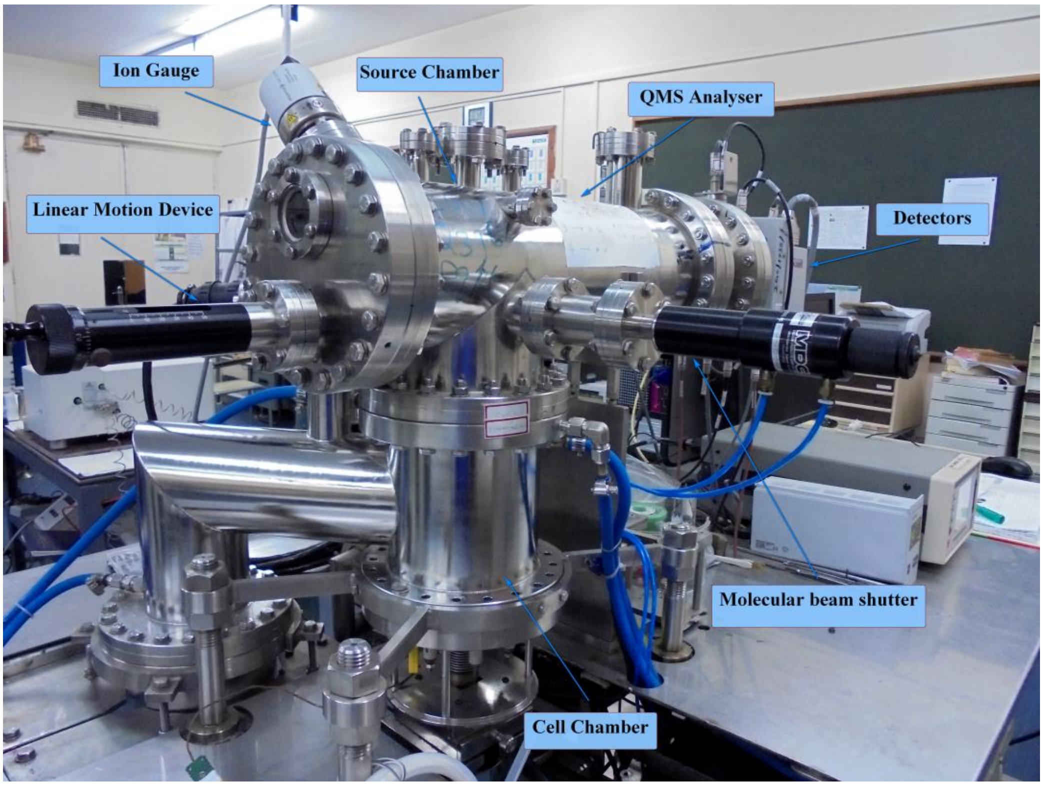

Fig. 1B.2 Photograph of KEMS used in present work.

1B.12.1 Cell Chamber

The sample is placed inside a suitable Knudsen cell, having lid with knife edged orifice of diameter 0.5 mm, which in turn is placed inside the tantalum cup having lid with opening at top (diameter 2.0 mm). A chromel-alumel thermocouple inserted through the bottom of the tantalum outer cup is used to measure the temperature. Samples were heated by bombarding with electrons emitted from the two tungsten filaments which surround the Knudsen cell assembly. Temperature of the Knudsen cell is maintained by thermocouple control mode that enables the temperature to be maintained within ±3 K through feedback mechanism. The Knudsen cell is enclosed by tantalum heat shields (three stages of shielding). These heat shields help in maintaining the uniform temperature of the cell, keeps the power requirement less, minimises the out-gassing that would result from the heating of the surroundings and also protects the inner wall of the vacuum chamber from getting heated up. The furnace could be safely heated to, and maintained at temperatures as high as ~ 1400 K. The Knudsen cell furnace assembly rests on a small platform attached to a X-Y positioner through a shaft and bellows, which makes it possible to align the Knudsen cell with the ion source of the mass spectrometer. The base of the X-Y positioner is attached to a water cooled flange having six feed through for providing power to the furnace. The entire cell chamber including the bellow that connects to the high vacuum pump is a annular vessel so as to have water cooling. The photograph of the electron bombardment furnace assembly is shown in Fig. 1B.3.

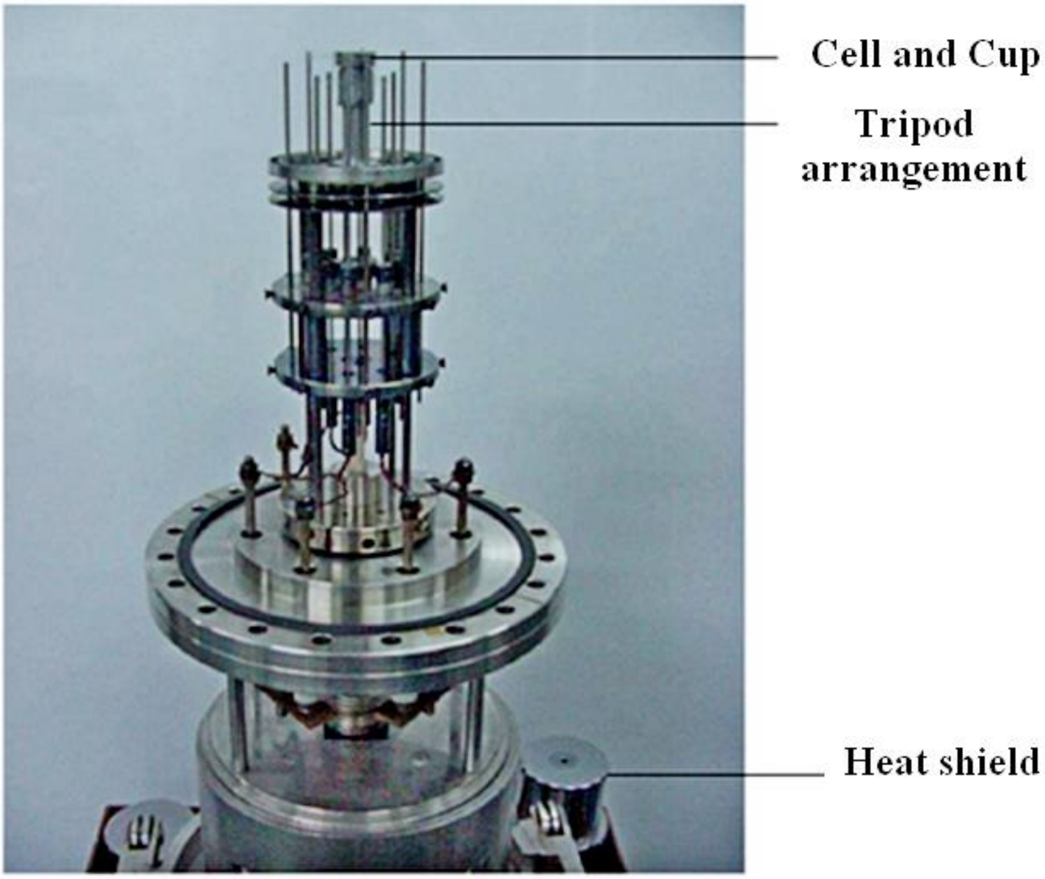

Fig. 1B.3 Photograph of home built electron bombardment furnace assembly [47].

1B.12.2 Source chamber

The top chamber which is also called as source chamber is connected to cell chamber (bottom chamber) through a 5.0 mm diameter hole. To be able to have the ion-source 'ON' even when the Knudsen cell chamber will be at ambient pressure (during sample changing), a specially designed vacuum isolation device has been installed. This essentially consists of a viton O-ring with 8.0 mm ID and 3.0 mm section diameter mounted on a 'O-ring carrier plate'. The design is such that the connectivity between the Knudsen cell and the ion source chambers can be readily restored when the vacuum level in the Knudsen cell chamber is satisfactory. The QMS lies just above the cell chamber and has three components, namely, ion source, mass filter and detector. The orifice of ion source is located coaxial with that of the cell. The configuration of ion source is such that the directions of molecular beam from the cell orifice, electron emission from the ion source filaments, and the resulting positive ion beam are mutually perpendicular to each other. The positive ions generated are directed into the mass analyser (QMS) by applying suitable voltages and mass analysed according to their m/z ratio. The mass analyser used is a quadrupole mass spectrometer (QMS) (M/s Hiden Analyticals, UK). The ions transmitted by the mass filter are detected by using a secondary electron multiplier operating in pulse counting mode. The extreme care in the design aspects of KEMS enabled measurement of vapour pressures as low as 10^{-6} Pa comfortably. The very high vacuum required for the operation of KEMS is provided by two turbo molecular pumps (pumping speed 500 L/sec; M/s Edwards UK) and backed by rotary pumps (M/s Edwards, UK). The residual pressures in the Knudsen cell furnace and ion source chambers are monitored by hot ionisation gauge (M/s SRS, U.S.A) and compact cold cathode gauge (M/s Pfeiffer, Germany) respectively; and in the fore vacuum region by Pirani gauges (M/s Edwards, UK). By making use of the provisions in the control electronics of these gauges, some safety interlocks, necessary for smooth functioning and round the clock operation of the HTMS, have been incorporated.

1B.13 Calibration

1B.13.1 Calibration of Thermocouple

Following procedure was adopted to ensure the accuracy of temperatures measured by thermocouple, an important factor for obtaining reliable partial pressures and thermodynamic data.

Before the thermocouple was installed in the K-cell furnace assembly, the temperatures of ice point and boiling point of water were measured with the thermocouple. After the installation of the thermocouple in the K-cell assembly, the calibration of thermocouple was carried out by visual examination method [47].

1B.13.1.1 Visual examination method

A NIST certified silver was used for thermocouple calibration. By this method, Ag(s) (pieces of irregular shape) was heated well below the (~ 25 K) expected melting point (T_m = 1235 K) [48] and the temperature was maintained for ~ 30 minutes to ensure stability. Then the temperature was raised and kept near the melting temperature for ~ 30 minutes. After cooling, the sample was visually examined. The appearance of sample in globule form is indicative of the melting process that could have occurred at the set temperature. Retention of sample appearance in the original shape indicates that the sample had not melted till then. This process of heating the sample and visual examination was repeated until the difference between melting and non-melting temperatures was less than 3 degrees. Then the melting point ($T_{m,\ obs}$) was taken as average of these two values. The equation to calculate the actual temperature of the sample (T_{actual}) was obtained as

$$T_{actual} = T_{app} + \Delta T \qquad (1B.18)$$

where T_{app} is the temperature corresponding to the millivolt output of the thermocouple and $\Delta T = (T_m - T_{m,obs})$ is the correction factor arrived from visual examination method.

Temperature calibration arrived by the above procedure was further ascertained by heating silver solid to different temperatures over a range of 100 degrees. From the measured ion intensities and partial pressures reported [44], pressure calibration constant, at different temperatures were calculated. Absence of trend in the calibration constant as a function of temperature was taken to further confirm the reliability of the temperature calibration and reliability of temperature measurement based on the above calibration.

1B.13.2 Calibration of electron energy scale

For the electron energy scale calibration, In(s), Ag(s), Hg(s), Ar(g) and He(g) were used. The first ionisation energies of the ions corresponding to these gaseous species are 5.8, 7.6, 10.4, 15.8 and 24.6 eV [49], respectively. While the solid samples were heated in the Knudsen cell, the gaseous species were admitted through the gas inlet system. The ion intensities of singly charged ions of the above species were measured as a function of electron energy (ionisation efficiency curve) and the appearance energies were obtained by linear extrapolation method. The equation corresponding to the linear relationship shown in the figure was used to deduce the actual electron energy. This procedure was used previously by Hilpert and Gingerich [50]. The species used for calibration were so chosen such that, the first ionisation energy of these ions cover a range of up to 20-25 eV in the electron energy scale. The electron energy calibration experiments were carried out periodically to check the validity of the existing calibration.

1B.14 Application of KEMS in nuclear industry

Loss of materials due to vaporisation, change from one form to another, undesirable changes in the mechanical properties due to decomposition and chemical reactivity are some of the aspects that alter the properties of materials and more significantly at high temperatures. Determination and understanding of the phase diagrams, the phase transformations, vapour pressures and the energies associated with phase transition in the range of temperatures of interest thus become essential in the evaluation of materials for many technologies and the realization of these technologies. In each and every stage of the nuclear fuel cycle, thermochemistry plays an important role. In a nuclear reactor, a fuel made of fissile material in a suitable chemical form is contained in a clad material. For the manufacture and use of oxide fuel of desirable stoichiometry, oxygen potential data are required as this plays a very important role in the determination of the physicochemical behavior of the fuel [51-54]. It is important to evaluate the various solid-gas and gas phase equilibria concerning the fuel at temperatures which it would experience. This requires knowledge of composition of vapour phase over the fuel. On the other hand, nuclear engineers require the values of the thermodynamic functions, for assessing the fuel life and integrity, from the safety analysis perspective [55]. Nuclear reactor fuels, especially after being subjected to high burn up, are some of the most complex high temperature materials, with host of fission products and heavy elements. Some of the fission products under the hot chemically reactive environment existing inside the reactor can attack the clad resulting in the formation of low melting alloys which may affect the mechanical strength of the clad. Other chemical interaction like fuel coolant, fuel-fission product can also occur and become more complicated with increase in burn-up. Assessment of such interactions is required to understand the behavior of the fuel under normal and under extreme conditions such as circumstances leading to accidents. The chemical states of irradiated fuel also influence its reprocessing and waste disposal processes [56]. Thermodynamic properties are also required for materials used in power plant boilers, gas turbines and other advanced energy devices that are exposed to corrosive and high operation temperatures. KEMS can effectively be employed to address many of the above issues through determining vapour pressure and thermodynamic properties of the concerned materials.

1.5 Scope of the present study

TIMS is one of the Nuclear Analytical Technique (NAT) for determining the isotopic composition of various elements like Li, B, Mg, Sr, Zr, Mo, Sb, Cs, Ba, La, Ce, Nd, Sm, Gd, Er, Lu, Pb, Th, U, Np, Pu, Am etc. In the present work, thermal ionisation mass spectrometric studies were carried out on elements like U, Pu, Nd, La, Mo, Mg, Li and Gd. TIMS provides isotopic ratios with very good precision and accuracy and hence is considered as gold standard for nuclear material accounting (NUMAC). ID-TIMS is also a certified method for reporting burn-up of irradiated fuels. Uranium plutonium mixed oxide (MOX) is the fuel which will be used for Prototype Fast Breeder Reactor (PFBR) and for future fast breeder reactors. Accurate and precise burn-up measurement of irradiated MOX fuel helps in validating its performance in the reactor. Hence it is important to obtain information on burn-up of MOX based fuel. Also ^{148}Nd is usually employed as fission product monitor for the determination of burn-up in thermal reactors. However in the case of fast reactors with different fuel compositions, it is important that accurate burn-up are measured using suitable fission product monitors. Taking into consideration the above aspects, the burn-up studies have been carried out on MOX dissolver solution; molybdenum and lanthanum are examined as alternate burn-up monitors. Studies on PHWR dissolver solution using TIMS by employing molybdenum and lanthanum as alternate fission product monitors have been taken up and burn-up data obtained are compared with those obtained using Nd-148 burn-up monitor. Also individual separations of lanthanides and actinides have been investigated on reversed phase supports such as small particle (1.8 μm) and monolith based supports. These methods were subsequently employed for the burn-up measurement on dissolver solutions of nuclear reactor fuels. The high ionisation energy of molybdenum results in poor thermal ionisation efficiency. Hence new sample loading procedure has been examined to improve the ionisation efficiency. To overcome the natural isobaric interference during analysis of lanthanum a new sample loading procedure has been developed to provide better ion intensities of its compound rather than as metallic species.

The precise isotopic ratio measurements of elements of interest are also crucial in isotope enrichment plants, radioactive waste management facility and reprocessing plants. Magnesium is an aspirant tracer element for accurate measurement of volume in reprocessing input tank. Hence, TIMS has been used for determining isotopic ratio measurement of magnesium in SRM-980 standard solution by employing new sample loading method. Glass bonded sodalite (GBS) is a promising candidate for the immobilisation of the chloride waste resulting from pyrometallurgical reprocessing of nuclear fuels. Accurate and precise quantification of the constituent elements in sodalite is essential to develop a suitable waste storage matrix. TIMS along with IDMS is employed for quantification of lithium and neodymium in sodalite sample. Gadolinium (particularly ^{155}Gd and ^{157}Gd isotopes) acts as an effective neutron poison due to its high neutron absorbing cross section and plays an important role in nuclear fuel cycle. Hence the use of enriched gadolinium ($^{155, 157}$Gd) will reduce the gadolinium inventory and this provides a good economic incentive. TIMS analysis on gadolinium samples collected using HPLC separation, using multiple columns with different experimental conditions, have been studied for gadolinium enrichment.

Knudsen effusion mass spectrometer is a versatile and dynamic technique that provides reliable vapour pressure and thermodynamic data of nuclear material of interest. It helps in determining the basic thermodynamic properties of the compounds that are formed due to interaction of, fuel - clad, fuel - fission products, fission product - fission product and those relevant to reprocessing. In the present work studies on following system have been undertaken by KEMS to determine vapour pressure and other thermodynamic properties.

(i) U-Al system: These alloys are used as fuel in research reactors,

(ii) U-Sn system: Intermetallic compounds of uranium and plutonium with tin and noble metal fission products are relevant in irradiated mixed oxide fuel,

(iii) Gd-Al system: Intermetallics of the Gd-Al system are of interest to understand the behaviour of gadolinium during electro refining.

Hence, KEMS has been employed to determine vapour pressure and thermodynamic properties over (UAl_2+UAl_3), (USn_3+U_3Sn_7) and ($GdAl_2$+$GdAl_3$) biphasic region of U-Al, U-Sn, Gd-Al system, respectively.

References

[1] H. J. Bhabha, Proc. Int. Conf. on the Peaceful uses of Atomic Energy, 1, Geneva (1955) 103.

[2] I. T. Platzner, “Modern isotope ratio mass spectrometry” John Wiley & Sons (1997).

[3] J. Roboz, “Introduction to mass spectrometry” John Wiley & Sons (1968).

[4] J. H. Gross, “Mass spectrometry” Springer (2011).

[5] S. K. Aggarwal, H. C. Jain, “Introduction to mass spectrometry” Indian Society for Mass spectrometry (1997).

[6] D. A. Skoog, D. M. West, F. J. Holler, S. R. Crouch, “Fundamental of analytical chemistry” Brooks Cole (2013).

[7] J. Griffiths, Anal. Chem. 80 (2008) 5678.

[8] S. E. Van Bramer, “An introduction to mass spectrometry” (1998).

[9] K. G. Heumann, Isotope Dilution Mass Spectrometry, Int. J. Mass Spec. Ion Processes, 118 (1992) 575.

[10] S. K. Aggarwal, Anal. Methods, 8 (2016) 942.

[11] J. E. Rein and B. F. Rider, “TID-17385, Progress Report, AEC Research and Development Report (1962).

[12] W. J. Maeck, W. A. Emel, J. E. Delmore, F. A. Duce, L. L. Dickerson, J. H. Keller, R. L. Tromp, Report No. EY-76-C-07-1540 (1976).

[13] A. J. Fudge, A. J. Wood, M. F. Banham, Report TID-7629, 152 (1961).

[14] ASTM Standards E 321 - 96 (Reapproved 2005); “Standard Test Method for Atom Percent Fission in Uranium and Plutonium Fuel (Neodymium-148 Method)”, PA 19428 2959, United States.

[15] P. Deregge, R. Boden, J. Radioanal. Chem. 35 (1977) 173.

[16] D. Karunasagar, M. Joseph, B. Saha, C. K. Mathews, Sep. Sci. Tech. 23 (1988) 1949.

[17] C. H. Knight, R. M. Cassidy, B. M. Recoskie, L.W. Green, Anal. Chem. 56 (1984) 474.

[18] N. Sivaraman, S. Subramaniam, T.G. Srinivasan, P. R. Vasudeva Rao, J. Radioanal. Nucl. Chem. 253 (2002) 35.

[19] R. M. Cassidy, S. Elchuk, N. L. Elliot, L. W. Green, C. H. Knight, B. M. Recoskie, Anal. Chem. 58 (1986) 1181.

[20] P. A. Sewell, B. Clarke, Chromatographic separations, analytical chemistry by open learning, John Wiley & Sons, New York (1987).

[21] L. R. Snyder, J. J. Kirkland, Introduction to modern liquid chromatography, 2nd Ed., John Wiley & Sonc, Inc, New York (1979).

[22] E. Sugrue, P. N. Nesterenko, B. Paull, Anal. Chim. Acta, 553 (2005) 27.

[23] J. Scancar, R. Milacic, Trends in Anal. Chem. 28 (2009) 1048.

[24] E. Browne, R. B. Firestone; Ed. V. S. Shirley; Table of Radioactive Isotopes; Lawrence Berkeley Laboratory, University of California; John Wiley & Sons, USA (1986).

[25] Physico-Chemical Measurements in Metals Research, Ed. R.F. Bunshah, John Wiley, New York (1970).

[26] K. D. Carlson, P. W. Gilles, R. J. Thorn, J. Chem. Phys. 38 (1963) 2064.

[27] Kleykamp, G. Chattopadhyay, PSB-Ber. 1549 (K1-II) Institut für Material and Festkörperforschung, KFK, Karlsruhe (1982).

[28] K. Hilpert, Ber. Bunsenges. Phys. Chem. 91 (1984) 724.

[29] K. Hilpert, Structure and Bonding 73, Springer-Verlag Berlin (1990) 97.

[30] Proceedings of the 10th Materials Research Symposium on Characterisation of High Temperature Vapors and Gases, Gaithersburg, Maryland, Sep. 18-22, 1978, Ed: J. W. Hastie, Nat. Bur. Std. Spc. Pub. 561/1, 3 (1979).

[31] Physico-Chemical Measurements in Metals Research, Ed. R. A. Rapp, Part I, Techniques of Metals Research, Vol. IV, Series Ed. R.F. Bunshah, John Wiley, New York (1970).

[32] K. D. Carlson, The Molecualr and Viscous Effusion of Saturated Vapours, ANL-6156 (1960).

[33] J. Drowart, P. Goldfinger, Angew. Chem., Intl. Ed. 6 (1967) 581.

[34] Electron Impact Phenomenon and the Properties of Gaseous Ions, Ed. F. H. Field, J. L. Franklin, Acad. Press (1970).

[35] P. Graber, K. G. Weil, Ber. Bunsenges. Phys. Chem. 76 (1972) 410.

[36] O. Bernauer, K. G. Weil, Ber. Bunsenges. Phys. Chem. 78 (1974) 1339.

[37] R. Viswanathan, Ph. D. Thesis (University of Madras) (1991).

[38] R. F. Pottie, J. Chem. Phys. 44 (1966) 916.

[39] J. W. Otvos, D. P. Stevenson, J. Am. Chem. Soc. 78 (1956) 546.

[40] J. B. Mann, in: Recent Developments in Mass Spectroscopy, Ed. K. Ogata, T. Hayakawa, University of Tokyo Press (1970) 814.

[41] C. K. Mathews, M. Sai Baba, T. S. Lakshmi Narasimhan, R. Balasubramanian, N. Sivaraman, T. G. Srinivasan, P. R. Vasudeva Rao, J. Phys. Chem. 96 (1992) 3566.

[42] C. K. Mathews, M. Sai Baba, T. S. Lakshmi Narasimhan, R. Balasubramanian, N. Sivaraman, T. G. Srinivasan, P. R. Vasudeva Rao, Full. Sci. Tech. 1 (1993) 101.

[43] R. Viswanathan, M. Sai Baba, D. Darwin Albert Raj, R. Balasubramanian, T. S. Lakshmi Narasimhan, C. K. Mathews, Spectrochim. Acta, 49B (1994) 243.

[44] R. C. Paule, J. Mandel, Analysis of Inter-laboratory Measurements on the Vapour Pressures of Cadmium and Silver, Nat. Bur. Std. (U.S.) Spl. Pub. 260-21 (1971).

[45] O. Kubaschewski, C. B. Alcock, Metallurgical Thermochemistry, 5th Ed., Pergamon Press, Oxford (1989).

[46] D. R. Gaskell, Introduction to Metallurgical Thermodynamics, McGraw-Hill Kogakusha Ltd. Tokyo (1973).

[47] T. S. Lakshmi Narasimhan, Ph. D. Thesis (Madras University) (2000).

[48] R. Hultgren, P. D. Desai, D. T. Hawkins, M. Gleiser, K. K. Kelley, D. D. Wagman, “Selected values of the Thermodynamic properties of Metals and Alloys”, American Soc. Metal, Metal Park, Ohio (1973).

[49] C. E. Moore, Ionisation Potentials and Ionisation Limits Derived from the Analyses of Optical spectra, NSRDS-NBS 34 (US Nat. Std. Ref. Data Ser., Nat. Bur. Std., U.S., 34) (1970).

[50] K. Hilpert, K. A. Gingerich, Int. J. Mass Spectrom. Ion Phys. 47 (1983) 247.

[51] High Temperature Chemistry of Inorganic and Ceramic Materials (Spl. Pub. No. 30), Ed. F. P. Glasser, P. E. Potter, The chem. Society, September (1976).

[52] E. H. P. Cordfunke, J. Nucl. Mater. 130 (1985) 82.

[53] D. Darwin Albert Raj, Ph. D. Thesis (University of Madras) (2008).

[54] P. Manikandan, Ph. D. Thesis (Homi Bhabha National Institute) (2017).

[55] Thermodynamics of Nuclear Materials, Proceedings Series, 1 (1979) (Proceedings of International Symposium on Thermodynamics of Nuclear Materials, IAEA, Julich, Germany, 29th - 2nd February (1979).

[56] Hj. Matzke, Science of Advanced LMFBR Fuels, North-Holland, Amsterdam (1986).

CHAPTER 2

===

Burn-Up Measurements on Dissolver Solution of Mixed Oxide Fuel Using HPLC-Mass Spectrometric Method

This chapter deals with determination of burn-up on irradiated mixed oxide fuel using thermal ionisation mass spectrometric and high performance liquid chromatographic techniques [1].

2.1 Introduction

During nuclear chain reaction, heavy elements undergo fission reaction to produce, a series of daughter products, ~2-3 neutrons (which helps in sustaining the chain reaction) and energy of ~200 MeV per atom fission. The burn-up of a fuel is a measure of the number of fissions undergone by the fuel [2]. Determination of burn-up is an important parameter for the study of nuclear fuel performance and is a measure of energy produced from unit mass of the fuel. The atom percent burn-up expression is essentially the ratio of the number of fissions that have occurred to the total heavy atoms initially present. The measurement of burn-up on dissolver solution of fuel subjected to high burn-up is challenging due to the high levels of radioactivity associated with the fuel. Various methods have been reported to measure the burn-up of spent nuclear fuels [2-9]. Among these, isotope dilution mass spectrometry (IDMS) using thermal ionisation mass spectrometry is recognised as ASTM standard method [3]. HPLC based techniques have been developed for rapid separation and determination of burn-up of nuclear reactor fuels [6, 8].

Fission product monitor method is a well established method for the determination of burn-up in an irradiated nuclear fuel [2]. The mass spectrometric method uses the isotopic dilution technique to measure the concentration of the burn-up monitor and the residual heavy elements present in the spent fuel to deduce the burn-up. As described in chapter 1A, the criteria for choosing a particular fission product monitor stems from the desired nuclear properties such as fission yield, neutron absorption cross section, decay constant and its migration into the fuel matrix to give reliable burn-up value [2]. Based on the above considerations, ^{148}Nd is by far the most widely used burn-up monitor using mass spectrometric measurements [2, 3, 7].

The burn-up (BU) is obtained from the relation:

$$BU\ (atom\ \%\ fission) = \frac{N(^{M}Nd)/Y(^{M}Nd)}{[N(U)+N(Pu)+(N(^{M}Nd)/Y(^{M}Nd))]} \times 100 \qquad (2.1)$$

Where "*N*" represents the concentration (number of atoms per gram of the dissolver solution) of the nuclide or element given in the parentheses; and "*Y*" represents the fractional fast fission yield for ^{M}Nd. In this study, "M" refers to mass numbers of Nd: 148, 145, and 146 wherever applicable and the rationale behind considering these isotopes for computing the burn-up is discussed later.

In the present study, results on the determination of burn-up on dissolver solution of nuclear reactor fuel, namely uranium-plutonium mixed oxide (MOX) spent fuel by mass spectrometric method are discussed. The HPLC based techniques using dynamic ion-exchange (for the separation of individual lanthanides) and reversed phase chromatography (for the separation of uranium and plutonium) were employed for the determination of concentration of lanthanides and actinides [4-6, 8].

The pure fractions of neodymium, uranium and plutonium required for mass spectrometric studies are conventionally obtained using time consuming traditional ion-exchange chromatographic procedure using gravity flow. However, in the present study, these metal ion fractions were rapidly isolated employing HPLC technique, i.e.

the dissolver solution was injected into the HPLC system after appropriate dilutions for the isolation of desired fractions of fission products and actinides. The neodymium fraction required for TIMS measurements was obtained by its isolation from other lanthanide fission products using dynamic ion exchange chromatographic method, whereas pure fractions of uranium and plutonium were obtained using reversed phase chromatographic technique. The fractional fission and the atom percent fission were computed using isotopic ratios and concentrations of neodymium, uranium and plutonium obtained employing ID-TIMS technique.

2.2 Experimental

Mass spectrometric and HPLC determination of burn-up of MOX fuel pellets were carried out on a test irradiated fuel, discharged from Fast Breeder Test Reactor (FBTR) at Kalpakkam. The U-Pu mixed oxide fuel with 29% ± 1% PuO_2 (76% ^{239}Pu in total plutonium) and rest UO_2 enriched in ^{233}U (53.5% ^{233}U in total uranium) was used. One of the irradiated fuel pellet was dissolved in 11 M HNO_3 medium in the hot cells. An aliquot of the dissolver solution containing uranium, plutonium, lanthanides and other fission products in HNO_3 medium (with permissible external dose) was taken inside a fume hood, evaporated to near dryness under IR lamp and re-dissolved in 8 M HNO_3 medium. Subsequently, the solution was diluted with a solution of alpha hydroxy isobutyric acid (α-HIBA) and directly injected into the HPLC system with appropriate dilutions for the determination of lanthanide fission products, uranium and plutonium. The pure fraction of Nd was collected at an appropriate retention time and was analysed for isotopic analysis by TIMS. Similarly, the pure U and Pu fractions for TIMS were collected from reversed phase chromatographic technique. Identical separation procedures were followed after the addition of spikes viz. ^{238}U, ^{239}Pu and

^{142}Nd to the dissolver sample for concentration measurement by TIMS. The samples (about 2 μg in the case of uranium and plutonium and 1 μg in the case of neodymium) were loaded onto a side filament of the triple filament assembly with Ta-Re-Ta configuration.

2.2.1 HPLC analysis

The HPLC system (M/s JASCO, Japan) was set-up in fume hood for separation of fission product monitors and actinides. The details of the instrument are explained in chapter 1AA.4. Reversed phase monolithic column (Merck) with dimensions: 100 mm (length) × 4.6 mm (inner diameter), surface area: 300 m^2g^{-1}, macroporous structure: 2 μm and mesoporous structure: 13 nm, was used. The lanthanide and actinide (U and Pu) complexes were detected at 655 nm. For the preparation of calibration plots, 20 μL of lanthanide samples (La - Sm) over the concentration range of 2 - 50 μg/mL were injected into the HPLC system. In the reversed phase chromatographic study, uranium *i.e.* UO_2^{+2} (10 - 100 ppm) and plutonium *i.e.* Pu (IV) (10 - 75 ppm) nitrate solutions were injected into the HPLC system for getting the calibration graph. Sodium nitrite solution (~50 µL) was added to an aliquot of dissolver solution to ensure plutonium is retained in Pu(IV) oxidation state.

2.2.2 Separation of lanthanide fission products using HPLC with dynamic ion exchange column

The reversed phase monolith column was modified into a dynamic ion-exchange support using water soluble modifier, e.g., ion-pairing reagent, camphor-10-sulfonic acid (CSA) as reported earlier [10-12]. The lanthanides were separated and eluted using alpha hydroxy isobutyric acid (α-HIBA). About 30 mL of mobile phase (0.02 M CSA + 0.1 M α-HIBA, pH adjusted to 3.1 with dil. NH_3) was passed through the monolithic reversed phase column to establish a dynamic ion-exchange surface. The chromatogram of HPLC separated lanthanides in MOX dissolver solution is given in Figure 2.1.

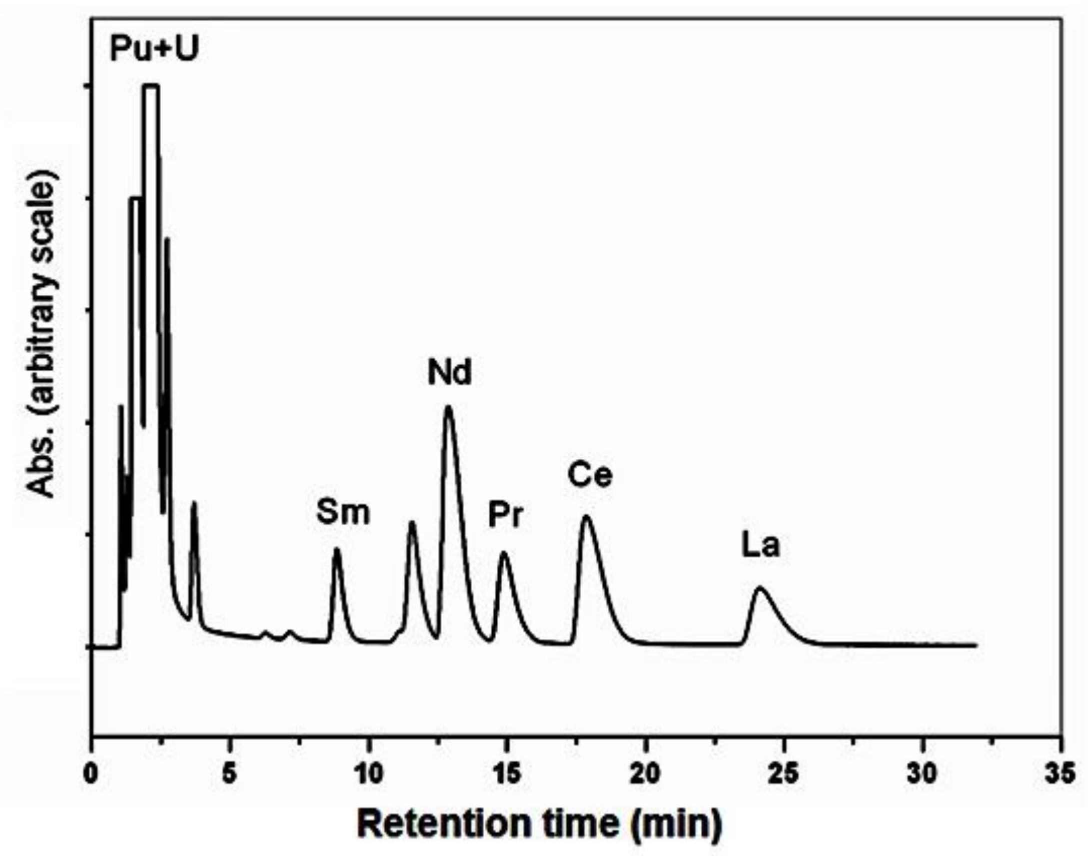

Fig. 2.1 Direct injection of MOX dissolver solution into HPLC for separation and determination of lanthanide fission products. Mobile phase: 0.02 M CSA + 0.1 M HIBA, pH: 3.1, Flow rate: 2 mL/min; post-column reagent (PCR): Arsenazo (III) (10^{-4} M); flow rate: 1 mL/min; detection of lanthanide-arsenazo(III) complexes: 655 nm. Sample: aliquot of MOX fuel ~110 GWd/t dissolved in mobile phase and injected into HPLC.

2.2.3 Separation and determination of uranium and plutonium with HPLC using reversed phase chromatography

Uranium and plutonium present in the dissolver solution were separated and determined by both dynamic ion-exchange and reversed phase chromatographic techniques. Uranium as well as plutonium were not determined in the same run along with lanthanides since the U and Pu peaks showed near saturation during the assay of the lanthanide fraction in the dynamic ion-exchange experiments. The dissolver solution was directly injected after appropriate dilution for the determination of uranium or plutonium. The spectra of uranium and plutonium separated by HPLC from dissolver solution are shown in Fig. 2.2.

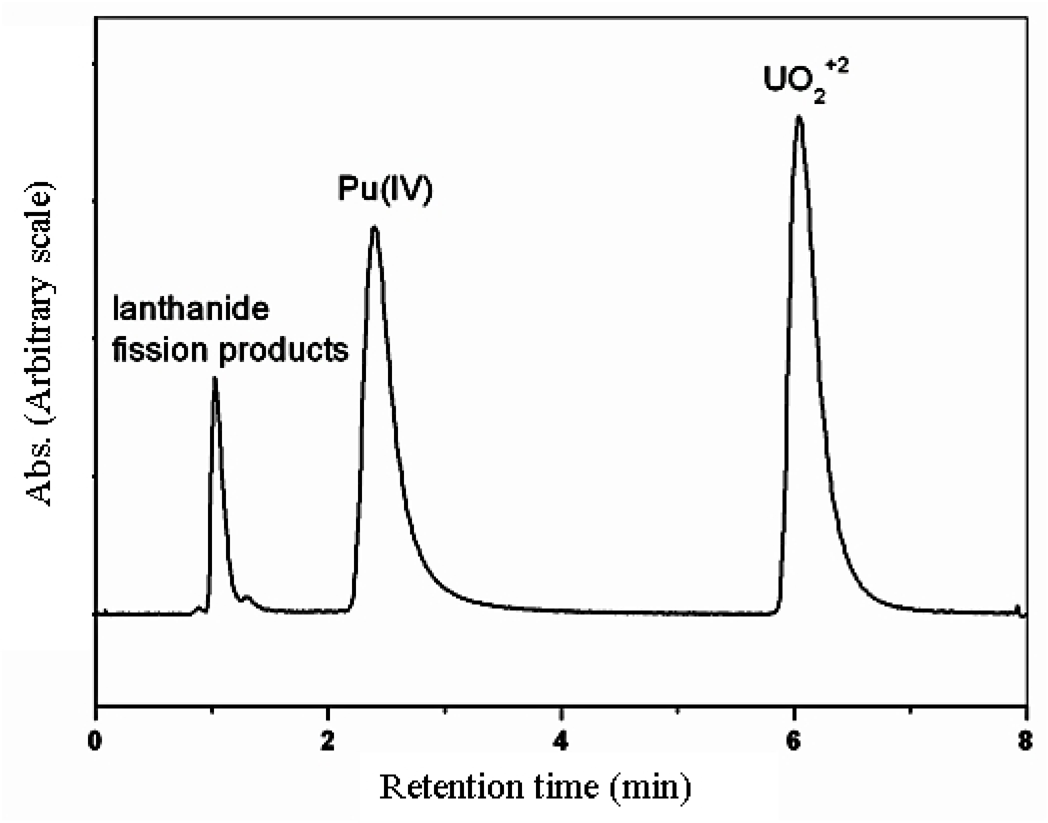

Fig. 2.2 Separation and determination of uranium and plutonium present in dissolver solution of MOX fuel by reversed phase chromatography. Mobile phase: 0.1 M α-HIBA, pH: 3.75, Flow rate: 2 mL/min; PCR Arsenazo (III) at 655 nm. Sample: dissolver solution of MOX.

The reversed phase HPLC technique using monolith support was also employed in the present work for the separation and determination of uranium (UO_2^{+2}) and plutonium Pu (IV).

2.2.4 Sample preparation for TIMS

The pure neodymium, uranium and plutonium fractions obtained from HPLC separations were evaporated to near dryness and were re-dissolved in 8 M HNO_3. This procedure *i.e.* dissolution of fractions in HNO_3 medium was repeated three times to minimise the organics (CSA and HIBA) during the loading of neodymium, uranium and plutonium fractions on the tantalum filament. The conditioned samples (pure fractions of Nd, U and Pu) were loaded with 0.75 M HNO_3 medium on tantalum side filaments using triple filament assembly (Ta-Re-Ta). This filament configuration provides better control on sample evaporation with effective ionisation. The samples were loaded on filament surface using an external sample loading instrument. Samples were dried on filament surface by passing a constant current of 1.2 A. Once dried, filament current was increased to 1.4 A for ~20 second to remove any moisture in samples. Unspiked (pure fraction) and spiked samples of neodymium, uranium and plutonium were loaded in duplicate on filament surface for acquiring reproducible isotopic composition data during measurements.

2.2.5 Experimental condition for TIMS

The isotopic ratios were measured using a multicollector thermal ionisation mass spectrometer (ISOPROBE-T, M/s ISOTOPX, UK). The details of the instrument have already been described in chapter 1A.10. Prior to running the isotopic ratio measurement program, it is necessary to performe collector gain calibration, since the measurements were done in static multi collector mode. The samples were first heated using an in-built program to ramp up the filament current slowly to 4.0 A and 1.0 A for central (ionisation) and side (vaporisation) filaments, respectively. At this stage, Re^+ signal (usually about 60 - 70 mV) was measured and the focus conditions were optimised using the controls provided for various focus plates. Subsequently, the side filament currents were slowly increased to get minimum ion intensity for the peaks of interest. After proper focusing, flat topped isotopic peaks were obtained and all the peaks corresponding to different isotopes of an element were checked for coincidence which signifies the exact placement of collectors for the dispersed beams. Subsequently, the sample filament current was slowly ramped to obtain the ion intensity around 1 - 2 V for major peak. In general, central filament and side filaments were heated at 5.4 A and 2.3 A, respectively for a satisfactory analysis. The isotope ratios were obtained by comparing the ion intensities of all the beams acquired by the software. The isotopic ratios were obtained for pure fraction and mixture (sample + spike) for neodymium, uranium and plutonium.

The mass spectra of neodymium obtained from TIMS analysis for MOX dissolver solution is shown in Fig. 2.3. The non-existence of peak at mass number 142 indicates absence of any natural neodymium contamination in dissolver sample.

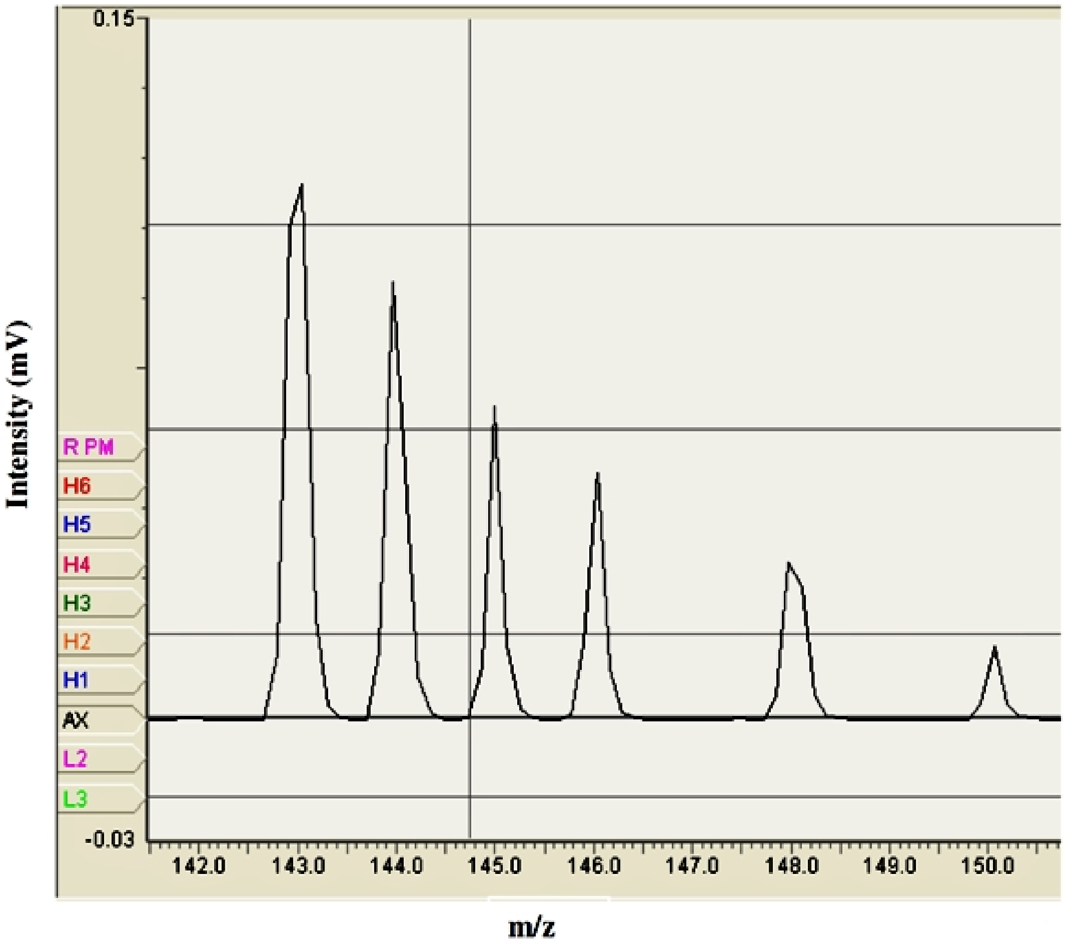

Fig. 2.3 Mass spectrum of neodymium in MOX dissolver solution.

Similarly, pre-treated uranium and plutonium fractions, collected after HPLC separation were subjected to TIMS analysis, to ascertain their isotopic composition and are shown in Figure 2.4. It gives credence to HPLC method for effective separation of uranium and plutonium from each other.

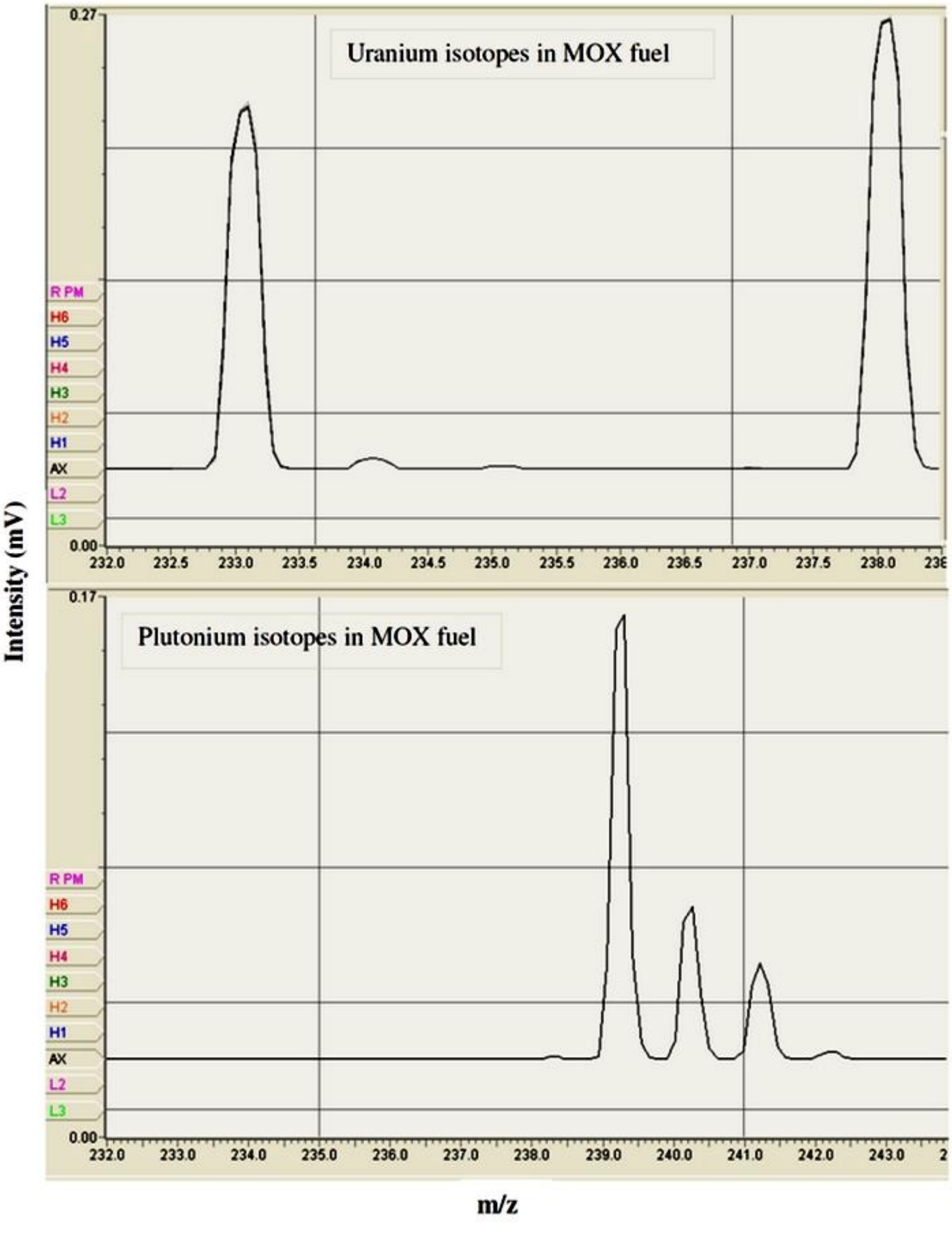

Fig. 2.4 Mass spectra of uranium (top) and plutonium (bottom) in MOX dissolver solution.

2.3 Results and Discussion

The fission product monitors, neodymium/lanthanum present in the dissolver solution were separated from each other as well as resolved from uranium and plutonium under dynamic ion-exchange conditions using HPLC is represented in chromatogram (Fig. 2.1). The concentrations of La, Ce, Pr, and Nd were determined in the dissolver solution using a calibration plot. Uranium and plutonium were also separated and determined by reversed phase chromatographic technique (Fig. 2.2). The concentrations of lanthanides (La, Ce, Pr, Nd and Sm) and actinides (U and Pu) in the dissolver solution of MOX fuel were estimated and the results are shown in Table 2.1. The isotopic ratios of neodymium (Table 2.2), uranium and plutonium (Table 2.3) were determined using TIMS. The concentrations of these elements (Nd, U and Pu), in MOX dissolver solutions was obtained using suitable spikes by employing IDMS technique and are listed in Table 2.4.

2.3.1 Computation of burn-up using HPLC technique

The HPLC technique can provide only an elemental rather than an isotopic yield. Thus the equation 2.1 can be rewritten in a simpler form to deduce burn-up using HPLC technique. Accordingly, the burn-up equation can be presented as follows:

$$\text{Atom \% fission} = \frac{(A/Y)}{[H+(A/Y)]} \times 100 \qquad (2.2)$$

where “A” is the number of atoms of fission product monitor (Nd or La), ‘Y’ is the effective fractional fission yield for “A” [13] and “H” is the residual heavy element (U + Pu) atoms in the dissolver solution. When sum of concentrations of all isotopes of a fission product monitor element is used (total elemental yield) for determination of “A”, the fractional fission yield, “Y” is obtained by summing up the fractional fission yield of all isotopes of the fission monitor and dividing by 100 [2]. In the present study, for computing burn-up, we have examined the possibility of using three different lanthanides as fission product monitors, namely, Nd, La and Pr. One of the necessary criteria for selecting a suitable fission product monitor is, it should have similar fission yield for all neutron energies from different fissioning elements.

Table 2.1 Estimation of lanthanides, uranium and plutonium in MOX dissolver solution.

Lanthanide fission products/ actinides	**Amount per gram of dissolver solution**	**Atom % burn-up**
Lanthanum (La-139)	204.9 μg	10.8
Cerium (Ce-140, 142)	401.1 μg	
Praseodymium (Pr-141)	201.6 μg	
Neodymium (Nd-143, 144, 145, 146, 148, 150)	573.2 μg	10.5[a)] 11[b)] 10.7[c)]
Samarium	123.1 μg	
Europium	8.5 μg	
Uranium	32.85 mg	
Plutonium	13.28 mg	

HPLC experimental conditions: mobile phase: 0.02 M CSA; 0.1 M HIBA; pH: 3.1 (lanthanide fission products separation); 0.1 M HIBA; pH: 3.75 (U-Pu separation).

[a)] ‘Y’ value used was 0.1743, where ‘Y’ was cumulative yield of all Nd isotopes exclusively from ^{233}U fast fissions [13].

[b)] ‘Y’ value used was 0.1641, where ‘Y’ was cumulative yield of all Nd isotopes exclusively from ^{239}Pu fast fissions [13].

[c)] ‘Y’ value used was 0.1696, where ‘Y’ was computed based on 54.2 % fast fissions from ^{233}U and 45.8 % fast fissions from ^{239}Pu. Fractional fissions were computed using TIMS. Burn-up was computed (HPLC technique) using equation (2.2)

The neodymium isotopes produced in the nuclear fission are ^{143}Nd, ^{144}Nd, ^{145}Nd, ^{146}Nd, ^{148}Nd and ^{150}Nd from both ^{233}U and ^{239}Pu fissile nuclides. The total neodymium yield is 16.41% and 17.43% for ^{239}Pu and ^{233}U (fast neutron fission) respectively, differing by about 6% [13]. During nuclear fission, the fission product lanthanum is formed with major isotope of ^{139}La and negligible amount of ^{138}La. Hence it necessitates, assessing total lanthanum using suitable chemical technique. However, the lanthanum yields for ^{239}Pu and ^{233}U fissions are 5.83% and 6.55% respectively, differing by about 11% [13]. Similarly, use of praseodymium (produced as ^{141}Pr) also results in a difference in the “Y” between ^{239}Pu (5.62 %) and ^{233}U fissions (7.00 %) by about 20% [13]. Thus, use of total Nd as fission product monitor can be regarded as better option than use of Pr or La. Further, the difference in “Y” gets minimised by employing fractional fission contributions from ^{233}U and ^{239}Pu for computing atom % burn-up. The atom % fission deduced from the HPLC measurements are summarised in Table 2.1.

2.3.2 Isotopic ratio measurements and atom % burn-up determination using TIMS

The isotopic ratios listed in Tables (2.2 and 2.3) for neodymium, uranium and plutonium are the mean of six individual runs and each run consisted of 36 measurements. The isotopic composition (in mass percent) of fission product neodymium was found to be: ^{143}Nd: 29.23; ^{144}Nd: 23.81; ^{145}Nd: 18.75; ^{146}Nd: 15.06; ^{148}Nd: 8.69; and ^{150}Nd: 4.46. The isotopic ratios, atom fractions and mass percent for neodymium are listed in Table 2.2.

Table 2.2 Isotopic ratios and abundances of neodymium in MOX dissolver solution.

Isotope M(i)	**Isotope ratio M(i)/M(ref)**	**Relative error in % in isotope ratio [a)]**	**Atom fraction of the isotope M(i)**	**Relative error in % in atom fraction [b)]**	**Mass % of the isotope M(i)**
Neodymium: M (ref) = 143; Average atomic weight = 144.70					
143	1	-	2.959×10^{-1}	0.05	29.230
144	8.090×10^{-1}	0.09	2.394×10^{-1}	0.11	23.812
145	6.324×10^{-1}	0.16	1.872×10^{-1}	0.17	18.745
146	5.045×10^{-1}	0.13	1.493×10^{-1}	0.14	15.058
148	2.873×10^{-1}	0.20	8.503×10^{-2}	0.21	8.692
150	1.456×10^{-1}	0.51	4.308×10^{-2}	0.51	4.464

[a)] Combination of internal and external error (standard deviation) associated with individual runs.

[b)] Derived from error associated with isotopic ratios using error propagation.

The isotopic composition (in mass percent) of uranium in the dissolver solution was observed to be: ^{238}U: 55.09; ^{233}U: 43.23; ^{234}U: 1.25; ^{235}U: 0.397; and ^{236}U: 0.036; for Plutonium, the values (in mass percent) are: ^{239}Pu: 72.80; ^{240}Pu: 24.27; ^{241}Pu: 1.56; ^{242}Pu: 1.14; and ^{238}Pu: 0.23. The atom fraction value for ^{238}Pu was taken from alpha spectrometric analysis to avoid any isobaric interference from ^{238}U. The details of isotopic ratios, atom fraction and mass percent for residual heavy elements (U and Pu) are listed in Table 2.3.

Table 2.3 Isotopic ratios and abundances of uranium and plutonium in MOX dissolver solution.

Isotope M(i)	**Isotope ratio M(i)/M(ref)**	**Relative error in % in isotope ratio** [b)]	**Atom fraction of the isotope M(i)**	**Relative error in % in atom fraction** [c)]	**Mass % of the isotope M(i)**
Uranium: M (ref) = 238; Average Atomic Weight = 235.80					
238	1	-	5.457×10^{-1}	0.06	55.094
234	2.302×10^{-2}	1.13	1.256×10^{-2}	1.13	1.247
235	7.301×10^{-3}	3.23	3.984×10^{-3}	3.23	0.397
236	6.63×10^{-4}	25.54	3.62×10^{-4}	25.5	0.036
233	8.014×10^{-1}	0.12	4.374×10^{-1}	0.14	43.226
Plutonium: M (ref) = 239; Average Atomic Weight = 239.36					
239	1	-	7.289×10^{-1}	0.02	72.802
238 [a)]	3.149×10^{-3}	2.0	2.296×10^{-3}	2.0	0.228
240	3.320×10^{-1}	0.05	2.420×10^{-1}	0.05	24.272
241	2.125×10^{-2}	0.56	1.549×10^{-2}	0.56	1.560
242	1.543×10^{-2}	0.56	1.125×10^{-2}	0.56	1.137

[a)] Deduced by combining mass spectrometric and alpha spectrometric results; error estimated to be 2%.

[b)] Combination of internal and external error (standard deviation) associated with individual runs

[c)] Derived from error associated with isotopic ratios using error propagation

ID-TIMS was employed to determine concentration of neodymium and actinides (U and Pu) in dissolver solution. The total number of atoms of residual heavy element (U and Pu) determined per gram of dissolver solution was found to be 11.1×10^{23}. Similarly the total (elemental) and individual (isotopic) number of atoms of neodymium present per gram of dissolver solution were determined. Burn-up in dissolver solution was deduced using equation (2.1), by incorporating number of atoms of fission product monitor (Nd), residual heavy elements (U and Pu), and the fractional fission yields data (*Y*) was taken from literature [13]. Since the test fuel is a combination of Pu recycled from thermal reactor and uranium enriched in ^{233}U to provide more fissile content, the fissions would be mainly contributed by ^{239}Pu and ^{233}U. Since one of the criteria for choosing a burn-up monitor is uniform fission yield from various sources of fission [2], different isotopes of neodymium were examined for deducing burn-up for this type of test fuel and the pair $^{145+146}$Nd having closely similar fast fission yields from ^{233}U (5.65 %) and ^{239}Pu (5.59 %) was chosen [13]. The ratios of neodymium isotopes *i.e.* $^{(145+146)}$Nd/^{150}Nd are widely different for these two sources of fission (12.12 for ^{233}U and 5.48 for ^{239}Pu). Hence the mass spectrometric data for these isotopes have been chosen for computing the fractional fissions. A similar approach was followed to compute fractional fissions in our earlier studies using HPLC [6]. The fractional fission contribution of ^{233}U and ^{239}Pu towards total fission is 54.2 % and 45.8 %, respectively. The detail of this calculation is given in Appendix-1. The atom % burn-up deduced from the concentrations of U, Pu and Nd was 10.8 (total Nd as monitor), 10.9 (Nd^{148} as monitor) and 10.9 ($^{(145 + 146)}$Nd as monitors) and are given in Table 2.4.

Table 2.4 Computation of burn-up using different isotopes of Nd determined by IDMS technique.

Fission product monitors	Total number of atoms determined per gram of dissolver solution	Atom % burn-up[a)]
^{Total} Nd	2.28×10^{22}	10.8
^{148}Nd	1.94×10^{21}	10.9
$^{(145 + 146)}$Nd	7.68×10^{21}	10.9

[a)] Total residual heavy element atoms (U + Pu) determined per gram of dissolver solution: 11.1×10^{23}.

The possible source of errors contributing to the computed burn-up are those arising from i) assay of fission product monitor, uranium and plutonium, ii) data on the fission yield of the fission product monitor and iii) computation of fractional fissions from ^{233}U and ^{239}Pu from isotopic measurements. The uncertainties in the assay of fission monitor, and heavy elements are minimized by the use of certified standards to < 1%. The uncertainty in the yields of fission monitors (e.g. Nd) obtained from literature is ~ 1 - 2%. The overall uncertainty arising from the individual contributions to the atom percent fission could extend to a maximum of 3 - 5%.

2.4 Conclusion

Burn-up measurements on mixed oxide test fuel pellet irradiated in FBTR was carried out through measurements on the dissolver solution using HPLC as well as TIMS technique. In one case, both the separation and determination of neodymium and actinides (U and Pu) were carried out using HPLC; in another case, isotopic composition measurements and quantification of elements of interest after HPLC separation were performed using TIMS. The rapid separation technique using dynamic ion exchange chromatographic technique was demonstrated for the separation of pure fractions of lanthanide fission products present in the dissolver solution of a mixed oxide fuel. Reversed phase chromatographic technique was employed for isolation of pure fractions of uranium and plutonium as well as for their assay in the dissolver solution. The pure fractions of neodymium, uranium and plutonium required for TIMS were isolated from the dissolver solutions using HPLC technique. Isotope dilution mass spectrometric method along with TIMS was employed to quantify different isotopes of neodymium, uranium and plutonium present in the dissolver solution. Fractional fissions from ^{233}U and ^{239}Pu were determined from these measurements. The atom percent fission (burn-up) was computed from these data. The atom % burn-up, computed using HPLC by considering fractional fission data shows a good agreement with those obtained from TIMS analysis.

References

[1] S. Bera, R. Balasubramanian, A. Datta, R. Sajimol, S. Nalini, T. S. Lakshmi Narasimhan, M. P. Antony, N. Sivaraman, K. Nagarajan, P. R. Vasudeva Rao, Int. J. Anal. Spec. Chrom. 1 (2013) 55.

[2] J. E. Rein, B. F. Rider, "TID-17385, Progress Report, AEC, Research and Development Report (1962).

[3] ASTM Standards E, "Standard Test Method for Atom Percent Fission in Uranium and Plutonium Fuel (Neodymium-148 Method)," ASTM Standards E321-96 (2005).

[4] C. H. Knight, R. M. Cassidy, B. M. Recoskie, L. W. Green, Anal. Chem. 56, 3 (1984) 474.

[5] R. M. Cassidy, S. Elchuk, N. L. Elliot, L. W. Green, C. H. Knight, B. M. Recoskie, Anal. Chem. 58, 6 (1986) 1181.

[6] N. Sivaraman, S. Subramaniam, T. G. Srinivasan, P. R. Vasudeva Rao, J. Radioanal. Nucl. Chem. 253, 1 (2002) 35.

[7] R. Balasubramanian, D. Darwin Albert Raj, S. Nalini, M. Sai Baba, Int. J. Nucl. Energy Sci. Tech. 1, 2-3 (2005) 197.

[8] A. Datta, N. Sivaraman, T. G. Srinivasan, P. R. Vasudeva Rao, Nucl. Tech. 182 (2013) 84.

[9] P. G. Jaison, N. M. Raut, S. K. Aggarwal, J. Chrom. A, 1122, 1-2 (2006) 47.

[10] P. R. Vasudeva Rao, N. Sivaraman, T. G. Srinivasan, In: Encyclopedia of Chrom. Taylor & Francis (2005).

[11] A. Datta, N. Sivaraman, T. G. Srinivasan, P. R. Vasudeva Rao, Radiochimica Acta, 98 (2010) 277.

[12] A. Datta, N. Sivaraman, T. G. Srinivasan, P. R. Vasudeva Rao, Radiochimica Acta, 99 (2011) 275.

[13] E. A C. Crouch, "Atomic Data and Nuclear Data Tables: Fission Product Yields from Neutron Induced Fission," Academic Press, New York and London, 19 (1977).

CHAPTER 3

==

Studies on use of Molybdenum and Lanthanum as alternate burn-up monitors

During the nuclear fission of ^{235}U and ^{239}Pu, various fission products [1, 2] are produced in the mass ranges of 80 - 160 Da. Quantification of selected fission products can be used to evaluate the efficiency of fuel utilised in a nuclear reactor, commonly known as burn-up [3-7]. One of the well established methods for the determination of burn-up is by fission product monitor method [8-11]. The details of burn-up determination using fission product monitor method were discussed in chapter 1A. The equation governing burn-up calculation, used in the present work is given below.

$$\text{Burn-up (atom \% fission)} = \frac{(\mathrm{A}/\mathrm{Y})}{[\mathrm{H}+(\mathrm{A}/\mathrm{Y})]} \times 100 \tag{3.1}$$

where A is the numbers of atoms of fission product monitor (molybdenum or neodymium), Y is the effective fractional fission yield for ‘A’ and H is the number of residual heavy element atoms (uranium and plutonium) present in the dissolver solution. The required criteria for selecting a fission product monitor are mentioned in chapter 1A. There is no single nuclide that satisfies all the required criteria to qualify as an ideal burn-up monitor in nuclear reactors of different types with fuels of varying compositions (uranium based/ plutonium based). Burn-up monitor can be any fission product viz. Zr, Mo, Ru, La, Ce, Nd, Sm, which satisfies most of the criteria and the selection depend on the type of reactor and the fuel employed [12]. ^{148}Nd is one of the most commonly used and well established fission product monitor for thermal reactor fuels as it satisfies most of the desirable properties of a monitor [13]. For fast reactor fuels, where ^{239}Pu is the major source of fission, ^{233}U based fuel and U-Pu-Zr based metallic fuels need alternate burn-up monitors. In this context, molybdenum and lanthanum were explored as alternate fission product monitors in present investigation. Chromatographic and mass spectrometric methods have been developed for use of molybdenum and lanthanum as burn-up monitors.

Chapter 3A: discusses about the methodology adopted for molybdenum and

Chapter 3B: describes the procedure employed for lanthanum.

CHAPTER 3A

Molybdenum as alternate burn-up monitor

In this chapter, molybdenum as burn-up monitor was ascertained by employing HPLC and TIMS techniques is discussed.

3A.1 Introduction

Among fission products, molybdenum is the second most abundant fission product in the fission yield curve [1, 2], posses the required characteristics to get qualified as burn-up monitor. The advantage of molybdenum as fission product monitor over neodymium is that the cumulative thermal fission yields from ^{235}U and ^{239}Pu for the former is higher with the values of 24.49 and 22.94% respectively as compared to 20.69 and 16.40% of latter [14, 15]. Apart from this, molybdenum possesses a few other features like, a) low thermal neutron absorption cross section for its isotopes, b) shielded isotopes of same element (92, 94, 96) and c) stable isotopes. This makes molybdenum a suitable alternate for neodymium.

Molybdenum in nature has seven stable isotopes 92, 94, 95, 96, 97, 98, 100. Among these, $^{92,\ 94,\ 96}$Mo are not formed in the reactor due to stable isotopes of zirconium which is a precursor in the decay chain. The molybdenum isotopes produced in the nuclear reactor during the fission of ^{235}U and ^{239}Pu are 95, 97, 98 and 100. The high first ionisation energy of 7.1 eV for molybdenum results in low ionisation efficiency during TIMS analysis. Hence a suitable loading procedure is required to enhance its ionisation efficiency. Additionally, molybdenum (VI) has higher vapour pressure compared to molybdenum (III) and hence it is essential that molybdenum exists in (III) state to avoid vaporisation losses before the sample reaches the ionisation temperature, during TIMS analysis. This has been accomplished by reducing molybdenum (VI) to molybdenum (III) state using HCl medium.

Murthy [16] had separated microgram quantities of molybdenum from other elements in terrestrial and meteorites samples by employing Dowex anion exchange resin. Subsequently, the concentration was determined using TIMS by converting molybdenum to MoS_2 and loading onto a tantalum filament. Wetherill [17] also used a similar procedure to separate and analyse molybdenum from the same terrestrial and meteorite samples, however by using rhenium filament with double spike method. Moore et al. [18] had reported TIMS results for molybdenum-standard reference material by reducing ammonium molybdate to molybdenum metal in the presence of hydrogen gas on zone refined rhenium filament surface. Qi-Lu et al. [19, 20] had carried out solvent extraction and TIMS methods to extract molybdenum and zirconium from ruthenium using di-(2-ethylhexyl) phosphoric acid (HDEHP) - cyclohexane as the solvent. Molybdenum was selectively stripped to aqueous phase from zirconium by reducing with 3% H_2O_2 in 10 M HNO_3 solution. Molybdenum, thus separated was loaded as ammonium paramolybdate along with boric acid in 1 M HNO_3 medium on a side rhenium filament. Out-gassed triple rhenium filament assembly was used to avoid molybdenum contamination from filament surface and for better control on heating of the sample. Kawashima et al. [21] had measured the isotopic composition of molybdenum in a standard solution by converting it to molybdenum (VI) dichloride dioxide (MoO_2Cl_2) with 6 M HCl and subsequently reduced to molybdenum (III) by using a mixture of ascorbic acid and ammonium iodide. This was loaded on a rhenium filament and coated with rhenium - platinum slurry to enhance the ionisation efficiency. Wieser et al. [22] had used an ion exchange method to purify molybdenum from other impurities. Molybdenum thus separated was loaded in sub-microgram quantities on a rhenium single filament along with freshly prepared ascorbic acid solution in 4 M HCl medium and a silica gel suspension layer was deposited above this, to achieve enhancement in ion intensity. Forsyth [12] used molybdenum as fission product monitor for two different fuels and compared the burn-up with those obtained from heavy element difference (^{235}U depletion) and radiochemical methods. A good agreement was seen in the burn-up values obtained by these methods. One of the concerns in using molybdenum as fission product monitor is its redistribution or loss from fuel matrix at higher temperatures. However as long as the whole fuel pellet or pin is considered for analysis, there will not be any actual loss of molybdenum from specimen sample.

As can be seen, separation of molybdenum from various solutions had been carried out by using either ion exchange or solvent extraction methods. However the high radioactivity of the spent fuel, demands a quick and effective separation of molybdenum from the dissolver solution. Hence in the present study, we have developed a new HPLC method for quick and effective separation of molybdenum from zirconium, ruthenium and other fission products. For TIMS analysis, a sample loading method was developed, where a mixture of solution containing molybdenum and ascorbic acid in 4 M HCl was loaded on an out-gassed rhenium filament followed by deposition of a layer of silicic acid above the mixture.

HPLC method developed earlier [23-26] was used to separate neodymium and actinides (U and Pu) from other fission products. Concentration of molybdenum in the spent pressurised heavy water reactor (PHWR) dissolver solution was determined by using IDMS method. Subsequently burn-up was computed using molybdenum as fission product monitor. The burn-up data thus obtained was compared with the well established ^{148}Nd burn-up monitor method. For this, the fission product monitor neodymium was isolated from the dissolver solution.

3A.2 Experimental

HPLC separation followed by mass spectrometric analysis was employed for the quantitative determination of fission product monitors (molybdenum and neodymium) and residual heavy elements (uranium and plutonium) in irradiated UO_2 fuel (discharged from PHWR). The irradiated fuel pin, which was cooled for sufficient time (> 2 years) to allow decay of short lived fission products, was dissolved in 11.5 mol/L HNO_3 medium and heated to about 110 ^{o}C under reflux condition for about 12 hours in the hot-cell facility. For our experiments, an aliquot of (10 mL) dissolver solution was employed. From this about 250 µL was used for uranium and plutonium, 500 µL for molybdenum and another 500 µL for neodymium and lanthanum separation using HPLC.

3A. 2.1 HPLC separation

The HPLC system (M/s JASCO, Japan) was used for the separation of fission products such as molybdenum, neodymium and the actinides (uranium and plutonium) from the dissolver solution. The details of the instrument are given elsewhere (Chapter 1AA.4). The sample injector (Rheodyne), UV-Vis detector and the chromatographic column were placed inside a fume hood and the high pressure reciprocating pumps used for the delivery of mobile phase solution and post-column reagent and the data acquisition system are placed outside the fume hood. Reversed phase particle column (M/s Merck, Germany) of dimensions 50 mm (length) × 4.6 mm (inner diameter) and with particle size of 1.8 µm was used for the experiments. The data was acquired using

Borwin software which is interfaced with UV-Vis detector. Post-column derivatisation technique (using arsenazo (III)) was employed for the detection of lanthanides and actinides. The metal-arsenazo (III) complexes were detected at a wavelength of 655nm.

3A.2.1.1 Separation of molybdenum by reversed phase chromatography

Since molybdenum does not form complex with arsenazo (III) chromogenic agent, direct determination by post column reagent using UV-Visible detector is not feasible. In order to optimise the experimental conditions for the collection of molybdenum fraction and to determine its retention time, HPLC experiments were carried out using a simulated PHWR dissolver sample. The HPLC column was preconditioned with 0.1 M mandelic acid (adjusted to pH: 4 with ammonium hydroxide solution) and the feed solution containing molybdenum was injected into the column at a mobile phase flow rate of 1.0 mL/min. The eluted fractions were collected at regular time intervals (one-minute) and analysed by Inductively Coupled Plasma Mass Spectrometer (ICP-MS) (Spectro MS, Model: MSS001, M/s AMETEK, Germany). The retention time of molybdenum was established from these studies. Subsequently experiments on dissolver solution were carried out under identical experimental conditions for the separation of molybdenum. An aliquot of PHWR stock solution was evaporated to near dryness under infrared lamp and re-dissolved in a mixture of 0.1 M HNO_3 and 0.1 M mandelic acid. From this 100 μL of sample was injected into the HPLC column. The molybdenum fraction was collected during 2nd - 3rd minute time interval.

3A.2.1.2 Separation of neodymium by dynamic ion exchange chromatography

The values of ionic radii of lanthanides are very close to each other due to “lanthanide contraction”. Hence, a suitable complexing reagent is required for the effective separation of individual lanthanides. In the present study, the reversed phase columns were modified into a dynamic ion-exchange support using suitable water soluble modifier, e.g., ion-pairing reagent, camphor sulphonic acid (CSA). The fission product monitor neodymium was separated and eluted with alpha hydroxy isobutyric acid (α-HIBA) as a complexing agent from the dissolver solution. An aliquot of the PHWR stock solution was subjected to solvent extraction with 1.1 M tributyl phosphate (TBP) in n-dodacane to remove bulk of uranium (present in mg level compared to μg level of neodymium) from the sample. The above aqueous phase containing all the lanthanide fission products with some uranium and plutonium was evaporated to near dryness and re-dissolved in 0.1 M HNO_3 before being injected into the HPLC column. About 15-20 mL of the mobile phase (0.01 M CSA + 0.05 M α-HIBA, adjusted to pH: 3.9 with ammonium hydroxide solution) was passed through the particle HPLC column to establish a dynamic ion exchange surface. The neodymium fraction was collected at retention time corresponding to 14th to 16th minute interval.

3A.2.1.3Separation of uranium and plutonium by reversed phase chromatography

About 20 mL of mobile phase (0.1 M HIBA, adjusted to pH: 3.75 with ammonium hydroxide solution) was used to condition the column and also to separate uranium and plutonium. To ensure that plutonium is retained in Pu (IV) oxidation state, a small quantity of sodium nitrite was added to the aliquot of dissolver solution. Reversed phase chromatography method was used to separate and determine uranium and plutonium present in the dissolver solution. Separation of uranium and plutonium was not carried out along with those of lanthanides by dynamic ion-exchange experiments, since the peaks of actinides obtained during HPLC analysis showed near saturation during the assay of the lanthanides. After appropriate dilution, the dissolver solution was directly injected into the HPLC system for the separation and determination of uranium and plutonium using a reversed phase column.

Both the unspiked and spiked (an internal standard enriched in particular isotope were added to the samples) samples were subjected to the identical chemical separation procedures as described above.

3A.2.2 Mass spectrometric analysis

Thermal ionisation mass spectrometer (ISOPROBE-T, M/s ISOTOPX, UK) was used for precise and accurate measurement of isotopic ratios. Description of the TIMS instrument used for present work is given in chapter 1A.10. Required samples were loaded on filament surface using external sample loading instrument. After complete evaporation, the filaments were placed in the sample magazine inside the source chamber of TIMS. The samples were heated slowly by ramping up the filament current to the desired values. Initially central (ionisation) filament and side (vaporisation) filament currents were increased independently to 4.8 A and 1.0 A until rhenium ion signals were observed. At this setting, sufficient rhenium signal (~ 100 mV) required for focusing of ion beam using various focus plates was obtained. Subsequently central and side filament currents were increased slowly to get signals of metal ions of interest. The ion beam of a particular metal species was focused to obtain a flat “trapezoidal” isotopic peak. Depending on the number of isotopes of an element, collectors were arranged to have “coincidence” of isotopes, which indicate the exact positioning of the collectors for dispersed ion beams.

Prior to loading in TIMS, the pure fractions of molybdenum and actinides obtained from HPLC separation were evaporated to near dryness and re-dissolved in 8M HNO_3 medium. This procedure was repeated thrice to minimise the presence of organics (mandelic acid, CSA and α-HIBA) in the samples. Before loading of samples, the blank rhenium filaments were out-gassed at 5.4 A (current corresponding to sample analysis temperature) for 2-3 h in vacuum, until no signal for molybdenum was detected to avoid isobaric interferences during analysis of samples.

3A.2.2.1 Experimental conditions for mass analysis of molybdenum by TIMS

The molybdenum fraction which is present in nitrate form was converted to chloride form by conditioning with 4 M HCl. The solution was then mixed with ~4 μL of 1.0 M ascorbic acid solution (prepared with 4 M HCl) to reduce Mo (VI) to Mo (III) state. The above mixture was loaded onto the outer rhenium filament of a Re-Re-Re triple filament geometry and above this a layer of silicic acid (~2 μL) slurry was deposited. The sample was dried on the filament by passing current, initially at 0.8 A and finally at 1.8 A to remove any moisture or organics in the sample. For the analysis of molybdenum, centre and side filaments were kept at 5.4 and 1.5 A so as to have sufficient ion signal.

3A.2.2.2 Experimental condition for mass analysis of neodymium, uranium and plutonium by TIMS

The pre-conditioned fractions of neodymium, uranium and plutonium were re-dissolved in 0.7 M HNO_3 prior to loading onto the filaments. These fractions (uranium, plutonium, and neodymium) were loaded on a tantalum side filament in Ta-Re-Ta filament configuration. It was dried by passing a constant current of 0.8 A. Finally filament current was raised to 1.2 A for ~20 sec to facilitate complete dryness. The filament assembly was loaded in source chamber for mass spectrometric analysis. Central filament and side filaments were heated at 5.4 and 2.0 - 2.4 A, respectively for the satisfactory analysis of neodymium, uranium and plutonium.

3A.3 Results and Discussion

The retention time of molybdenum (in simulated PHWR sample) in HPLC was determined by subjecting the various fractions collected to ICP-MS analysis. Molybdenum could be detected in the fraction collected during the time interval 2-3 minutes. Subsequently, the fraction collected in the 2-3 minutes interval of PHWR dissolver solution was subjected to TIMS analysis for determining the isotopic ratios. The molybdenum sample was loaded on filament surface and placed inside the source chamber. Under the optimal filament current conditions, ion current of the order 1 x 10^{-11} A could be measured which was stable for 2-3 hours. Molybdenum isotopic ratios were computed from the measured ion intensities at m/z: 95, 97, 98, and 100 in four different faraday cups under static multi collector method. Fig. 3A.1 represents individual isotopic ratio of molybdenum (97/95, 98/95, 100/95) and mean isotopic ratio of all the run are given in Table 3A.1.

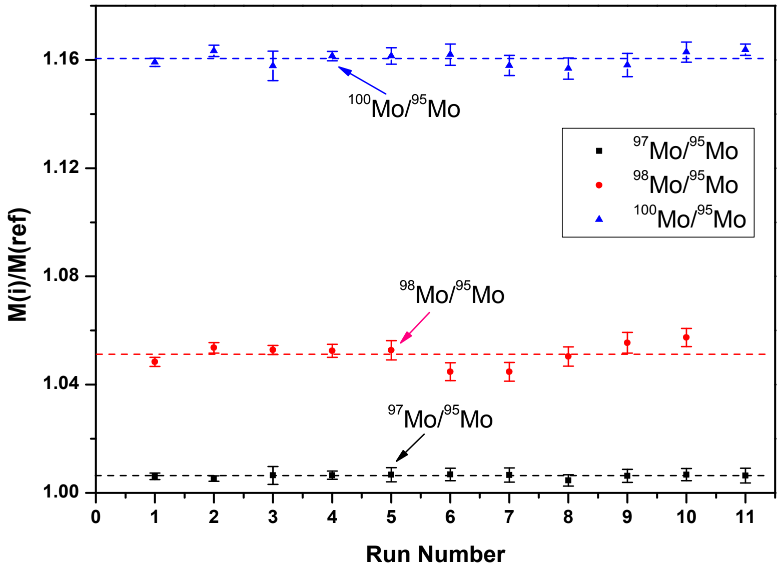

Fig. 3A.1 Individual isotopic ratio of molybdenum [M(i)/M(ref)] for PHWR dissolver solution. The dashed lines represent mean of individual isotopic ratios. Where M(i) = 97, 98, 100 and M(ref) = 95, isotopes of molybdenum.

Table 3A.1 Isotopic ratios and abundances of fission product monitor molybdenum in PHWR dissolver sample.

Isotope M(i)	Isotope ratio M(i)/M(ref)	Relative error in % in the isotope ratio [a)]	Atom fraction of the isotope M(i)	Relative error in % in atom fraction[b)]	Mass % of the isotope M(i)
Molybdenum: M (ref) = 95; Average atomic weight = 97.507					
95	1	-	2.371×10^{-1}	0.17	23.078
97	1.0062	0.23	2.386×10^{-1}	0.29	23.709
98	1.0512	0.47	2.492×10^{-1}	0.50	25.025
100	1.1603	0.38	2.751×10^{-1}	0.42	28.189

a) Combination of internal and external error (standard deviation) associated with individual runs

b) Derived from error associated with isotopic ratios using error propagation

During TIMS analysis, no signal was observed at mass numbers corresponding to 91 and 93 ensuring the absence of zirconium in the molybdenum fraction. Similarly, absence of ion signals at mass numbers 101, 102 and 104 ensured no contamination from ruthenium either. During the mass spectrometric runs, ion signals for isotopes of 92, 94, and 96 (which were not expected for reactor produced molybdenum) were also observed, indicating presence of some natural molybdenum. Probably, the reaction of sample with the inner surface of the filament might have resulted in these peaks. Contamination during dissolution of fuel pin in the dissolver vessel is another possibility. However, the interference from this contamination at mass numbers corresponding to reactor produced isotopes (95, 97, 98, 100) were corrected using intensity of ^{92}Mo (natural abundance) with the help of "interference correction" program in TIMS software. The isotopic abundance of natural and reactor produced (PHWR) molybdenum are represented in Fig. 3A.2.

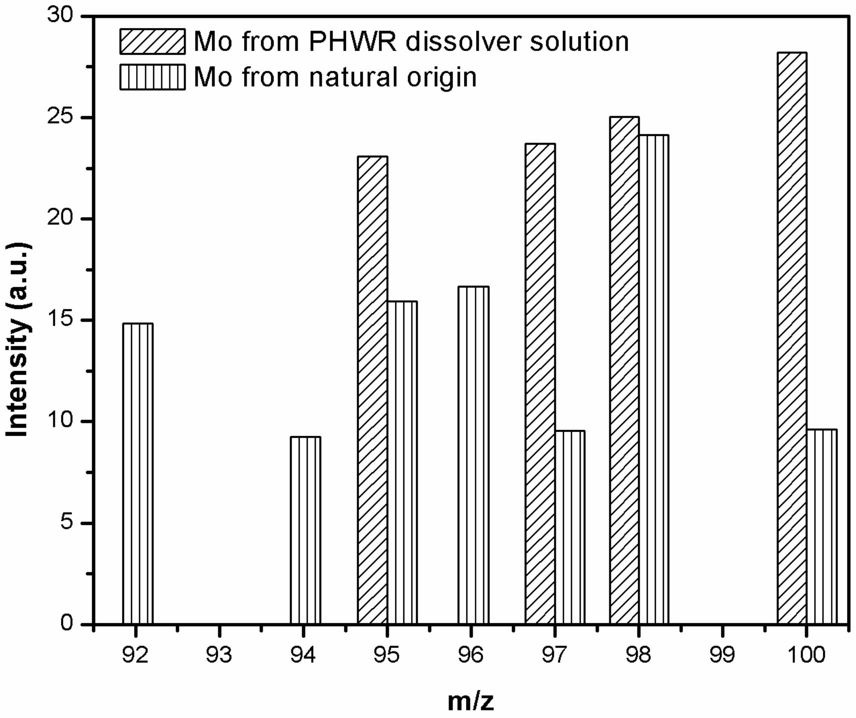

Fig. 3A.2 Isotopic abundance of molybdenum in natural sample and PHWR dissolver solution.

The interference correction which was carried out by software with respect to ^{92}Mo, using raw intensity data of Mo at mass numbers 92, 95, 97, 98, 100, are executed by using the following equations

For unspiked molybdenum sample:

$$^{95}I^{+}_{Rec} = {}^{95}I^{+}_{(Rec+Nat)} - \left[\left({}^{92}I^{+}_{Nat}\right) \times \left(\frac{^{95}(At.\ frct.)_{Nat}}{^{92}(At.fract.)_{Nat}}\right)\right] \tag{3A.2}$$

$$^{97}I^{+}_{Rec} = {}^{97}I^{+}_{(Rec+Nat)} - \left[\left({}^{92}I^{+}_{Nat}\right) \times \left(\frac{^{97}(At.\ frct.)_{Nat}}{^{92}(At.fract.)_{Nat}}\right)\right] \tag{3A.3}$$

$$^{98}I^{+}_{Rec} = {}^{98}I^{+}_{(Rec+Nat)} - \left[\left({}^{92}I^{+}_{Nat}\right) \times \left(\frac{^{98}(At.\ frct.)_{Nat}}{^{92}(At.fract.)_{Nat}}\right)\right] \tag{3A.4}$$

$$^{100}I^{+}_{Rec} = {}^{100}I^{+}_{(Rec+Nat)} - \left[\left({}^{92}I^{+}_{Nat}\right) \times \left(\frac{^{100}(At.\ frct.)_{Nat}}{^{92}(At.fract.)_{Nat}}\right)\right] \tag{3A.5}$$

For spiked molybdenum sample:

$$ {}^{95}I^{+}_{(Rec+Spk)} \;=\; {}^{95}I^{+}_{(Rec+Spk+Nat)} - \left\{ {}^{92}I^{+}_{(Spk+Nat)} \times \left(\frac{{}^{95}(At.\ frct.)_{Nat}}{{}^{92}(At.fract.)_{Nat}}\right) \times \left(\frac{{}^{92}(At.\ frct.)_{Nat}}{\left({}^{92}(At.fract.)_{Nat} + {}^{92}(At.fract.)_{Spk}\right)}\right)\right\} \quad (3A.6) $$

$$ {}^{97}I^{+}_{(Rec+Spk)} \;=\; {}^{97}I^{+}_{(Rec+Spk+Nat)} - \left\{ {}^{92}I^{+}_{(Spk+Nat)} \times \left(\frac{{}^{97}(At.\ frct.)_{Nat}}{{}^{92}(At.fract.)_{Nat}}\right) \times \left(\frac{{}^{92}(At.\ frct.)_{Nat}}{\left({}^{92}(At.fract.)_{Nat} + {}^{92}(At.fract.)_{Spk}\right)}\right)\right\} \quad (3A.7) $$

where ${}^{97}I^{+}_{(Rec+Spk+Nat)}$ represents intensity of ^{97}Mo due to reactor produced (Rec), spike used (Spk) and natural contamination (Nat), ${}^{92}(At.\ frct.)_{Nat}$ represents atom fraction value of ^{92}Mo in the natural sample. Atom fraction values for isotopes (92, 95, 97, 98, 100) of Mo in natural and spike were taken from literature [27] and certified materials data, respectively. The corrected intensity data were used to derive isotopic composition of reactor produced molybdenum.

Mass spectra of un-spiked and spiked (with ^{142}Nd) neodymium in PHWR dissolver solution is presented in Fig. 3A.3 and 3A.4, respectively.

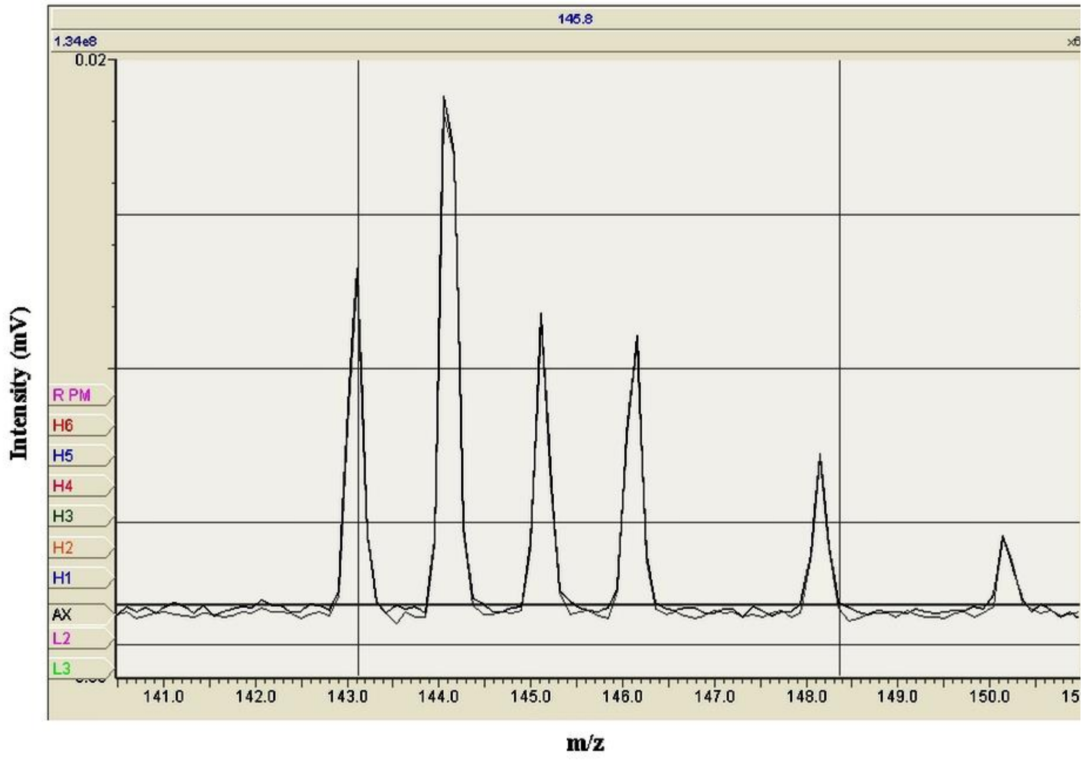

Fig. 3A.3 Mass spectrum of un-spiked neodymium in PHWR dissolver solution.

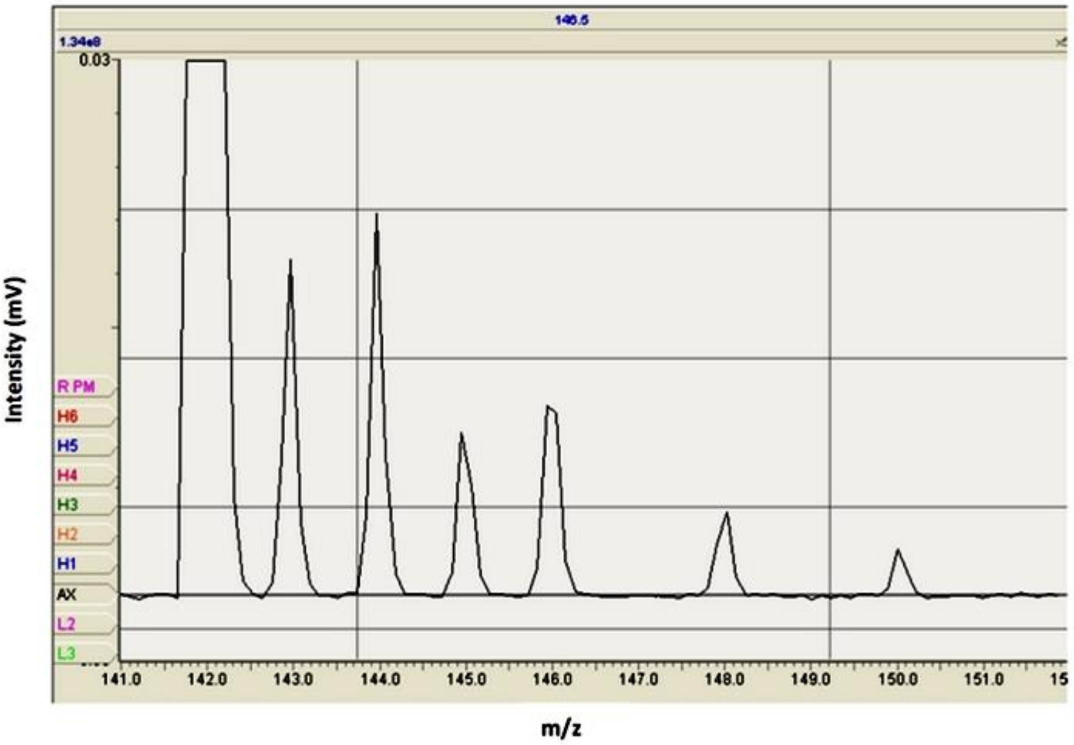

Fig. 3A.4 Mass spectrum of spiked (with ^{142}Nd) neodymium in PHWR dissolver solution.

The absence of peak at mass number 142 in Figure 3A.3 for neodymium in reactor produced sample is attributed to shielding of precursor ^{142}Ce. Due to high thermal neutron capture cross section for ^{143}Nd (~325 barns [13]), it had undergone neutron capture reaction which is reflected in the higher abundance of ^{144}Nd compared to ^{143}Nd in the dissolver solution. The isotopic composition values for reactor produced neodymium are listed in Table 3A.2.

Fig. 3A.5 represents mass spectra of uranium and plutonium in PHWR solution. It shows a complete separation of uranium and plutonium from each other using HPLC method and the corresponding values are listed in Table 3A.3. The isotopic ratios given in the Tables (3A.1, 2 and 3) for all the elements are mean of five individual runs and each run consisted of 36 measurements. Relative % errors for isotopic ratios were calculated by considering internal and external errors (standard deviation) associated with individual runs.

Table 3A.2 Isotopic ratios and abundances of fission product neodymium in PHWR dissolver sample.

Isotope M(i)	Isotope ratio M(i)/M(ref)	Relative error in % in the isotope ratio [a)]	Atom fraction of the isotope M(i)	Relative error in % in atom fraction [b)]	Mass % of the isotope M(i)
Neodymium: M (ref) = 143; Average atomic weight = 144.843					
143	1	-	1.999×10^{-1}	0.03	19.723
144	1.6385	0.05	3.275×10^{-1}	0.06	32.543
145	8.806×10^{-1}	0.09	1.760×10^{-1}	0.09	17.611
146	7.991×10^{-1}	0.09	1.597×10^{-1}	0.09	16.091
148	4.635×10^{-1}	0.18	9.265×10^{-2}	0.19	9.461
150	2.210×10^{-1}	0.20	4.417×10^{-2}	0.20	4.572

a) Combination of internal and external error (standard deviation) associated with individual runs.

b) Derived from the errors associated with isotopic ratios using error propagation.

Concentrations of molybdenum, neodymium, uranium and plutonium were determined using IDMS method. For determining the concentration of Mo, Nd, U and Pu in dissolver solution, spikes enriched with ^{94}Mo, ^{142}Nd, ^{233}U, ^{239}Pu isotopes respectively, were used.

The isotopic composition and concentration of spikes used in these experiments were determined by employing reverse IDMS procedure.

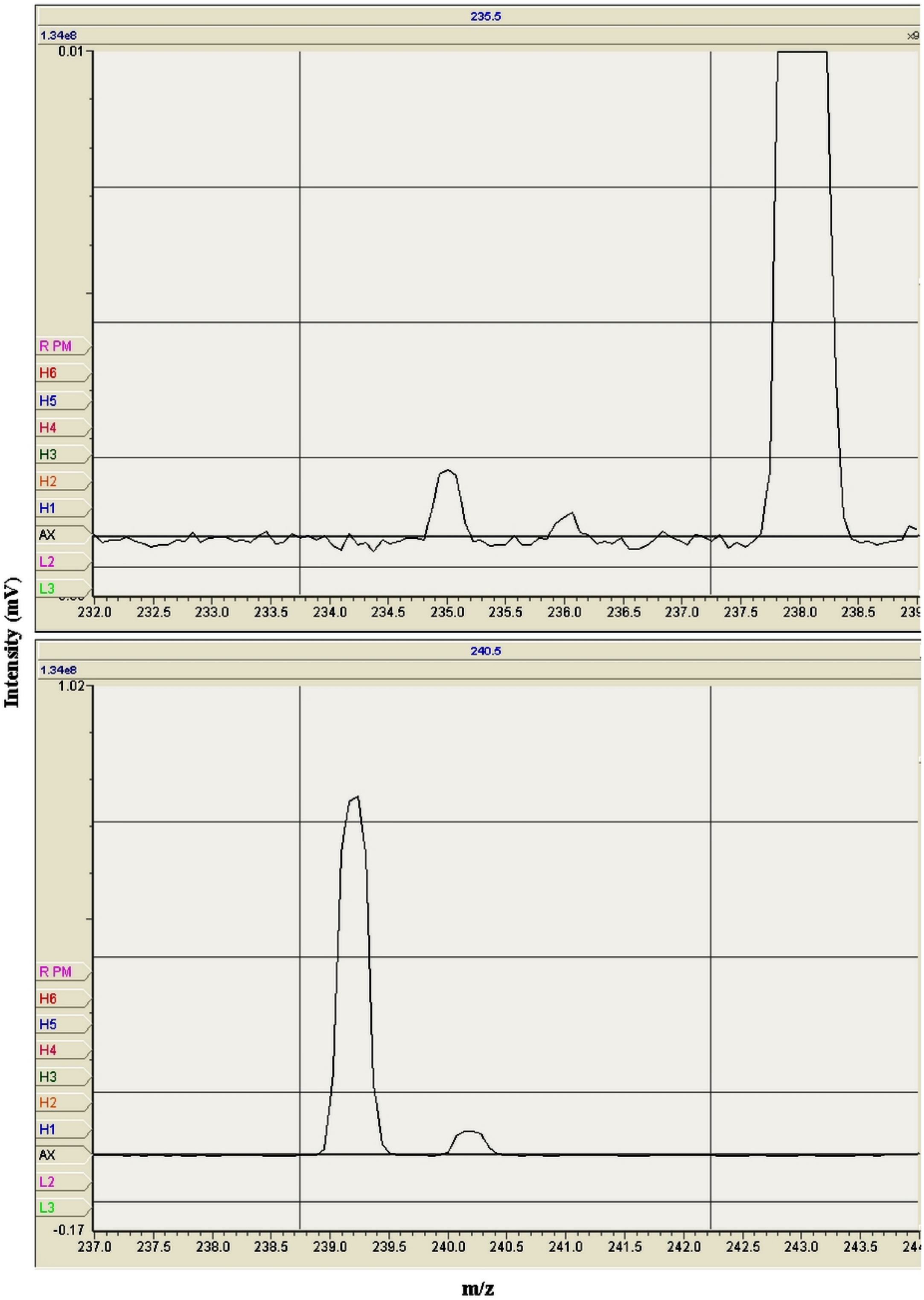

Fig. 3A.5 Mass spectra of uranium (top) and plutonium (bottom) in PHWR dissolver solution.

Table 3A.3 Isotopic ratios and abundances of heavy elements (U and Pu) in PHWR dissolver sample.

Isotope M(i)	Isotope ratio M(i)/M(ref)	Relative error in % in the isotope ratio [b)]	Atom fraction of the isotope M(i)	Relative error in % in atom fraction [c)]	Mass % of the isotope M(i)
Uranium: M (ref) = 238; Average atomic weight = 238.042					
238	1	-	9.970×10^{-1}	0.001	99.702
234	4.5×10^{-5}	9.13	4.5×10^{-5}	9.13	0.004
235	2.201×10^{-3}	0.16	2.194×10^{-3}	0.16	0.217
236	7.75×10^{-4}	0.40	7.73×10^{-4}	0.40	0.077
Plutonium: M (ref) = 239; Average atomic weight = 239.446					
239	1	-	6.711×10^{-1}	0.01	66.995
238[a)]	2.839×10^{-3}	2.0	1.905×10^{-3}	2.0	0.189
240	4.194×10^{-1}	0.03	2.814×10^{-1}	0.03	28.216
241	3.386×10^{-2}	0.23	2.272×10^{-2}	0.23	2.287
242	3.410×10^{-2}	0.20	2.288×10^{-2}	0.20	2.313

[a)] Deduced by combining mass spectrometric and alpha spectrometric results; the error estimated to be ~2%.

[b)] Combination of internal and external error (standard deviation) associated with individual runs

[c)] Derived from error associated with isotopic ratios using error propagation

3A.3.1 Computation of burn-up

The values for A, Y and H given in equation (3.1) which are required for computation of burn-up were deduced as follows. Effective fractional fission yield (Y) for different isotopes of molybdenum and neodymium with respect to ^{235}U and ^{239}Pu fissions were taken from fission yield data from literature [14]. The number of atoms of fission product monitor, A (isotopic yield of neodymium or molybdenum) and the total residual heavy elements, H (uranium and plutonium) in a given aliquot of a dissolver solution were computed from the concentration, using IDMS technique. Subsequently, the burn-up (atom % fission) values were computed using equation (3.1) are given in Table 3A.4. The total residual heavy element atoms (H) determined per gram of dissolver solution was found to be 3.79 x 10^{19} (U: 3.78 x 10^{19} and Pu: 1.45 x 10^{17}).

Table 3A.4 Total number of atoms and burn-up computed using different isotopes of Mo and Nd determined by IDMS technique.

Fission product monitors	Total no. of atoms determined per gm of dissolver soln.(A) [a)]	Atom % burn-up[b)]
^{100}Mo	1.98 x 10^{16}	0.79
^{Total} Mo	7.20 x 10^{16}	0.80
^{148}Nd	5.25 x 10^{15}	0.82
^{Total} Nd	5.66 x 10^{16}	0.80

[a)] Corresponding to "A" given in equation (3.1)

[b)] Total residual heavy element atoms (U+Pu) determined per gram of dissolver solution (H): 3.79 x 10^{19} (U: 3.78 x 10^{19} and Pu: 1.45 x 10^{17}).

As can be seen from Table 3A.4, the atom % burn-up computed using fission product monitor, molybdenum of PHWR dissolver solution are in good agreement with those obtained using well established Nd-148 method. Isotopic composition (in mass percent) of U in PHWR dissolver solution was found to be ^{238}U: 99.70; ^{235}U: 0.22; and ^{236}U: 0.08; for Plutonium, the isotopic composition (in mass percent) was: ^{239}Pu: 67.0; ^{240}Pu: 28.22; ^{241}Pu: 2.29; ^{242}Pu: 2.31; and ^{238}Pu: 0.19. The isotopic composition (in mass percent) of fission product neodymium was: ^{143}Nd: 19.72; ^{144}Nd: 32.54; ^{145}Nd: 17.61; ^{146}Nd: 16.09; ^{148}Nd: 9.46; and ^{150}Nd: 4.57; and for molybdenum (in mass percent) the values were ^{95}Mo: 23.08; ^{97}Mo: 23.71; ^{98}Mo: 25.03; and ^{100}Mo: 28.19. The fractional fission contribution from ^{235}U and ^{239}Pu is computed to be 50-50 using isotopic ratio of ^{97}Mo / ^{95}Mo. This value was arrived at by correlating the data of isotopic ratio derived from experiments (TIMS) with the literature data [14]. The atom % burn-up determined from concentrations of U, Pu, Mo and Nd was found to be 0.79 (^{100}Mo as fission monitor), 0.80 (elemental Mo as monitor), 0.82 (^{148}Nd as fission monitor) and 0.80 (elemental Nd as monitor). The errors associated with burn-up are due to uncertainties in the fission yield data and uncertainties associated with experimental determination of Mo/Nd, U, Pu. The overall uncertainty is expected to be in the region of about 2-3%.

3A.4 Conclusion

A quick and effective separation technique using 1.8 µm particle HPLC column was demonstrated for the separation of fission products, Mo, Nd and actinides (U, and Pu) from PHWR dissolver solution. The pure fractions of Mo, Nd, U and Pu were subjected to TIMS analysis. New sample loading method was developed for molybdenum analysis and they provide stable and enhanced ion intensity during TIMS analysis. IDMS method was employed for accurate and precise determination of Mo, Nd, U and Pu concentrations in the dissolver solution. Fractional fission contribution from ^{235}U and ^{239}Pu towards total fission was computed. The atom % burn-up was derived for PHWR dissolver solution using different isotopes of alternate fission product monitor (molybdenum) and the data were in good agreement with established ASTM standard (Nd-148) method. Burn-up using molybdenum as fission product monitor is being reported for the first time for PHWR dissolver solution using HPLC and TIMS techniques.

CHAPTER 3B

Lanthanum as alternate burn-up monitor

In this chapter HPLC and TIMS methodologies developed to ascertain lanthanum as burn-up monitor are discussed.

3B.1 Introduction

Among fission products, other than neodymium and molybdenum, lanthanum which appears in the second range of masses in the fission yield curve [1, 2] posses the required characteristics as a burn-up monitor. This makes lanthanum a prospective candidate as fission product monitor, alternate to neodymium. Lanthanum on the other hand, apart from possessing some of the required features of fission product monitor, have almost near similar fission yields for ^{233}U (6.45 (thermal); 6.55 (fast)), and ^{235}U (6.65 (thermal); 6.65 (fast)). The fission yields for ^{139}La from ^{239}Pu fissions are (5.73 (thermal): 5.83 (fast)) [14, 15]. Thus for uranium and thorium based fuels as fission yields are similar for lanthanum, even without considering fractional fission contributions, the atom % burn-up can be computed. However in the case of uranium-plutonium based fuels, since there is difference in the fission yields, fractional fission contributions from U and Pu is required for computing the burn-up. This makes lanthanum a suitable fission product monitor not only for fuels pertaining to thermal reactor, but also for fast reactor like mixed oxide and metallic fuels, which are proposed nuclear fuels for future Indian nuclear programme.

Lanthanum exists as two stable isotopes with mass number 138 and 139 in nature with abundances of 0.089% and 99.911%, respectively [27]. In a nuclear reactor, La-139 is the major isotope that is produced. ^{138}La is a “shielded isotope” since the decay chain stops at precursor stable isotope, i.e. ^{138}Ba. However, a minute quantity of ^{138}La is produced through direct fission and this was used for isotopic ratio measurements in the dissolver spent fuel solution. Isobaric interference from ^{138}Ce was overcome by separating it from La using HPLC method. Lanthanum with first ionisation energy of 5.6 eV is quite sensitive to TIMS analysis. Natural impurities of ^{138}Ba (abundance of 71.66%) from sample loading filaments can interfere with the analysis of lanthanum and hence lanthanum was analysed for the intensities of its compound rather than as metallic species. Inghram et al. [28] used oxide of lanthanum in nitric acid medium to get stable ion intensity of LaO$^+$ ion. Single tantalum filament was used for loading the sample. White et al. [29] had deposited lanthanum oxide in chloride medium on a tantalum filament to measure the isotopic ratio. Elliot et al. [30] had reported the isotopic composition of spiked lanthanum (with ^{138}La) in nuclear fuel solution. Lanthanum was converted to lanthanum oxide by heating (~600 ^{o}C) the sample on a rhenium filament surface for overnight in air. Reversed phase column with dynamic ion exchange modifier (0.01 M ammonium octanesulfonate at pH 3.8) was used to separate spiked lanthanum fraction from fuel solution. Makishima et al. [31] had determined the isotopic ratio of lanthanum by loading lanthanum oxide sample on a rhenium single filament. Shen et al. [32, 33] used double filament assembly using out-gassed zone refined rhenium filament for loading the sample. Cation exchange resin was used to separate lanthanum from barium and other rare earth elements. Lanthanum in chloride form was converted to LaO$^+$ through controlled oxygen supply in the source chamber and this LaO$^+$ was used for TIMS analysis. De Laeter et al. [34] had employed pure LaCl$_3$ solution and loaded on two sides of a triple rhenium filament system to have enhanced ion intensity of LaO$^+$ ion. In earlier studies from our laboratory, lanthanides and actinides were separated and quantified using HPLC for atom percent fission determination [23-26].

For lanthanum analysis using TIMS, a new procedure has been developed as it was realised that the procedures reported earlier were either not suitable for radioactive samples or did not yield sufficient ion intensity of LaO^+ as compared to La^+. A new sample loading procedure, wherein lanthanum contained in a mixture of (graphite + H_3BO_3 + silica gel) in HCl medium loaded onto a side filament of out-gassed rhenium triple filament system (Re-Re-Re) was developed. Also this is the first time where use of lanthanum is demonstrated as fission product monitor using TIMS. The HPLC methods developed earlier [23-26] for lanthanides and actinides were used to separate lanthanum, neodymium and actinides from other fission products. Concentration of lanthanum in the spent PHWR dissolver solution was determined using IDMS method. Subsequently burn-up was determined. The burn-up data thus obtained was compared with the well established ^{148}Nd burn-up monitor method.

3B.2 Experimental

An aliquot from the same stock solution of irradiated UO_2 fuel discharged from pressurised heavy water reactor (PHWR), used in the previous work on molybdenum, was used. Separation using HPLC, followed by mass spectrometric analysis was performed for the determination of fission product monitors (lanthanum and neodymium) and residual heavy elements (uranium and plutonium) of irradiated UO_2 fuel dissolver solution.

3B. 2.1 HPLC separation

The HPLC set up for radioactive sample handling (described in chapter 1AA.4) employed a reversed phase particle column (M/s Merck, Germany) of dimensions 50 mm (length) × 4.6 mm (diameter) and with particle size of 1.8 μm has been used in the present study. Post-column derivatisation technique was employed for the detection of lanthanides and actinides. The arsenazo (III) is used as chromogenic reagent to form metal - arsenazo (III) complexes, which can be detected at a wavelength of 655 nm.

3B.2.1.1 Separation of neodymium and lanthanum by dynamic ion exchange chromatography

The modified dynamic ion-exchange reversed phase column was used for present study. The fission product monitors neodymium and lanthanum were separated and eluted with alpha hydroxy isobutyric acid (α-HIBA) as a complexing agent from the dissolver solution. Experimental conditions discussed earlier in the chapter (3A.2.1.2) were followed for solvent extraction to remove bulk of uranium from the sample, followed by HPLC separation to collect pure fraction of neodymium and lanthanum from dissolver solution. The neodymium fraction was collected at a retention time interval of 14th to 16th minutes and lanthanum at 20th to 22nd minutes. Identical separation procedure was adopted for dissolver solution after mixing with a known quantity of ^{142}Nd and ^{138}La spikes.

3B.2.1.2 Separation of uranium and plutonium by reversed phase chromatography

As same PHWR dissolver solution was taken for present study, HPLC separation for un-spiked sample was not carried out. Dissolver solution spiked with required amount of ^{233}U and ^{239}Pu were added before HPLC separation. About 20 mL of mobile phase (0.1 M α-HIBA, adjusted to pH: 3.75 with NH_4OH solution) was used to condition the column and also to separate uranium and plutonium. To ensure that plutonium is retained in Pu (IV) oxidation state, a small quantity of sodium nitrite was added to the aliquot of dissolver solution. Similar procedure (as described in section 3A.2.1.3) was followed for separation of uranium and plutonium spiked samples. The separated fractions ware collected and subjected to TIMS analysis for determination of their concentrations.

3B.2.2 Mass Spectrometric Analysis

The samples in suitable chemical form (lanthanum in chloride form and neodymium, uranium and plutonium in nitrate form) were loaded above the filament surface before inserting into the source chamber. For TIMS analysis, similar analytical procedures as described in section 3A.2.2 was adopted.

Prior to loading on filament surface, the pure fractions of lanthanides and actinides obtained from HPLC separation were evaporated to near dryness and re-dissolved in 8 M HNO_3. This procedure was repeated thrice to minimise the presence of organics (CSA and α-HIBA) in the samples. The radioactive samples (La, Nd, U, Pu) were loaded on filament surface inside the fume hood.

3B.2.2.1 Experimental condition for mass analysis of lanthanum by TIMS

The pre-conditioned HPLC separated lanthanum fractions were re-dissolved in 0.5 M HCl. A layer of graphite slurry was placed on the out-gassed rhenium side filament of triple Re-Re-Re filament assembly. It was dried by passing a constant current of 0.8 A. Above this; a mixture of boric acid with silica gel along with the lanthanum sample in 0.5 M HCl medium was loaded. The filament current was raised to 1.2 A for complete dryness. Lanthanum was analysed in the form of LaO^+ by carrying out experiment at current values 4.8 and 2.0 A respectively for central and side filaments.

3B.2.2.2 Experimental condition for mass analysis of neodymium, uranium and plutonium by TIMS

The pre-conditioned fractions of neodymium, uranium and plutonium were re-dissolved in 0.7 M HNO_3 prior to loading onto the filaments. Uranium, plutonium, and neodymium fractions corresponding to spiked samples were loaded onto the tantalum side filament in Ta-Re-Ta filament configuration. Heating procedure similar to that adopted for lanthanum was employed. Finally, the central filament and side filaments were heated at 5.4 and 2.0 to 2.4 A respectively for the satisfactory analysis of neodymium, uranium and plutonium.

3B.3 Results and Discussion

Lanthanum isotopic ratios in the form of LaO^+ were measured at mass numbers, 154 and 155 corresponding to $^{138}La^{16}O^+$ and $^{139}La^{16}O^+$, and are given in Fig. 3B.1.

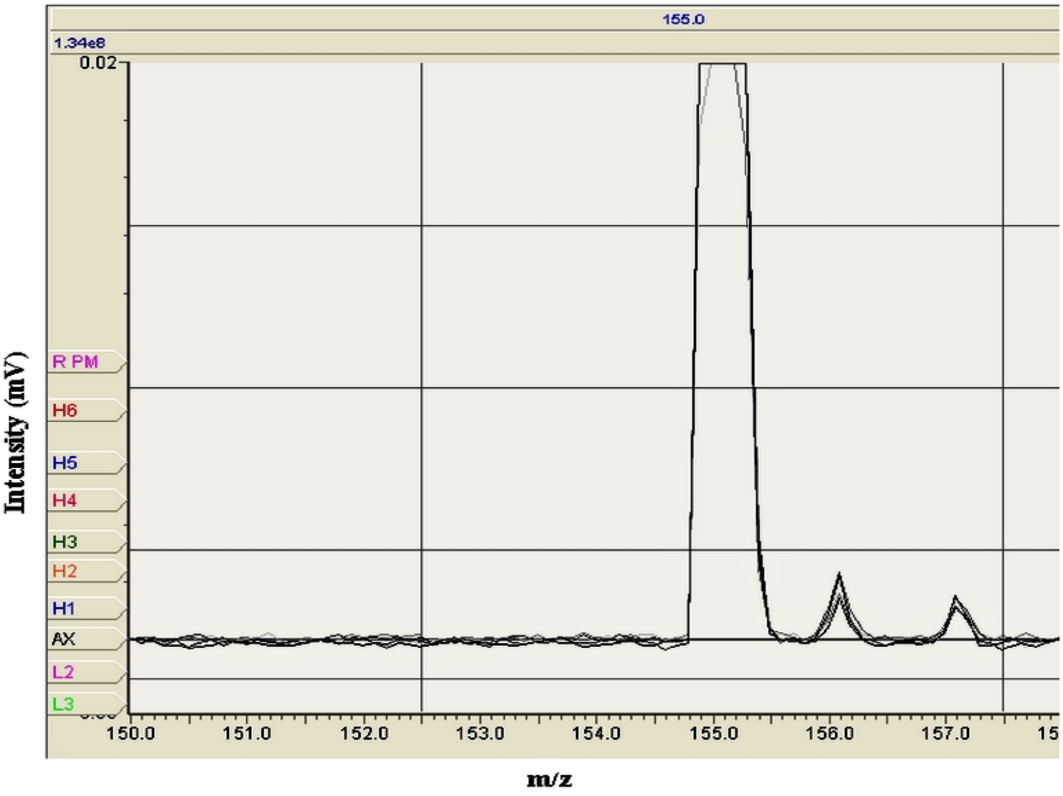

Fig. 3B.1 Mass spectrum of un-spiked lanthanum (as LaO^+) in PHWR dissolver solution.

The fission yield of ^{138}Ba (as decay chain stops at ^{138}Ba), ^{140}Ce, and ^{142}Ce from ^{235}U (thermal) fission are 6.91, 6.31 and 5.91 respectively. Any contamination from the reactor produced or from natural impurities corresponding to mass number 154 should be reflected in higher peak intensity at mass number 154 compared to the peaks at mass number 156 and 158. Absence of intense peak at the mass number 154 corresponding to ^{138}CeO and ^{138}BaO confirmed the absence of these impurities in the samples. This gives credence to effective separation of lanthanum from cerium. Non formation of BaO^{+} ions ensured no isobaric interference due to this species.

Static multicollector mode was employed for measuring the ion intensities. The minor isotope ^{138}LaO was measured using SEM and the major isotope ^{139}LaO was measured using a faraday cup. The gain factor for SEM with respect to faraday cup was calculated using La-138 (La isotopic standard) by dynamic multicollector mode. In this method, ion signal of ^{138}LaO was collected simultaneously using SEM and faraday cup by changing the magnetic current of mass analyser to obtain the gain factor. The gain factor determined thus was incorporated in the calculation of isotopic ratio measurements of lanthanum. The ionisation and vaporisation filament currents were varied so as to obtain maximum signal for LaO^{+} as compared to La^{+}. At filament current values of 4.5 A and 2.0 A, respectively for ionisation and vaporisation filament, high ion intensity ratio of LaO^{+}/La^{+} (40-50 times) was observed. Further measurements were carried out at these optimised filament current settings. It needs to be mentioned here that various sample loading procedures [28, 29, 31, 34] described in literature and applied to radioactive samples were attempted and none of these yielded such high LaO^{+}/La^{+} ratio. The procedure mentioned in literature [30] was not adopted for this study as it required longer time for sample treatment and safety issue associated with this method. As there is no provision in our instrument to pass oxygen during measurements, the procedure described in literature [32, 33] was not attempted either. The peaks at m/z: 155 is a composite of $^{139}La^{16}O^+$ and $^{138}La^{17}O$. In order to get the true value of $^{138}La^{16}O/^{139}La^{16}O$, the correction procedure as described in references [35, 27] was employed to subtract the contribution due to $^{138}La^{17}O$. The oxygen corrected isotopic ratio of lanthanum in PHWR dissolver solution with error bars for different runs is plotted in Fig. 3B.2.

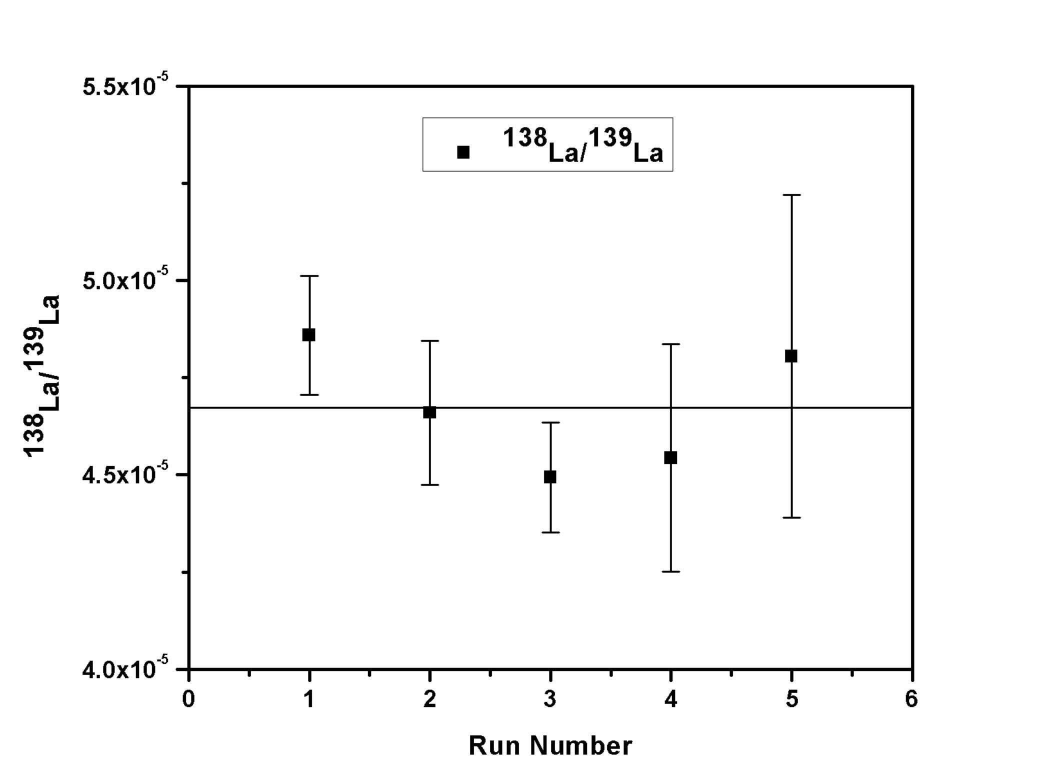

Fig. 3B.2 Isotopic ratio of lanthanum ($^{138}La/^{139}La$) measured using SEM and Faraday cup detectors for PHWR dissolver solution. The horizontal line at 4.7×10^{-5} ($\pm 3 \times 10^{-6}$) represents the mean isotopic ratio of all runs.

It can be seen from the figure that a good reproducibility in the data was obtained indicating better precision in the measurements. The isotopic composition of lanthanum in PHWR dissolver solution thus obtained after incorporating the correction is given in Table 3B.1.

Table 3B.1 Isotopic ratios and abundances of fission product monitor lanthanum in PHWR dissolver sample.

Isotope M(i)	Isotope ratio M(i)/M(ref)	Relative error in % in the isotope ratio [a)]	Atom fraction of the isotope M(i)	Relative error in % in atom fraction [b)]	Mass % of the isotope M(i)
Lanthanum: M (ref) = 139; Average atomic weight = 138.906					
138	4.7×10^{-5}	7.14	4.7×10^{-5}	7.14	0.0046
139	1	-	1.00	0.0003	99.9954

[a)] Combination of internal and external error (standard deviation) associated with individual runs

[b)] Derived from error associated with isotopic ratios using error propagation

Mass spectrum of neodymium in PHWR dissolver solution is presented in Fig. 3B.3 and observed to be of same pattern as that of Fig. 3A.3. For the present work, the isotopic composition data for unspiked neodymium in PHWR solution was taken from Table 3A.2. The isotopic composition data for pure uranium and plutonium were taken from that given in previous chapter (Table 3A.3).

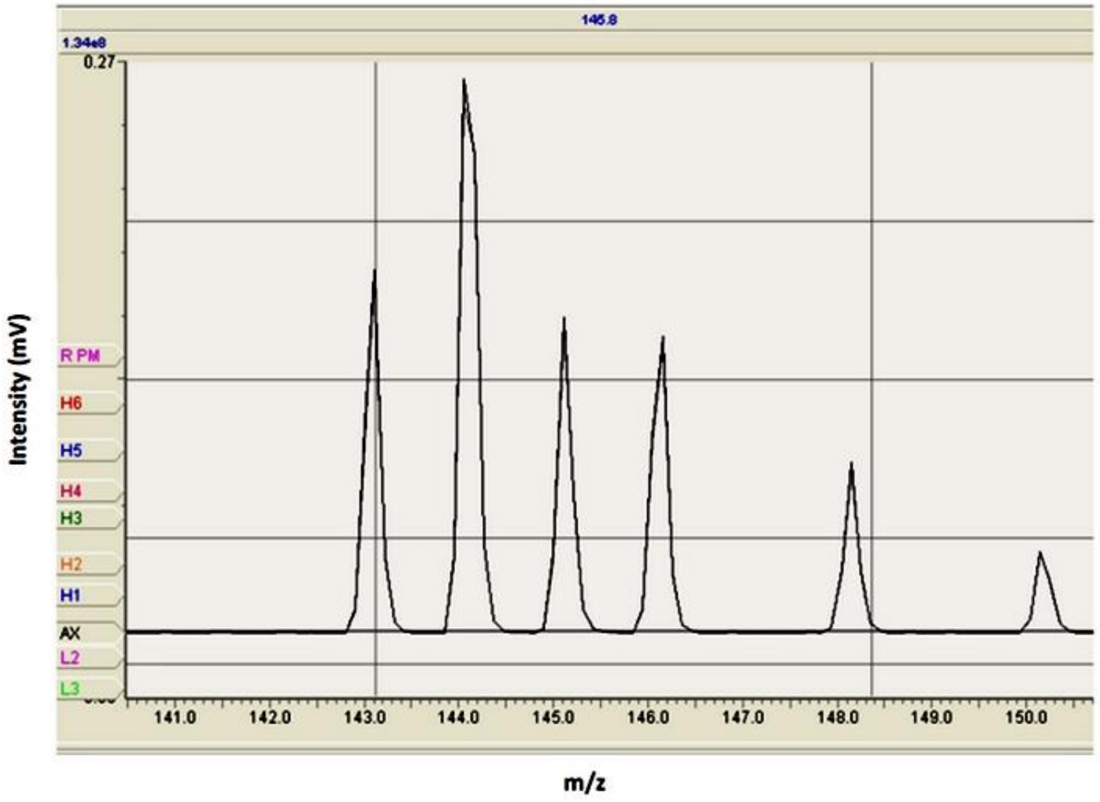

Fig. 3B.3 Mass spectrum of neodymium in PHWR dissolver solution.

The isotopic ratio for lanthanum is given in the Table 3B.1, and is the mean of five individual runs and each run consisted of 36 measurements. Relative % error for isotopic ratio was calculated by considering internal and external errors (standard deviation) associated with individual runs.

Concentration of lanthanum was determined using IDMS method. The mass spectrum of lanthanum, spiked with ^{138}La is shown in Fig. 3B.4. For the present study, the concentration alone was derived for neodymium, uranium and plutonium by taking different combinations of spike and sample. It is worth to mention here that the reproducibility of concentration (number of atoms per gram of dissolver solution) values for Nd, U and Pu in dissolver solution (Table 3A.4 and Table 3B.2) confirm the reliability of burn-up data.

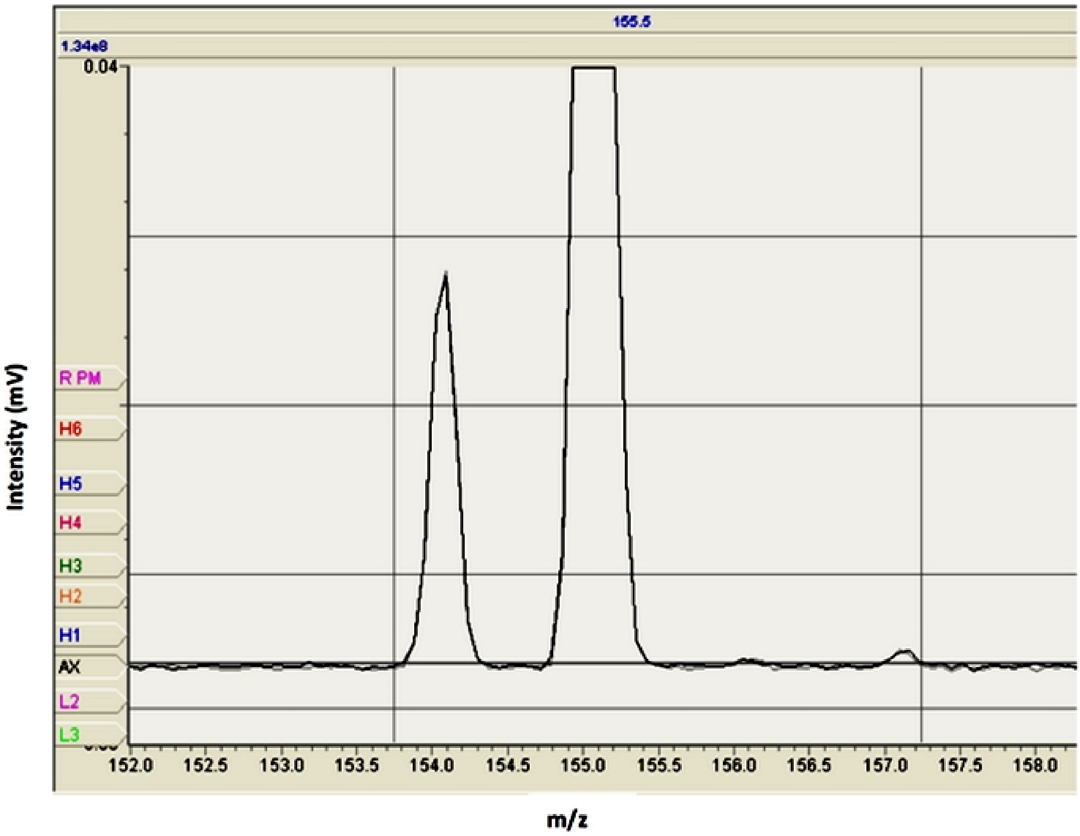

Fig. 3B.4 Mass spectrum of spiked lanthanum (as LaO^{+}) in PHWR dissolver solution.

The isotopic composition and concentration of lanthanum spike used in these experiments were determined by employing reverse IDMS procedure.

3B.3.1 Computation of Burn-up

The burn up for dissolver solution was computed using equation 3.1. The effective fractional fission yields (Y) of ^{139}La from ^{235}U and ^{239}Pu fissions were taken from literature [15]. The numbers of atoms of fission product monitor, A and the total residual heavy elements, H (uranium and plutonium) in a given aliquot of a dissolver solution were computed from the concentration, using IDMS technique. Subsequently, the burn-up (atom % fission) values were computed and given in Table 3B.2.

Table 3B.2 Total number of atoms and burn-up computed using different isotopes of La and Nd determined by IDMS technique.

Fission product monitors	Total no. of atoms determined per gm of dissolver soln.(A) [a)]	Atom % burn-up[b)]
^{139}La	1.91×10^{16}	0.81
^{148}Nd	5.26×10^{15}	0.82
^{Total}Nd	5.68×10^{16}	0.80

[a)] Corresponding to “A” given in equation (3.1)

[b)] Total residual heavy element atoms (U+Pu) determined per gram of dissolver solution (H): 3.79×10^{19} (U: 3.78×10^{19} and Pu: 1.44×10^{17}).

The total residual heavy element atoms (H) was determined per gram of dissolver solution for present work and was found to be 3.79×10^{19} (U: 3.78×10^{19} and Pu: 1.44×10^{17}). As can be seen, the atom % burn-up computed using fission product monitor, lanthanum for PHWR dissolver solution is in good agreement with that obtained using the well established Nd-148 method. The isotopic composition of fission product lanthanum is: ^{139}La: 99.99%. The atom % burn-up determined from concentrations of U, Pu, La and Nd was found to be 0.82 (^{148}Nd as fission monitor) and 0.80 (elemental Nd as monitor), 0.81 (^{139}La as fission monitor). The details of all the steps to arrive at the final burn-up value for PHWR dissolver solution are given in Appendix-2. The errors associated with burn-up are due to uncertainties in the fission yield data and uncertainties associated with experimental determination La/Nd, U and Pu. The overall uncertainty is in the region of about 2-3%.

3B.4 Conclusion

A rapid HPLC and TIMS methods have been developed for the separation and estimation of fission product element lanthanum for the burn-up measurements on the PHWR dissolver solution. A dynamic ion exchange chromatography technique was used for the separation of lanthanum as well as neodymium from the dissolver solution. The pure fractions of La and spiked mixture of La, Nd, U and Pu were subjected to TIMS analysis. New sample loading method was developed for lanthanum analysis by TIMS and they provide enhanced and steady ion beam formation of LaO^+. IDMS method was employed for accurate and precise determination of La, Nd, U and Pu concentrations in the dissolver solution. The atom % burn-up was derived for PHWR dissolver solution using lanthanum as alternate fission product monitor and the data obtained are in good agreement with those obtained using ASTM procedure employing Nd-148 as monitor. For the first time, lanthanum is used as fission product monitor for determining burn-up using TIMS.

References

[1] I. G. Cuninghame, The Mass-Yield Curve for Fission of Natural Uranium by 14-MeV Neutrons. J. Inorg. Nucl. Chem. 5 (1957) 1.

[2] P. Moller, D. G. Madland, A. J. Sierk, A. Iwamoto, Nuclear fission modes and fragment mass asymmetries in a five-dimensional deformation space. Int. J. Science, Nature 409 (2001) 785.

[3] W. N. Bishop, Nuclear Regulatory Commission, Washington D.C., Vol. 1, Report NUREG /CP 004 (1977) 469.

[4] J. E. Rein, B. F. Rider, Burn-up Determination of Nuclear Fuels. AEC Research and Development Report, 18th Ed., TID-17385, TID-4500 (1963).

[5] W. J. Maeck, R. P. Larsen, J. E. Rein, A review and status of the nuclear data and analytical chemistry methodology requirements. U.S. Atomic Energy Commission (1973).

[6] J. E. Rein, Analytical Methods in the Nuclear Fuel Cycle. IAEA - SM-149, IAEA, Vienna (1972).

[7] R. M. Cassidy, in: J. F. Lawrence, (Ed.): Trace Analysis. Vol. 1, Academic Press, New York (1981) 121.

[8] W. J. Maeck, W. A. Emel, J. E. Delmore, F. A. Duce, L. L. Dickerson, J. H. Keller, R. L. Tromp, Report No. EY-76-C-07-1540 (1976).

[9] A. J. Fudge, A. J. Wood, M. F. Banham, Report TID-7629 (1961) 152.

[10] N. Sivaraman, S. Subramaniam, T. G. Srinivasan, P. R. Vasudeva Rao, Burn-up measurements on nuclear reactor fuels using high performance liquid chromatography. J. Radioanal. Nucl. Chem. 253 (2002) 35.

[11] P. De Regge, R. Boden, Determination of neodymium isotopes as burn-up indicator of highly irradiated (U, Pu)O_2 LMFBR fuel. J. Radioanal. Chem. 35 (1977) 173.

[12] R. S. Forsyth, Some Studies on the Burn-up of Nuclear Fuel. Chem. Comm. No. II (1970).

[13] ASTM Standards, E321-96: Standard Test Method for Atom Percent Fission in Uranium and Plutonium Fuel (Neodymium-148 Method). PA 19428-2959, United States (2005).

[14] J. Magill, G. Pfennig, R. Dreher, Z. Sóti, Karlsruhe Nuclide Chart. (2012).

[15] E. A. C. Crouch, Atomic Data and Nuclear Data Tables: Fission Product Yields from Neutron Induced Fission. Academic Press, New York and London, Vol.19 (1977).

[16] V. R. Murthy, Elemental and isotopic abundances of molybdenum in some meteorites. Geochim. Cosmochim. Acta, 27 (1963) 1171.

[17] G. W. Wetherill, Isotopic Composition and Concentration of Molybdenum in Iron Meteorites. J. Geophys. Res. 69, No.20 (1964) 4403.

[18] L. J. Moore, L. A. Machlan, W. R. Shields, E. L. Garner, Internal Normalization Techniques for High Accuracy Isotope Dilution Analyses-Application to Molybdenum and Nickel in Standard Reference materials. Anal. Chem. 46 (1974) 1082.

[19] Qi-Lu, A. Masuda, High Accuracy Measurement of Isotope Ratios of Molybdenum in Some Terrestrial Molybdenites. J. Am. Soc. Mass Spectrom. 3 (1992) 10.

[20] Qi-Lu, A. Masuda, The isotopic composition and atomic weight of molybdenum. Int. J. Mass Spectrom. Ion Processes 130 (1994) 65.

[21] A. Kawashima, K. Takahashi, A. Masuda, Positive thermal ionisation mass spectrometry of molybdenum. Int. J. Mass Spectrom. Ion Processes 115 (1993) 115.

[22] M. E. Wieser, J. R. De Laeter, Thermal ionisation mass spectrometry of molybdenum isotopes. Int. J. Mass Spectrom. 197 (2000) 253.

[23] A. Datta, N. Sivaraman, T. G. Srinivasan, P. R. Vasudeva Rao, Rapid Separation of Lanthanides and Actinides on Small Particle Based Reverse Phase Supports. Radiochim. Acta, 98 (2010) 277.

[24] A. Datta, N. Sivaraman, T. G. Srinivasan, P. R. Vasudeva Rao, Single Stage Coupled Column HPLC Technique for the Separation and Determination of Lanthanides in Uranium Matrix-Application to Burn-up Measurement on Nuclear Reactor Fuel. Nucl. Tech. TN-12-45 (2013).

[25] A. Datta, K. Sujatha, R. Kumar, N. Sivaraman, T. G. Srinivasan, P. R. Vasudeva Rao, High Performance Separation and Supercritical Extraction of Lanthanides and Actinides. Energy Procedia, 8 (2011) 425.

[26] S. Bera, R. Balasubramanian, A. Datta, R. Sajimol, S. Nalini, T. S. Lakshmi Narasimhan, M. P. Antony, N. Sivaraman, K. Nagarajan, P. R. Vasudeva Rao, Burn-Up Measurements on Dissolver Solution of Mixed Oxide Fuel Using HPLC-Mass Spectrometric Method. Int. J. Anal. Mass Spect. Chrom. 1 (2013) 55.

[27] J. Meija, T. B. Coplen, M. Berglund, W. A. Brand, P. De Bievre, M. Groning N. E. Holden, J. Irrgeher, R. D. Loss, T. Walczyk, T. Prohaska, Isotopic compositions of the elements 2013, Pure Appl. Chem. 88, 3 (2016) 293.

[28] M. G. Inghram, R. J. Hayden, D. C. Hess, The Isotopic Constitution of Lanthanum and Cerium. Phys. Rev. 72 (1947) 967.

[29] F. A. White, T. L. Collins, F. M. Rourke, Search for Possible Naturally Occurring Isotopes of Low Abundance. Phys. Rev. 101 (1956) 1786.

[30] N. L. Elliot, L. W. Green, B. M. Recoskie, R. M. Cassidy, Mass Spectrometric Determination of Lanthanum in Nuclear Fuels. Anal. Chem. 58 (1986) 1178.

[31] A. Makishima, H. Shimizu, A. Masuda, Precise Measurement of cerium and Lanthanum Isotope Ratios. J. Mass Spect. Soc. Japan, 35 (1987) 64.

[32] J. J. -S. Shen, T. Lee, C. T. Chang, Detecting Small Isotopic Shifts in Two-Isotope Elements Using Thermal Ionisation Mass Spectrometry. Anal. Chem. 64 (1992) 2216.

[33] J. J. -S Shen, T. Lee, C. T. Chang, Lanthanum isotopic composition of meteoritic and terrestrial matter. Geochim. Cosmochim. Acta 58 (1994) 1499.

[34] J. R. De Laeter, N. Bukilic, The isotopic composition and atomic weight of lanthanum. Int. J. Mass Spect. 244 (2005) 91.

[35] A. J. Spivack, J. M. Edmond, Determination of Boron Isotope Ratios by Thermal Ionisation Mass Spectrometry of the Dicesium Metaborate Cation, Anal. Chem. 58 (1986) 31.

CHAPTER 4

==

Other TIMS studies on materials of relevance to nuclear fuel cycle

This chapter describes the application of TIMS in some of the areas in nuclear fuel cycle like reprocessing plants, radioactive waste management facility and isotope enrichment plants. It contains three subchapters namely,

Chapter 4A: Development of new sample loading method for magnesium analysis, which is used as tracer in reprocessing plants.

Chapter 4B: Simultaneous quantification of lithium and neodymium in sodalite matrix used for immobilization of radioactive waste.

Chapter 4C: Feasibility and optimisation of gadolinium enrichment process using HPLC and use of TIMS as verification of enrichment process.

CHAPTER 4A

Improved magnesium loading method to employ MAGnesium Tracer Technique for the Accountability of Plutonium (MAGTRAP)

This subchapter describes the importance of magnesium as tracer for volume measurement and accountability of plutonium in the input tank of the reprocessing plant. It highlights the usefulness of new sample loading method developed for improving the accuracy in the determination of magnesium.

4A.1 Introduction

Precise and accurate isotopic analysis of magnesium finds wide applications in areas like geology, oceanography, biology and nuclear technology [1-3]. As mentioned previously, Indian nuclear reactors follow closed fuel cycle, which involve reprocessing and recycling of uranium and plutonium. The closed fuel cycle have benefits like effective utilisation of fissile material, minimisation of high level waste and proliferation resistance. The reprocessing of spent nuclear fuel involves separation, extraction and consolidation of uranium, plutonium and some of the important fission products (for societal applications) from dissolver fuel solutions. Accounting of these nuclear materials, especially plutonium at input end of the reprocessing plant is very important, where it appears for the first time in the nuclear fuel cycle after being produced in the reactor. In a reprocessing plant, the fuels cooled for sufficient time, after irradiation in reactor, were dissolved in concentrated HNO_3 for the separation of uranium and plutonium using a process called Plutonium Uranium Redox Extraction (PUREX) [4]. After dissolution, the clear solution containing these nuclear materials is stored in accountability tank before carrying out further chemical processing. The accounting of nuclear materials in reprocessing input tank is essential for efficient and economic operation, propensity for criticality, health and safety of the facility workers and the public, proliferation resistance of nuclear materials and providing assurance that all material quantities are present in the correct amount.

For nuclear material accounting (NUMAC), it is important to determine accurately and precisely the amount of uranium and plutonium present in accountability tank. Among all mass spectrometric techniques, thermal ionisation mass spectrometry (TIMS) plays a vital role in the determination of uranium and plutonium present in input tank and isotopic dilution mass spectrometry (IDMS) is the only accepted measurement technique for this purpose especially since separation need not be quantitative. The accounting of nuclear materials in the input accountability tank is based on the measurement of three quantities 1) volume of dissolver solution in reprocessing tank, 2) density of the solution, 3) uranium and plutonium concentration.

The non-destructive techniques available for volume measurements in reprocessing tank are electro manometer, dip U-tube manometer, the acoustic system (SONAR) and the Time Domain Reflect meter (TDR). The use of electro manometer system over the conventional U-tube manometric system has improved the sensitivity and the accuracy of pressure measurements, by a factor of ten. However, it suffers from the problem of run-to-run difference in tank calibration. Other liquid level measurement systems such as TDR and SONAR are in the phase of development to accommodate inside the confinement box, where reprocessing tank is located. Thus, there is a need for alternative techniques for volume measurement in reprocessing tank due to the following reasons

1. None of the above nondestructive methods can account the holdup volume or dead volume in the tank.

2. The precision of destructive analytical techniques in most cases is superior because the effect of the sample matrix can be eliminated or corrected.
3. The detection limit of destructive analysis technique is usually lower than non-destructive techniques.
4. The role of destructive analytical techniques is to calibrate the non-destructive analytical instruments available for volume measurement.
5. It provides an alternative and independent verification method.

The better way for the determination of the volume of reprocessing input tank solution is by tracer techniques.

4A.2 Principle of tracer technique

The “tracer technique” is based on the addition of a known amount of a specific element (tracer/spike) to the dissolver solution and the measurement of its concentration in an aliquot of the solution drawn from the tank after homogenisation. The ratio between the concentration of the tracer added and the concentration of the tracer found after mixing gives the volume of the solution in the tank. The measurement of the tracer concentration in the drawn sample is performed by isotopic dilution mass spectrometry method with the aid of a well calibrated spike.

The main criteria for selection of a suitable tracer are

1) The tracer element should have at least two stable (or long-lived) isotopes, one of which must be available in a highly enriched form to be used as spike for isotope dilution.
2) It should be chemically inert and not lost by adsorption, plating and other reactions.
3) It should, preferably, not have different oxidation states (among which isotopic exchange is slow).
4) A chemical assay standard must be available, i.e., it must have a compound which is available in pure and stoichiometric form.

5) It should not interfere with plant operation, especially in product purity, decontamination factor, extraction efficiency, etc.
6) Preferably, it should not be a fission product with high fission yield, i.e. low blank in process solution.
7) It should be inexpensive and readily available.
8) Minimum risk of contamination in handling.
9) It should be possible to measure its isotopic abundances (at least the ratio of an abundant natural isotope to the spike isotope) very accurately.
10) Absence of isobaric interferences

Based on above criteria suitable elements which can be selected as tracer elements are Li, Mg, K, Ca, Zn, Sr, Nd, Gd, Er, Yb, Lu, Re, Pb and U. Among these, Li, Mg, Lu and Pd were short listed for the present study since the possibility of natural contamination is less during analysis, availability of the element in reprocessing tank (back ground source) and isotopic abundance. Out of these, based on isotopic fractionation effect and availability of standard solution, magnesium was selected as tracer for measurement of input tank volume. The volume of input tank can be determined by the following procedure.

A known weight (W_{Tracer}) of tracer (^{24}Mg: natural magnesium), is added to the input tank. After complete homogenisation, a known aliquot (W_{al}) of the solution is collected from the reprocessing tank and mixed with a known quantity of spike (^{26}Mg). Using IDMS technique the concentration of magnesium (C_s) in aliquot solution is determined. The weight of the total solution (W_{TS}) in the tank is given by

$$W_{TS} = (W_{Tracer} / C_s) \cdot W_{al} \tag{4A.1}$$

If $R_{(j/i)S}$, $R_{(j/i)Sp}$ and $R_{(j/i)mix}$ are the relative abundance of two isotopes (j: ^{26}Mg and i: ^{24}Mg) in the sample (S), spike (Sp), and mixture (mix) respectively, then the concentration of the element (Mg) in the sample (C_S) is given by

$$C_S = \frac{C_{Sp*}\,W_{Sp}}{W_S} \times \left(\frac{R_{(j/i)Sp} - R_{(j/i)mix}}{R_{(j/i)mix} - R_{(j/i)S}} \times \frac{1}{R_{(j/i)Sp}}\right) \times \frac{<AF_{j,Sp}>}{<AF_{i,S}>} \times \frac{(AW)_S}{(AW)_{Sp}} \qquad (4A.2)$$

where $AF_{j,Sp}$ and $AF_{i,S}$: are atom fractions of isotopes j and i in spike and sample, respectively. $(AW)_S$ and $(AW)_{Sp}$: are average atomic weight of sample and spike, respectively. Figure 4A.1 shows pictorial representation of above method for volume measurement of input tank.

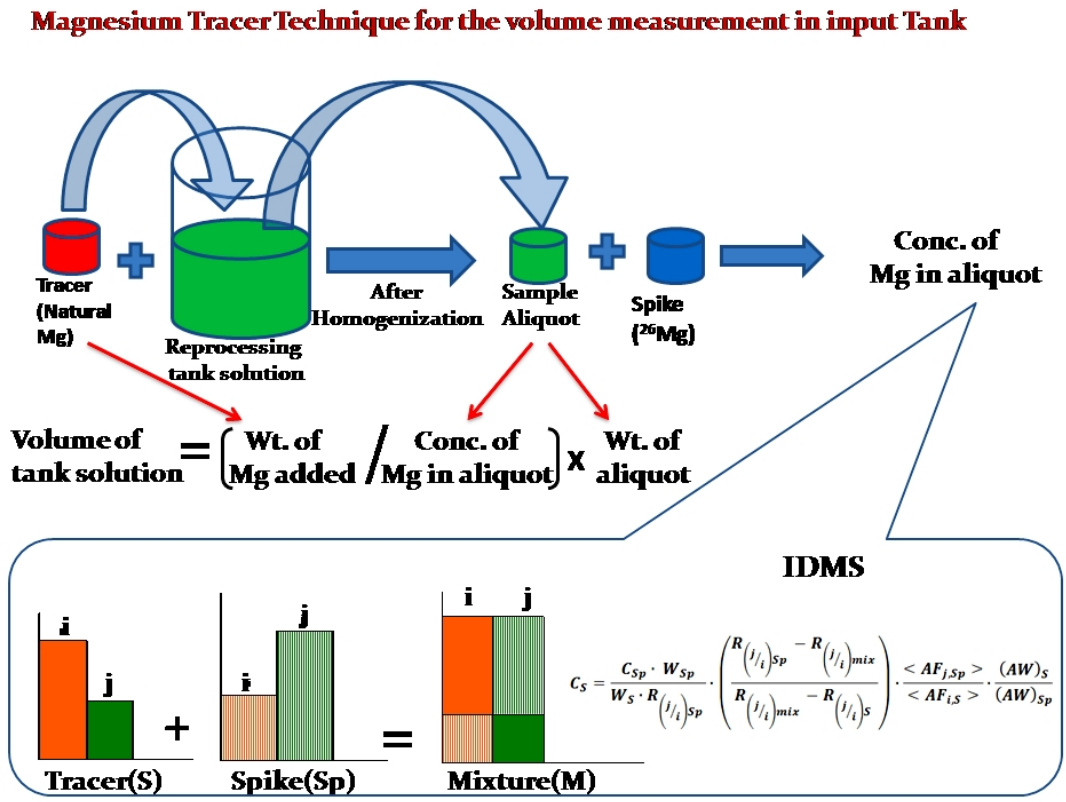

Fig. 4A.1 Pictorial representation of magnesium tracer technique for the volume measurement in input tank.

To determine the amount of plutonium present in the input tank, following procedure is adopted. A known amount of natural magnesium (W_{Mg}) is added to the reprocessing tank containing plutonium solution. After homogenisation (by mechanical mixing), small quantity of the solution is withdrawn and mixed with tracers (^{26}Mg and

^{240}Pu) in an accurately known ratio (R_t). The quantity of sample withdrawn and the tracer added need not be known. The ratios ^{240}Pu/^{239}Pu [$R_{\left(240/_{239}\right)mix}$] and ^{26}Mg/^{24}Mg [$R_{\left(26/_{24}\right)mix}$] are measured in the spiked solution. Using isotopic ratios of natural magnesium added to tank solution ^{26}Mg/^{24}Mg ($R_{\left(26/_{24}\right)Nat}$) and isotopic ratio of plutonium($R_{\left(240/_{239}\right)S}$) in the sample, the total amount of plutonium (W_{Pu}) in the tank can be given as

$$\boldsymbol{W_{Pu} = W_{Mg} \cdot R_t \cdot \frac{\left[R_{(26/_{24})mix} - R_{(26/_{24})Nat}\right]}{\left[R_{(240/_{239})mix} - R_{(240/_{239})S}\right]} \cdot \frac{\left[1 - \left(R_{(240/_{239})mix} / R_{(240/_{239})Sp}\right)\right]}{\left[1 - \left(R_{(26/_{24})mix} / R_{(26/_{24})Sp}\right)\right]} \cdot \frac{<AF_{(26),S}>}{<AF_{(239),S}>} \cdot \frac{(AW)Pu_{(S)}}{(AW)Mg_{(S)}}} \quad (4A.3)$$

where $< AF_{(26),S} >$, $< AF_{(239),S} >$ are atom fractions of ^{26}Mg and ^{239}Pu in sample, $(AW)Mg_{(S)}$, $(AW)Pu_{(S)}$ are the average atomic weights of magnesium and plutonium in the sample. The only assumption in this procedure is that no magnesium is present in accountability tank. If some amount of magnesium is present in blank, then blank correction for magnesium can be incorporated by measuring the magnesium in tank solution by IDMS method. Magnesium as tracer employed in different laboratories, worldwide is listed in Table 4A.1.

Table 4A.1 Magnesium as tracer employed in different laboratories across the world [5].

Year of experiment	Site	Volume of the reprocessing tank (litres)	Research institutes involved
1975	Tarapur, Atomic power station	1500	Bhabha Atomic Research Centre, Mumbai, India.
1979	La Hague, Nuclear fuel reprocessing plant	3000	CEN Saclay, France
1980	WAK, Karlsruhe reprocessing plant	800	International Atomic Energy Agency (IAEA)-Federal Republic of Germany (FRG) Support Programme.
1982	Marcoule, Nuclear site	500	CEN Saclay, France.
1982	EUREX, Nuclear fuel reprocessing facility	300	ENEA EUREX-JRC ISPRA, Italy.
1983	ALKEM, Karlsruhe reprocessing plant	300	IAEA-FRG Support Programme.

Magnesium has three natural isotopes namely 24, 25 and 26 having abundances 78.60%, 10.11% and 11.29%, respectively. It has first ionisation energy of 7.65 eV. Due to high ionisation energy and low mass, magnesium isotopes are more prone to fractionation and hence direct loading of sample during TIMS analysis is challenging. Isotopic fractionation is a process where relative evaporation of lighter isotope of an element is higher compared to the heavier isotope which leads to decrease in isotopic ratio of the lighter to the heavier isotope with time, during TIMS analysis. Mathews et al. [6] had employed magnesium as tracer for accountability of plutonium in reprocessing tank and coined the name MAGnesium TRacer technique for the Accountability of Plutonium (MAGTRAP) in the year 1975. Calanzaro et al. [7] had determined the isotopic ratio of magnesium in nitric acid medium, loaded with uranyl nitrate on rhenium side filament of triple filament assembly. Aggarwal et al. [8] had loaded magnesium in nitrate and chloride form on rhenium triple filament assembly to minimise fractionation effect during isotopic ratio measurements. Stegmann et al. [9] had reported the isotopic composition of magnesium by loading magnesium chloride with silica gel and boric acid on a rhenium single filament. Midwood et al. [10] had employed silica gel and phosphoric acid mixture loaded on rhenium single filament to determine magnesium isotopic ratio of standard solution (Standard Reference Material (SRM-980) in chloride medium.

The present work was confined to the magnesium isotopic ratio measurements. The equations (4A.2 and 4A.3) presented for determination of volume and amount of plutonium respectively in input reprocessing tank required only isotopic ratios, weight of tracer and concentration of tracer added for analysis. The isotopic ratio measurement of magnesium using TIMS is a crucial step in volume measurement using tracer technique. This in turn will provide accurate determination of volume of input tank and avoid error due to non accounting of dead volume. For magnesium analysis, a new sample loading method was employed in the present study. In this method, magnesium with tantalum activator in chloride medium was loaded on rhenium side filament of Re-Re-Re triple filament assembly. To ascertain the usefulness of present sample loading method employed for magnesium analysis, a standard reference material of magnesium was considered. The developed method was compared with other literature procedures by taking SRM-980 certified magnesium. For the present investigations, samples in four chemical forms were selected: a) natural magnesium in nitrate form, b) SRM-980 solution in chloride form, c) SRM-980 solution with silica gel and boric acid in chloride medium, and d) SRM-980 with tantalum activator in chloride medium.

4A.3 Experimental

4A.3.1 Sample preparation

To minimise isotopic fractionation effect and to produce stable magnesium ion at low temperature a suitable activator was prepared. For this, ~ 0.2 mL of concentrated hydrofluoric acid (50%, M/s Sigma Aldrich), ~ 0.15 mL of concentrated phosphoric acid (85%, M/s Fisher scientific), ~ 20 mL of concentrated nitric acid (70%, M/s Merck) were added sequentially to the ~ 0.15 g tantalum pentoxide (purity 99.99%, M/s Sigma Aldrich) powder taken in a Teflon beaker. The solution was kept under IR lamp for complete dissolution, followed by addition of 30 mL of Millipore water to it. The above mixture is referred as tantalum activator solution. The silica gel suspension was prepared by mixing 0.1 g of well grounded powder (supplied as 60-120 mesh size) with about 2 mL of Millipore water and allowed to settle overnight. The supernatant solution was used for the experiment. 0.5 M boric acid solution was prepared by dissolving boric acid powder in Millipore water. Natural magnesium nitrate solution was prepared by dissolving magnesium oxide powder (purity, ≥ 97%, M/s Merck) in HNO_3 medium. The SRM-980 standard solution was prepared by dissolving magnesium metal in HCl medium.

4A.3.2 Sample loading

About 4 µL of tantalum activator solution was deposited on the surface of a rhenium side filament and dried by passing a constant current of 0.8 A. Above it, ~ 10 µL of magnesium containing solution was added and heated to 0.8 A. Finally, filament current was raised to 1.6 A for complete evaporation of solution mixture.

4A.4 TIMS analysis

After complete evaporation, sample filaments were loaded on sample holder magazine in Re-Re-Re, triple filament assemblies. Central and side filaments (one of it contained sample) were heated to identify and focus rhenium pilot peak. Then central filament was raised to 5.4 A and side filament to 2.0 A for effective analysis of magnesium ions. Figure 4A.2 shows mass spectrum of magnesium in SRM-980 sample and its isotopic composition is listed in Table 4A.2.

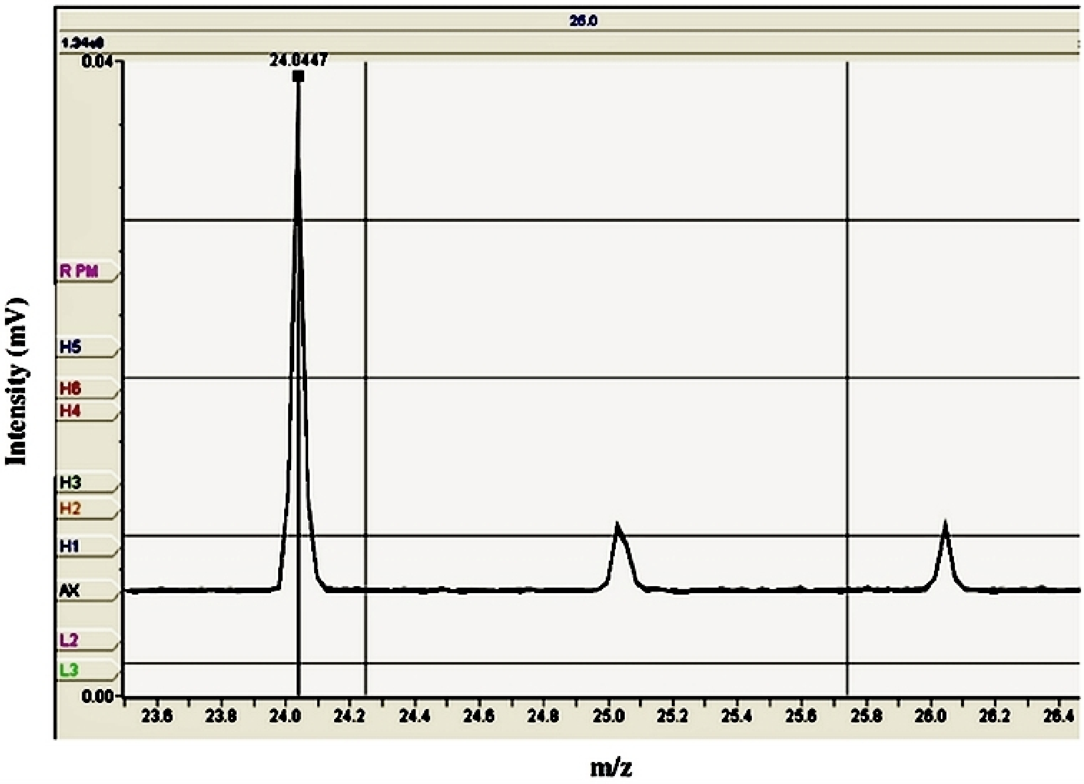

Fig. 4A.2 Mass spectrum of magnesium in SRM-980.

Table 4A.2 Isotopic ratios and abundances of magnesium in SRM-980.

Isotope M(i)	Isotope ratio M(i)/M(ref)	Relative error in % in the isotope ratio [a)]	Atom fraction of the isotope M(i)	Relative error in % in atom fraction [b)]	Mass % of the isotope M(i)
Magnesium: M (ref) = 24; Average atomic weight = 24.305					
24	1	-	7.897×10^{-1}	0.08	77.930
25	1.268×10^{-1}	0.54	1.001×10^{-1}	0.55	10.295
26	1.395×10^{-1}	0.51	1.102×10^{-1}	0.52	11.775

a) Combination of internal and external error (standard deviation) associated with individual runs.

b) Derived from error associated with isotopic ratios using error propagation.

4A.5 Results and Discussion

The main objective of adding tantalum activator during magnesium analysis is to (i) overcome the high ionisation energy barrier (by enhancing work function of the filament surface, that reflects in increase in ion intensity of magnesium), (ii) minimising the isotopic fractionation effect (which can be observe from accuracy and precision of isotopic ratios) during acquisition of isotopic ratio data. Loading techniques with two types of additives viz. silica gel-boric acid and tantalum activator were employed to examine ion enhancing ability for magnesium ion emission. The isotopic ratios of magnesium were measured with static multicollector mode using three Faraday cup detectors (Ax, H3 and H6). The coincidence of magnesium isotopes, which indicate proper focusing of ions onto the faraday cup detector, is shown in Figure 4A.3.

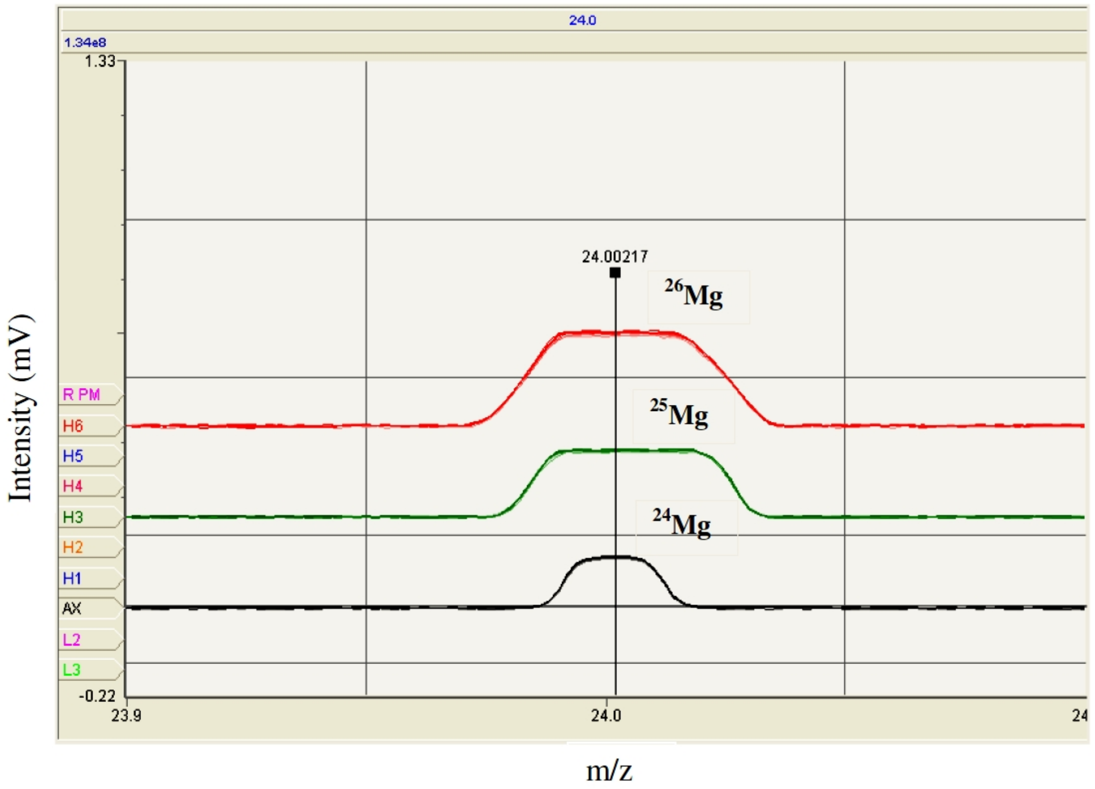

Fig. 4A.3 Coincidence of magnesium isotopes.

Table 4A.3 gives the isotope ratios obtained in various loading and heating conditions along with the precision and accuracy of the measurements. The ratio of observed (from experiment) and certified values (from reference) for the natural magnesium [11] and SRM-980 certified magnesium are also given in the same table. As can be seen from the table, the isotope ratios from samples loaded as nitrate and chloride show better reproducibility but poorer accuracy possibly due to fractionation effects. On the other hand, silica gel technique yielded poorer precision but better accuracy than the above loading methods. It was observed that magnesium loaded in chloride form provides sufficient ion intensity at low temperature, compared to magnesium loaded in nitrate form, indicating less fractionation effect in the former. Hence for the present work, magnesium was loaded in chloride medium along with tantalum activator. The tantalum activator method provided isotopic ratio of magnesium for SRM-980 with better accuracy (less isotopic fractionation), stable and intense ion beam. This loading method provided better precision than (silica gel + boric acid) loading method.

Table 4A.3 Comparison of results for different loading techniques for magnesium isotopic analysis.

Chemical forms of sample	Sample amount (µg)	Filament Current (A)		^{25}Mg/^{24}Mg		^{26}Mg/^{24}Mg	
		IFC*	VFC*	Observed Value (%RSD)[a]	*Observed* / *Certified* Value	Observed Value (%RSD)[a]	*Observed* / *Certified* Value
Mg as nitrate form (Natural)	6	4.9	1.2	0.12815 (0.2%)	1.01224	0.14266 (0.26%)	1.02353
Mg as chloride form (SRM-980)	12	4.7	0.2	0.12840 (0.38%)	1.01398	0.14185 (0.63%)	1.01816
Mg as chloride form with silica gel and boric acid (SRM-980)	12	2.6		0.12600 (1.0%)	0.99502	0.138357 (1.57%)	0.99309
Mg as chloride form with "Ta" activator (SRM-980)	12	5.4	2.0	0.12682 (0.54%)	1.00150	0.13948 (0.51%)	1.00115
Certified values for magnesium samples used in this study				**Natural Mg**		**SRM-980 Mg Standard**	
				^{25}Mg/^{24}Mg	^{26}Mg/^{24}Mg	^{25}Mg/^{24}Mg	^{26}Mg/^{24}Mg
				0.12660	0.13938	0.12663 (0.10%)	0.13932 (0.19%)

* IFC: Ionisation Filament Current, VFC: Vaporisation Filament Current

[a] Combination of internal and external error (standard deviation) associated with individual runs

The distribution (25 data points) of $^{26}Mg/^{24}Mg$ isotopic ratios obtained using tantalum activator loading method with respect to SRM-980 is shown in Figure 4A.4 and the mean isotopic ratio was found to be 0.13948 ± 0.00071 and the SRM-980 certified data is 0.13932 ± 0.00026.

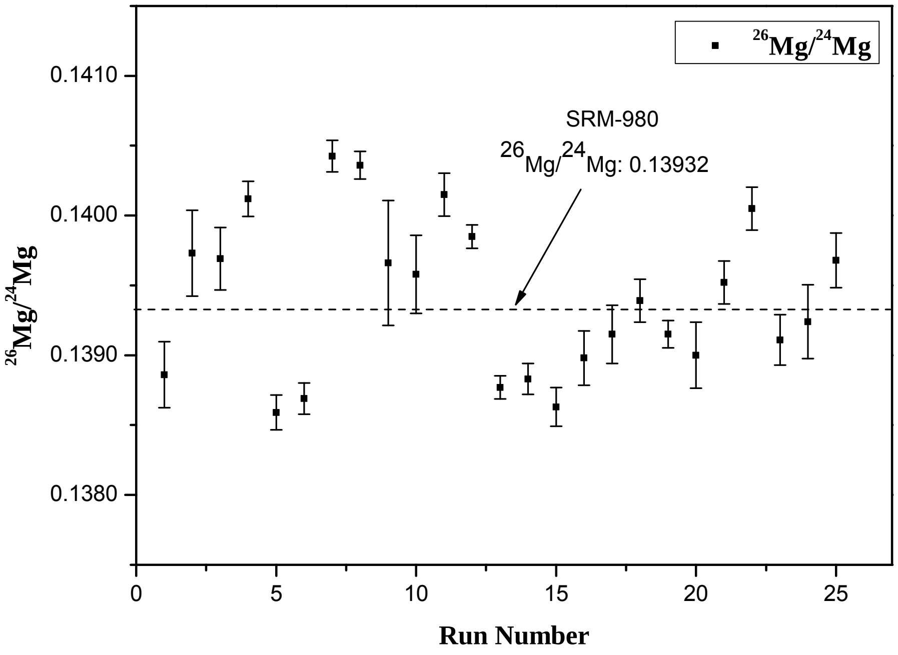

Fig. 4A.4 Distribution of isotopic ratios of $^{26}Mg/^{24}Mg$ in SRM-980 measured using tantalum activator loading method.

The isotopic ratio of $^{26}Mg/^{24}Mg$ obtained using present work is shown in Table 4A.4 along with those reported in literature. It can be seen from the data that the sample loaded using tantalum activator method provides more accurate result compared to data reported using (silica gel+ phosphoric acid) [9] and (silica gel + boric acid) [3] methods.

Table 4A.4 Comparison of results of isotopic ratio of ^{26}Mg/^{24}Mg in SRM-980.

Loading technique	^{26}Mg/^{24}Mg	References	Standard/ technique used
Mg as chloride form with "Ta" activator	0.13948 ± 0.00071	Present study	SRM-980 / TIMS
Mg as chloride form with silica gel and phosphoric acid	0.13979 ± 0.00013	Midwood et al. [9]	SRM-980 / TIMS
Mg as chloride form with silica gel and boric acid	0.139733 ± 0.000028	Stegmann et al. [3]	Mg standard (Titrisol soln., Merck, Germany) / TIMS
Direct injection of Mg standard solution	0.1393 ± 0.0003	Becker et al. [11]	SRM-980 / ICP-MS

4A.6 Conclusion

The accurate and precise isotopic ratio measurement of tracer (magnesium) is an important criterion for accurate and precise determination of volume of input reprocessing tank. A new sample loading method was employed for magnesium isotopic ratio analysis. In this method magnesium in chloride form, mixed with tantalum activator, loaded on a rhenium side filament provided stable ion beam with less isotopic fractionation. The isotopic ratio of magnesium obtained using above sample loading method was compared with other sample loading techniques. The tantalum activator method has proven to be better in terms of accuracy (lesser degree of fractionation), providing stable ion beam intensity and extended sample life. The isotopic ratio of $^{26/24}$Mg obtained using tantalum activator method was found to be 0.13948 ± 0.00071. When compared to literature work [3, 9], the result obtained in the present work using TIMS is more accurate though the precision obtained is fair. Additional experiments with actual dissolver solution to implement above method for determination of volume in input tank was not attempted as subsequently it was observed that magnesium solution formed a layer on the inner surface of the container holding stock solution, which may affect the chemical properties of structural material holding the actual dissolver solution in input tank.

CHAPTER 4B

IDMS Studies on Sodalite - a Candidate Material for Nuclear waste Immobilisation

This subchapter describes the implementation of IDMS technique for determination of lithium and neodymium concentration in sodalite sample. Present work involved on measurement of these elements loaded on single filament, without chemical separation.

4B.1 Introduction

Nuclear fuels after irradiation, are subjected to reprocessing to separate uranium and plutonium from spent fuel after sufficient cooling. During reprocessing either by aqueous route (PUREX process for oxide fuels) [4] or by non-aqueous route (pyro-metallurgical reprocessing for metallic fuels) [12], radioactive high level waste (solid and liquid) is generated. The high level waste (HLW) is immobilised using suitable matrices. There are various kinds of waste storage matrices depending on the nature of waste. Glass bonded sodalite (GBS) [Na_8 $(AlSiO_4)_6Cl_2$], a glass-ceramic, is a promising candidate for the immobilisation of the chloride waste resulting from pyro-metallurgical reprocessing of nuclear fuels [13]. Characterisation of individual components (waste matrix constituents) is essential for the development of this matrix, which is expected to encounter different physicochemical conditions. For this purpose, concentration of individual components in GBS were determined by employing Isotope Dilution Mass Spectrometry (IDMS) owing to its capability to ensure precise and accurate data for multi element analysis in a matrix.

Two set of experiments were carried out by taking up lighter element lithium and heavier element neodymium to examine whether without chemical separation one can determine the concentration in a given sample loaded on a single filament. These two elements were selected (out of Li, Cs, Ba and Nd) based on the availability of spike solution. Though natural cesium (^{133}Cs) is mono isotopic in nature, cesium isotopes (133, 134, 135 and 137) produced from nuclear reactor can be considered for concentration measurement using IDMS method. Precise isotopic ratio measurements for lithium is challenging due to its low mass (mass number 6 and 7), which is more prone to isotopic fractionation during TIMS analysis. It required low and slow heating rate of sample filament during analysis. For the determination of lithium, enriched ^{6}Li obtained from AERE, Harwell and for neodymium ^{150}Nd obtained from ORNL, USA were used as spikes. The solutions were standardised by a reverse IDMS procedure using pertinent standards with natural abundance available in our laboratory. The IDMS data on actual sodalite sample is presented in this work.

4B.2 Experimental

4B.2.1 Sample preparation

A simulated GBS waste form prepared by high temperature (900^{o} C) equilibration of dehydrated zeolite4A with a simulated chloride waste (containing Li, Cs, Ba, and Nd) and blending the salt occluded zeolite with boroaluminosilicate glass ceramic composite [14] was used for TIMS analysis. Cesium, barium and neodymium were selected because these elements are representative fission products belonging to the (IA, IIA, IIIB) periods of the periodic table and lithium from the chloride matrix (LiCl-KCl) used for pyro-metallurgical reprocessing. About 10 mg of powdered sample (two set; A & B) was weighed and dissolved in an acid mixture (2 mL of conc. HCl + 1 mL of conc. HNO_3 + 0.5 mL of conc. HF + 5 mL Millipore H_2O) contained in a sealed Teflon vessel heated on a mantle at 140 ˚C. This was diluted with known volume of 0.75 M HNO_3 and referred as stock solution for further experiments. For concentration measurements of lithium and neodymium, spikes (enriched in ^{6}Li and ^{150}Nd) in the form of nitrates were added to the aliquot of stock solution.

4B.2.2 TIMS analysis

Lithium and neodymium (first ionisation energy 5.39 and 5.53 eV, respectively) are easily ionised by thermal ionisation. A portion of stock solution (~ 4 μL) was loaded onto side filaments with Ta-Re-Ta configuration for thermal ionisation mass spectrometric analysis (ISOPROBE-T). Data were acquired in static multicollector mode using Faraday cups. Lithium and neodymium samples were loaded in nitrate medium on tantalum filament surface. For lithium analysis, potassium pilot peak was initially focused at 2.8 A and 0.5A for central and side filaments respectively, then central filament was raised to 3.6 A and side filaments to 0.7A at a heating rate of 0.001A/s. This current was sufficient enough to ionise lithium from side filament by radiation from central filament. Neodymium was analysed using normal procedure as mentioned in earlier chapter (chapter 2). The mass spectra of lithium isotopes in sodalite sample (^{7}Li is the highest abundant isotope) and in spike solution (enriched in ^{6}Li isotope) are presented in Figure 4B.1. Similarly Figure 4B.2 shows mass spectra of neodymium in sodalite and in spike, which is enriched with ^{150}Nd isotope.

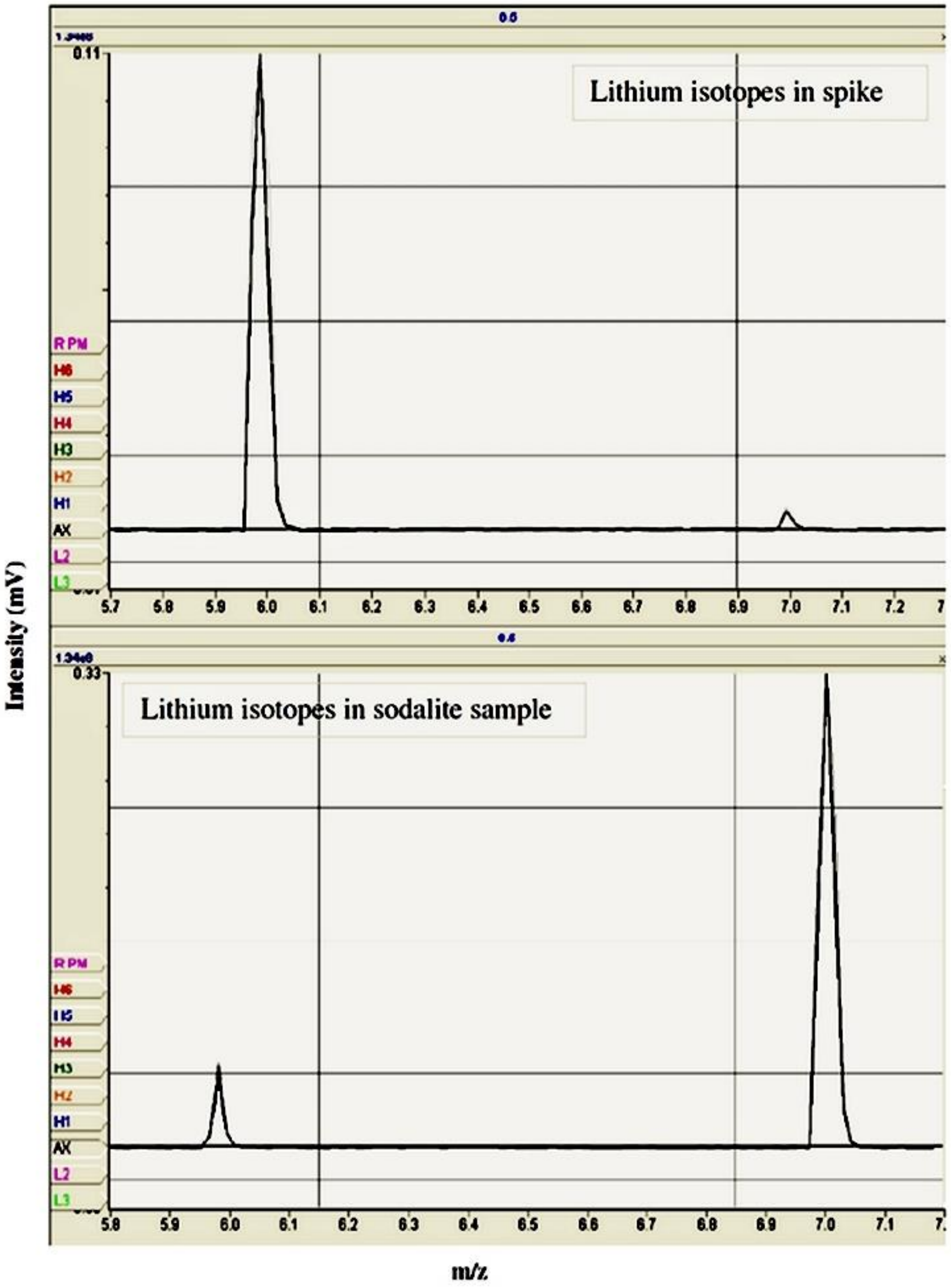

Fig. 4B.1 Mass spectra of lithium in sodalite (bottom) and in spike enriched with ^{6}Li (top).

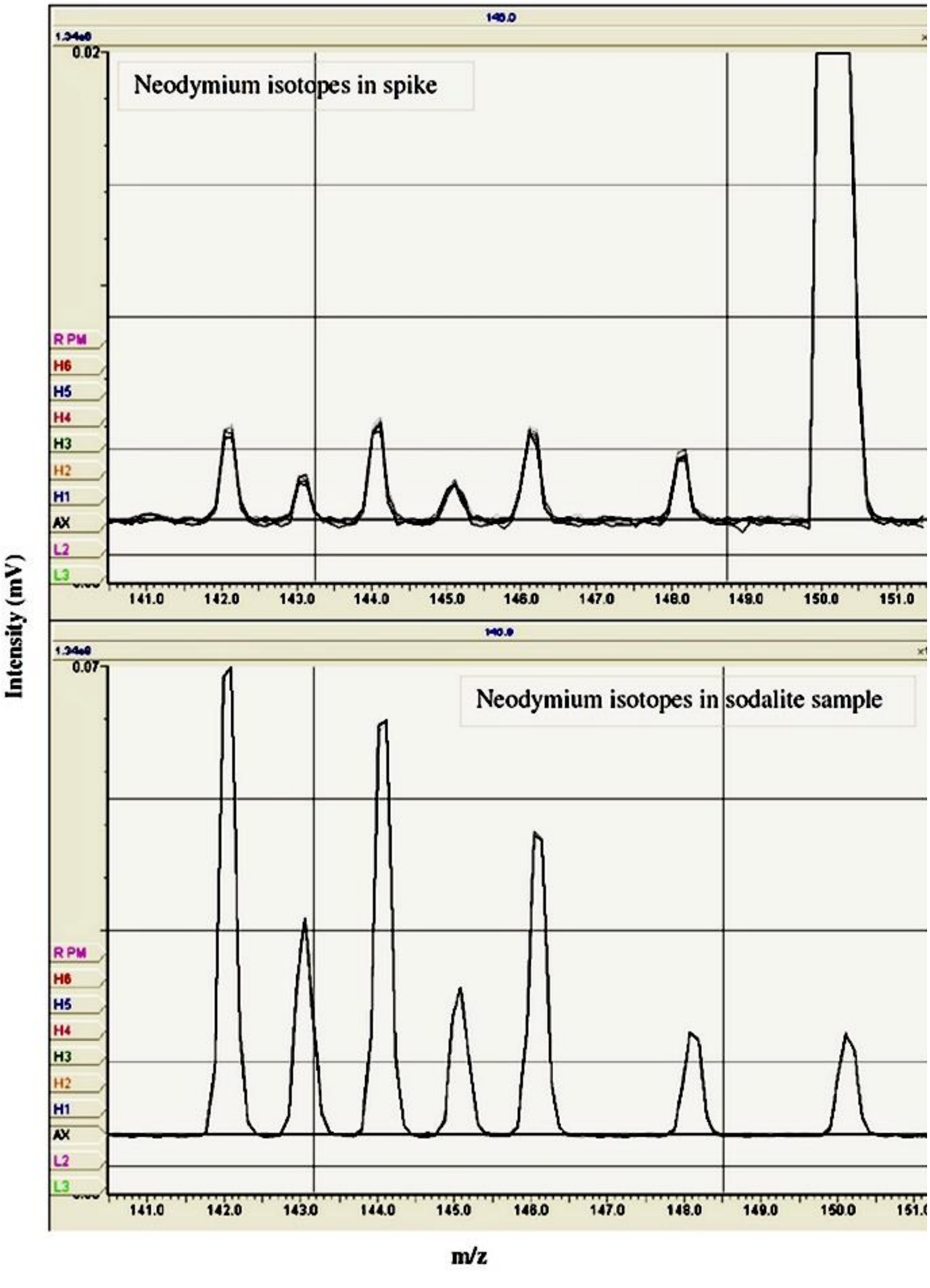

Fig. 4B.2 Mass spectra of neodymium in sodalite (bottom) and in spike enriched with ^{150}Nd (top).

4B.3 Results and Discussion

To achieve precise isotopic ratio of lithium, different sample loading conditions were attempted like loading in nitrate, chloride form, using single and triple filament assembly etc. It was observed that lithium loaded in nitrate form with minimum current to side and centre filaments, provides better results of isotopic ratio. The isotopic compositions of lithium and neodymium in sodalite were measured and the respective isotopic compositions are listed in Table 4B.1 and 4B.2.

Table 4B.1 Isotopic ratios and abundances of lithium in sodalite sample.

Isotope M(i)	Isotope ratio M(i)/M(ref)	Relative error in % in the isotope ratio [a)]	Atom fraction of the isotope M(i)	Relative error in % in atom fraction [b)]	Mass % of the isotope M(i)
Lithium: M (ref) = 7; Average atomic weight = 6.937					
6	8.598×10^{-2}	0.96	7.917×10^{-2}	0.97	6.865
7	1	-	9.208×10^{-1}	0.08	93.135

[a)] Combination of internal and external error (standard deviation) associated with individual runs.

[b)] Derived from error associated with isotopic ratios using error propagation.

The measured relative isotopic abundances for lithium (in atom percent) are: ^{6}Li: 7.92 and ^{7}Li: 92.08. For ^{142}Nd, ^{143}Nd, ^{144}Nd, ^{145}Nd, ^{146}Nd, ^{148}Nd, ^{150}Nd the abundances are: 27.25, 12.19, 23.81, 8.29, 17.14, 5.73 and 5.59 respectively. These values are in agreement with those of natural isotopic abundance [9]. Since there is a wide gap in temperature of appearance for Li and Nd ions (Li: central filament current (CFC): 3.6 A, side filament current (SFC): 0.7 A and for Nd: CFC: 5.5 A and SFC: 2.2 A), it was possible to carry out the analysis of these elements without any chemical separation.

Table 4B.2 Isotopic ratios and abundances of neodymium in sodalite sample.

Isotope M(i)	Isotope ratio M(i)/M(ref)	Relative error in % in isotope ratio [a)]	Atom fraction of the isotope M(i)	Relative error in % in atom fraction [b)]	Mass % of the isotope M(i)
Neodymium: M (ref) = 142; Average atomic weight = 144.235					
142	1	-	2.725×10^{-1}	0.05	26.812
143	4.473×10^{-1}	0.09	1.219×10^{-1}	0.10	12.077
144	8.737×10^{-1}	0.06	2.381×10^{-1}	0.08	23.756
145	3.040×10^{-1}	0.36	8.286×10^{-2}	0.37	8.325
146	6.291×10^{-1}	0.14	1.714×10^{-1}	0.15	17.343
148	2.101×10^{-1}	0.34	5.727×10^{-2}	0.35	5.873
150	2.053×10^{-1}	0.37	5.594×10^{-2}	0.37	5.814

[a)] Combination of internal and external error (standard deviation) associated with individual runs.

[b)] Derived from error associated with isotopic ratios using error propagation.

Reproducibility of measured concentrations was affected due to inhomogeneity during dissolution in the first set of experiments. Hence, the second set of experiment was optimised with respect to following conditions (i) increasing the heating conditions from 100 ˚C to 140 ˚C, and (ii) changing composition of the acid mixture by including hydrofluoric acid, and this lead to an improvement in the dissolution of sodalite sample. This resulted in achieving the value within an error of less than 1% (i.e. 0.64% for lithium and 0.22% for neodymium) from the mean concentrations. The data obtained after improving the dissolution conditions are presented in Table 4B.3.

Table 4B.3 IDMS data on lithium and neodymium in sodalite sample.

Lithium[a)]						
Sample	IR sample (6/7)	Relative error in % in isotopic ratio	IR mixture (6/7)	Relative error in % in isotopic ratio	Conc. (µg/g)	Mean Conc. (µg/g) (Error in %)
A	0.0864	0.76	1.4551	0.28	615.83	619.81 (0.64%)
B	0.0855	0.34	1.1644	0.90	623.78	
Neodymium[b)]						
Sample	IR sample (150/142)	Relative error in % in isotopic ratio	IR mixture (150/142)	Relative error in % in isotopic ratio	Conc. (µg/g)	Mean Conc. (µg/g) (Error in %)
A	0.2057	0.23	0.6422	0.17	4.66	4.65 (0.22%)
B	0.2048	0.19	0.3946	0.23	4.63	

[a)] Isotopic ratio (IR) for Li spike (^{6}Li/^{7}Li): 20.3697

[b)] Isotopic ratio (IR) for Nd spike (^{150}Nd/^{142}Nd): 124.844

4B.4 Conclusion

The challenges of precise isotopic ratio measurements and quantification of lithium in sodalite sample was overcome by loading the sample in nitrate form and controlled sample heating procedure to minimise isotopic fractionation effect. The studies revealed that lighter and heavier elements like lithium and neodymium can be conveniently determined by IDMS in sodalite sample without any prior chemical separation. This experiment also explored the capability of TIMS to analyse required element in presence of high salt containing matrix without interference. Further these experiments open up the possibilities for study on leaching behaviour of these elements from sodalite matrix in actual corrosive environments.

CHAPTER 4C

Gadolinium enrichment studies by using HPLC and TIMS

This subchapter describes about HPLC and TIMS analysis carried out for the enrichment studies of gadolinium isotopes.

4C.1 Introduction

Isotope enrichment is the process of concentrating specific isotope of interest of a chemical element by separating from other isotopes. Some of the principal factors that contribute to the separation process are gravitational or centrifugal effects which are proportional to the molecular masses, electric or magnetic forces affecting ionized molecules, and inter atomic or inter molecular forces.

Gadolinium has high neutron absorbing cross section and hence plays an important role in nuclear fuel cycle. Gadolinium has seven natural isotopes viz. 152, 154, 155, 156, 157, 158 and 160, having natural abundance (in atom percent) of 0.20, 2.18, 14.80, 20.47, 15.65, 24.84 and 21.86, respectively [10]. Among these isotopes, ^{155}Gd and ^{157}Gd have high thermal neutron absorption cross section of 60,900 and 2,54,000 barn (10^{-24} cm^{2}) respectively. Natural gadolinium is used as a burnable poison in nuclear fuel but the use of gadolinium enriched with 155 and 157 isotopes would create more effective burnable poison [15, 16]. Hence the use of enriched gadolinium ($^{155,\ 157}$Gd) will reduce the gadolinium inventory and this provides a good economic incentive. Also, in the reprocessing tanks, especially in plutonium rich fuels, enriched gadolinium which acts as neutron poison is added to prevent criticality. For enrichment of gadolinium isotopes, distillation [17], centrifugation [18], electromagnetic separation, and laser based separation [19, 20] methods are generally used. Each of these methods has its own merits and demerits.

Chen et al. [21] had carried out gadolinium isotope enrichment using strong cation exchange resin by displacement chromatographic method. Boda et al. [22] had reported, the possibility of gadolinium isotope enrichment, by carrying out ion exchange column experiments using crown ether grafted resin. Conventional ion exchange isotope separation has small separation coefficients and needs long time to obtain desired enrichment. On the other hand, HPLC technique is a quick method to achieve the desired enrichment due to its large number of theoretical plates (ion exchange steps). Hence HPLC technique was explored for gadolinium enrichment. In the present study, in order to enrich these two isotopes (^{155}Gd, ^{157}Gd), gadolinium samples were passed through HPLC columns. The fractions collected were subjected to pretreatment to remove unwanted organics and subsequently analysed using TIMS.

4C.2 Experimental

4C.2.1 Sample preparation

Isotopes of gadolinium have isobaric interference from those of samarium and dysprosium. Thus for this experiment gadolinium stock solution was prepared from spectroscopic grade gadolinium standard solution.

4C.2.2 HPLC enrichment method

The reversed phase monolithic column (M/s Merck) used in the present experiments had dimensions, surface area, macroporous and mesoporous structure of 100 mm × 4.6 mm, 300 m^2g^{-1}, 2 μm, and 13 nm, respectively. For this study, the feed solution containing natural gadolinium was passed through a 10 cm monolithic column. Initially the column was conditioned by passing 20 mL of mobile phase (mixture of αhydroxyl butyric acid (α-HIBA) and camphor sulfonic acid (CSA)) and then gadolinium sample of desired concentration was injected through the same. The mobile phase pH was adjusted with the help of ammonium hydroxide solution. In all the experiments, a constant flow rate of 1 mL/min was maintained for mobile phase. For metal ion detection by HPLC, Arsenazo (III) was used as post-column reagent, which complexes with gadolinium (655 nm wavelength). For TIMS analysis, gadolinium sample (100µL) of particular concentration was injected into the HPLC column and gadolinium was displaced with mobile phase (0.025 M CSA + 0.05 M α-HIBA) at a particular pH. The effluent fractions containing gadolinium was collected directly at the column exit for ten mL volumes until complete elution of gadolinium (the complete elution of gadolinium was indicated from the distinct colour of metal-arsenazo (III) complex). Different set of experiments were carried out by varying the column length, mobile phase, pH and concentration of feed solution. The column length was increased by connecting "columns in series" (up to three columns).

4C.2.3 Sample pretreatment

Gadolinium samples collected after HPLC separation, contained organics like CSA and α-HIBA. These organics are hygroscopic in nature and have a high decomposition temperature (e.g. 195 ˚C for CSA) and hence difficult to load the sample effectively onto a filament for TIMS analysis. It also affects the analysis and vacuum of the instrument. Hence, pretreatment of sample was required prior to loading onto a filament and accordingly different methods were explored. To eliminate the effect of organics, natural gadolinium samples with organic contents were heated at different temperatures (200, 400, 600 and 800 ˚C) inside a furnace. These preheated gadolinium samples were analysed by TIMS and the results were compared with those obtained from natural gadolinium sample without organics, to check for any fractionation due to heating (Table 4C.1).

Table 4C.1 Isotopic ratio (IR) of gadolinium at different pre-treatment conditions.

Gd Isotopic ratios	IR without organics (Relative error in %)	IR with organic (Relative error in %)	IR after heated to 600 ˚C (Relative error in %)	IR after heated to 800 ˚C (Relative error in %)
152/158	0.00823 (1.27)	0.00824 (2.87)	0.00827 (1.04)	0.00826 (2.58)
154/158	0.08835 (0.21)	0.08850 (0.31)	0.08858 (0.13)	0.08865 (0.30)
155/158	0.59878 (0.12)	0.5999 (0.12)	0.60036 (0.16)	0.60155 (0.26)
156/158	0.82644 (0.09)	0.82785 (0.07)	0.82880 (0.30)	0.83005 (0.21)
157/158	0.63067 (0.06)	0.63126 (0.04)	0.63090 (0.04)	0.63104 (0.06)
160/158	0.87582 (0.07)	0.87454 (0.05)	0.87442 (0.10)	0.87398 (0.07)

4C.3 TIMS analysis

All the preheated samples were analysed for their isotopic composition. Gadolinium with first ionisation energy of 6.15 eV, is quite sensitive to thermal ionisation. Samples were loaded onto a rhenium side filament in a triple filament configuration. To enhance the gadolinium ion intensity, samples were loaded with graphite slurry coating over the filament. Filaments were then mounted in mass spectrometer for TIMS analysis. The filaments were heated slowly to focus the rhenium ion, followed by heating side and central filament to achieve minimum ion intensity of gadolinium. Isotopic ratios were measured by keeping the central and side filament currents at 5.4 and 2.3 A, respectively. The coincidence ensuring proper collimation and placement of Faraday cups for all the isotopes of gadolinium is shown in Fig. 4C.1. Fig. 4C.2 shows the mass spectrum of natural gadolinium.

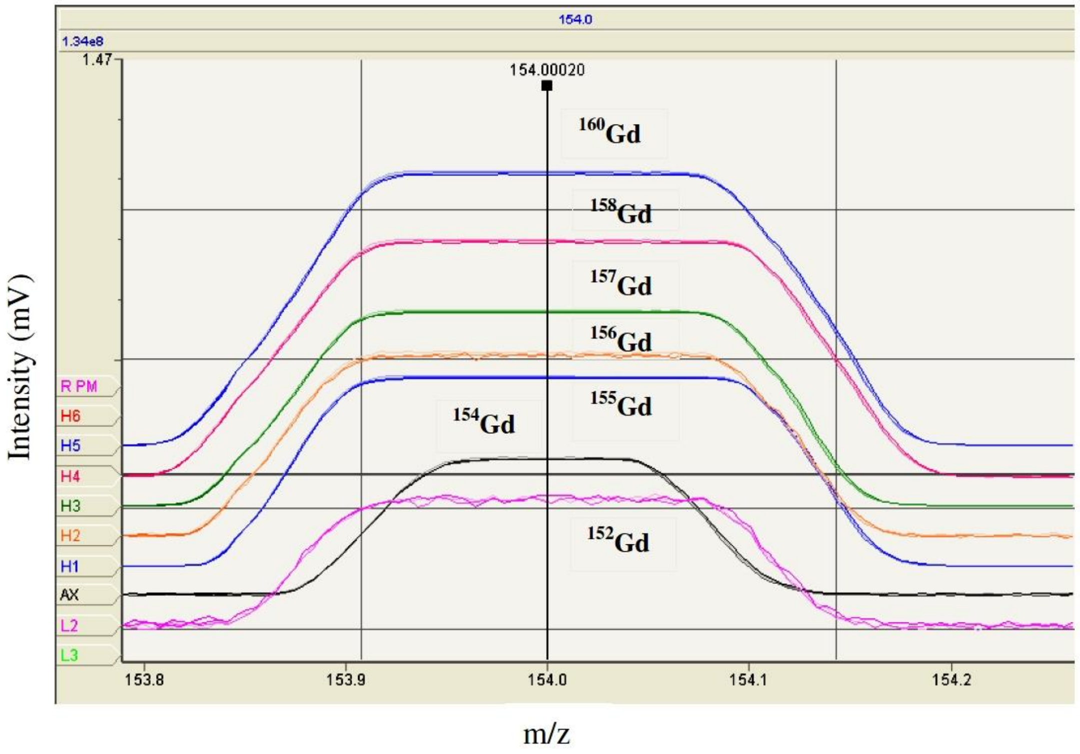

Fig. 4C.1 Coincidence of gadolinium isotopes.

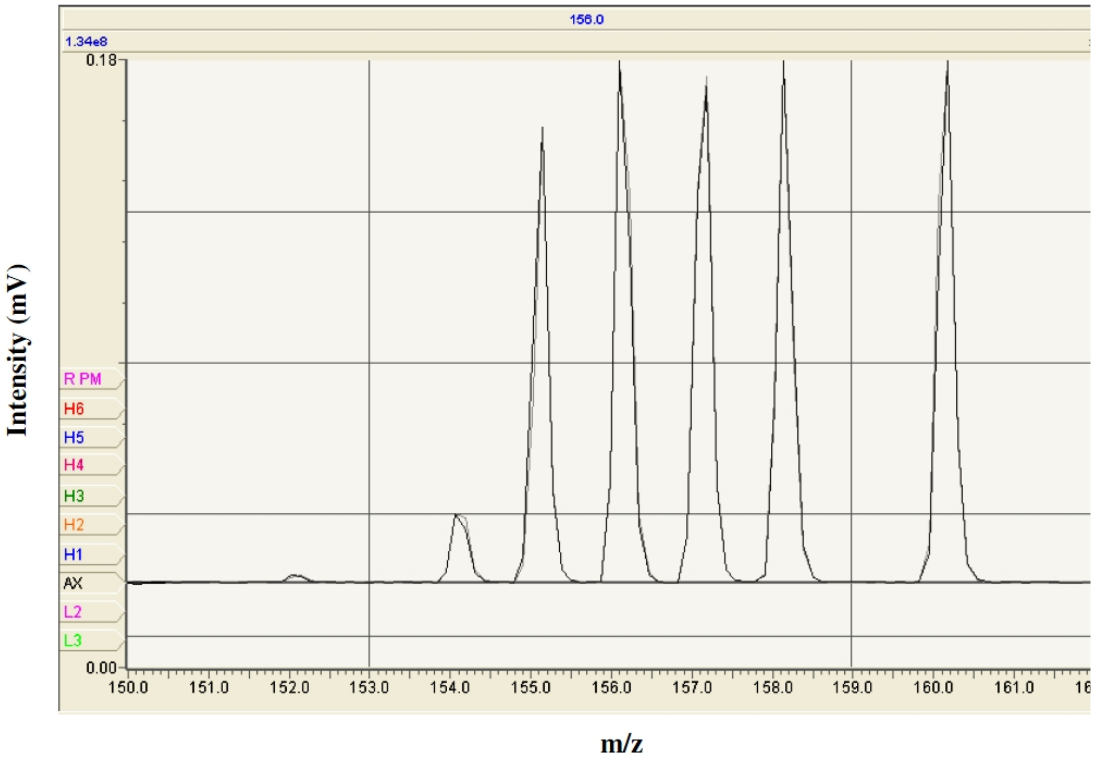

Fig. 4C.2 Mass spectrum of natural gadolinium.

4C.4 Results and Discussion

In the present study, up to three columns were connected in series to increase the column length. With single column, two set of experiments were carried out at pH 2.70 and 2.80 with a gadolinium concentration of 5.34 mg/mL. With two columns in series, three set of experiments were carried out having gadolinium concentration of 5.34 and 10.74 mg/mL at pH: 2.70 and 2.80 (i.e. two set of experiments with feed concentration of 5.34 mg/mL at pH: 2.70 and 2.80, one set of experiment with feed concentration of 10.74 mg/mL at pH 2.8). With three columns in series, an experiment was carried out at pH 2.80 with 10.74 mg/mL of gadolinium as feed solution.

It was observed that at temperatures of 200 and 400 ˚C, organics could not be decomposed completely. From Table 4C.1, it can be seen that at higher temperature (>600 ˚C), there is slight deviation in isotopic ratios for heavier isotopes. Therefore, it was decided to pre heat all the samples at 550 ˚C before loading onto a filament surface. During pretreatment, it was noticed that some of the gadolinium samples which were charred due to combustion of organics, gave better ion intensity during TIMS analysis. Subsequently all the gadolinium samples were pretreated and loaded along with graphite slurry for achieving better ion signal.

Figures 4C.3 to 4C.6 shows the isotopic ratios of gadolinium as a function of effluent volume for different experimental conditions. The first point i.e. zeroth effluent volume in all the plots correspond to the isotopic ratio of gadolinium of natural origin. From the pattern observed in these figures and taking into the consideration the scatter and uncertainty associated with experimental parameters, one can make the following broad observations,

(i) Among all isotopes, lighter isotopes with mass number 152, 154, 155, 156, 157 and 158 were enriched in the initial fractions whereas heavier isotope (160) relatively got enriched in later fractions (Figure 4C.3).

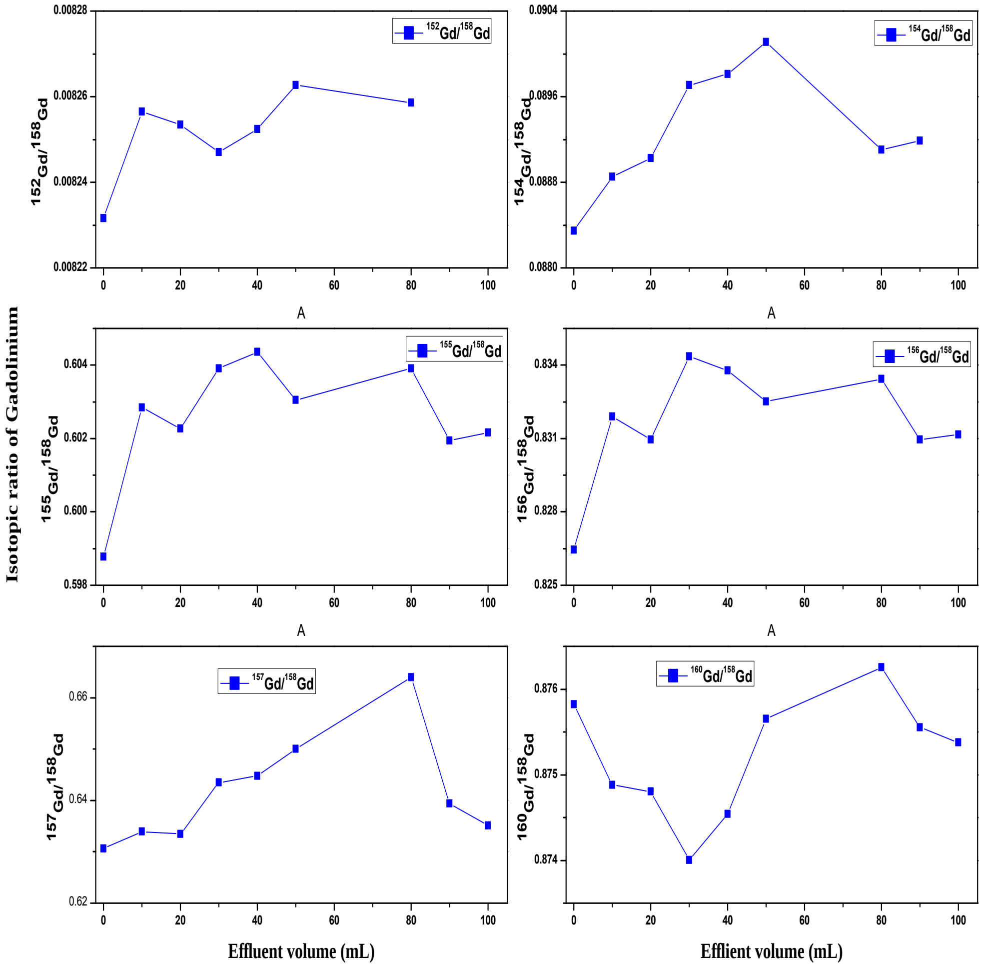

Fig. 4C.3 Isotopic ratios of gadolinium with feed concentration of 10.47 mg/mL, triple chromatographic columns, mobile phase: 0.025 M CSA + 0.05 M α-HIBA, pH: 2.80, flow rate: 1 mL/min.

Isotopic abundance of gadolinium obtained from HPLC separation with experimental condition like feed concentration: 10.47 mg/mL, three chromatographic columns in series, mobile phase: 0.025 M CSA + 0.05 M α-HIBA (pH: 2.80), flow rate: 1 mL/min, show a maximum enrichment of 1.54 % for ^{157}Gd with respect to natural abundance under these experimental conditions.

(ii) Enrichment of ^{157}Gd decreases with increase in feed concentration of gadolinium (Figure 4C.4).

(iii) Enrichment of ^{157}Gd increases with increase in pH of mobile phase (2.70 to 2.80), might be due to better desorption kinetics of gadolinium from the stationary phase (Figure 4C.5).

(iv) Higher the column length better is the enrichment of gadolinium of ^{157}Gd, since number of separation stages increases with length (Figure 4C.6).

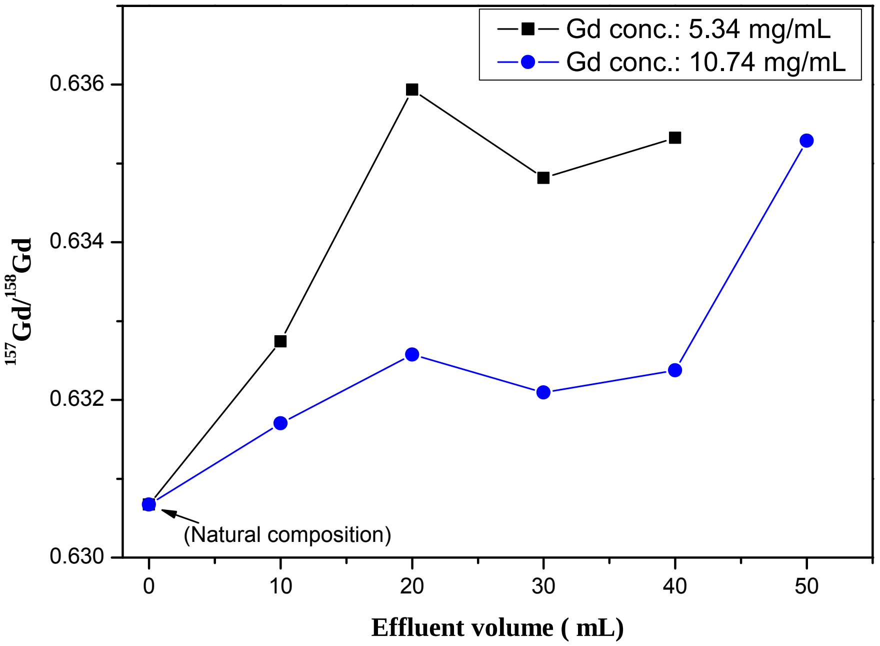

Fig. 4C.4 Isotopic ratios of ^{157}Gd/^{158}Gd at feed concentration of 5.34 mg/mL and 10.47 mg/mL, double chromatographic columns, mobile phase: 0.025 M CSA + 0.05 M α-HIBA, pH: 2.80, flow rate: 1 mL/min.

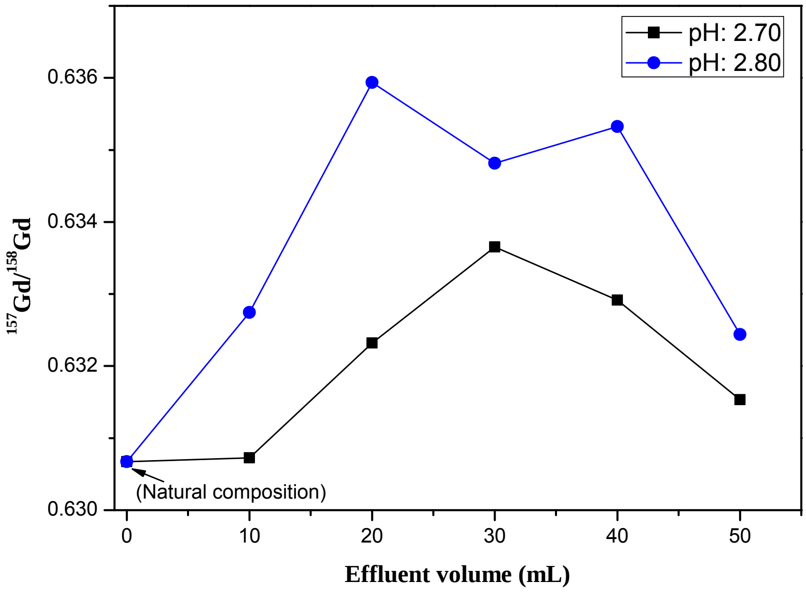

Fig. 4C.5 Isotopic ratios of ^{157}Gd/^{158}Gd at feed solution pH: 2.70 and 2.80, feed concentration: 5.34 mg/mL, double chromatographic columns, mobile phase: 0.025 M CSA + 0.05 M α-HIBA, flow rate: 1 mL/min.

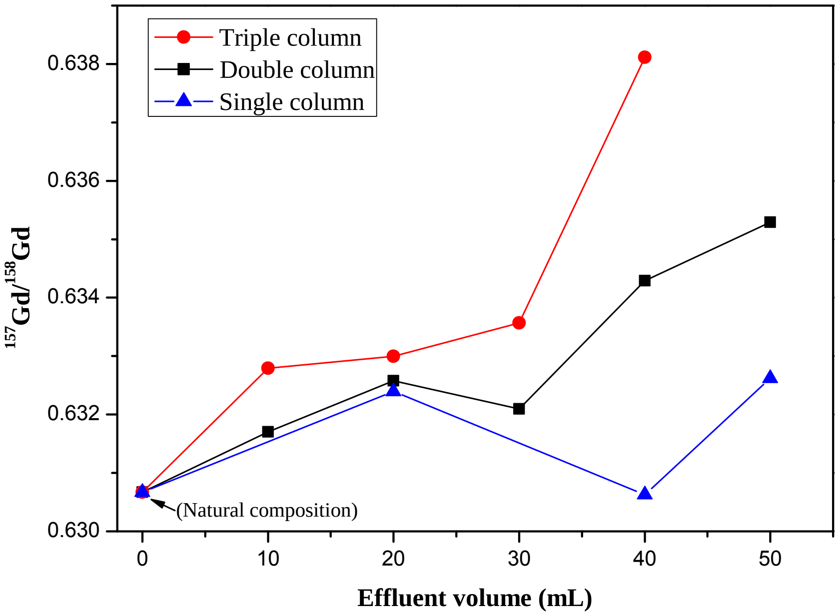

Fig. 4C.6 Isotopic ratios of ^{157}Gd/^{158}Gd obtained using single, double and triple columns in series, feed concentration of 10.74 mg/mL and 5.34 mg/mL (for single column), mobile phase: 0.025 M CSA + 0.05 M α-HIBA, pH: 2.80, flow rate: 1 mL/min.

It can be ascertained that the isotopic ratios for lighter mass isotopes (^{152}Gd/^{158}Gd, ^{154}Gd/^{158}Gd, ^{155}Gd/^{158}Gd, ^{156}Gd/^{158}Gd and ^{157}Gd/^{158}Gd) increased with increase of effluent volume up to a certain maximum value, followed by reduction in latter fractions. This trend is in contrast for heavier mass isotopic ratios i.e. for ^{160}Gd/^{158}Gd, where the initial fractions have lower isotopic ratios for ^{160}Gd/^{158}Gd and later fractions have higher isotopic ratio. From this pattern, it may be concluded that the lighter isotopes were enriched in initial fractions and heavier isotope (^{160}Gd) in later fractions. Similar pattern of enrichment was reported by Chen et al. [21] using ion exchange column of one meter long, operated in merry-go-round fashion.

4C.5 Conclusion

In the present study HPLC method was explored for gadolinium isotope enrichment. Enrichment up to 1.54% for ^{157}Gd with respect to natural was observed. Further studies with five to six columns in series is expected to provide better enrichment though these columns will provide back pressure and accordingly the pressure at pump head should be managed. The inference derived from these experiments will be helpful in setting up a pilot scale plant for gadolinium enrichment using conventional cation exchange resin.

References

[1] E. T. Tipper, E. Lemarchand, R. S. Hindshaw, B. C. Reynolds, B. Bourdon, Chem. Geol. 312 (2012) 80.

[2] S. de Villiers, J. A. D. Dickson, R. M. Ellam, Chem. Geo. 16 (2005) 133.

[3] W. Stegmann, S. L. Goldstein, M. Georgieff, Analyst, 121 (1996) 901.

[4] A. Ramanujam, IANCAS Bulletin, July (1998) 11.

[5] G. Guzzi, P. R. Trincherini, Report on Workshop on “Determination of the Volume of Reprocessing Input Solutions by Tracer Techniques” held at CEC, JRC-Ispra, Italy, on 8th-9th November (1983).

[6] C. K. Mathews, H. C. Jain, S. A. Chitambar, V. D. Kavimandan, S. K. Agarwal, B.A.R.C.-809 (1975).

[7] E. J. Calanzaro, T. J. Murphy, E. L. Garner, W. R. Shields, J. Res. Nat. Bur. Std.-A, Physics and Chemistry, 70A, 6 (1966) 453.

[8] S. K. Agarwal, V. D. Kavimandan, C. K. Mathews, Talanta, 24 (1977) 701.

[9] A. J. Midwood, M. F. Proe, J. J. Harthill, Analyst, 125 (2000) 487.

[10] J. Meija, T. B. Coplen, M. Berglund, W. A. Brand, P. De Bievre, M. Groning, N. E. Holden, J. Irrgeher, R. D. Loss, T. Walczyk, T. Prohaska, Isotopic compositions of the elements 2013, Pure Appl. Chem. 88, 3 (2016) 293.

[11] J. S. Becker, H. J. Dietze, J. Anal. At. Spectrom. 13, 9 (1998) 1057.

[12] T. Inoue, Pergamon, Prog. Nucl. Eng. 40, 3-4 (2002) 547.

[13] W. L. Ebert, N. L. Dietz, D. E. Janney, chem. Eng. Divn. ANL, IL (USA) ANL-05/32, August (2005).

[14] I. W. Donald, B. L. Metcalfe, S. K. Fong, L. A. Gerrard, D. M. Strachan, R. D. Scheele, J. Nucl. Mater. 361 (2007) 78.

[15] V. F. Sears, Thermal-neutron scattering lengths and cross sections for condensed-matter research, Chalk River Nuclear Laboratories Chalk River, Ontario (1984).

[16] K. H. Bejmer, O. Seveborn, PHYSOR 2004, Amer. Nucl. Soc., Lagrange Park, II. (2004).

[17] M. Abdollahi, S. J. Ahmadi, Chemical Engineering and Processing: Process Intensification 76 (2014) 26.

[18] A. A. Artyukhov, A. P. Babichev, I. Y. Knyasev, Y. M. Kravets, et al., Nuclear Instruments and Methods in Physics Research Section A: Accelerators, Spectrometers, Detectors and Associated Equipment 401 (1997) 281.

[19] B. J. Egle, K. J. Hart, W. S. Aaron, J. Radioanal. Nucl. Chem. 299 (2014) 995.

[20] C. P. Keim, Annual review of nuclear science 1 (1952) 263.

[21] J. Chen, M. Nomura, Y. Fujii, F. Kawakami, M. Okamoto, J. Nucl. Sci. Tech. 29, 11 (1992) 1086.

[22] A. Boda, S. K. Arora, A. K. Singha Deb, J. M. Joshi, M. Jha, S. Govalkar, P. V. Kadale, Sk. M. Ali, S. Mukhopadhyay, K. T. Shenoy, B.A.R.C. News let. May-June (2015).

CHAPTER 5

==

Knudsen effusion mass spectrometric studies on some of the systems relevant to fuel, structural materials and reprocessing

Knudsen effusion mass spectrometry plays an important role at different stages of nuclear fuel cycle. It helps in determining the basic thermodynamic properties of the compounds that are formed due to interaction of, fuel and clad materials, fuel materials with fission products, which are formed during nuclear chain reaction, and structural materials with fission products and those relevant to reprocessing. This chapter brings out the importance of KEMS studies on some of the systems like U-Al, U-Sn and Gd-Al. This chapter is divided into three subchapters namely:

Chapter 5A: Derivation of partial pressure and thermodynamic data over (UAl_2+UAl_3) biphasic region of U-Al system.

Chapter 5B: Determination of thermodynamic properties over two phase region of (USn_3+U_3Sn_7) in U-Sn system.

Chapter 5C: Derivation of thermodynamic properties on Gd-Al system, over ($GdAl_2$+$GdAl_3$) two phase mixture.

CHAPTER 5A

Knudsen effusion mass spectrometric studies on U-Al system: Thermodynamic properties over (UAl_2+UAl_3) biphasic region

This subchapter describes about the utilisation of KEMS technique to deduce thermodynamic properties over (UAl_2+UAl_3) biphasic region [1].

5A.1 Introduction

Thermodynamic properties of U-Al alloys are of interest in nuclear technology, since these alloys are used as fuel in research reactors [2]. Thermodynamic properties of U-Al phases serve as useful inputs for fuel design as well as in understanding their "in-pile" behaviour. The phase diagram of the U-Al system has been reviewed in detail by Kassner et al. [3] and subsequently evaluated by Wang et al. [4]. The experimental studies used to establish the phase diagram include thermal analyses, X-ray diffraction, determination of electrical resistivity, and metallography [3-8]. The optimised phase diagram for the system U-Al proposed by Wang et al. [4] is shown in Figure 5A.1. This phase diagram is characterized by three intermetallics viz., UAl_2, UAl_3 and UAl_4. The thermodynamic properties pertaining to the system U-Al had been reviewed by Johnson [9], Chiottiet et al. [10] and later by Kassner et al. [3]. The experimental techniques used for the determination of thermodynamic properties include measurement of electromotive force (e.m.f.) and calorimetric methods [11-15]. Chiotti and Kateley [11] and Lebedev et al. [12] have carried out e.m.f. measurements on U-Al system by using fused salt galvanic cells (KCl-LiCl-UCl_3) in the temperature ranges of 672 -1113 K and 672 - 1153 K, respectively, and derived the Gibbs energies of formation of these intermetallic compounds.

Chiotti and Kateley [11] and Ivanov et al. [13] have deduced the enthalpies of formation of all the three phases at 298.15 K by using adiabatic calorimetry and acid solution calorimetry, respectively. Dannohl et al. [14] had obtained the enthalpy of formation of UAl_2 at 298.15 K by employing high temperature solution calorimetry. Nagarajan et al. [15] had reported the enthalpies of formation of UAl_3 and UAl_4 at 298.15 K by carrying out high temperature solution calorimetry and obtained the data at high temperature (at 1086 K for UAl_3; at 978 K for UAl_4) by precipitation calorimetry. By using the enthalpies of formation of the three intermetallic compounds in the system U-Al, reported in the literature, Johnson et al. [9] had estimated their Gibbs energy of formation. No study has so far been reported on the vaporisation behavior of this binary system.

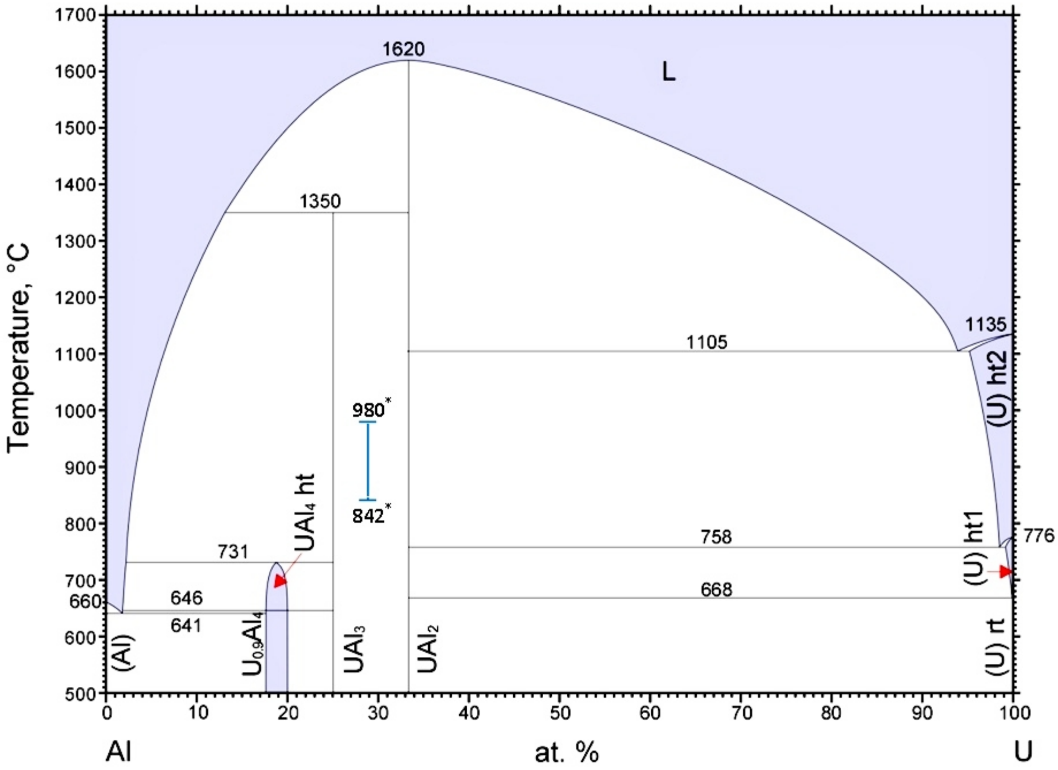

Fig. 5A.1 Phase diagram of U-Al system [4].

*The temperature range of present work, 842 - 980 ˚C (1115-1253 K) is indicated by a vertical line.

Hence, the objective of the present work has been to conduct systematic vaporisation studies on U-Al system by using the Knudsen effusion mass spectrometry and derive vapour pressure and other thermodynamic properties. The thermodynamic information pertinent to the two phase region of (UAl_2+UAl_3) and also the enthalpy and Gibbs energy of formation of UAl_3 (s) phase is reported in this chapter.

5A.2 Experimental

The samples with compositions 28 and 30 at.% U and pertaining to the two phase region (UAl_2+UAl_3) were used for the vaporisation experiments. These alloy samples were prepared by arc melting procedure by melting appropriate quantities of aluminium and uranium in an arc melting apparatus procured from M/s Edmund Buehler, Germany**.** Prior to the alloy preparation, uranium chunks which were stored in oil were cleaned with tissue paper, subsequently with 1:1 HNO_3 to remove the superficial oxide layer and finally with acetone. After loading uranium and aluminium in the arc melting chamber, it was evacuated and flushed with high purity argon thrice before melting. Generally uranium alloys are sensitive to oxidation. Hence, prior to melting of sample constituents, a freshly cleaned uranium chunk was melted to scavenge the oxygen present inside the chamber. To ensure homogeneity of the samples prepared, the sample buttons were flipped and melted thrice.

The as-prepared samples were wrapped in cleaned tantalum sheet and sealed under vacuum in a quartz tube at a residual pressure of 10^{-5} Torr under an atmosphere of argon. Before use, the tantalum sheet was cleaned by immersing in a solution of 10 vol.% HF, 30 vol.% HNO_3 and 60 vol.% H_2SO_4 to strip off any layer of oxide or other impurities from the surface. The samples were heated, initially at 950 K for 50 h and then at 1100 K for two weeks. The annealed samples were stored inside an argon atmosphere glove box in which the oxygen and moisture levels were maintained at values less than 10 ppm. This was accomplished by passing the argon through a purification tower consisting of molecular sieves and copper de-oxo catalyst, which trap respectively the moisture and oxygen present in the argon gas. These alloy samples were crushed into smaller chunks, powdered, and stored in a sealed vial and kept inside an argon glove box. These alloys were characterised by using X-ray diffraction (XRD) (Cu K-α, Xpert pro XRD, M/s. Philips, The Netherlands) to identify the co-existing phases present.

Vaporisation studies on these samples were carried out by using a home built Knudsen effusion mass spectrometric system. A schematic detail of this instrument is described in chapter 1B.12 (Fig. 1B.1). The samples were contained in Knudsen cell made of zirconia with a lid at the top with a knife edged orifice of 0.5 mm diameter and this was placed inside a tantalum outer cup and lid. The samples were heated by radiation as well as by the bombardment of electrons emitted from two encircling tungsten filaments. The temperature of the sample was measured by using a chromel - alumel thermocouple inserted through the bottom of the outer tantalum cup. The vapour effusing out of the cell was ionised by electron impact and the energy of the latter can be varied (up to 100 eV). In the present work, electrons energy of 13.3 eV (emission current = 100 µA) was used to ionise vapour species coming out of Knudsen cell through orifice. The ions produced were mass analysed by a quadrupole mass analyser and detected by a Secondary Electron Multiplier (SEM) operating in pulse counting mode.

The sample was loaded into the Knudsen cell inside the glove box. In a typical vaporisation experiment, samples with a mass of around 300 mg were taken in the

Knudsen cell and heated slowly in steps of 100 K up to 1000 K and then in steps of 15-25 K. Two lots of samples were used for each of the composition. At each temperature above 1000 K, the mass spectrum was recorded looking for shutterable peak or ion intensities. Al^+ was the ion observed in the mass spectrum of the equilibrium vapour and was identified from the mass number of the shutterable peak. The ionisation efficiency (IE) curve was recorded by measuring the Al^+ intensity as a function of electron energy and the same is shown in Figure 5A.2.

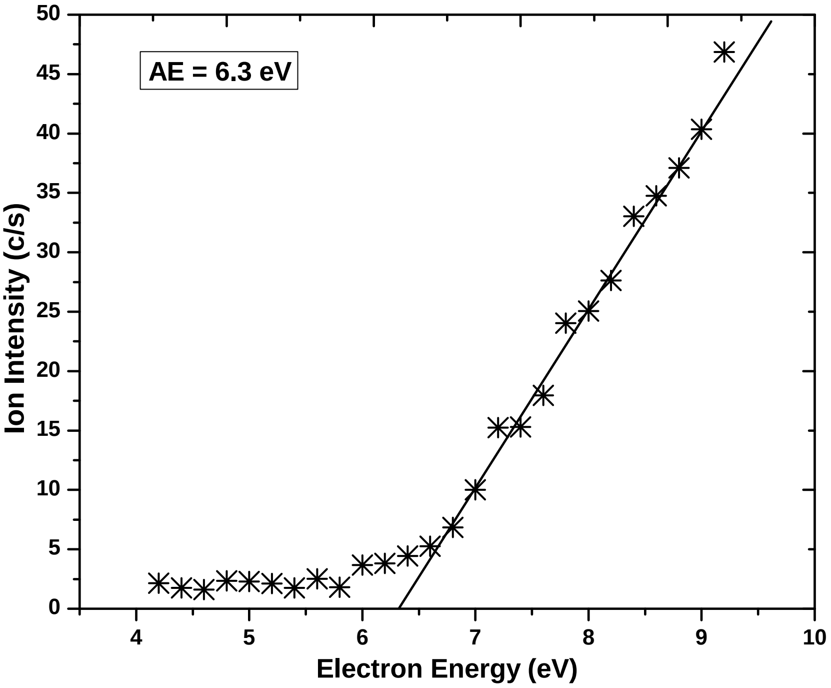

Fig. 5A.2 Typical ionisation efficiency curve for $^{27}Al^+$ over (UAl_2+UAl_3).

From this curve, the appearance energy was obtained by extrapolating the linear portion of the plot to the electron energy axis. The temperature dependence of ion intensities was measured in the temperature range of 1115-1253 K. For these experiments, the sample was kept at the first temperature of measurement for about an hour and the constancy of ion intensity of Al^+ with time ensured that thermodynamic equilibrium was established inside the Knudsen cell. The ion intensity of Al^+ measured as a function of time (at constant temperature) during vaporisation experiment is shown in Figure 5A.3.

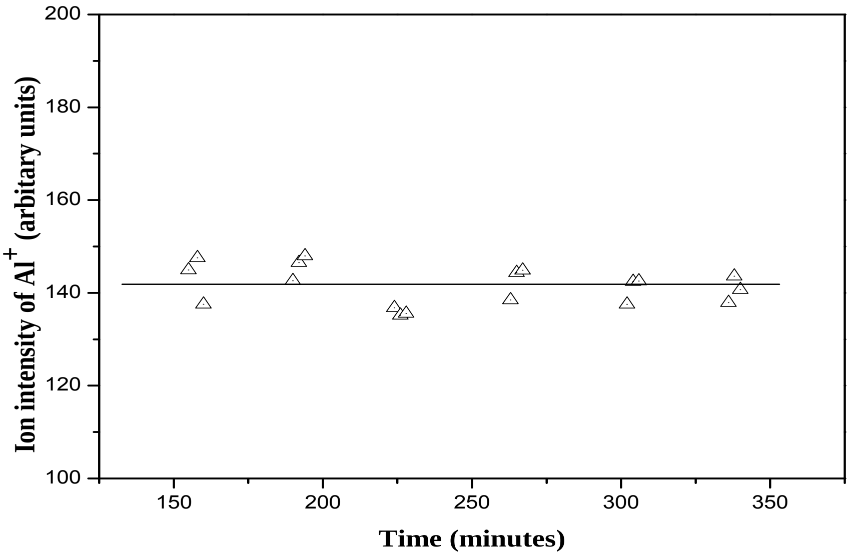

Fig. 5A.3 Ion intensity of Al^+ as a function of time.

Subsequently the sample was heated in steps of 15-20 K, keeping at each temperature for about 25-30 minutes. A range of 100 K or more was covered in each set of measurements and this constituted one run. The temperature of the sample was varied in cycles about the mean temperature. At the end of each run, the sample was taken back to the first temperature of that run to check for the reproducibility of ion intensities. The temperature corresponding to a measurement was read from the thermocouple output. The Al^+ ion intensity measured during a temperature dependence experiment is presented in Table 5A.1.

Table 5A.1 Ion intensities of Al^+ over ($UAl_2(s) + UAl_3(s)$) two phase field in one of the temperature dependance experiment (sample: 28 at.% U Lot 1, Run 2).

Slr. No.	Temperature (K)	Ion Intensity of Al^+ (cps)
1	1129	47
2	1148	85
3	1173	143
4	1183	269
5	1203	447
6	1222	716
7	1243	1221
8	1253	1506
9	1211	558
10	1192	323
11	1173	172
12	1135	56
13	1116	30

Totally four lots of sample (two from each composition) were used in these experiments. In all, twelve runs of temperature dependence of intensity of $^{27}Al^+$ (six runs on each composition) were performed. The post mass spectrometric residues were characterised by XRD to identify the co-existing phases. Figure 5A.4 shows the XRD patterns of samples before and after KEMS measurements. The pressure calibration experiments were carried out by taking pure aluminium in an alumina liner and placed in the same zirconia Knudsen cell, which was used for performing the experiments over the U-Al alloy samples. These calibration experiments were carried out both before and after the experiments with these samples. Prior to the measurements on samples, the Knudsen cell was thoroughly degassed by heating it to ~1400 K, and the ion intensity of Al^+ was measured as a function of time. The degassing experiment was continued until the shutterable ion intensities were below the detection limits.

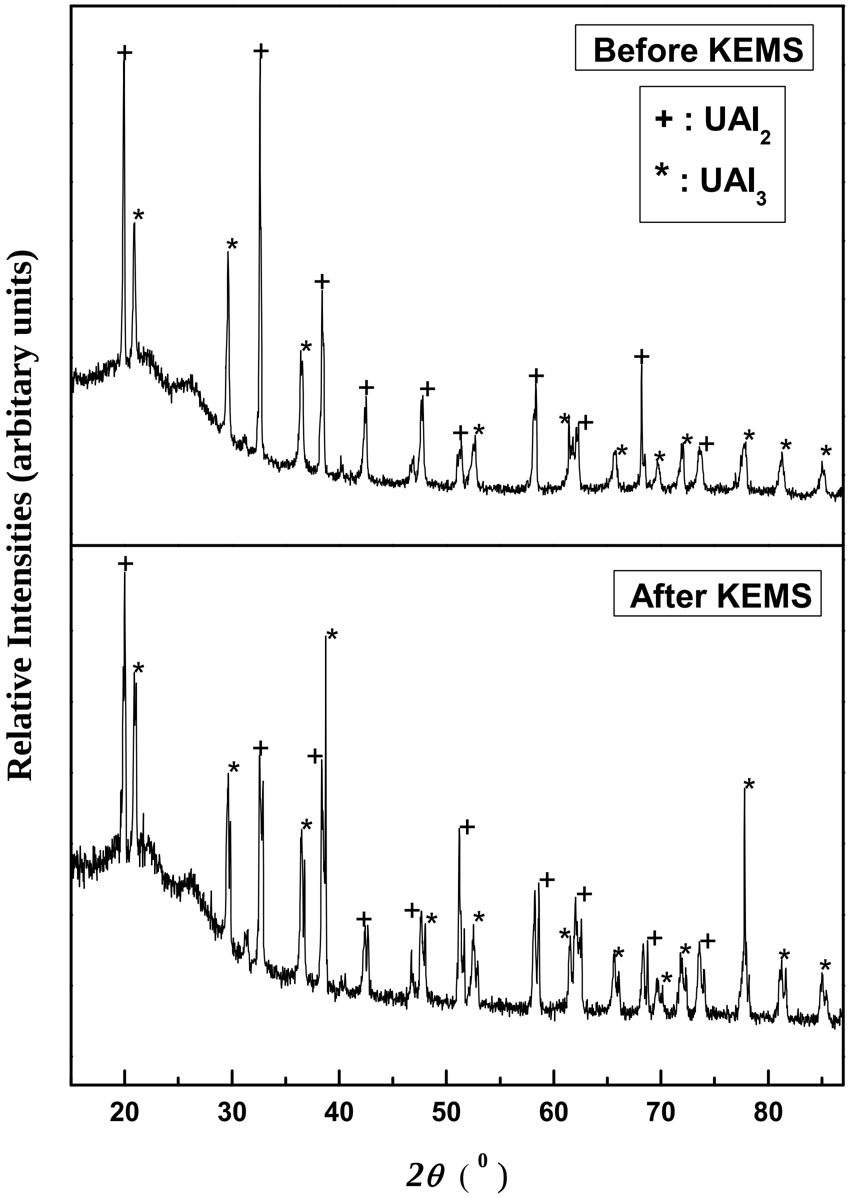

Fig. 5A.4 XRD of the sample ($U_{0.28}Al_{0.72}$) over (UAl_2(s) + UAl_3(s)) biphasic region before and after KEMS.

5A.3 Results and Discussion

5A.3.1 Partial pressure of Al(g) over (UAl_3+UAl_2)

Appearance energy deduced from the IE curve (6.3 eV) (Fig. 5A.3) was in good agreement within error limits (± 0.5 eV) with the first ionisation energy of Al(g) reported in the literature [19]. From the mass number of the shutterable peak in the mass spectrum of the equilibrium vapour and appearance energy (AE), the neutral precursor of Al^+ was identified as Al(g). X-ray diffraction results carried out on the samples before and after Knudsen effusion mass spectrometric studies (Fig. 5A.3) showed the presence of the co-existing phases (UAl_3+UAl_2). This ensured that the partial pressure data derived belonged to the above two-phase region. The measured ion intensities were converted to partial pressures by using the relation

$$p_{Al} = k'_{Al^+} \cdot I_{Al^+} \cdot T \qquad (5A.1)$$

where $k'_{Al^+} = \frac{k}{(\sigma\gamma n)_{Al^+}}$ is the pressure calibration constant; k is the instrument calibration constant, I_{Al^+} is the intensity of Al^+; T is the temperature in Kelvin; σ is the ionisation cross section of Al(g); γ is the multiplier yield and n is the isotopic abundance. The required ionisation cross section data was taken from Mann's compilation [20]. Al(g) is monoisotopic (n=1) and γ is independent of mass (hence equal to one) since ion detection was carried out in pulse counting mode. The instrument calibration constant k was derived from the mean of pre- and post-calibration experiments conducted over pure aluminium. A good reproducibility of the pre- and post-calibration values provided the confidence that the sensitivity, within the uncertainty levels, had not changed during the experiments over the samples. The mean of these values was considered to avoid bias towards a particular value. The required partial pressure of Al(g) over pure aluminium (p°_{Al}) was taken from reference [21]. The logarithmic values of partial pressures of Al(g) in a given run were least-squares fitted to the reciprocal of the temperature to derive the partial pressure (p) - temperature (T) relation. The p-T relations thus obtained for various runs are given in Table 5A.2 along with the combined relation which was obtained by least-squares fitting of all the data points (156 points) from the individual runs.

Table 5A.2 Partial pressure - temperature relations for (UAl_2(s) + UAl_3(s)) two phase field.

Sample	**Run**	**Temperature range/(K)**	**log(p_{Al}/Pa) = –A/T(K) + B**		**p(Al)/Pa × 10^4 at 1184 K[a)]**
			A	B	
28 at.% U Lot 1	1	1125 - 1245	18084 ± 456	12.06 ± 0.39	6.11
	2	1116 - 1253	18111 ± 342	12.08 ± 0.29	6.08
	3	1116 - 1232	18007 ± 564	12.0 ± 0.48	6.19
28 at.% U Lot 2	4	1134 - 1248	18183 ± 300	12.14 ± 0.25	6.06
	5	1126 - 1248	18325 ± 487	12.19 ± 0.41	5.16
	6	1127 - 1249	18538 ± 441	12.38 ± 0.37	5.28
30 at.% U Lot 1	7	1115 - 1248	18246 ± 237	12.17 ± 0.20	5.75
	8	1128 - 1243	18355 ± 350	12.21 ± 0.29	5.10
	9	1129 - 1245	18454 ± 456	12.27 ± 0.38	4.83
30 at.% U Lot 2	10	1126 - 1253	18589 ± 647	12.41 ± 0.55	5.13
	11	1115 - 1247	18371 ± 441	12.24 ± 0.37	5.30
	12	1138 - 1250	18370 ± 450	12.22 ± 0.37	5.07
	All points	1115 - 1253	18215 ± 157	12.12 ± 0.13	5.44
	Pure Aluminium	1115 - 1253	16211	10.92	16.9

a) Mean temperature of the investigation

Figure 5A.5 shows the plot of log(p_{Al}/Pa) vs. 1/T (K^{-1}) corresponding to the combined run. The p-T relation thus derived is given below

$$\log (p_{Al}/pa) = (-18215 \pm 157)/T + (12.12 \pm 0.13) \qquad (1115\text{-}1253\ K) \qquad (5A.2)$$

As can be seen from Table 5A.2, there is a very good reproducibility in the partial pressure values amongst the individual runs, giving credence to the partial pressures derived in the present work. The estimated uncertainty in the partial pressure (u(p)) values of Al(g) is u(p) = 0.2p.

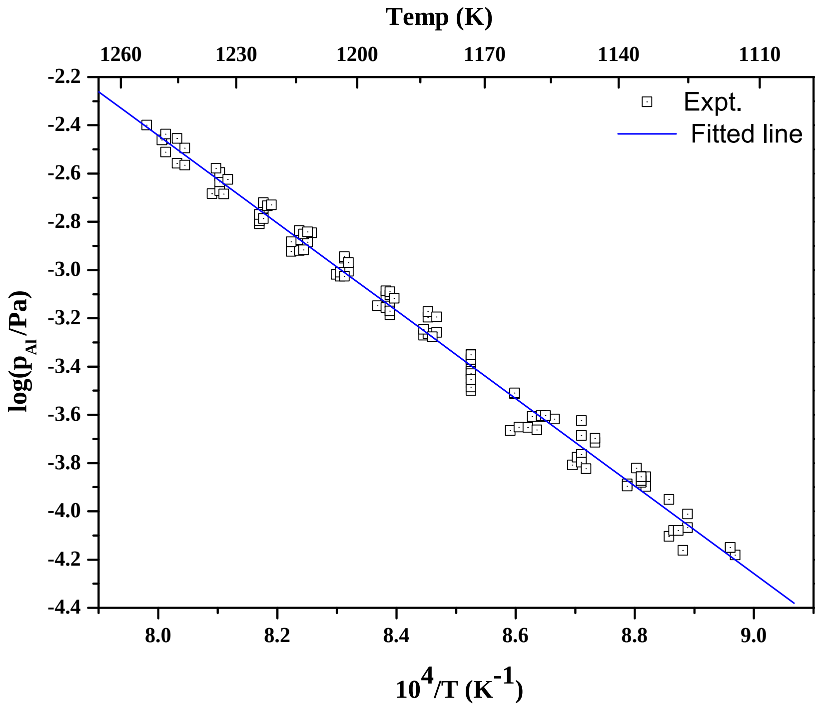

Fig. 5A.5 Combined plot of log ($p_{Al\,(g)}$/ Pa) vs. 1/T (K^{-1}) over (UAl_2(s) + UAl_3(s)) biphasic mixture.

5A.3.2 Thermodynamic quantities

From the information on the neutral vapour species and the co-existing phases identified, in the XRD patterns obtained on samples, before and after KEMS studies, the vaporisation reaction occurring in the Knudsen cell can be written as

$$UAl_3(s) \rightleftharpoons UAl_2(s) + Al(g) \qquad (5A.3)$$

The enthalpy of the above reaction at 298.15 K was deduced by second and third law methods of thermodynamics [21]. The required enthalpy increments (for second law method) and Gibbs free energy functions (third law method) were taken from the literature [22]. The values thus derived are given in Table 5A.3.

Table 5A.3 Reaction enthalpies (kJ mol^{-1}) $UAl_3(s) \rightleftharpoons UAl_2(s) + Al(g)$.

Sample	Run	$T_m/(K)^{a)}$	Second law		Third law $\Delta_r H°_{298.15}$	Recommended $\Delta_r H°_{298.15}$
			$\Delta_r H°_T$	$\Delta_r H°_{298.15}$		
28 at.% U Lot 1	1	1185	346.3 ± 8.7	351.9 ± 8.7	342.2 ± 1.0	349.8 ± 12.8
	2	1185	346.8 ± 6.5	352.4 ± 6.5	342.9 ± 0.9	
	3	1174	344.8 ± 10.7	350.3 ± 10.7	342.7 ± 1.0	
28 at.% U Lot 2	4	1191	348.2 ± 5.7	353.9 ± 5.7	342.3 ± 0.7	
	5	1187	350.9 ± 9.3	356.5 ± 9.3	343.2 ± 1.6	
	6	1188	354.9 ± 8.4	360.5 ± 8.4	343.7 ± 1.0	
30 at.% U Lot 1	7	1182	349.3 ± 4.5	354.9 ± 4.5	342.9 ± 0.7	
	8	1186	351.4 ± 6.7	357.0 ± 6.7	344.0 ± 0.8	
	9	1187	353.3 ± 8.7	358.9 ± 8.7	344.5 ± 1.0	
30 at.% U Lot 2	10	1190	355.9 ± 9.5	361.6 ± 9.5	344.2 ± 1.8	
	11	1181	351.8 ± 8.4	357.3 ± 8.4	343.6 ± 1.2	
	12	1194	351.7 ± 8.6	357.4 ± 8.6	344.0 ± 0.9	
	Mean		350.4 ± 8.7	356.1 ± 8.7	343.4 ± 1.3	

[a)] Mean temperature of the investigation

There is a fair agreement in the values of enthalpies obtained by these two methods. For a given run, the uncertainty quoted in the value of second law enthalpy was obtained from the uncertainty in the slope of the corresponding partial pressure - temperature relation. For the mean third law enthalpy, it is the standard deviation of the mean of the values calculated from each partial pressure data of the given run. The recommended value given in Table 5A.3 was obtained by taking the average of the mean second and third law values of all the runs. The error quoted in the recommended value includes error in temperature (±3 K), estimated uncertainty in pressure (20%) and the precision of the measurements. The values of enthalpy of reaction (5A.3) obtained by third law method for all the temperature points are shown in Figure 5A.6. The individual data are scattered symmetrically about the mean third law enthalpy of reaction indicating that the data is devoid of temperature dependent systematic error and gives further credence to the derived values of the partial pressure.

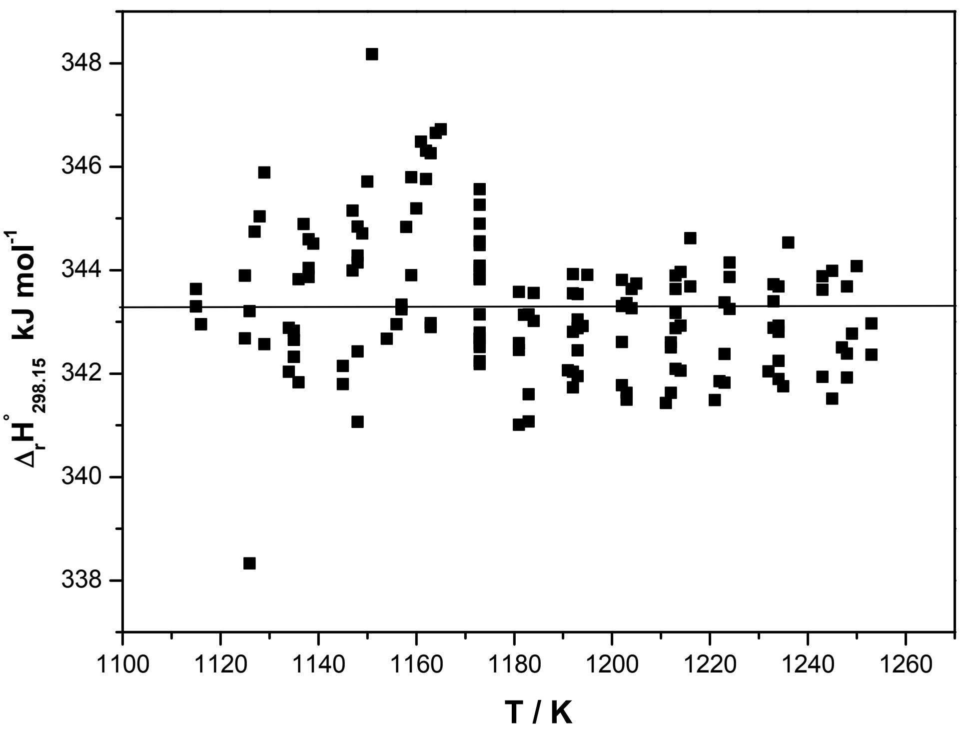

Fig. 5A.6 A 'third law analysis' plot for $\Delta_r H^\circ_{298.15}$. The line represents the mean third law enthalpy of reaction at 298.15 K, 343.4 (kJ mol^{-1}).

Subsequently, the enthalpy of formation of $UAl_3(s)$ at 298.15 K was deduced from the recommended enthalpy change of reaction (5A.3) and by using auxiliary data on the enthalpies of formation at 298.15 K of $UAl_2(s)$ and Al(g) reported in ref. [23]. The value of the standard enthalpy of formation of this intermetallic was found to be –112.1 ± 12.8 (kJ mol^{-1}). Table 5A.4 compares the enthalpy of formation of this compound obtained in the present work along with those reported in the literature [3, 11, 13, 15, 23]. Our value lies in between other values reported in the literature [3, 11, 13, 15, 23].

Table 5A.4 Comparison of the enthalpies of formation (in kJ mol^{-1}) of UAl$_3$ at 298.15 K.

Compound	$\Delta_f H°_{298.15}$	**Method**	**References**
UAl$_3$ w.r.t. α-U and solid Al	– 112.1 ± 12.8	KEMS	Present study
	– 108.4 ± 8.4	Solution and adiabatic calorimetry	Chiotti et al. [11]
	– 105.4 ± 9.2	Solution and adiabatic calorimetry	Ivanov et al. [13]
	– 117.6	Estimation	Kassner et al. [3]
	– 118.1 ± 8.2	High temperature calorimeter	Nagarajan et al. [15]
	– 104.6	Compilation	Barin [23]

5A.3.2.1 Gibbs energy of formation of UAl$_3$(s)

The Gibbs energy of formation of UAl$_3$ as a function of temperature was derived by using equations (5A.4) and (5A.5) which relates the Gibbs energy change for the reaction with the equilibrium constant.

$$\Delta_r G^\circ_T = -2.303\ RT\ \log(K) \qquad (5A.4)$$

where R is the gas constant. The relation thus obtained could be written as

$$\Delta_r G^\circ_T = (348.8 \pm 3.4) - (0.136 \pm 0.0029)\ T\ (\text{kJ mol}^{-1}) \quad (1115\text{-}1253\ \text{K}) \quad (5A.5)$$

The above relation was used to obtain the Gibbs energy of formation of UAl$_3$(s). The Gibbs energy change of the reaction (equation 5A.3) could also be represented by the equation given below:

$$\Delta_r G_T^\circ = \Delta_f G_{T,UAl_{2(s)}}^\circ + \Delta_f G_{T,Al(g)}^\circ - \Delta_f G_{T,UAl_{3,(s)}}^\circ \qquad (5A.6)$$

By using the relations (5A.5) and (5A.6), the Gibbs energy of formation of UAl_3(s) was obtained. The reference states of uranium and aluminium are γ-uranium and liquid aluminum, respectively. The values of the Gibbs energy of formation of UAl_2(s) and that of Al(g) were taken from the references [10] and [23], respectively. The expression of the temperature dependence of the Gibbs energy of formation of Al(g) was derived by least-squares linear regression analysis of the data [23] in the temperature range 1000-1300 K. This expression is given as equation (5A.7). For UAl_2, the Gibbs energy of formation of $\Delta_f G_{T,UAl_{2(s)}}^\circ$ reported in the assessment by Chiotti et al., [6] valid in the temperature range 1049-1400 K was used and the same is given as equation (5A.8).

$$\Delta_f G_{T,Al(g)}^\circ = 311.3 - 0.114\ T\ (\text{kJ mol}^{-1}) \qquad (1000 - 1300\ \text{K}) \qquad (5A.7)$$

$$\Delta_f G_{T,UAl_{2(s)}}^\circ\ (\text{w.r.t. } \gamma\text{-U, liq. Al}) = -121.3 + 0.0371\ T\ (\text{kJ mol}^{-1})\ (1049 - 1400\ \text{K})\ (5A.8)$$

The Gibbs energy of formation of UAl_3(s) thus derived could be represented as

$$\Delta_f G_{T,UAl_{3(s)}}^\circ\ (\pm 3.4) = -158.8 + 0.0591\ T\ (\text{kJ mol}^{-1}) \qquad (1115 - 1253\ \text{K}) \qquad (5A.9)$$

The Gibbs energy of formation of UAl_3(s) derived is given in Table 5A.5 along with those reported in the literature. The Gibbs energy of formation of this intermetallic compound at 1184 K derived by interpolation from the analytical expression (eqn. (5A.9)) is in good agreement with those determined by using e.m.f. methods reported in references [11, 12, 23] and is marginally more negative than that estimated by Kassner et al. [3].

Table 5A.5 Comparison of Gibbs energy of formation of UAl_3 (kJ mol^{-1}).

Compound	$\Delta_f G°_T$ = A + BT		T/K	$\Delta_f G°_T$ (T=1184K)	Method	References
	A	B				
UAl_3 w.r.t. γ-U and liq. Al	– 158.8 ± 3.4	0.0591	1115 - 1253	− 88.9 ± 3.4	KEMS	Present study
	– 145.4	0.045	672 - 979	– 92.1	e.m.f.	Chiotti et al. [11]
	– 161.5	0.062	1003 - 1143	– 88.1	e.m.f.	Lebedev et al. [12]
	– 157.5	0.0645	-	– 81.1	Estimation	Kassner et al. [3]
	-	-	-	– 90.2	Compilation	Barin [23]

5A.4 Conclusion

The high temperature mass spectrometric studies on U-Al system have been carried out for the first time. The partial pressures of Al(g) over the (UAl_2+UAl_3) biphasic region were determined in the temperature range of 1115-1253 K and the p-T relation is deduced was found to be $\log(p_{Al}(g)/Pa) = (–18215 \pm 157)/T + (12.12 \pm 0.13)$. The enthalpy of the reaction $UAl_3(s) \rightleftharpoons UAl_2(s) + Al(g)$ was derived through both the second and third law methods. Subsequently the enthalpy of formation of UAl_3(s) was deduced from the enthalpy of reaction and is given as $\Delta_f H^{\circ}_{298.15,UAl_{3(s)}} = –112.1 \pm 12.8$ (kJ mol^{-1}). The temperature dependence of the Gibbs energy of formation of UAl_3 was found to be $\Delta_f G^{\circ}_T$. (± 3.4) = –158.8 + 0.0591 T (kJ mol^{-1}).

CHAPTER 5B

Knudsen Effusion Mass Spectrometric studies over (USn_3+U_3Sn_7) two-phase region of U-Sn System

This subchapter deals with the derivation of thermodynamic properties on U-Sn system over (USn_3+U_3Sn_7) biphasic region using KEMS technique [24].

5B.1 Introduction

Intermetallic compounds of uranium and plutonium with tin (typical fission yield 0.3% in fast reactors) and noble metal fission products have been reported to exist in irradiated mixed oxide fuel [25]. Post irradiation examination of the defective mixed oxide fuel pins has revealed the presence of (U, Pu)Sn(Rh, Pd)$_2$ [25]. Further, the actinide-tin alloys are of interest from the point of view of molten tin process [26], an alternate method to pyro reprocessing of the spent oxide fuel. In this process, the spent oxide fuel is dissolved in the molten tin bath in a graphite crucible maintained at 1900 K. The solution consisting of actinides and the fission products is treated with nitrogen at 1 atm and the actinide nitrides get precipitated out while the fission products remain in the solution. In the next step, the molten bath is cooled to 700-900 K to precipitate any residual actinide left over in the solution. Hence, it is useful to derive thermodynamic data on U-Sn system to assess the thermodynamic stabilities of different U-Sn intermetallic compounds.

The phase diagram of U-Sn system has been reported by many workers [27-34]. Rough et al. [27] had reported the U-Sn phase diagram based on the results of metallographic, X-ray and thermal analysis of the earlier studies [28, 29] and indicted the presence of USn_3(s), U_3Sn_5(s) and U_5Sn_4(s) phases. Alcock et al. [30] had carried out vaporisation studies over various compositions in the range 17 to 82 at.% Sn by Knudsen Effusion Mass Loss method (KEML) in the temperature range 1150-1300 K using Knudsen cells made of BeO. They chose to present their results graphically rather than giving any pressure-temperature analytical relation. Based on total pressures and thermodynamic activities, presence of a new phase namely U_3Sn_2 had been reported by them. The vapour pressure data reported pertains to the biphasic regions of (USn_3+U_3Sn_5), (U_3Sn_5+U_3Sn_2) and (U_3Sn_2+U). Subsequently, the Gibbs energies of formation of USn_3(s), U_3Sn_5(s) and U_3Sn_2(s) phases have been deduced. Sari et al. [31] had reinvestigated the U-Sn system by Electron Probe Micro Analysis (EPMA), Differential Scanning Calorimetry (DSC), micro hardness measurements and XRD and identified, in addition to USn_3 and U_5Sn_4, four new phases namely U_3Sn_7(s), USn_2(s), U_4Sn_5(s) and USn(s). However, Sheldon et al. [32], based on their detailed assessment, concluded the presence of USn_3(s), U_3Sn_5(s) and U_3Sn_2(s) phases in this system. Subsequently, Palenzona and Manfrinetti [33] had reinvestigated the phase diagram of U-Sn system by employing differential thermal analysis, metallography, electron microscopy and XRD and confirmed the existence of only USn_3, U_3Sn_7(s), USn_2(s), USn(s) and U_5Sn_4(s) phases. According to this phase diagram, the co-existing intermediate two-phase fields are (USn_3+U_3Sn_7), (U_3Sn_7+USn_2), (USn_2+USn) and (USn+U_5Sn_4). Very recently Wang et al. [34] had carried out a comprehensive literature survey and thermodynamic evaluation and proposed an optimized phase diagram, which is consistent with the results obtained by Palenzona and Manfrinetti [33]. They have also calculated the enthalpies and entropies of formation of the various intermetallic compounds. Figure 5B.1 shows the latest phase diagram as given in reference [34]. Johnson [35] reviewed the thermodynamic data pertaining to the U-Sn intermetallic compounds. Johnson and Feder [36] as well as Kadochnikov et al. [37] had determined the Gibbs energies of formation of USn_3 by employing e.m.f. method in the temperature ranges 363-677 K and 813-1117 K, respectively. Ashit Pattanaik et al. [38] had carried out e.m.f studies and reported the Gibbs energies of formation of USn_3(s), U_3Sn_7(s), USn_2(s) and USn(s) in the temperature range 682-905 K. Colinet et al. [39] had deduced the enthalpies of formation of USn_3 at 298 K and 1145 K by using aluminium and tin, solution and precipitation calorimetric methods, respectively. As evident from the above, no mass spectrometric studies have been reported on this system so far. Hence, in this work the vapour pressure over the two phase field (USn_3+U_3Sn_7) by Knudsen effusion mass spectrometry (KEMS), in the temperature range 1050-1226 K, thermodynamic data pertaining to USn_3 phase have been deduced.

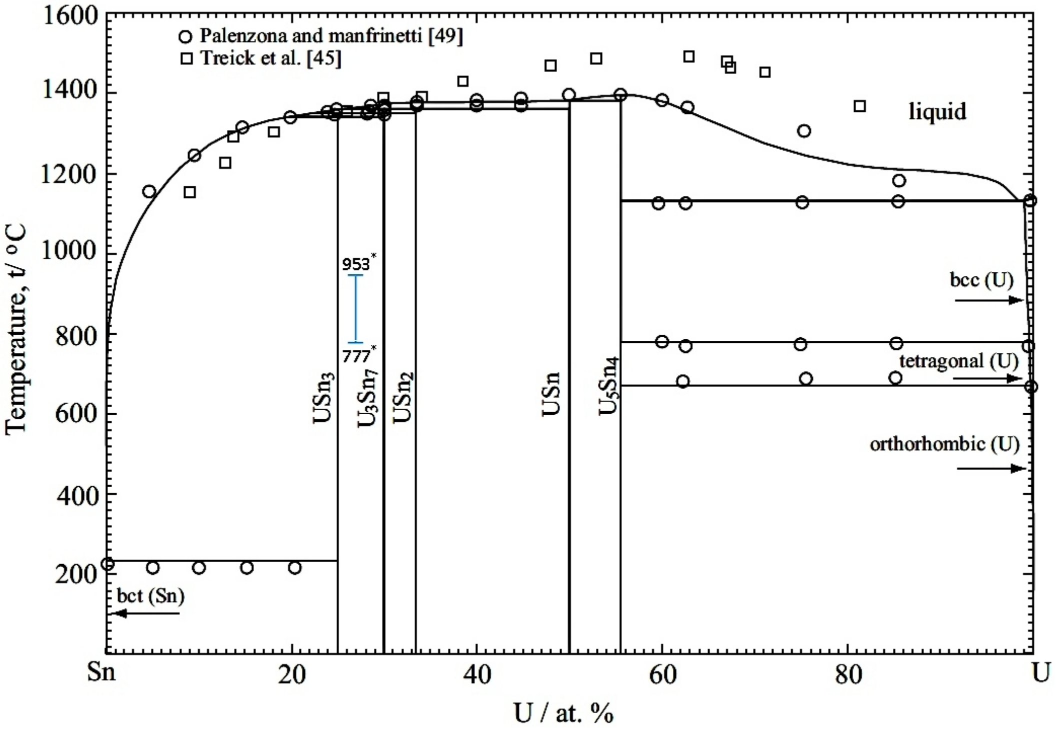

Fig. 5B.1 Phase diagram of U-Sn system [34].

*The temperature range of present work, 777 - 953 ˚C (1050 - 1226 K) is indicated by a vertical line.

5B.2 Experimental

U-Sn alloys corresponding to 71.5 and 73 at.% Sn and belonging to biphasic region (USn_3+U_3Sn_7) were prepared by taking stoichiometric amounts of uranium (nuclear grade purity, Bhabha Atomic Research Centre, Mumbai, India) and tin (purity: 99.99%, M/s Nuclear Fuel Complex, Hyderabad, India) and arc melting them under high pure argon atmosphere. Before arc melting, the uranium pieces stored in oil were wiped using a tissue paper, then immersed in acetone to remove the oil and finally cleaned in 1:1 HNO_3 to etch out the oxide layer. Tin shots were used as received. As additional precaution, during arc melting a freshly cleaned uranium chunk was used as a getter for oxygen. The alloy buttons were flipped and re-melted thrice, to ensure homogeneity. These samples were wrapped in tantalum sheets, sealed in a quartz tube under vacuum (10^{-5} Torr) and annealed at 1073 K for 14 days. Prior to use, same cleaning procedure as described in chapter 5A.2 was employed to remove any oxide layer or any other impurities on tantalum sheet. The samples prepared were characterised by X-ray diffraction (XRD) (Cu K-α, Xpert pro XRD, M/s Philips, The Netherlands). In order to prevent the oxidation of alloys, the samples were handled in an argon atmosphere glove box.

The vaporisation studies were carried out by using a home built KEMS as described in chapter 1B.12. The sample was held in an yttria cup which in turn was kept in an alumina Knudsen cell (knife edged orifice, diameter 0.5 mm) enclosed in an outer cup made of tantalum. The vapour effusing through the orifice was ionised by electrons (energy = 28.3 eV; emission current = 100 µA) from an oxide coated iridium filament.

Sn^+ was the only ion observed in the mass spectrum of the equilibrium vapour over the samples which was identified from the mass and isotopic abundances. The ion intensities were measured as a function of electron energy in order to establish the ionisation efficiency curve. Intensities of $^{120}Sn^+$ were measured as a function of temperature in the range 1050-1226 K. Three samples, one containing 71.5 at.% Sn and the other two lots with 73.0 at.% Sn were used in the vaporisation experiments and totally twelve runs were carried out. In each of these runs, the first temperature was repeated at the end of the run to verify the reproducibility of ion intensities. The ion intensities were recorded as a function of temperature in heating, cooling and cyclic modes. The pressure calibration constant was obtained by conducting experiments by using pure tin, both before and after the experiments with these samples. The residues of the samples obtained after KEMS studies were characterised by X-ray diffraction in order to confirm the co-existing phases.

5B.3 Results and Discussion

5B.3.1 Partial pressure of Sn(g) over (USn_3+U_3Sn_7)

Figure 5B.2 shows the ionisation efficiency curve of Sn^+ over the alloy sample. From the curve, the appearance energy of Sn^+ was derived by linear extrapolation method and the value is 7.7 eV. This is comparable with the first ionisation energy value of 7.4 eV reported in the literature [18].

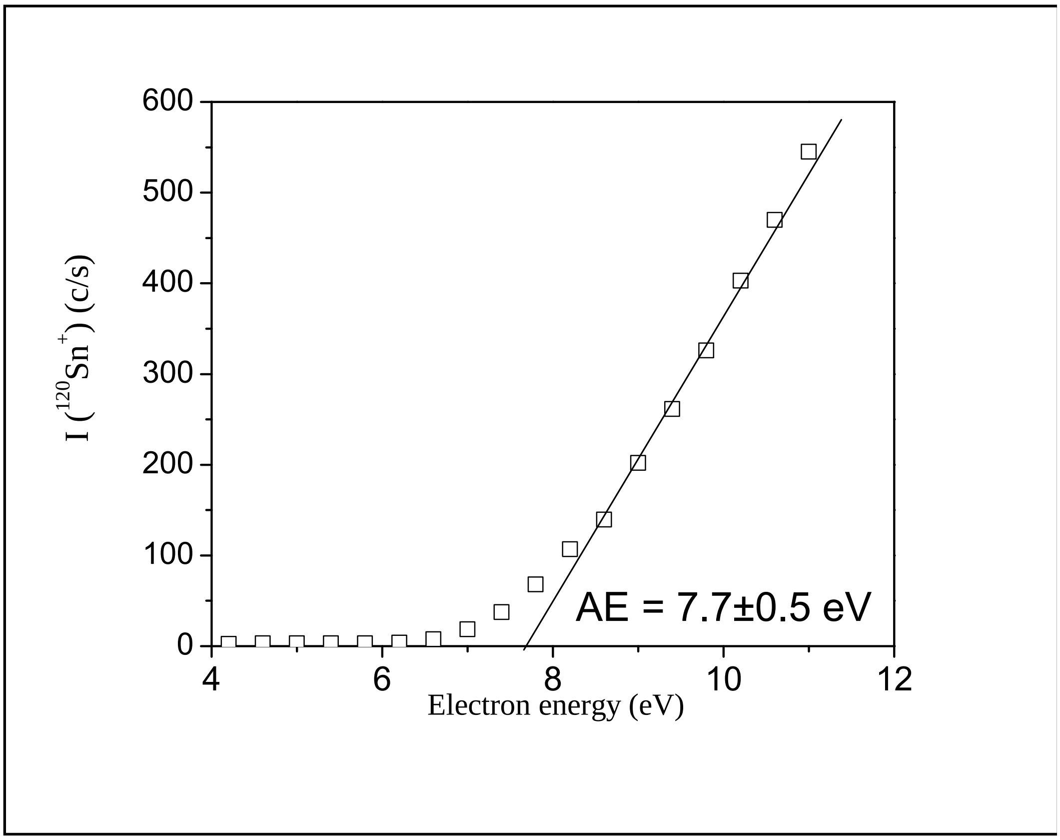

Fig. 5B.2 Ionisation efficiency curve of $^{120}Sn^+$ over the ($USn_3+U_3Sn_7$) "two- phase" field.

From the mass, isotopic abundance and appearance energy, the neutral precursor was established as Sn(g). The intensity of $^{120}Sn^+$ measured was converted into the corresponding value of partial pressure by using the relation given in equation 5B.1.

$$p'_{Sn} = k'_{Sn} \cdot I_{Sn} \cdot T \qquad (5B.1)$$

where $k'_{Sn} = k/(\sigma\gamma n)_{Sn}$ is the pressure calibration constant, k: the instrument calibration constant, I_{Sn^+}: the ion intensity of tin, σ: the ionisation cross section, γ : multiplier yield, n: the isotopic abundance and T: the temperature in Kelvin. The required parameters e.g. ionisation cross section, isotopic abundance electron multiplier yield and instrument calibration constant for Sn(g) were deduced by adopting a procedure similar to that described in chapter 5A.3.1. Table 5B.1 gives the least-square regression analysis of the dependence of vapour pressure on temperature along with the partial pressures for Sn(g) computed at the mean temperature of this investigation.

Table 5B.1 Partial pressure - temperature relations over (USn_3+U_3Sn_7) two-phase region.

Sample USn_3+U_3Sn_7	**Run**	**No of points**	**Temp. range (K)**	**$\log(p_{Sn}/Pa) = -A/T + B$**		**$p_{Sn}/Pa \times 10^5$ at 1138 K**[a)]
				A	B	
71.5 at.% Sn Lot 1	1	12	1058-1195	14656 ± 221	8.89 ± 0.20	10.26
	2	13	1056-1197	14575 ± 343	8.80 ± 0.31	9.83
	3	11	1059-1173	14730 ± 253	8.93 ± 0.23	9.69
	4	10	1050-1172	14390 ± 152	8.62 ± 0.13	9.44
73 at.% Sn Lot 2	5	13	1057-1209	14330 ± 184	8.64 ± 0.16	11.16
	6	13	1057-1196	14558 ± 142	8.84 ± 0.13	11.15
	7	9	1056-1173	14627 ± 284	8.87 ± 0.25	10.39
	8	13	1057-1195	14451 ± 182	8.72 ± 0.16	10.51
73 at.% Sn Lot 3	9	9	1056-1160	14713 ± 158	8.94 ± 0.14	10.26
	10	12	1067-1202	14697 ± 119	8.95 ± 0.10	10.85
	11	9	1082-1225	14756 ± 260	8.92 ± 0.23	8.98
	12	12	1062-1226	14666 ± 228	8.87 ± 0.20	9.61
	All points	137	1050-1226	14580 ± 91	8.82 ± 0.08	10.19
	Pure Sn		1050-1226	15332	10.26	61.27

[a)] Mean temperature of the study

Figure 5B.3 shows a typical plot of log (p_{Sn}/Pa) vs. 1/T (K^{-1}) obtained over (USn_3+U_3Sn_7) two-phase field.

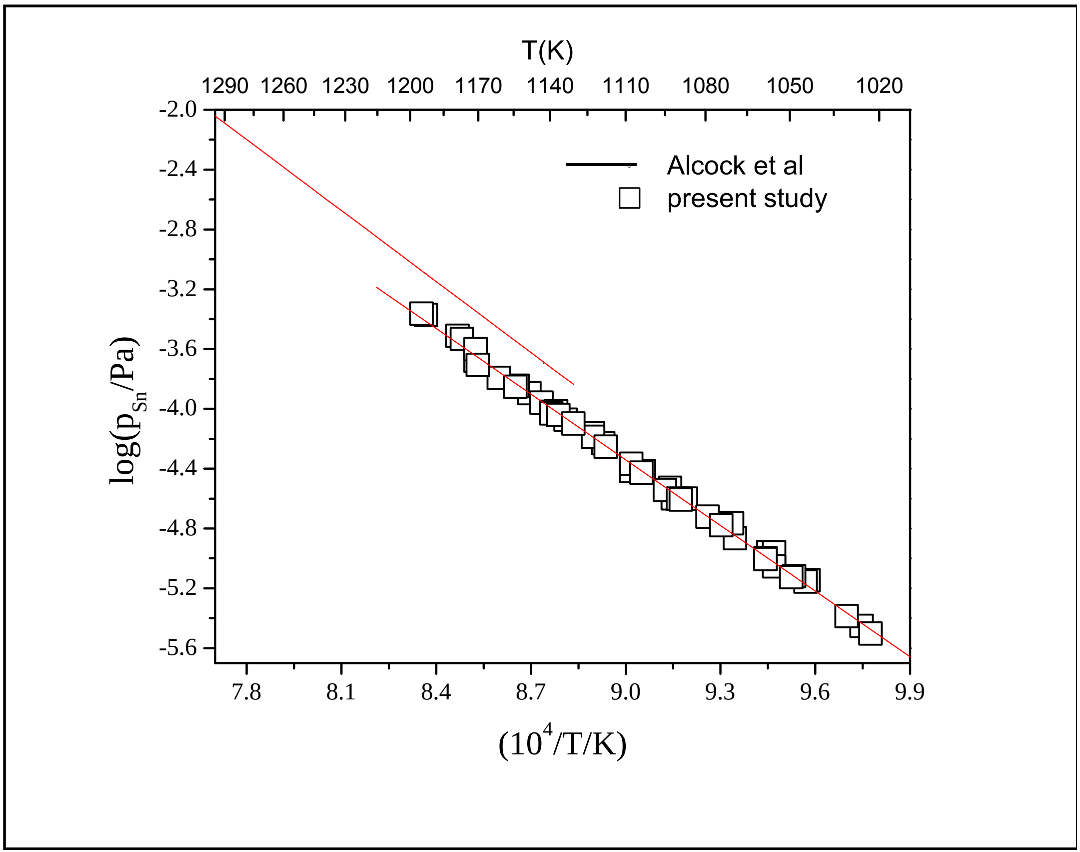

Fig. 5B.3 Plot of log(p_{Sn}/Pa) vs. 1/T (K^{-1}) over (USn_3+U_3Sn_7) “two- phase” field.

The combined equation was obtained by least-squares regression analysis of all the individual partial pressure points (137 points) obtained from different runs and is given as

$$\log(p_{Sn}/\mathrm{Pa}) = (-14580 \pm 91)/T + (8.82 \pm 0.08) \quad (1050\text{-}1226\ \mathrm{K}) \qquad (5B.2)$$

Figure 5B.3 also shows the vapour pressure data reported by Alcock et al. [30] for a sample with a composition 73 at.% Sn. It needs to be mentioned that Alcock et al. [30] had wrongly assumed that this alloy falls in the two-phase region (USn_3+U_3Sn_5). Subsequent evaluation had shown that their sample would have comprised a mixture of USn_3 and U_3Sn_7. The partial pressure data of Sn(g) corresponding to the composition 73 at.% Sn was extracted from the plot of log(p_{Sn}/Pa) vs. 1/T reported in reference [30] and is shown in Figure 5B.3 along with those obtained in the present study. As can be seen from this figure, data from present study are lower by a factor of about two than that reported by Alcock et al. [30]. The fact that the partial pressures obtained in the present work show a very good reproducibility (for 12 runs) indicate that the data obtained in the present work are more reliable and supersede the earlier values [30].

5B.3.2 Thermodynamic quantities

The partial pressure (p_{Sn}) and enthalpy of vaporisation are related by the equation given below

$$-Rdln(p_{Sn})/d(1/T) = \Delta_v H_T^{\circ} \tag{5B.3}$$

From the vapour phase information, XRD and the reproducibility of ion intensities during temperature dependence experiments, the vaporisation reaction corresponding to the p-T relation given in equation (5B.2) can be written as

$$3USn_3(s) \rightleftharpoons U_3Sn_7(s) + 2\,Sn(g) \tag{5B.4}$$

The reference states for uranium and tin are U(γ) and Sn(l) in the temperature range of present investigation. Table 5B.2 shows the log(K)-T relation for the individual runs as well as for the combined equation obtained by second law evaluation [40] where K^o is the equilibrium constant pertaining to reaction (5B.4). These were obtained by using linear least-square regression analysis of the experimental data. The combined equation could be represented as

$$\log(K) = (-29160 \pm 182)/T + (7.63 \pm 0.16)\ (1050\text{-}1226\ K) \tag{5B.5}$$

The enthalpy of vaporisation of Sn(g) was calculated from the slope of the above equation. The mean of enthalpies obtained from individual runs is reported as the enthalpy of reaction represented by equation (5B.4). For any given run, the uncertainty quoted for the second law enthalpy was derived from the error in the slope of the corresponding log(K) vs. 1/T plot.

Table 5B.2 Enthalpy of the reaction $3USn_3(s) \rightleftharpoons U_3Sn_7(s) + 2Sn(g)$.

Sample $USn_3 + U_3Sn_7$	Run	Temp. range (K)	$\log(K°/atm^2) = -A/T + B$		$\Delta_r H_T^\circ$ (kJ mol^{-1}) [a)]
			A	B	
71.5 at.% Sn Lot 1	1	1058-1195	29312 ± 442	7.76 ± 0.39	560.5 ± 8.4
	2	1056-1197	29149 ± 687	7.59 ± 0.61	557.4 ± 13.1
	3	1059-1173	29461 ± 507	7.85 ± 0.46	563.4 ± 9.7
	4	1050-1172	28780 ± 303	7.22 ± 0.27	550.3 ± 5.8
73 at.% Sn Lot 2	1	1057-1209	28660 ± 367	7.27 ± 0.32	548.0 ± 7.0
	2	1057-1196	29116 ± 284	7.67 ± 0.25	556.8 ± 5.4
	3	1056-1173	29254 ± 567	7.71 ± 0.51	559.4 ± 10.8
	4	1057-1195	28901 ± 365	7.42 ± 0.32	552.6 ± 7.0
73 at.% Sn Lot 3	1	1056-1160	29426 ± 316	7.86 ± 0.29	562.7 ± 6.0
	2	1067-1202	29395 ± 238	7.89 ± 0.21	562.1 ± 4.6
	3	1082-1225	29512 ± 520	7.83 ± 0.45	564.3 ± 9.9
	4	1062-1226	29333 ± 455	7.74 ± 0.40	560.9 ± 8.7
	Mean	1050-1226	29160 ± 182	7.63 ± 0.16	558.2 ± 9.7 [b)]

[a)] Mean temperature of each run.

[b)] Includes errors in individual values and the standard deviation of the mean.

5B.3.2.1 Gibbs energy of formation of USn_3

The Gibbs energy of formation of USn_3 was computed by using the following expression.

$$\Delta_r G_T^\circ = \Delta_f G^\circ_{T,U_3Sn_{7,(s)}} + 2\Delta_f G^\circ_{T,Sn(g)} - 3\Delta_f G^\circ_{T,USn_{3,(s)}} \tag{5B.6}$$

The temperature dependence of Gibbs energy of the reaction 5B.4 was obtained by combining equation 5B.5 and the following expression

$$\Delta_r G_T^\circ = -2.303\ RT \log(K) \tag{5B.7}$$

The relation thus obtained is given as

$$\Delta_r G^\circ_T\ (\pm 3.5) = 558.3\ T - 0.146\ (\text{kJ mol}^{-1}) \qquad (5B.8)$$

The auxiliary data viz., $\Delta_f G^\circ_{T,U_3Sn_{7,(s)}}$ and $\Delta_f G^\circ_{T,Sn(g)}$ required for deriving $\Delta_f G^\circ_{T,USn_{3,(s)}}$ were taken from references [38] and [40], respectively. The reference states of U and Sn in the two-phase field, (USn_3+U_3Sn_7) in the temperature range of the present investigation (1050-1226 K) are U(γ) and Sn(l), whereas the reference states considered in reference [38] are U(α) and Sn(l). Hence, the appropriate contributions of α ⇌ β and β ⇌ γ [41] were taken into account in the calculation of $\Delta_f G^\circ_{T,U_3Sn_{7,(s)}}$. The Gibbs energy of formation of U_3Sn_7(s), thus computed, could be represented as

$$\Delta_f G^\circ_{T,U_3Sn_{7,(s)},(U(\gamma),Sn(l))}\ (\pm 4.2) = -550.6 + 0.223\ T\ (K)\ (\text{kJ mol}^{-1}) \qquad (5B.9)$$

For Sn(g), the values of the Gibbs energy of formation in the range 1000-1200 K, taken from the reference [42] was subjected to linear least square regression analysis and the expression obtained is given as

$$\Delta_f G^\circ_{T,Sn(g)} = 294.3 - 0.101\ T\ (K)\ (\text{kJ mol}^{-1}) \qquad (5B.10)$$

By using all the above data, the Gibbs energy of formation of USn_3 could be represented as

$$\Delta_f G^\circ_{T,USn_{3,(s)}}(\pm 5.4) = -173.4 + 0.055\ T\ (K)\ (\text{kJ mol}^{-1})\ \ (1050\text{-}1226\ K) \qquad (5B.11)$$

The Gibbs energy of formation of USn_3(s) thus obtained is given in Table 5B.3 along with the data cited in the literature. The latter have been corrected for the appropriate standard reference states of the constituent elements (U(γ) and Sn(*l*)). The value obtained in the present study is in reasonable agreement with those reported by e.m.f. studies but are more negative than that reported by Alcock et al. [30] by about 18 kJ mol^{-1}. One possible reason could be that Alcock et al. [30] had used BeO crucible and it is reported that BeO can react with uranium [41] and this could have influenced their values of the Gibbs energy of formation. Wang et al. [34] have optimised their data using the thermodynamic data reported by Ashit et al. [38].

Table 5B.3 Gibbs energy of formation of USn_3(s).

Compound	$\Delta_r G_T^\circ$ (kJ mol^{-1})	Method	Temp. range (K)	$\Delta_f G^\circ$ (kJ mol^{-1}) at 1138K$^{a)}$	Reference
USn_3 w.r.t. (U(γ), Sn(*l*)	– 103.8 + 0.010 T	KEML	1150 - 1300	– 92.4	Alcock et al. [30]
	– 184 + 0.063 T	Calculation		– 112.3	Wang et al. [34]
	– 171.53 + 0.048 T + 12.8 × 10^{-6} T^2	e.m.f.	636 - 950	– 100.3	Johnson et al. [36]
	– 180.4 + 0.069 T	e.m.f.	682 - 908	– 101.9	Ashit et al. [38]
	– 173.4 + 0.055 T	KEMS	1023 - 1209	– 110.8	Present study

$^{a)}$ Mean temperature of the present investigation

5B.3.2.2 Variation of enthalpy of formation of USn_3 with temperature

The mean value of the enthalpy of reaction 5B.4 was found to be 558.2 ± 9.7 (kJ mol^{-1}) at 1138 K, the mean temperature of the present study. No heat capacity or enthalpy increment data have been reported so far in the literature for either USn_3(s) or U_3Sn_7(s). Hence, the value of $\Delta_f H^\circ_{298.15,USn_3(s)}$ was not deduced directly from the enthalpy of reaction at 1138 K. However, a relation for the enthalpy of formation of USn_3 as a function of temperature was derived by following the procedure explained by Chiotti et al. [10]. The expression for the variation of enthalpy of formation of USn_3 with temperature was obtained by using the enthalpies of formation of USn_3 at 298.15 K reported by Colinet et al. [39] who had determined the same by employing the Sn-solution and Al-solution calorimetric methods. For the present calculation, the mean of the values of the enthalpy of formation (–140.5 kJ mol^{-1}) obtained from the above two calorimetric methods was used. The expression was derived by using the Kirchoff's equation [43] given below:

$$\Delta_f H^\circ_{T_2} = \Delta_f H^\circ_{T_1} + \Delta C_p\,[T_2\text{-}T_1] \qquad \text{5B.12)}$$

ΔC_p was first deduced between 298.15 and 1138 K. $\Delta_f H^\circ_{T_2}$ is the enthalpy of formation of USn_3 (U(γ), Sn(l) at 1138 K, which was taken from the intercept of equation 5B.11. For $\Delta_f H^\circ_{T_1}$ the value of –140.5 kJ mol^{-1} was used. Using the ΔC_p thus obtained, a temperature dependence relation for the $\Delta_f H^o_T$ of USn_3 in the range 298.15-1138 K was deduced as

$$\Delta_f H^\circ_{T,USn_{3,(s)}}\ (\pm 5.4) = -128.8 - 0.039\ T\ (K)\ (kJ\ mol^{-1}) \qquad (5B.13)$$

Similar procedure was followed earlier by us for deriving the data for the compound UGa_3 in the U-Ga system [44]. Colinet et al. [39] had reported the enthalpy of formation of USn_3 at 1145 K as –173.9 kJ mol^{-1} which was determined by the precipitation in tin. The above relation, on extrapolating to 1145 K, gives a value of –173.2 (kJ mol^{-1}), which is in good agreement with the value of reported by Colinet et al. [39].

5B.3.2.3 Calculation of uncertainty in the values of thermodynamic quantities

The estimated uncertainty (u) in the measured partial pressure of Sn(g) is u(p) = 0.2p. The uncertainty quoted in the enthalpy of reaction (5B.4) was computed by error propagation taking into account the errors within the individual values and the standard deviation of the mean. The error in the Gibbs energy of reaction (5B.4) was deduced from the statistical errors associated with the slope of the fitted equation for the experimental temperature and pressure data points. The errors quoted for the Gibbs energy of formation for USn_3(s) was computed by error propagation due to errors in the Gibbs energy of reaction (5B.4) and due to those cited in the literature data for the other phases involved in the reaction. Similar computation was performed to calculate the error in the enthalpy of formation of USn_3(s).

5B.4 Conclusion

Vaporisation studies on two compositions 71.5 and 73 at.% Sn pertaining to (USn_3+U_3Sn_7) two-phase field have been conducted by using high temperature mass spectrometry for the first time. Partial pressure-temperature relation for Sn(g) was derived in the temperature range 1050-1226 K and is given as $\log (p_{Sn}/Pa) = (-14580 \pm 91)/T + (8.82 \pm 0.08)$ (1050-1226 K). The vaporisation reaction $3USn_3(s) \rightleftharpoons U_3Sn_7(s) + 2Sn(g)$ was evaluated by the second law method and the enthalpy of this reaction at the mean temperature of investigation (1138 K) was found to be 558.2 ± 9.7 kJ mol^{-1}. The temperature dependence of enthalpy and Gibbs energy of formation of USn_3(s) could be represented as $\Delta_f H^{\circ}_{T,USn_{3,(s)}} (\pm 5.4) = -128.8 - 0.039\ T\ (K)$ (kJ mol^{-1}); $\Delta_f G^{\circ}_{T,USn_{3,(s)}} (\pm 5.4) = -173.4 + 0.055\ T\ (K)$ (kJ mol^{-1}) (1050-1226 K), respectively.

CHAPTER 5C

Thermodynamic properties over ($GdAl_3$+$GdAl_2$) of Gd-Al system: A High temperature mass spectrometric study

This chapter deals with the thermodynamic properties of Gd-Al system over ($GdAl_2$+$GdAl_3$) biphasic region, deduced using KEMS technique [45].

5C.1 Introduction

Pyrochemical reprocessing is considered as the most appropriate method for reprocessing of irradiated metallic fuels of fast reactors. This process employs molten chloride/ fluoride salts and liquid metals for effecting the separation of actinides from spent fuel. Many metals such as Bi, Zn, Ga, Cd, Al and Sn in the molten form had been investigated for their suitability for use as solvents to achieve actinide-lanthanide separation from the spent metallic fuel by applying a technique called reductive extraction [46-48]. Among these metals, aluminium was ascertained to exhibit superior selectivity for actinides than for lanthanides [49]. Cassayre et *al*. [50] had investigated the feasibility of carrying out electro refining process of U-Zr and U-Pu-Zr metallic fuels by using solid aluminium cathode instead of liquid cadmium cathode. They selectively deposited the actinides, while the lanthanides remained in the salt. Among the lanthanides, the study of the electrochemical behavior of gadolinium is interesting because the reduction potential of Gd^{3+} ion in molten LiCl-KCl, is close to those of actinides, making the mutual separation of actinides and lanthanides difficult [51]. In this context, determinations of thermodynamic properties of the intermetallics in the Gd-Al system are of interest to understand the behaviour of gadolinium during electro refining.

The binary system Gd-Al had been studied over the whole composition range by Buschow [52] by employing different techniques, namely, metallographic, thermal analysis and X-ray diffraction (XRD) methods. This system was found to comprise of the phases Gd_2Al, Gd_3Al_2, GdAl, $GdAl_2$ and $GdAl_3$. Subsequently, Runnalls and Boucher [53] had investigated this binary system in the aluminium rich region by using the techniques described above and identified it to consist of yet another compound, $GdAl_4$. Gschneidner and Calderwood [54] had critically assessed the Gd-Al phase diagram by using the data reported up to the year 1986 and later Saccone et al. [55] had studied the phase diagram of this system experimentally over the composition range of 0-66.7 at.% Al by employing XRD, differential thermal analysis (DTA), quantitative electron probe microanalysis and metallographic methods. These authors verified the existence of the intermetallic compounds Gd_2Al, Gd_3Al_2, GdAl and $GdAl_2$. Subsequently, Cacciamani et al. [56] had performed thermodynamic modeling of the Gd-Al system by using the compound energy formalism and Liling Jin et al. [57] had conducted thermodynamic evaluation and optimisation of this system by employing a modified quasi chemical model for the liquid component. Recently, Bo et al. [58] had re-assessed Gd-Al system by using CALPHAD and the phase diagram reported by them is given in Fig. 5C.1. As can be seen, there exist five intermetallic compounds, i.e., $GdAl_3$, $GdAl_2$, GdAl, Gd_3Al_2 and Gd_2Al. Colinet et al. [59] had determined the formation enthalpies of these intermetallic compounds at 298.15 K by employing aluminum solution calorimetry while Sommer and Keita [60] had determined for $GdAl_2$, GdAl, and Gd_2Al by solution calorimetry in liquid aluminium. Caravaca et al. [51] and Bermejo et al. [61] had deduced the Gibbs energy of formation of $GdAl_3(s)$ employing open-circuit chronopotentiometry over the temperature ranges, 723-823 and

673-823 K. As can be seen from the above, no vaporisation studies had been carried out so far in the system Gd-Al. Vaporisation behavior of Gd-Al intermetallics at high temperatures, are useful for deriving reliable thermodynamic data pertaining to this system. Hence in the present study, Knudsen effusion based mass spectrometric studies has been conducted over the ($GdAl_2$+$GdAl_3$) two phase region with an objective to derive partial pressures and other thermodynamic properties.

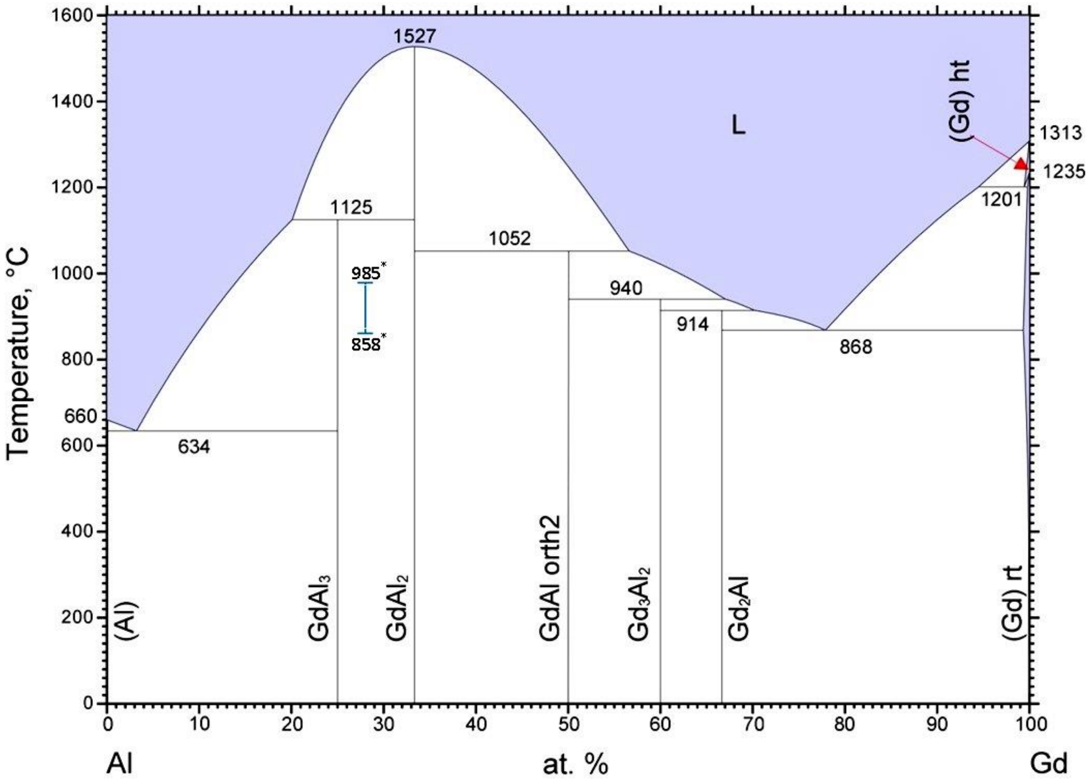

Fig. 5C.1 Phase diagram of Gd-Al system reproduced from ref. [58].

* The temperature range of present work, 858 - 985 °C (1131 - 1258 K) is indicated by a vertical line.

5C.2 Experimental

5C.2.1 Preparation of the samples

Two samples corresponding to ($GdAl_2$+$GdAl_3$) two phase region with the gross compositions 70 and 72 at% Al were prepared by taking required amounts of gadolinium (Purity, 99.9%, M/s. Johnson Matthey, UK) and aluminium (Purity, 99.999%, M/s Leico Industries Inc, New York) and arc melting them in a facility procured from M/s Edmund Buehler, Germany. About two grams of sample was prepared for each composition. During the arc melting, the sample constituents corresponding to a given composition were loaded in the enclosure of the arc melting facility. Subsequently, the enclosure was evacuated and filled with high pure argon and this was repeated thrice and finally the constituents were melted under an atmosphere of high pure argon. The sample was re-melted thrice and flipped between melts in order to ensure homogenisation.

The melted buttons were placed inside a cleaned tantalum sheet and vacuum sealed inside the quartz tubes under a vacuum of 10^{-5} Torr in argon atmosphere. The tantalum sheets used were etched using similar procedure as described in chapter 5A.2 to remove oxide layer, if any formed or impurities from the surface before the alloy sample was placed on it. The alloys were annealed at 800 K for 700 h and were stored inside a high pure argon glove box.

5C.2.2 Characterisation by X-Ray diffraction

The samples were characterised by employing X-ray diffractometer (M/s PANalytical X'Pert Pro MPD system) with Cu K_α radiation, to ascertain the equilibrium phases in them. Powder diffraction patterns of these samples were recorded in the range $2\theta = 25$ to 80° in steps of 0.02° with a count time of 5 s for each step.

5C.2.3 Knudsen effusion mass spectrometric studies

High temperature vaporisation behaviour of the above samples was investigated using an in-house built Knudsen effusion mass spectrometric system. The complete details about the mass spectrometric system are given in chapter 1B.12 with a schematic of KEMS (Fig. 1B.1) used for present work.

For the vaporisation experiments conducted in the present study, the samples (~500 mg) were loaded in zirconia Knudsen cell fitted with a lid having an orifice of 0.5 mm diameter (knife edged) at its centre and kept inside an outer cup and lid both made of tantalum. The heating of sample, ionisation, mass analysis etc. were carried out as described in chapter 5A.2. For ionisation electron with energy of 13.3 eV was used.

Initially, the sample was heated in increments of 100 K up to a temperature of 1000 K and subsequently in steps of 25 K, looking at each temperature above 1000 K for shutterable peaks in the mass spectra of the ions obtained from the molecular beam of the equilibrium vapour over the condensed samples inside the Knudsen cell. Two aliquots of samples, (~500 mg) from each composition were used for the vaporisation studies. Al^+ was detected as ionic species and its intensities were measured as a function of electron energy to obtain the ionisation efficiency curve. The curve thus obtained is given in Figure 5C.2 and from this the appearance energy was derived by the method of linear extrapolation. Subsequently, temperature dependence of the intensity of $^{27}Al^+$ ions was measured in the temperature range 1131-1258 K. In a given run, the sample was kept at the first temperature of that run for about an hour during which the variation in ion intensity of $^{27}Al^+$ with time was recorded at intervals of 5 to 10 minutes. The invariance of ion intensity with time at a given temperature confirmed that thermodynamic equilibrium was established in the Knudsen cell. After ensuring this, the temperature was varied in steps of 10-15 K in increasing, decreasing or in cyclic fashion. The sample was held at each temperature, for about 30 minutes. In all, twelve such runs were carried out. The pressure calibration experiments were performed both before and after the experiments on Gd-Al samples, using the same zirconia Knudsen cell that was used for the samples. The post KEMS residues were analysed by using XRD to confirm the presence of co-existing condensed phases.

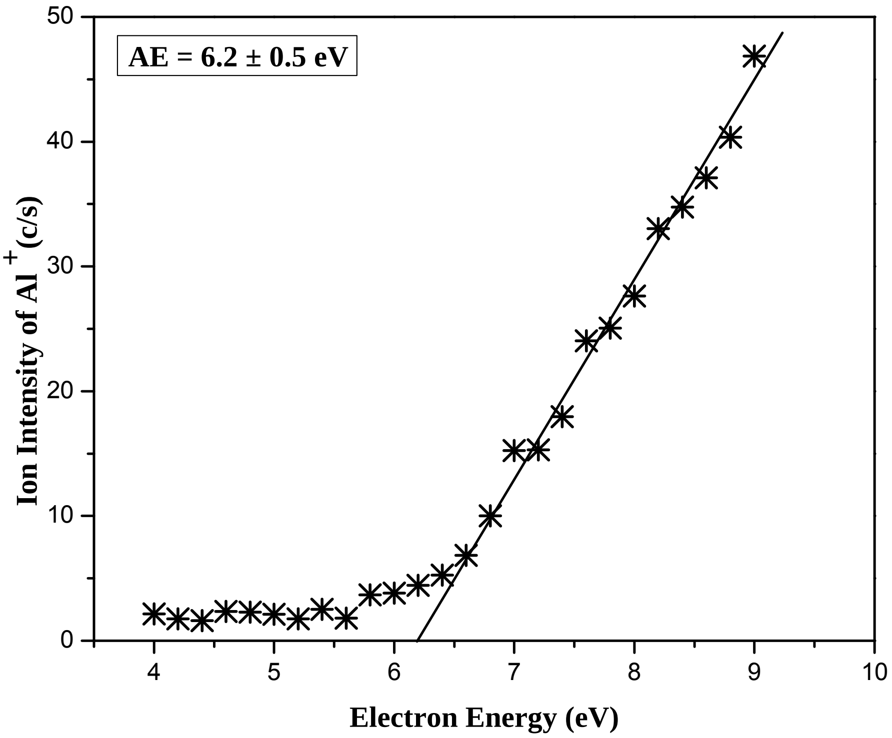

Fig. 5C.2 Typical ionisation efficiency curve for $^{27}Al^+$ over ($GdAl_2$+$GdAl_3$).

5C.3 Results and Discussion

The XRD patterns of the as prepared samples and the post KEMS residues are shown in Fig. 5C.3. The presence of $GdAl_2$ and $GdAl_3$ in both XRD patterns indicates that these samples remained in the same two-phase region during the vaporisation studies. The appearance energy (6.2 eV) obtained from the plot of ion intensity vs. the electron energy shown in Fig. 5C.2 was found to be in good accord with the value cited in ref. [18], evidencing that the neutral precursor corresponding to Al^+ was Al(g).

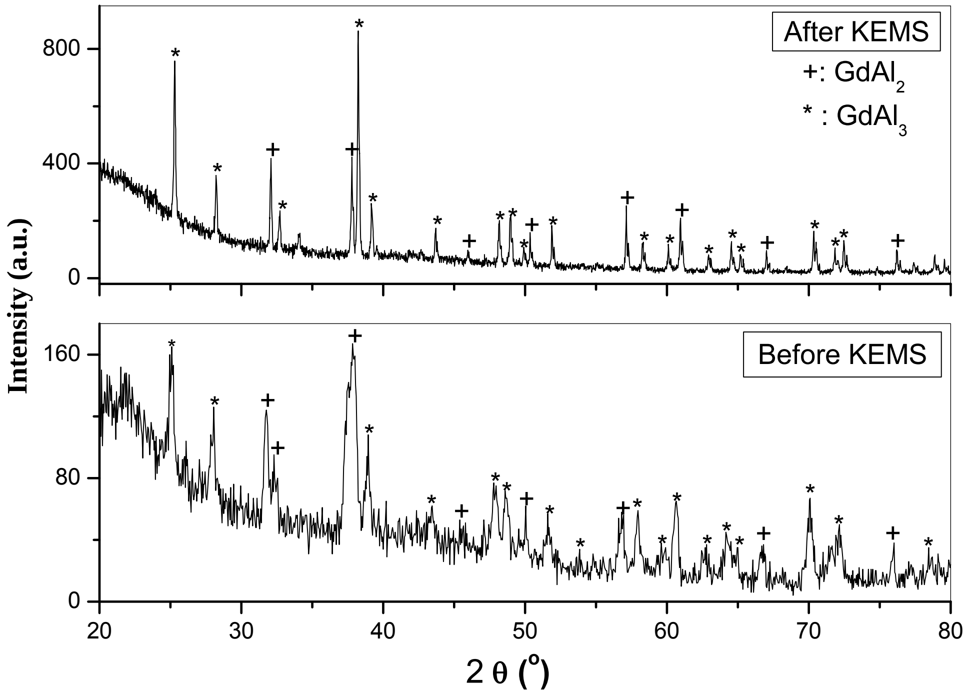

Fig. 5C.3 XRD of the sample ($Gd_{0.28}Al_{0.72}$) over ($GdAl_3$+$GdAl_2$) biphasic region before and after KEMS.

5C.3.1 Partial pressure-temperature relation of Al(g) over ($GdAl_3$+$GdAl_2$)

The measured ion intensities of $^{27}Al^+$ were converted into partial pressure by using the following relation

$$p_{Al} = k'_{Al^+} \cdot I_{Al^+} \cdot T \qquad (5C.1)$$

where $k'_{Al^+} = \frac{k}{(\sigma\gamma n)_{Al^+}}$ is the pressure calibration constant; k is the instrument calibration constant; I_{Al^+} is the measured intensity of Al^+; T is the temperature of the sample in Kelvin; σ is the ionisation cross section pertaining to Al(g); γ is the yield of secondary electron multiplier and n is the isotopic abundance. The parameters like ionisation cross section, isotopic abundance, secondary electron multiplier yield and calibration constant for Al(g) were derived using similar procedure as described in chapter 5A.3.1.

For a given temperature dependence run, the partial pressure of Al(g) (logarithmic values) were least-squares fitted with the reciprocal of the temperature to derive the partial pressure - temperature relation (p-T). There is a good agreement in the partial pressure values (~30%) obtained in the individual runs. The combined p-T relation for Al(g) was derived by pooling the partial pressure points from all twelve temperature dependence runs (total of 137 points) and following the same fitting procedure that was used in every individual run. The p-T relation thus obtained could be represented as,

$$\log(p_{Al\,(g)}/\ Pa) = (-18743 \pm 213)/T + (12.61 \pm 0.18) \qquad (1131\text{-}1258\ K) \qquad (5C.2)$$

The above relation along with those obtained for the individual runs are listed in Table 5C.1 and the corresponding plot is shown in Fig. 5C.4.

Table 5C.1 Partial pressure - temperature relations over ($GdAl_2$(s) + $GdAl_3$(s)).

Sample	**Run**	**Temperature range/(K)**	**T_m/(K)**	**$\log(p_{Al}/Pa) = -A/T(K) + B$**		**p(Al)/Pa x 10^4 at 1195 K$^{a)}$**
				A	B	
70 at.% Al Lot 1	1	1133-1258	1196	18547 ± 196	12.44 ± 0.16	8.31
	2	1132-1257	1195	18649 ± 411	12.52 ± 0.34	8.21
	3	1138-1257	1196	18493 ± 344	12.39 ± 0.29	8.22
70 at.% Al Lot 2	4	1131-1255	1193	18412 ± 344	12.34 ± 0.29	8.56
	5	1142-1256	1199	18776 ± 322	12.66 ± 0.27	8.87
	6	1138-1228	1183	18524 ± 241	12.30 ± 0.20	6.29
72 at.% Al Lot 3	7	1136-1253	1195	18445 ± 188	12.44 ± 0.16	10.1
	8	1141-1255	1198	18366 ± 350	12.41 ± 0.29	11.0
	9	1137-1255	1196	18781 ± 322	12.66 ± 0.27	8.78
72 at.% Al Lot 4	10	1137-1243	1190	18582 ± 422	12.52 ± 0.36	9.34
	11	1141-1251	1196	18536 ± 527	12.38 ± 0.44	7.39
	12	1134-1251	1193	18662 ± 470	12.44 ± 0.39	6.66
	All points	1131-1258	1195	18743 ± 213	12.61 ± 0.18	8.42
	Pure Al	1131-1258		16211	10.92	24.45

$^{a)}$ Mean temperature (T_m) of the investigation

The estimated uncertainty (u) in the partial pressure values of Al(g) is u(p) = 0.2p. The uncertainties associated with the slope and intercept of the above equation are statistical errors resulting from the least-squares fitting of data points.

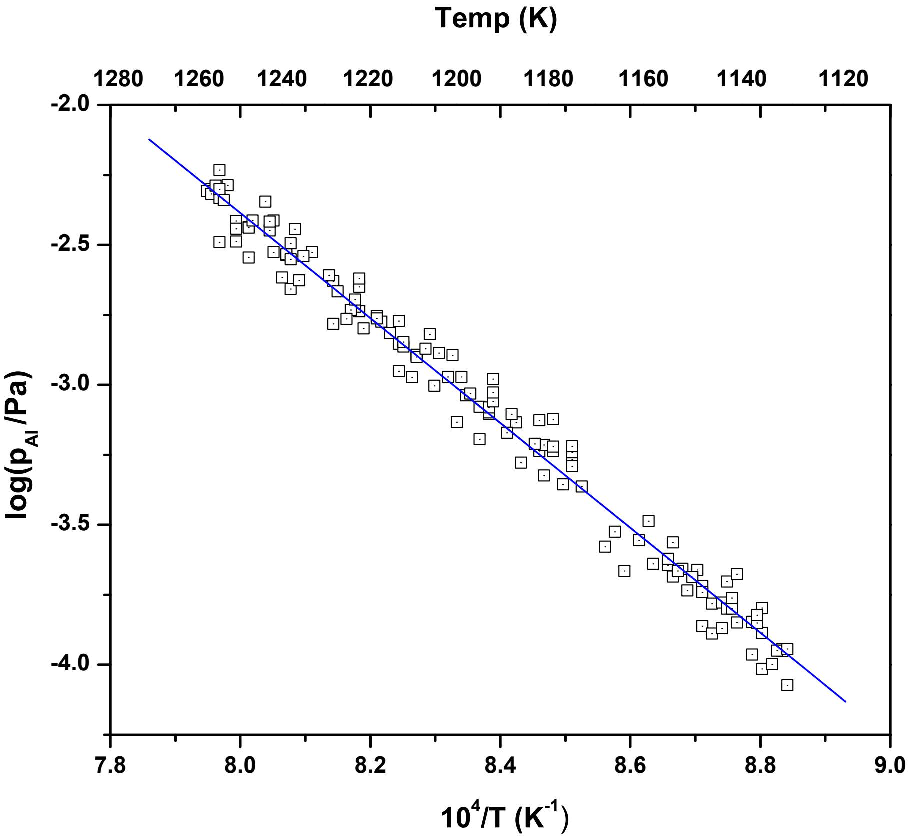

Fig. 5C.4 Combined plot of log($p_{Al\,(g)}$/ Pa) vs. 1/T (K^{-1}) over ($GdAl_2$(s) + $GdAl_3$(s)) biphasic mixture.

5C.3.2 Thermodynamic Properties

From the knowledge of the equilibrium phases present in the samples prior to and after KEMS studies and the information of the vapour species in equilibrium with the samples inside the Knudsen cell, the vaporisation reaction could be written as

$$GdAl_3(s) \rightleftharpoons GdAl_2(s) + Al(g) \tag{5C.3}$$

5C.3.2.1 Standard enthalpy of reaction and standard enthalpy of formation of $GdAl_2$

The standard enthalpy of reaction (5C.3) was derived by second and third law methods of thermodynamics [21]. The “second law enthalpy” of the reaction (5C.3), was derived through Vant Hoff’s equation given below:

$$-\mathrm{R}\,\mathrm{dln}(\mathrm{p_{Al}}) = \Delta_\mathrm{r}\mathrm{H}^\circ_\mathrm{T} \cdot \mathrm{d}(1/\mathrm{T}) \qquad (5C.4)$$

where $\Delta_r H^\circ_T$ is the standard enthalpy of reaction (5C.3) at temperature ‘T’. This corresponds to the mean temperature of the particular run. The enthalpy thus obtained was converted to that at 298.15 K, $\Delta_r H^\circ_{298.15}$ by using Kirchoff’s law [43]. The enthalpy of reaction by third law method was deduced using the following relation,

$$\Delta_r H^\circ_{298.15} = -T\{Rlnk_p + \Delta_r[(G^\circ_T - H^\circ_{298.15})/T]\} \qquad (5C.5)$$

where $(G^\circ_T - H^\circ_{298.15})/T$ is the free energy function. The required auxiliary thermal functions, enthalpy increments and Gibbs energy functions for $GdAl_3$(s) and Al(g) for evaluating the reaction enthalpies were taken from ref. [63] for $GdAl_3$(s), and ref. [22] for Al(g). In the case of $GdAl_2$(s), where the thermal functions are not available, the following procedure was adopted for estimating the enthalpy increments (for second law evaluation) and Gibbs energy functions (for third law evaluation). Such a procedure was used by us earlier to obtain thermal functions for Mo-Te [64] and Mn-Te [65]. The enthalpy increment data of $GdAl_2$(s) were estimated by using the following equation:

$$\mathrm{f_1} = \frac{(\mathrm{H^\circ_T}\text{-}\,\mathrm{H^\circ_{298.15}})_{\mathrm{GdAl_3(s)}}}{(\mathrm{H^\circ_T}\text{-}\,\mathrm{H^\circ_{298.15}})_{\mathrm{Gd(s)}} + 3\,(\mathrm{H^\circ_T}\text{-}\,\mathrm{H^\circ_{298.15}})_{\mathrm{Al(l)}}} \qquad (5C.6)$$

and $(H^\circ_T - H^\circ_{298.15})_{GdAl_2(s)} = f_1 \times \left\{(H^\circ_T - H^\circ_{298.15})_{Gd(s)} + 2(H^\circ_T - H^\circ_{298.15})_{Al(l)}\right\}$ (5C.7)

Subsequently the enthalpy of reaction at 298.15 K was derived for each run. The mean enthalpy was deduced by taking the average of enthalpy of reaction obtained from each run. These are given in Table 5C.2. The following equation was employed to derive the Gibbs Energy Functions (GEF) of $GdAl_2(s)$

$$f_2 = \frac{GEF_{GdAl_3(s)}}{GEF_{Gd(s)} + 3\,(GEF)_{Al(l)}} \tag{5C.8}$$

where $GEF = -\frac{G^\circ_T - H^\circ_{298.15}}{T}$

$GEF_{GdAl_2(s)}$ was deduced by multiplying f_2 by $\{(GEF)_{Gd(s)} + 2(GEF)_{Al(l)}\}$.

Subsequently the enthalpy of reaction for individual runs and the mean value were computed. These values are also given in Table 5C.2. The mean second and third law enthalpies of reaction at 298.15 K thus obtained are 365.3 ± 7.3 and 343.9 ± 1.9 (kJ mol^{-1}), respectively.

Table 5C.2 Reaction enthalpies (kJ mol^{-1}) of $GdAl_3(s) \rightleftharpoons GdAl_2(s) + Al(g)$.

Sample	Run	T_m/(K)[a]	Second law		Third law	Recommended $\Delta_rH^\circ_{298.15}$
			$\Delta_rH^\circ_T$	$\Delta_rH^\circ_{298.15}$	$\Delta_rH^\circ_{298.15}$	
70 at% Al Lot 1	1	1196	355.1 ± 3.8	365.0 ± 3.8	344.3 ± 1.1	354.6 ± 17.1
	2	1195	357.1 ± 7.9	367.0 ± 7.9	344.3 ± 1.2	
	3	1196	354.1 ± 6.6	364.0 ± 6.6	344.3 ± 1.0	
70 at% Al Lot 2	4	1193	352.5 ± 6.6	362.3 ± 6.6	345.0 ± 2.8	
	5	1199	359.5 ± 6.2	369.4 ± 6.2	343.4 ± 1.2	
	6	1183	354.7 ± 4.6	364.4 ± 4.6	342.5 ± 1.0	
72 at% Al Lot 3	7	1195	353.2 ± 3.6	363.1 ± 3.6	342.3 ± 0.8	
	8	1198	351.7 ± 6.7	361.6 ± 6.7	341.4 ± 0.9	
	9	1196	359.6 ± 6.2	369.5 ± 6.2	343.8 ± 1.1	
72 at% Al Lot 4	10	1190	355.8 ± 8.1	365.6 ± 8.1	343.3 ± 1.0	
	11	1196	354.9 ± 10.1	364.8 ± 10.1	345.6 ± 1.1	
	12	1193	357.3 ± 9.0	367.1 ± 9.0	346.5 ± 1.1	
	Mean	1195	355.5 ± 7.3	365.3 ± 7.3	343.9 ± 1.9	

[a] Mean temperature (T_m) of the investigation

The uncertainty in the mean second (or third) law enthalpy of reaction at 298.15K was calculated by carrying out error propagation on the uncertainties in the individual enthalpies and the standard deviation of the mean. The agreement between second and third law values can be termed “fair” considering the approximations used in calculating thermal functions of $GdAl_2$. The recommended value was computed by taking the average of the mean second and third law enthalpies and is given as 354.6 ±17.1 (kJ mol^{-1}). The uncertainty in the recommended value was deduced by applying error propagation, taking into consideration the error of ±3 K in the measured temperatures, estimated uncertainty of 20% in the calculated partial pressures and the statistical uncertainties associated with the “second” and “third law” enthalpies. The standard enthalpy of formation of $GdAl_2$(s) at 298.15 K was derived from the recommended enthalpy of reaction (5C.3), at 298.15 K and enthalpies of formation of $GdAl_3$(s) [59] and Al(g) [22]. The value obtained is given as $\Delta_f H^{\circ}_{298.15} = -148.7$ ±17.1 (kJ mol^{-1}). Table 5C.3 gives standard enthalpy of formation of $GdAl_2$(s) obtained in the present study along with the data available in literature [59, 60]. As can be seen from the table, our data are less negative than other two values and is in closer agreement with the data reported by Sommer and Keita [60].

Table 5C.3 Comparison of the enthalpies of formation of $GdAl_2$ (kJ mol^{-1}).

Compound	$\Delta_f H^{\circ}_{298.15}$	Method	Reference
$GdAl_2$ w. r. t. Gd(s) and Al(s)	– 148.7 ± 17.1	KEMS	Present study
	– 159.6	Solution calorimetry in aluminium	Colinet et al. [59]
	– 154.2 ± 9.0	Solution calorimetry in aluminium	Sommer and Keita [60]

5C.3.2.2 Standard Gibbs energy of formation of $GdAl_2$(s)

The Gibbs energy change of the reaction 5C.3 was calculated by using the following fundamental thermodynamic relation,

$$\Delta_r G^\circ_T = -2.303\ RT \log (K) \qquad (5C.9)$$

The standard Gibbs energy change of the reaction 3 derived from the pressure temperature relation for Al(g) (equation 5C.2) by employing the equation (5C.4) is expressed as given below

$$\Delta_r G^\circ_T = (358.9 \pm 4.1) - (0.1456 \pm 0.0034)\ T \quad (1131\text{-}1258\ K) \qquad (5C.10)$$

The Gibbs energy change of the reaction 5C.3 could also be written as

$$\Delta_r G^\circ_T = \Delta_f G^\circ_{T,GdAl_{2(s)}} + \Delta_f G^\circ_{T,Al(g)} - \Delta_f G^\circ_{T,GdAl_{3,(s)}} \qquad (5C.11)$$

The standard Gibbs energy of formation of $GdAl_2$(s) was obtained by using the equations (5C.10) and (5C.11). The other required thermodynamic properties viz., the standard Gibbs energies of formation of $GdAl_3$(s) and Al(g) were taken from the references [61, 22]. By using the data given in reference [22] for Al(g), an analytical expression was deduced by least-square fitting of the $\Delta_f G^\circ_T$ data as a function of temperature in the range 1000-1300 K.

$$\Delta_f G^\circ_{T,Al(g)} = 311.9 - 0.114\ T\ (kJ\ mol^{-1}) \qquad (1000 - 1300\ K) \qquad (5C.12)$$

The analytical expression for the standard Gibbs energy of formation of $GdAl_3$(s) reported in the reference [61] with respect to Gd(s) and Al(s) were converted into the appropriate reference states viz., Gd(s) and Al(l) (the reference states of gadolinium and aluminium in the temperature range of present work) by incorporating the Gibbs energy of solid - liquid transition of aluminium and the expression thus derived is given as,

$$\Delta_f G^\circ_{T,GdAl_3(s)} = (-226.2 \pm 1.7) + (0.0786 \pm 0.002)\ T\ (kJ\ mol^{-1})\ (1131\text{-}1258\ K)\ (5C.13)$$

The standard Gibbs energy of formation of $GdAl_2$(s) calculated, thus is given by the following expression

$\Delta_f G^\circ_{T,GdAl_2(s)} = (-179.2 \pm 4.4) + (0.0470 \pm 0.0039)\ T$ (kJ mol^{-1}) (1131-1258 K) (5C.14)

The reference states of gadolinium and aluminium in the above equation are solid gadolinium and liquid aluminium, respectively. The Gibbs energy of formation of $GdAl_2$(s) is reported for the first time.

The uncertainty in the standard Gibbs energy of formation of $GdAl_2$(s) was evaluated by error propagation of the uncertainties in the standard enthalpy of reaction (intercept of equation 5C.10), the standard Gibbs energy of formation of Al(g) and the standard enthalpy of formation of $GdAl_3$(s) (intercept of equation 5C.13).

5C.4 Conclusion

High temperature mass spectrometric studies on ($GdAl_2$+$GdAl_3$) of the Gd-Al binary system was conducted in the range T = 1131-1258 K. Vaporisation occurs incongruently and Al(g) was identified to be the neutral species in the vapour phase in equilibrium with the condensed phases corresponding to the above two phase mixture. The p-T relation for Al(g) was deduced as $\log(p_{Al\,(g)}/\text{Pa}) = (-18743 \pm 213)/T + (12.61 \pm 0.18)$. Using this relation, the standard enthalpy of reaction, $\Delta_r H^\circ_{298.15}$ of $GdAl_3(s) \rightleftharpoons GdAl_2(s) + Al(g)$ was deduced by second and third law methods of thermodynamics. Subsequently the standard enthalpy of formation, $\Delta_f H^\circ_{298.15}$ of $GdAl_2$(s) was computed. The values are 354.6 ± 17.1 and −148.7 ± 17.1(kJ mol^{-1}), respectively. From the above p-T relation, the standard Gibbs energy of formation of $GdAl_2$(s) was deduced to be $\Delta_f G^\circ_{T,GdAl_2(s)} = (-179.2 \pm 4.4) + (0.0470 \pm 0.0039)\ T$ (kJ mol^{-1}) (1131-1258 K). The vaporisation studies and the Gibbs energy of formation of $GdAl_2(s)$ are being reported for the first time.

References

[1] S. Bera, V. V. Trinadh, P. Manikandan, T. S. Lakshmi narasimhan, J. Nucl. Mater. 509 (2018) 613.

[2] S. Usha, R. R. Ramanarayanan, P. Mohanakrishnan, R. P. Kapoor, Nucl. Engg. Design 236 (2006) 872.

[3] M. E. Kassner, P. H. Adler, M. G. Adamson, J. Nucl. Mater. 167 (1989) 160.

[4] J. Wang, X. J. Liu, C. P. Wang, J. Nucl. Mater. 374 (2008) 79.

[5] P. Gordon, A. R. Kaufman, Trans. AIME 188 (1950) 182.

[6] G. Cabane, M. Englander, J. Lehmann, Proceedings of UN International Conference on Peaceful Uses of Atomic Energy 9 (1955) 120.

[7] P. R. Roy, J. Nucl. Mater.11 (1) (1964) 59.

[8] G. Petzow, S. Steeb, I. Ellinghaus, J. Nucl. Mater.4 (1961) 316.

[9] I. Johnson, in; Nuclear Metallurgy, Vol.10, AIME, New York, (1964) 171.

[10] P. Chiotti, V. V. Akhachinskji, I. Ansara, M. H. Rand, The Chemical Thermodynamics of Actinide Elements and Compounds, part 5 (1981).

[11] P. Chiotti, J. A. Kateley, J. Nucl. Mater. 32 (1969) 135.

[12] V. A. Lebedev, V. I. Salnikov, I. F. Nichkov, S. P. Rapopin, Atom. Energy 32 (1972) 115.

[13] M. I. Ivanov, V. A. Tumbakov, N. S. Podoo'skaia, J. Atom. Energy 4 (1958) 1007.

[14] H. D. Dannohl, H. I. Lukas, Z. Metallkd. 65 (1974) 642.

[15] K. Nagarajan, R. Babu, C. K. Mathews, J. Nucl. Mater. 201 (1993) 142.

[16] P. Manikandan, Ph.D Thesis (Homi Bhabha National University) (2017).

[17] R. Hultgren, P. D. Desai, D. T. Hawkins, M. Gleiser, K. K. Kelley, D. T. Wagman, Selected Values of the Thermodynamic Properties of Elements, American Society for Metals, Metal Park, OH (1973).

[18] K. Hilpert, K. A. Gingerich, Int. J. Mass Spectrom. 47 (1983) 247.

[19] C. E. Moore, Ionisation Potentials and ionisation limits derived from the analysis of Optical Spectra, NSRDS-NBS 34 Nat. Stand. Ref. Data Ser. Nat. Bur. Stand, vol. 34 (1970).

[20] J. B. Mann, K. Ogata, T. Hayakawa (Ed.), Proc. Int. Conf. on Mass Spect. (1970).

[21] C. B. Alcock, V. P. Itkin, M. K. Horrigan, Can., Metall. Quart. 23 (1984) 309.

[22] The Characterisation of High Temperature Vapours, Ed., J. L. Margrave, Wiley, New York (1967).

[23] I. Barin, Thermochemical Data of Pure Substance 3rd Ed., VCH, Weinheim, New York (1995).

[24] P. Manikandan, V. V. Trinadh, S. Bera, T. S. Lakshmi Narasimhan, K. Ananthasivan, M. Joseph, U. Kamachi Mudali, J. Nucl. Mater. 491 (2017) 31.

[25] H. Kleykamp, S. G. Kang, J. Nucl. Mater. 230 (1996) 280.

[26] O. H. Krikorian, Review of the Thermodynamic and Kinetic Data for the Molten Tin Process, Lawrence Livermore Laboratory, Report No. UCID 18262, 6th August (1979).

[27] F. A. Rough, A. A. Bauer, Uranium-Tin in Constitution of uranium and thorium alloys, BMI Report-1300, UC-25 Metallurgy and Ceramics, Battelle Memorial Institute, Ohio, 2, June (1958) 71.

[28] D. A. Treick, J. H. Carter, A. I. Snow, R. Baldwin, A. Wilson, The Uranium-Tin System, M-3107 (1945).

[29] R. E. Rundle and A. S. Wilson, Acta. cryst. 2 (1949) 148.

[30] C. B. Alcock, P. Grieveson, J. Inst. Met. 93 (1961) 304.

[31] C. Sari, F. Vernazza, W. Müller, J. Less-common. Met. 92 (1983) 301.

[32] R. I. Sheldon, E. M. Foltyn, D. E. Peterson, Bull. Alloy. Phase. Diagr. 8 (1987) 347.

[33] A. Palenzona, P. Manfrinetti, J. Alloy. Comp. 221 (1995) 157.

[34] J. Wang, K. Wang, C. Ma, L. Xie, J. Chem. Thermodyn. 92 (2016) 158.

[35] I. Johnson, Thermodynamics of plutonium, thorium and uranium metallic systems, in: T. J. Waber, P. Chiotti, (Ed.), Proceedings of the Int. Symp. on Compounds of Interest in Nucl. Reactor Tech., 171, IMD Special Rpt. 13, The American Inst. of Mining, Metallurgical and Petroleum Engineers (1964) 185.

[36] I. Johnson, H. M. Feder, Thermodynamic study of the compounds of uranium with silicon, germanium, tin and lead, in: Proceedings of the International Symposium of Thermodynamics of Nuclear Materials, Int. Atomic Energy Agency Vienna (1962) 319.

[37] V. A. Kadochniko, V. A. Lebedev, I. F. Nichkov, S. P. Raspopin, zvestiya Akademii Nauk SSSR, Met. (1976) 67.

[38] A. K. Pattanaik, R. Kandan, K. Nagarajan, P. R. Vasudeva Rao, J. Alloys. Comp. 551 (2013) 249.

[39] C. Colinet, A. Bessound, A. Pasturel, W. Müller, J. Less-Common. Met. 143 (1988) 265.

[40] R. Grimley, J. L. Margrave (Ed.), The Characterisation of High-Temperature Vapours, John Wiley & Sons, New York, Chapter 8 (1967).

[41] J. Drowart, A. Pattoret, S. Smoes, J. Nucl. Mater. 12 (1964) 319.

[42] L. B. Pankratz, Thermodynamic properties of elements and oxides, Report No. Bumines, B 672, Bull. US Bur. Mines (1983) 397.

[43] O. Kubaschewski and C. B. Alcock, Metallurgical Thermochemistry, 5th Ed., Pergamon press, Oxford, UK (1979).

[44] P. Manikandan, V. V. Trinadh, S. Bera, T. S. Lakshmi Narasimhan, M. Joseph, J. Nucl. Mater. 475 (2016) 87.

[45] S. Bera, P. Manikandan, V. V. Trinadh, S. Nedumaran, T. S. Lakshmi Narasimhan, K. Ananthasivan, J. Nucl. Mater. In press (2018).

[46] L. M. Ferris, J. C. Mailen, F. J. Smith, J. Inorg. Nucl. Chem. 33 (1971) 1325.

[47] H. Morriyama, K. Yajima, Y. Tominaga, K. Moritani, J. Oishi, J. Nucl. Sci. Tech. 21, 12 (1984) 949.

[48] M. Kurata, Y. Sakamura, T. Matsui, J. Alloys Comp. 234 (1996) 185.

[49] O. Conocar, N. Douyere, J. Lacquement, J. Nucl. Mater. 344 (2005) 136.

[50] L. Cassayre, R. Malmbeck, P. Masset, J. Rebizant, J. Serp, P. Soucek, J. P. Glatz, J. Nucl. Mater. 360 (2007) 49.

[51] C. Caravaca, G. De Cordoba, presented at the EUCHEM Conference on Molten Salts and Ionic Liquids, Hammamet, Tunisia, 16th - 22nd September (2006).

[52] K. H. J. Buschow, J. Less-Common Metals. 9 (1965) 452.

[53] O. J. C. Runnalls, R. R. Boucher, J. Less-Common. Met. 13 (1967) 431.

[54] K. A. Gschneidner, F. W. Calderwood, Bull. Alloy Phase Diagrams. 9 (1988) 680.

[55] A. Saccone, A. M. Cardinale, S. Delfino, R. Ferro, Z. Metallkd. 91 (2000) 1.

[56] G. Cacciamani, S. De Negri, A. Saccone, R. Ferro, Intemetallics. 11 (2003) 1135.

[57] L. Jin, Y. Kang, P. Chartrand, C. D. Fuerst, CALPHAD 34 (2010) 456.

[58] H. Bo, L. B. Liu, J. L. Hu, X. D. Zhang, Z. P. Jin, Therm. Chim. Acta. 591 (2014) 51.

[59] C. Colinet, A. Pasturel, K. H. J. Buschow, Phy. B 150 (1988) 397.

[60] F. Sommer, M. Keita, J. Less-Common. Met. 136 (1987) 95.

[61] M. R. Bermejo, J. Gomez, J. Medina, A. M. Martinez, Y. Castrillejo, J. Electroanal. Chem. 588 (2006) 253.

[62] D. Darwin Albert Raj, R. Viswanathan, P. Manikandan, ECS Trans. 46 (1) (2013) 77.

[63] S. Nedumaran, R. Kandan, B. P. Reddy, presented at Proceedings of the 21st DAE-BRNS symposium on thermal analysis (Thermans-2018), P.76, held in Goa, India, 18th-20th January (2018).

[64] R. Viswanathan, D. Darwin Albert Raj, T. S. Lakshmi Narasimhan, R. Balasubramanian, C. K. Mathews, J. Chem. Thermodyn. 25 (1993) 533.

[65] T. S. Lakshmi Narasimhan, M. Sai Baba, R. Balasubramanian, S. Nalini, R. Viswanathan, J. Chem. Thermodyn. 34 (2002) 103.

CHAPTER 6

===

Summary and Conclusion

This chapter summarises the outcome of research carried out in this thesis. Present study has brought out the importance of mass spectrometry in some of the important areas of nuclear technology. The mass spectrometric techniques, TIMS and KEMS were employed for studies on nuclear material/process pertaining to three stages of Indian nuclear power programme.

Chapter 1: This chapter described the methodology, important components and application of TIMS. The IDMS technique in combination with TIMS provides accurate isotopic abundance and these aspects were highlighted. The principle of KEMS technique, the instrumentation and methodology adopted to derive thermodynamic properties of materials were also described.

Chapter 2: The uranium plutonium mixed oxide (MOX) fuel irradiated in FBTR was analysed for its burn-up, using two techniques, HPLC and TIMS. HPLC technique was used to determine burn-up (atom percent fission) using suitable fission product monitors by considering total elemental concentration. TIMS was used to determine burn-up by employing isotopes of a nuclide, e.g. $^{(145+146)}$Nd and ^{148}Nd isotopes. The fractional fission contribution which is unique for a nuclear reactor with particular fuel composition was deduced using $^{(145+146)/150}$Nd ratio for the first time for MOX fuel. These studies established that $^{(145+146)}$Nd as fission product monitor provides more reliable burn-up data for fast reactor fuel along with ^{148}Nd, which is conventionally used for thermal reactors.

Chapter 3: It is good practice to certify important experimental data e.g. burn-up by employing various methods. Though neodymium is used routinely as burn-up monitor, there is a need for alternate burn-up monitors. The need and use of alternate burn-up monitors like molybdenum, lanthanum were discussed in this chapter. Molybdenum whose fission yield (second highest) is higher compared to neodymium, was successfully employed as alternate fission product monitor for the determination of burn-up. The natural contamination of molybdenum, if any present in reactor fuel can be corrected using internal natural isotope correction and the same was carried out. Lanthanum possesses almost similar fission yield for the fissile materials (^{233}U, ^{235}U and ^{239}Pu) from thermal and fast reactors, making it as a suitable isotope, i.e. fission product monitor, not only for fuels pertaining to the thermal reactors, but also for the fast reactor fuels like mixed oxide, carbide and metallic fuels. The burn-up was computed using lanthanum as burn-up monitor and the data obtained from molybdenum and lanthanum were compared with those of neodymium. The results indicated that molybdenum and lanthanum can be used as burn-up monitors whenever required. New sample loading procedures for TIMS were developed, which resulted in, increased efficiency of ionisation for molybdenum and lanthanum. All radioactive samples (Mo, La, Nd, U, Pu) were loaded on filament surface in minimum time inside fume hood to minimise the radioactive expose to analyst and safety related issues.

Chapter 4: The work carried out pertaining to use of magnesium as a tracer for the determination of volume of input tank at reprocessing facility, which is vital with respect to accurate accounting of nuclear materials (U and Pu). New sample loading method was developed and employed for accurate and precise measurement of magnesium isotopes and the results obtained were in good agreement with the certified values. Additional experiments with actual dissolver solution to implement above method was not attempted as it was observed that magnesium solution formed a layer on the inner surface of the tank containing stock solution, which may affect the chemical properties of structural material holding the actual dissolver solution in input tank.

Single loading measurements for the analysis of lithium and neodymium for their isotopic ratios (in sodalite, a waste matrix) and concentration measurements were demonstrated using ID-TIMS without chemical separation of elements present in the sodalite sample. Accurate and precise quantification of these elements is essential to develop a suitable waste storage matrix to ascertain their retention capacity which is expected to encounter different physicochemical conditions and to study the leaching behaviour of these elements from matrix in corrosive environments.

Isotopic enrichment study on gadolinium was carried out with different experimental conditions using HPLC followed by TIMS analysis. Presence of seven gadolinium isotopes and contribution of organics during sample loading makes the isotopic analysis challenging using TIMS. This was overcome using suitable pre-treatment and precise TIMS analysis of gadolinium samples. The outcome of present work provided the base for further scaling-up of the enrichment.

Chapter 5: The thermodynamic studies on U-Al system, which is a fuel material in research reactors, are important to understand their behaviour under normal and transient condition during irradiation. KEMS study on U-Al system over (UAl_2 + UAl_3) two phase region was carried out for the first time in the temperature range of 1115-1253 K. The thermodynamic properties like enthalpy and Gibbs energy of formation for UAl_3 were derived from partial pressure of Al(g).

KEMS study on U-Sn system over (USn_3+U_3Sn_7) biphasic region was carried out for the first time. Partial pressure of Sn(g) and enthalpy of reaction for $3USn_3(s) \rightleftharpoons U_3Sn_7(s) + 2Sn(g)$ was deduced in the temperature range of 1050-1226 K. The enthalpy and Gibbs energy of reaction for USn_3 was deduced at 298.15 K. These data will be of significance to the spent molten salt process and to understand the thermodynamics of intermetallic compounds formed between fuel constituents and fission product, tin.

KEMS study on Gd-Al system over ($GdAl_2$+$GdAl_3$) biphasic region was carried out over the temperature range of 1131-1258 K. The thermodynamic properties pertaining to ($GdAl_2$+$GdAl_3$) biphasic regions were deduced for the first time using KEMS. High temperature thermodynamic data on $GdAl_3$ one of the intermetallic compounds of this system was deduced. The studies on this system will help to understand their thermodynamic stabilities and have direct relevance to molten salt electro-refining.

CHAPTER 7

===

Scope for future studies

In continuation of the work presented in this thesis, further studies can be carried out on the following:

The present study established molybdenum and lanthanum as potential burn-up monitors. The same can be implemented for future burn-up studies with dissolver solution of fast reactor fuels (Mixed oxide, carbide and U-Pu-Zr metallic fuels)

New sample loading methods for lithium can be explored to minimise isotopic fractionation effect, which can result in improved accuracy and precision of the result. The present work on sodalite can be extended to barium along with lithium and neodymium for quantitative measurement of these elements, employing single loading on filament surface.

The preliminary studies on gadolinium enrichment with HPLC have shown possibilities for isotope enrichment. Use of ultra high pressure liquid chromatography (UPLC) (where the number of separation stages (N) is expected to be higher) along with appropriate columns, mobile phase composition and temperature can result in better enrichment of desirable isotope. The effective isotope separation followed with TIMS can provide better understanding of the insights of the separation process.

Thermodynamic investigation on other phase region of U-Al, U-Sn and Gd-Al can be taken up for further study to cover the entire phase diagram. Accordingly, studies on the biphasic region of ($GdAl_2$ + GdAl) over Gd-Al system, (U_3Sn_7 + USn_2), (USn_2 + USn) and (USn + U_3Sn_4) over U-Sn system can be pursued. The absence of thermal functions such as enthalpy and entropy increments data for different phases of Gd-Al system necessitates calorimetric studies over this system.

Appendix-1

Computation of fractional fission from ^{233}U and ^{239}Pu for MOX fuel

To derive fractional fission contribution for ^{233}U and ^{239}Pu, $^{(145+146)}$Nd/^{150}Nd ratio was selected because their ratio are widely different for these two sources of fission, i.e. for ^{233}U it is 12.12 and for ^{239}Pu it is 5.48. Thus the difference is ~50%. Hence the fractional fission can be obtained

Table.2 The fission yield data for neodymium from fast fission of ^{233}U and ^{239}Pu [13].

	^{143}Nd	^{144}Nd	^{145}Nd	^{146}Nd	^{148}Nd	^{150}Nd
^{233}U	5.66	4.44	3.24	2.41	1.21	0.466
^{239}Pu	4.38	3.73	3.05	2.54	1.69	1.02

If “p” is the fractional fission contribution from ^{233}U and “q” is fractional fission contribution from ^{239}Pu. Then combined fractional fission contribution from uranium and plutonium for $^{(145+146)}$Nd/^{150}Nd can be written as

$$\frac{^{(145+146)}Nd}{^{150}Nd} = \frac{\left({}^{145}_{Nd}Y^{233}_{U} \times p + {}^{145}_{Nd}Y^{239}_{Pu} \times q\right) + \left({}^{146}_{Nd}Y^{233}_{U} \times p + {}^{146}_{Nd}Y^{239}_{Pu} \times q\right)}{\left({}^{150}_{Nd}Y^{233}_{U} \times p + {}^{150}_{Nd}Y^{239}_{Pu} \times q\right)} \tag{Ap.1.1}$$

where ${}^{145}_{Nd}Y^{233}_{U}$, ${}^{146}_{Nd}Y^{233}_{U}$, ${}^{150}_{Nd}Y^{233}_{U}$: fission yield of 145, 146, 150 neodymium from nuclear fission of initial hundred atoms of ^{233}U. ${}^{145}_{Nd}Y^{239}_{Pu}$, ${}^{146}_{Nd}Y^{239}_{Pu}$, ${}^{150}_{Nd}Y^{239}_{Pu}$: fission yield of 145, 146, 150 neodymium from nuclear fission of initial hundred atoms of ^{239}Pu. The fraction of ‘p’ and ‘q’ from ^{233}U and ^{239}Pu can be within zero to 100%.

Thus we can have another equation

$$\boldsymbol{p + q = 1} \tag{Ap.1.2}$$

Using equation (Ap.2.1), (Ap.2.2) and incorporating values from zero to 100 for ‘p’ and ‘q’ the theoretical contribution from uranium and plutonium can derive for $^{(145+146)}$Nd/^{150}Nd. These simulated values then compared with experimental values deduced from TIMS analysis for $^{(145+146)}$Nd/^{150}Nd. The agreement of theoretical data with experimental one gives identical fractional fission contribution, which is unique for a particular composition of fuel.

The isotopic ratio of $^{(145+146)}$Nd/^{150}Nd obtained from TIMS analysis = 7.808

This experimental data is agreeing with value obtained from theoretical simulation, i.e. 54.2% fission from ^{233}U and 45.8% fission from ^{239}Pu.

Appendix-2

Table.1 A typical example for burn-up determination on MOX fuel using TIMS

Steps		Lanthanum	Neodymium	Uranium		Plutonium	
				Spiked A	Spiked B	Spiked A	Spiked B
1	Weight of PHWR fuel sample taken (in g)	0.5804	0.5804	0.0473	0.0589	0.0473	0.0589
2	Weight of Spike solution taken (in g) b)	1.0534	0.5645	0.6731	0.9294	0.65	1.2246
3	Concentration of spike (µg/g) b)	12.166131	1.674024	6.684594	6.684594	10.399621	10.399621
4	Isotopic ratio of spike (j/i) a)	0.063282	132.809	1.740×10^{3}	1.740×10^{3}	0.066263	0.066263
5	Isotopic ratio of sample (j/i) a) (Table 3B.1, 3A.2 and 3A.3)	4.7×10^{-5}	0	4×10^{-6}	4×10^{-6}	0.419406	0.419406
6	Isotopic ratio of mixture (j/i) a)	0.052207	0.596164	6.536×10^{-3}	7.199×10^{-3}	0.144908	0.123022
7	Atom fraction of " j" in spike b)	5.9516×10^{-2}	9.79938×10^{-1}	0.996924	0.996924	0.062066	0.062066
8	Atom fraction of " i" in sample (Table 3B.1, 3A.2 and 3A.3)	9.99953×10^{-1}	1.99619×10^{-1}	0.996984	0.996984	0.671051	0.671051
9	Average atomic weight of sample (Table 3B.1, 3A.2 and 3A.3)	138.906307	144.845046	238.042442	238.042442	239.446499	239.446499
10	Average atomic weight of spike b)	138.846882	141.9511	233.045195	233.045195	239.116786	239.116786
11	IDMS equation (1A.6)	$\boldsymbol{C_S = \frac{C_{Sp} * W_{Sp}}{W_S} \times \left(\frac{R_{(j/i)Sp} - R_{(j/i)mix}}{R_{(j/i)mix} - R_{(j/i)S}} \times \frac{1}{R_{(j/i)Sp}} \right) \times \frac{< AF_{j,Sp} >}{< AF_{i,S} >} \times \frac{(AW)_S}{(AW)_{Sp}}}$						
12	Concentration of element in sample (µg/g)	4.41	13.62	14873.16	14973.95	57.23	57.88
				14923.55 (± 0.34 %)		57.55 (± 0.56 %)	
13	Number of atoms (A and H)	1.913×10^{16}	5.663×10^{16} ($^{\text{Total}}$Nd) 5.247×10^{15} (^{148}Nd)	3.776×10^{19}		1.448×10^{17}	
14	Burn-up equation (1A.7)	$\text{Burn-up (atom \% fission)} = \frac{(A/Y)}{[H + (A/Y)]} \times 100$					
15	Fission yield (Y) (chapter 3,[15]) 50% contribution from ^{235}U and ^{239}Pu	0.061565	0.185 ($^{\text{Total}}$ Nd), 0.017 (^{148}Nd)				
16	Burn-up (Atom % fission)	0.81(^{139}La)	0.80 ($^{\text{Total}}$ Nd) , 0.82 (^{148}Nd)				

a) j/i : 138/139 for Lanthanum, 142/143 for Neodymium, 233/238 for Uranium, 240/239 for Plutonium.

For IDMS, lanthanum, neodymium, uranium and plutonium enriched with 138, 142, 233 and 239 isotopes, respectively were used.